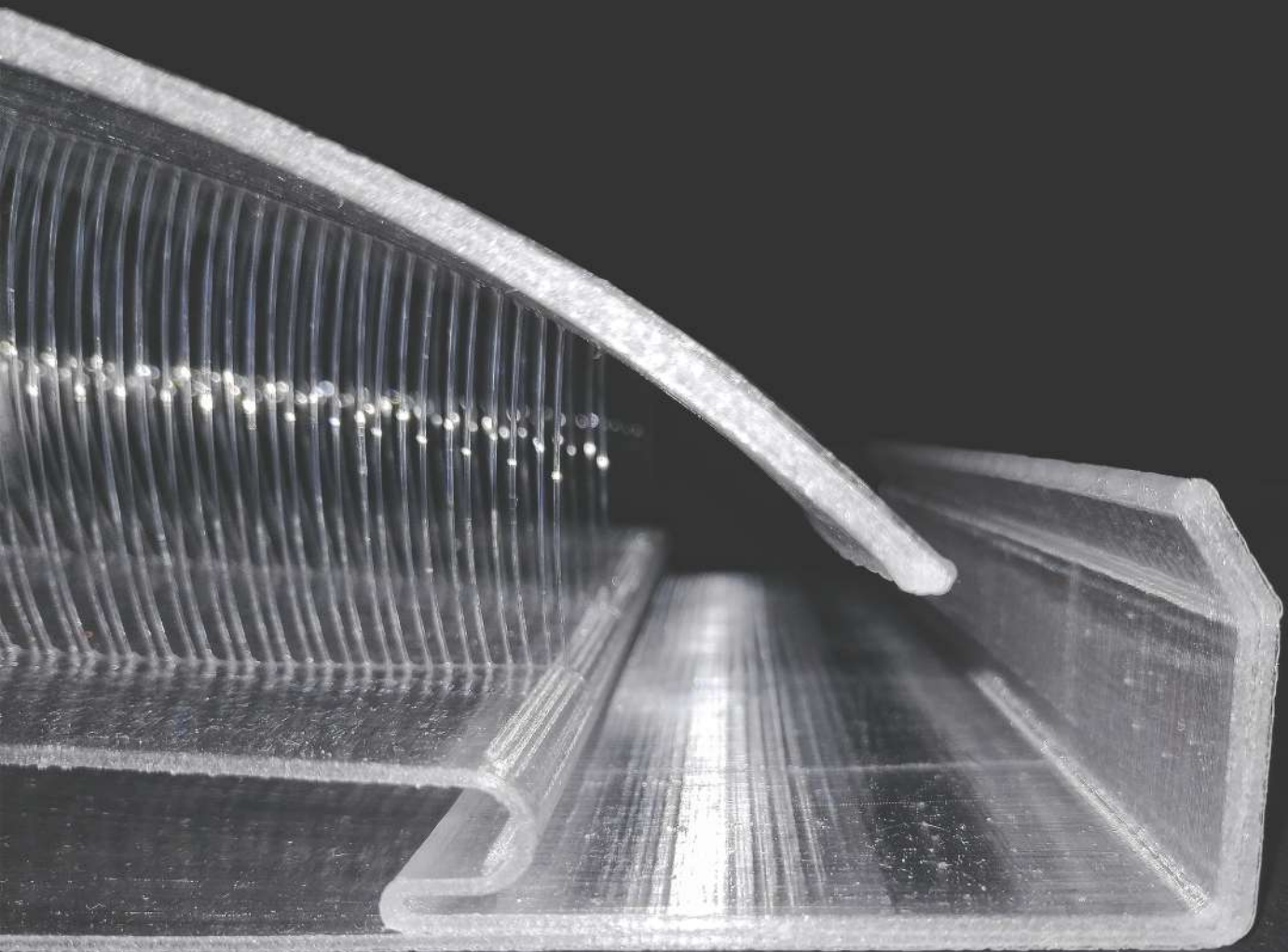


WATER - CATCHER

**A 3d-printed building component
to mitigate water stress in developing countries**



Master studio

MSc Architecture, Urbanism and Building Sciences
Track: Building Technology

Master's thesis

Title: WATER-CATCHER: a 3d printed building component to mitigate water stress in developing country
Author: Leonardo Caldoni
Student number: 5029058

Mentors

Ir. P. de Ruiter (AE+T: Design Informatics)
Ir. E. van den Ham (AE+T: Climate Design)

Delegate board of examiner

Ir. P. Kuitenbrouwer

University



Delft University of Technology
Faculty of Architecture and the Built Environment
Department of Building Technology

Julianalaan 134
2628BL Delft
The Netherlands

Abstract:

Urban population growth predictions and the threats posed by climate change will exacerbate social problems such as equal access to water worldwide. This will happen mostly in developing countries and will couple with other environmental issues such as the intensive use of raw materials and the production of new waste. New solutions need to be thought and atmospheric water supplies such as fog or dew water represent alternative sources still largely untapped.

Within the Living in a Bottle project, this research looks at computational design workflows and Additive Manufacturing as tools that can play a role in mitigating these risks, while transforming the perception of plastic waste from burden to construction material. Moreover, 3d-printing represents a flexible fabrication technology that could play a relevant educational and developing role in growing communities.

The goal of the research is to propose a solution for a mono-material building envelope component designed to enable and maximize atmospheric water collection in developing countries. The design aims to be adaptable to different climatic scenarios and easy to replicate locally. The task is approached systematically by defining all necessary functions and exploring the best strategy for each of them. Every step is performed considering both the optimization of functionality and 3d-printability. Functions are then combined in one element which is prototyped and tested. Computer simulations for the city of Rabat (Morocco), show that the combination of a dew and fog collector in one component would reduce by half the surface required to fulfill the water needs of one person. A feasibility analysis is also performed and the price of one module is estimated. The result is comparable to the cost of standard solutions in the field of atmospheric water harvesting and represents therefore an interesting achievement in the development of such technology.

Keywords:

Water scarcity, atmospheric water harvesting, fog collector, radiative condenser, rPET, additive manufacturing, 3d-printed roof, mono-material

Acknowledgements:

With this thesis, my adventure at TU Delft comes to an end. It has been an enriching experience that made me grow both professionally and personally. For this, many people need to be thanked.

First of all, I want to express my gratitude towards my two mentors Ir. Paul de Ruiter and Ir. Eric van den Ham. Their guidance and experience have been paramount to approach the research and the prototyping phase, which was totally new to me. Moreover, I am extremely thankful for all the additional support I received from them throughout the whole graduation. This ranged from giving me the possibility to prototype in my room during these pandemic times, to supporting and encouraging me with enthusiasm in the moments of confusion.

I also want to thank my family that has always been only one phone call away, supporting me during this period and believing in me more than myself. I thank my friends, for being next to me in the important moments for years now and a reference point in my life.

Lastly, I want to thank the friends with which I have shared this journey. Those with which I shared countless joyful nights, indelible memories, anxieties and moments of doubt. Thank you for being a constant inspiration.

Table of contents

PHASE 01 - RESEARCH FRAMEWORK			
1.1 Research context	4		
1.2 Problem statement	6		
1.3 Research questions	7		
1.4 Research objectives	7		
1.5 Research methodology	8		
PHASE 02 - FOUNDATION KNOWLEDGE			
2.1 Biomimetic inspirations	12		
2.2 Radiative condensers	14		
2.3 Fog collectors	15		
2.4 Architectural aerodynamics	16		
2.5 Additive manufacturing	18		
PHASE 03 - PRE-DESIGN			
3.1 Pre-Design: Radiative Condenser	24		
3.1.1 Condensation	24		
3.1.2 Collection	28		
3.2 Pre-Design: Fog Collector	29		
3.3 Specific case study definition	32		
3.4 Pre-Design: Additive Manufacturing	34		
PHASE 04 - DESIGN			
4.1 Design workflow and tools	38		
4.2 Condensing surface	38		
4.2.1 Temperature reduction	38		
4.2.2 Droplet nucleation and collection	41		
4.2.3 Radar charts	44		
4.3 Fog-catching surface	46		
4.3.1 Multilayer Harp Collector	46		
4.3.2 Three-dimensional Infill Collector	47		
4.3.3 Comparative analysis	48		
4.3.4 Radar charts	48		
4.4 Component design	50		
4.4.1 Conclusions from previous sections	50		
4.4.2 Water-catcher design method	50		
4.4.3 Building component's orientation	52		
4.5 Schematic Design	54		
4.5.1 Fog section	55		
4.5.2 Dew Section	58		
4.6 Design Development	60		
4.7 Final Design	61		
4.8 Optimization for 3d-printing	66		
4.9 Final Prototyping	71		
PHASE 05 - FINAL EVALUATION			
5.1 Workflow's flexibility		76	
5.1.1 Standalone component		77	
5.1.2 Modular wall system		78	
5.1.3 Facade system		79	
5.2 Water collection efficiency		80	
5.2.1 Experimental setup		80	
5.2.2 Experiment results		81	
5.2.3 Water collection potential		86	
5.3 Fabrication efficiency		90	
5.3.1 Printing quality		90	
5.3.2 Local production's feasibility		91	
5.4 Next steps		95	
5.4.1 Design improvements		95	
5.4.2 Water-catching performance		95	
5.4.3 3d-printability		96	
5.5 Discussion		100	
5.6 Conclusions		101	
5.7 Reflection		104	
REFERENCES			107
APPENDIX			109
Appendix I			109
Appendix II			111
Appendix III			112
Appendix IV			115
Appendix V			118
Appendix VI			119



1. Research context

The research question is developed in this section, through a first analysis of the societal problems and technological gap that aim to be addressed in this work. A methodology is set and presented to illustrate the structure of this report and of the rest of the thesis over time.

1.1 RESEARCH CONTEXT

1.1.1 Access to water and water scarcity

The sixth Sustainable Development Goal (SDG) approved by the UN in the 2030 Agenda for a Sustainable Development states “Ensure availability and sustainable management of water and sanitation for all”. According to the UN synthesis report on water and sanitation 2018 (UN, 2018)¹, 29% of world population had no access to a safely managed water service. In particular, **844 million people still lacked a basic drinking water service**, which consists of a safely managed water source within a 30 minutes walking distance (Fig.1).

In addition to this, climate change is increasingly threatening the availability and quality of water worldwide. In 2016, around 4 billion people experienced severe water scarcity for at least one month (Mekonnen and Hoekstra, 2016)² and, if unmitigated, water scarcity is expected to cause the displacement of 700 million people by 2030 (Global Water Institute, 2013)³ (Fig.2).

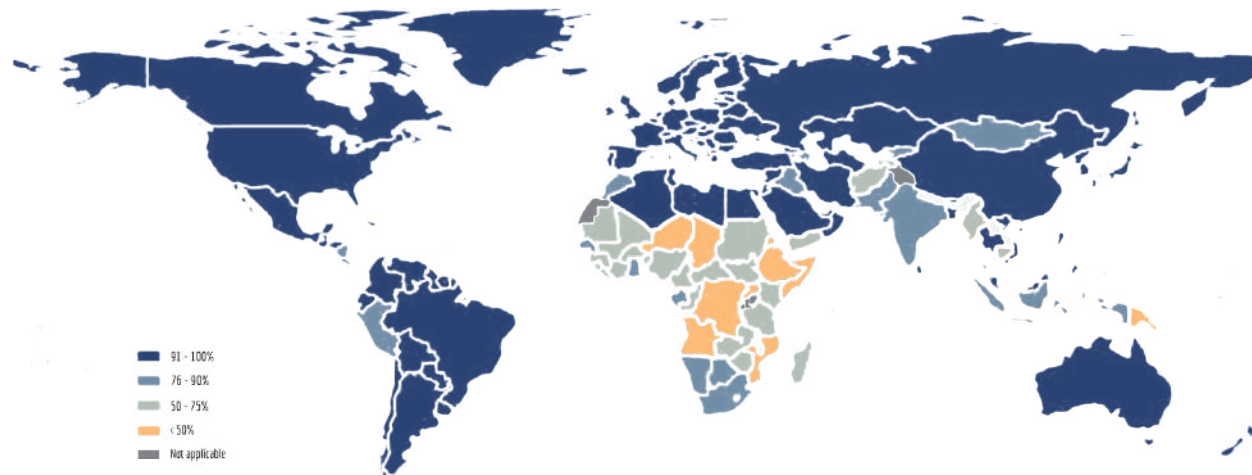


Fig.1: Share of population using at least basic water service. [Elaboration of image from UN, 2018]

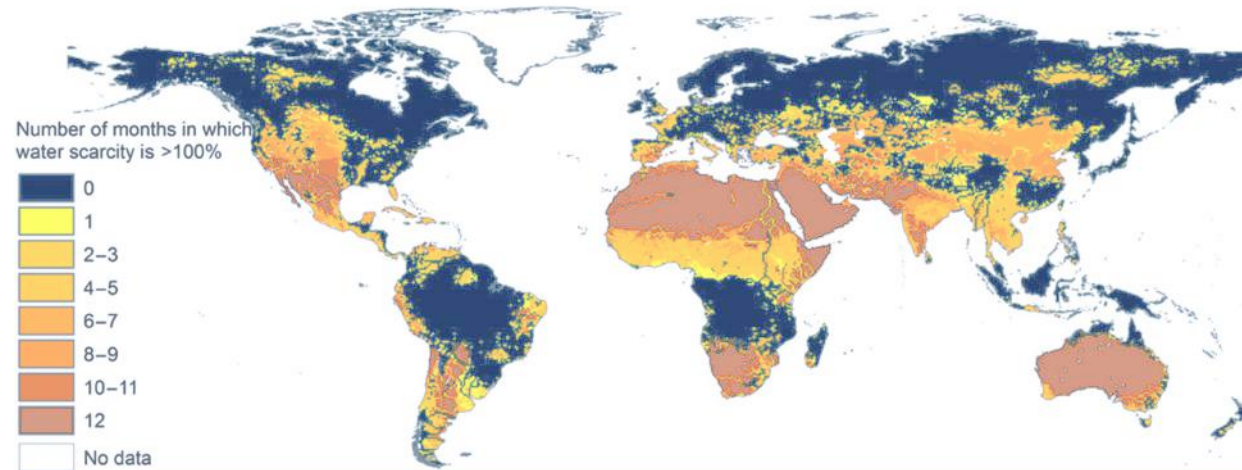


Fig.2: Months of severe water scarcity worldwide. [Elaboration of image from Mekonnen, 2016]

Different approaches can be explored to increase water availability in these environments (Schyns, Hamaideh, and others, 2015)⁴. The main options are:

- Dams for seasonal water storage
- Desalination of seawater
- Treatment and reuse of wastewater
- Rainwater harvesting
- Atmospheric water harvesting

These options have to be evaluated for specific site locations in terms of parameters such as local climate, distance from the coastline and affordability.

1.1.2 Urban population growth

According to the UN projections, the world population will keep growing until the end of the 21st century, reaching a peak value of around 10.88 billions by 2100 (Roser, 2019)⁵. However, the distribution of this growth will be uneven and the African population is expected to more than triple by 2100. According to the projections, by that time eight out of ten people will be living either in Asia or Africa.

This trend will go in parallel with the constant growth of cities. According to UN predictions, urban population is expected to be 60% of the total by 2030 (UN, 2019)⁶. Such a fast expansion, especially in developing countries, results in an increasing amount of slum dwellers. In 2018, over 1 billion people around the world lived in slums, accounting for the 23.5% of the urban population. People living in these areas often lack access to basic infrastructures such as freshwater supply and waste management. This share of the population was in 2018 concentrated mainly in Sub-Saharan Africa and Southern Asia (UN, 2020)⁷.

1.1.3 Mismanaged plastic waste

Pollution from plastic waste has become one of the most relevant environmental challenges. Plastic production has increased almost two hundred times from 1950 (2 million tonnes) to 2015 (381 million tonnes). 40% of this amount is estimated to be single-use plastic (Parker, 2019)⁸. Within the total amount of plastic waste, it is important to identify the share that is inadequately disposed of, meaning that it is not sufficiently managed after collection and has a high risk of being lost to the surrounding (Fig.3). This value is significant especially for low-to-middle income countries, reaching peak values of 80-90% (Ritchie and Roser, 2018)¹⁰.

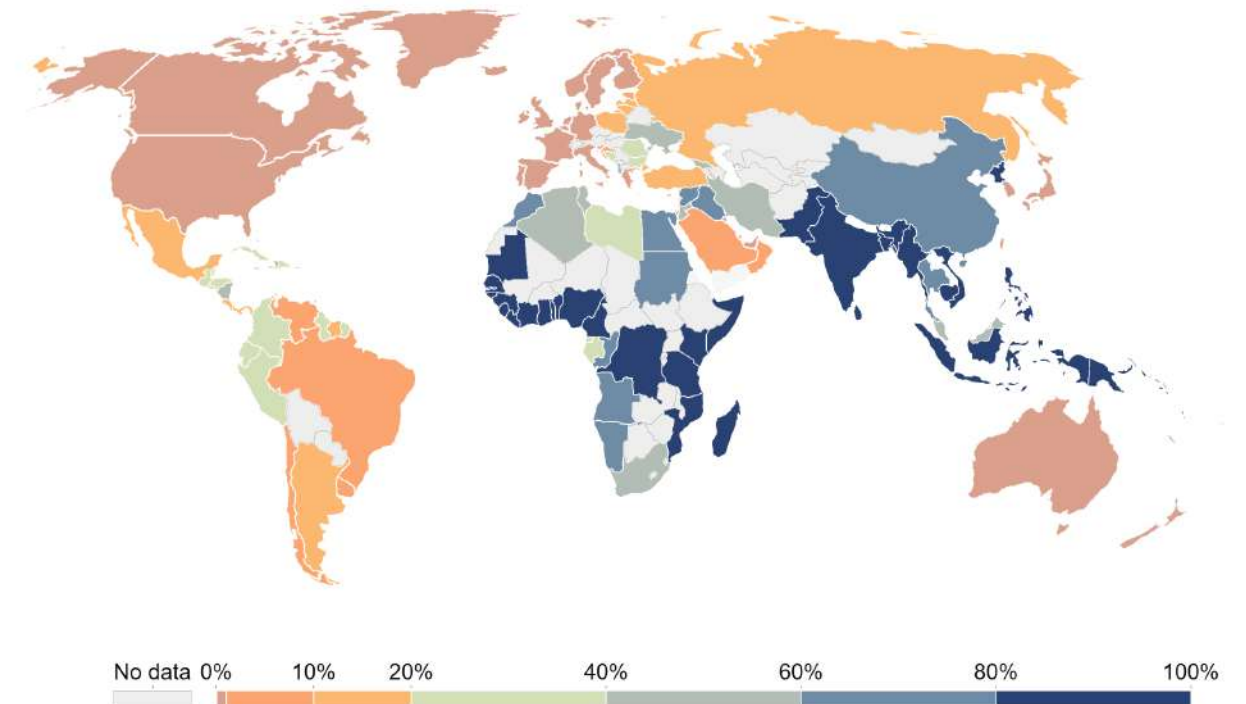


Fig.3: Mismanaged plastic waste share [Elaboration of image from Ritchie, 2018]

1.1.4 Additive manufacturing

Developments in additive manufacturing and printing filaments show a new alternative way to manage plastic waste. Filaments based on recycled PET plastic with different compositions are available on the market and could be evaluated according to specific design requirements. The use of waste materials is a growing trend in the 3d printing industry. One good example is BlueCycle¹¹, a company which is producing filament from marine waste, specifically from nylon fishing nets.

Beside this, AM offer multiple other advantages:

- Complex geometries can be achieved, as traditional manufacturing constraints and costs are not present.
- Volume optimization is necessary to minimize printing time. Minimum material consumption is a direct consequence of this requirement.
- The platform and community-based development and manufacturing system gives the possibility of developing knowledge and introducing new skills in developing countries

1.2 PROBLEM STATEMENT

As presented in the previous paragraphs, cities are expected to grow in the future. According to the projections (Roser, 2019)¹², the highest growth rate will be recorded in Africa. Current trends show the risk that the expansion of cities in these areas could lead to the growth of slums. In fact, especially in northern african countries informal settlements have been growing steadily over the last few years (UN, 2020).

Moreover, if the problem is not properly addressed, in the near future Northern Africa will also probably have to face a severe water stress level that would translate into poor health and living conditions. Being already semi-arid regions, precipitations are limited and alternative solutions to increase water availability need to be developed. Due to this reason and to the cost/complexity of desalination processes, atmospheric water harvesting represents an interesting option.

Lastly, when looking at the relatively high share of plastic waste that is mismanaged in developing countries such as those situated in Northern Africa (Ritchie and Roser, 2018), AM with recycled plastic represents an alternative point of view to transform the issue into a potential source for low cost building materials.

As it can be seen in Fig.4 the three main environmental and societal problems analyzed can be translated into design problems and tools:

- potential urban population growth leads to the need to develop adequate and affordable housing solutions or to upgrade the existing ones
- water scarcity leads to the necessity of developing alternative strategies to increase water availability (e.g. atmospheric harvesting systems)
- mismanaged plastic waste can be seen as an alternative source of construction material

AM represents an interesting approach to explore innovative solutions and address these issues. How can this technology provide a solution to address both the demands for better living conditions and freshwater supply, needs to be investigated.

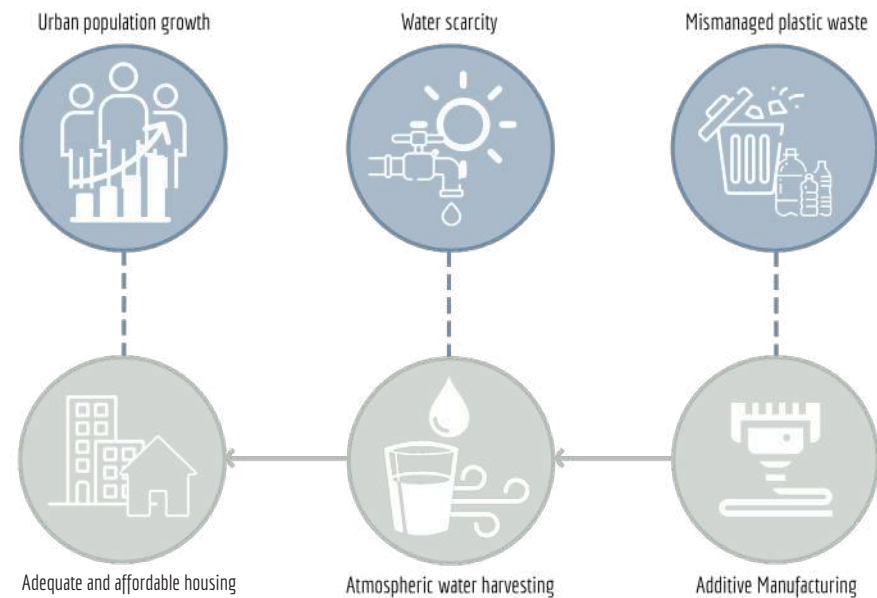
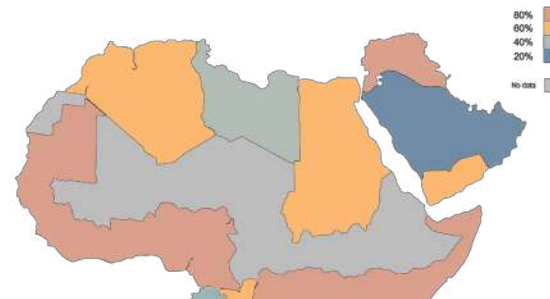


Fig.4: Research problems and potentials

Fig.5: Water scarcity in Northern African region



Fig.6: Mismanaged plastic waste in Northern African region



1.3 RESEARCH QUESTIONS

Based on the context analysis and the problem statement formulated above, the main research question for the research will be:

“How can AM (Additive Manufacturing) with rPET be used to design a building envelope component optimized for maximum passive atmospheric water harvesting and therefore mitigate water stress in semi-arid regions?”

Following the main research question, different sub-questions are formulated:

- What is the current state of the art in passive atmospheric water harvesting?
- Which physical parameters are involved in passive atmospheric water harvesting and how do they affect the collection yield?
- What are the material properties of rPET and how could they be translated into design constraints?
- What are the main fabrication constraints involved in the 3d printing process and how would they influence the design of a building component?
- Are there any previous examples of building envelope components produced through 3d printing?
- What is most efficient building envelope component type to be designed as an atmospheric water harvester?
- How can the performance of atmospheric water harvester be assessed and evaluated?

1.4 RESEARCH OBJECTIVE

This thesis does not have the presumption of trying to provide a final solution for complex problems such as those previously briefly presented. It rather recognizes some of the needs generated by these issues and explores the potentials that technologies like Additive Manufacturing could have in addressing them. Based on the research question and sub-questions, the main objective (Fig.7) of the research can be formulated as:

“The design of a mono-material modular building envelope component, optimized for atmospheric water harvesting and for Additive Manufacturing with recycled PET plastic. The design has to be easily manufacturable locally and on demand. The process of design through prototyping will be used to produce different design iterations and develop a final design, whose performances will be experimentally assessed, so that the potentials and limitations of such an application can be evaluated.”

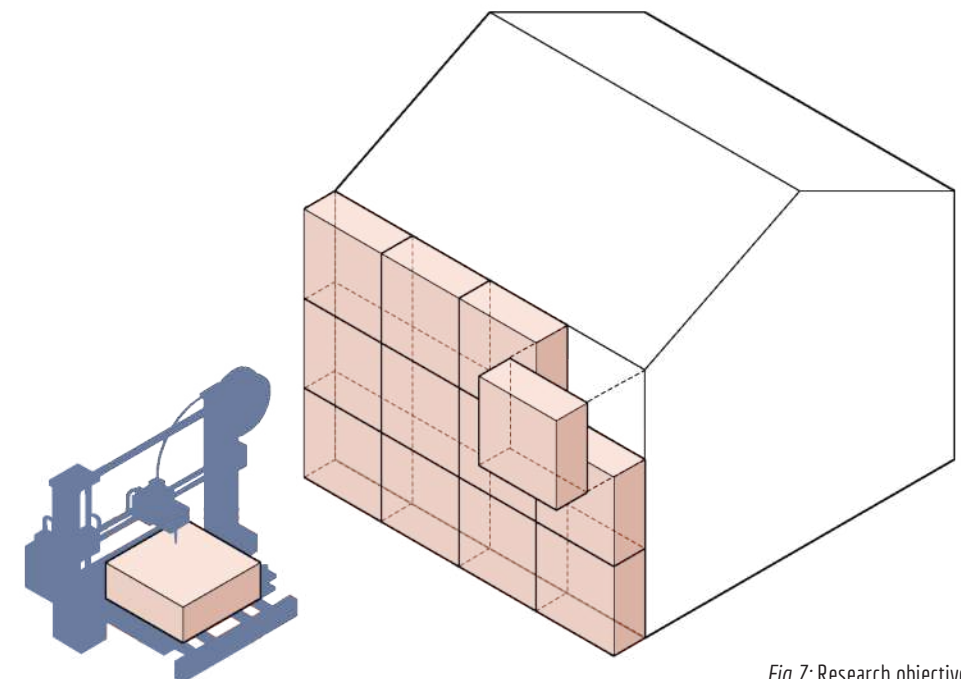


Fig.7: Research objective

1.5 RESEARCH METHODOLOGY

The research will be mainly based on research through design and design by prototyping methodologies. Five phases are identified and used to organize the work and its development over time (Fig.8). The main steps for each phase and their main products are identified and used to develop a first scheme of the research workflow.

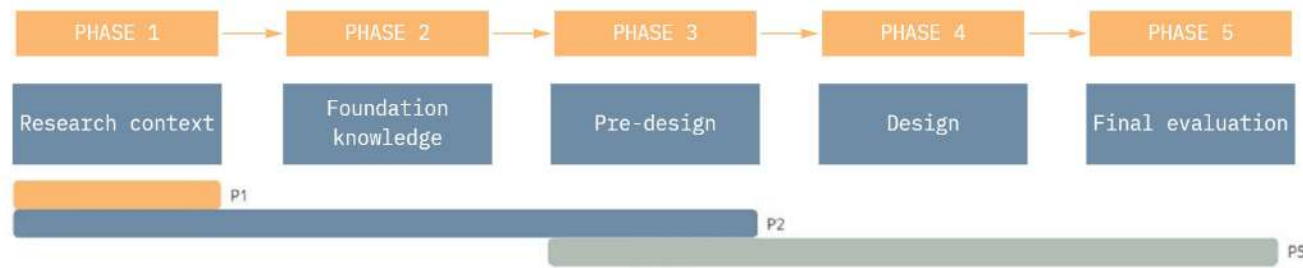


Fig.8: Research phases

The main phases are:

1) Research context. In this stage, whose results are already been presented, first literature research is performed to define the scope and relevance of the research. Societal problems that represent the framework of the thesis are studied more in depth, while the technological aspects are still vaguely researched. The main outcomes from this phase are the research question and a general case study location.

2) Foundation knowledge. After the definition of the main research question, literature review is performed on the main topics that will concur into answering it. The main research fields are:

- Atmospheric water harvesting (Biomimetic examples and state of the art).
- Architectural aerodynamics.
- Additive Manufacturing (techniques, materials and state of the art).

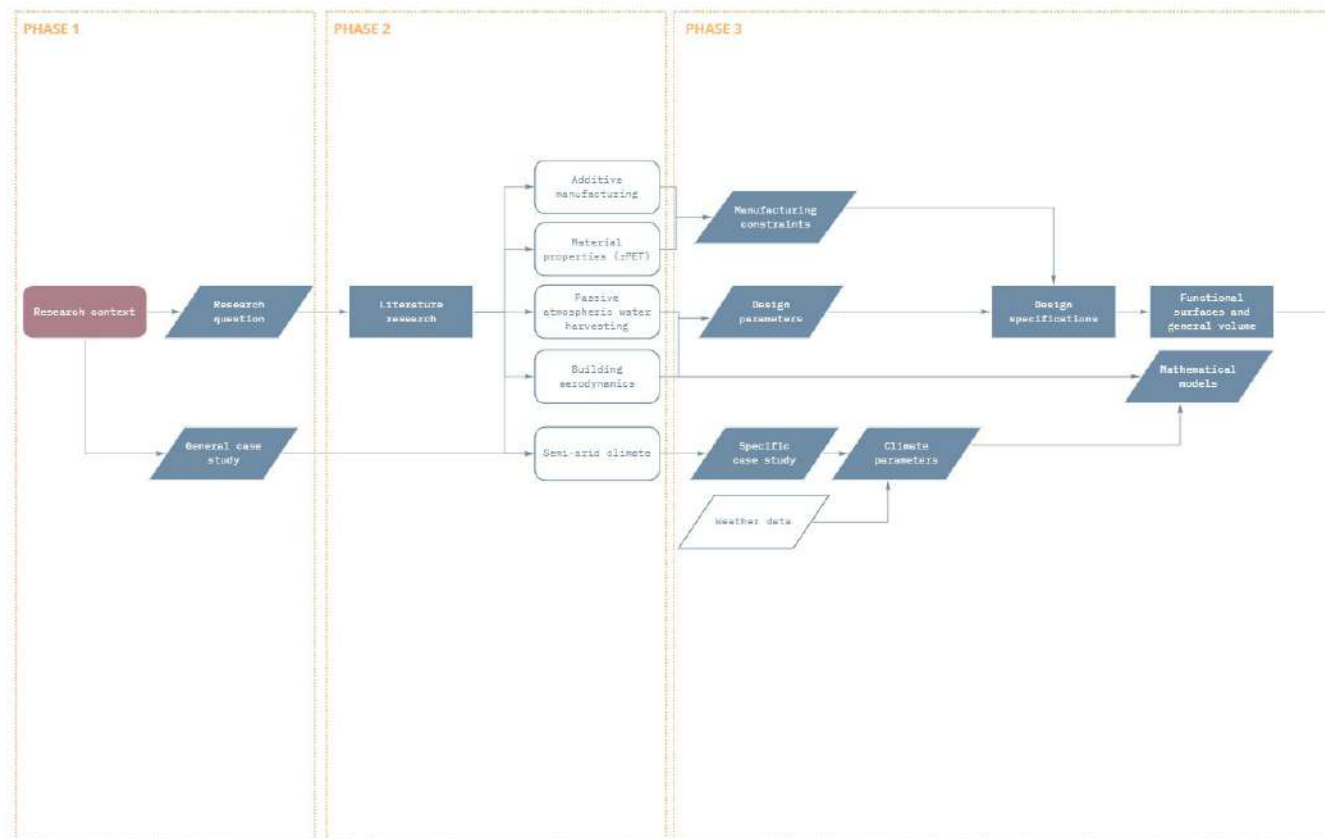


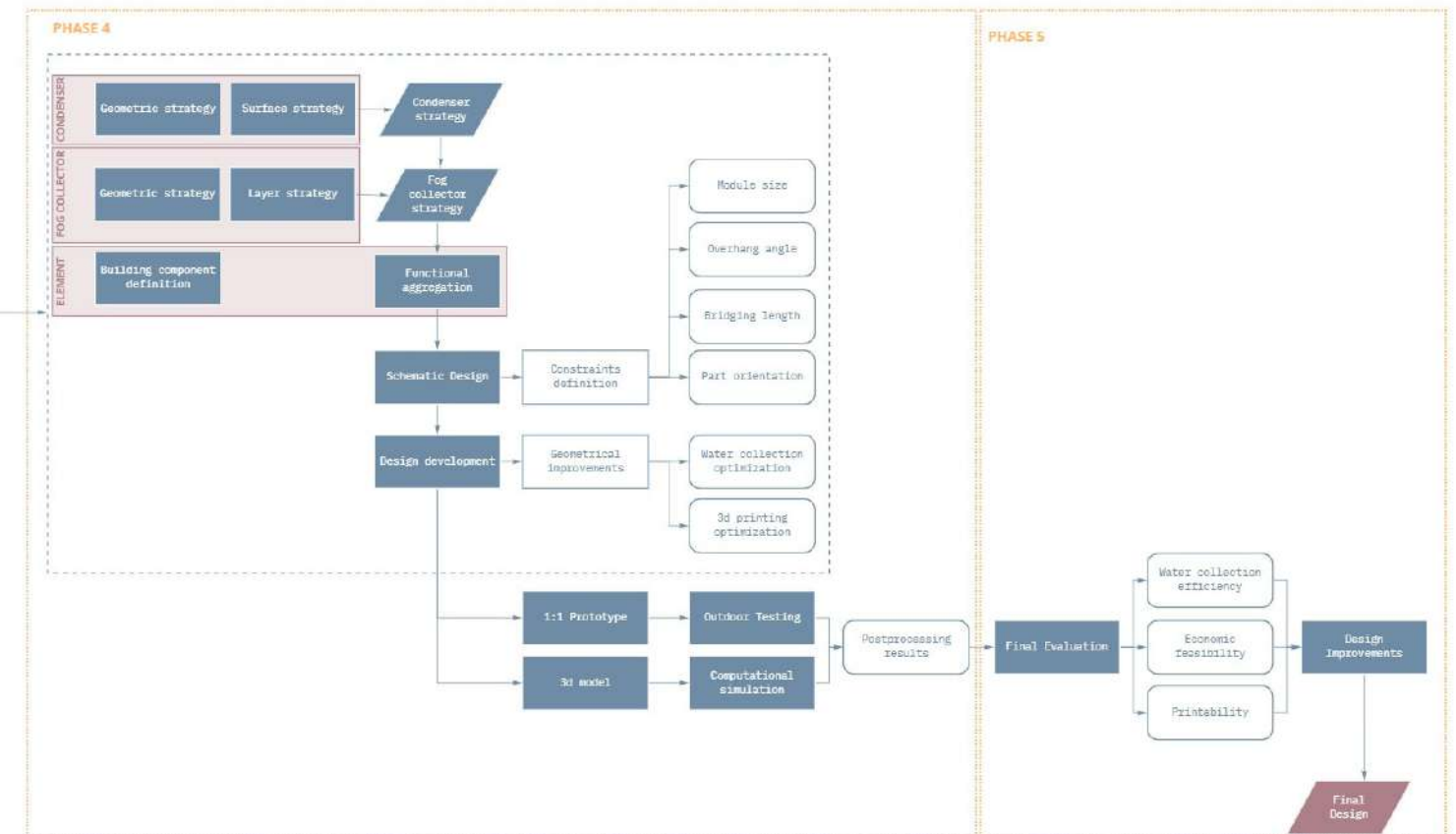
Fig.9: Research methodology

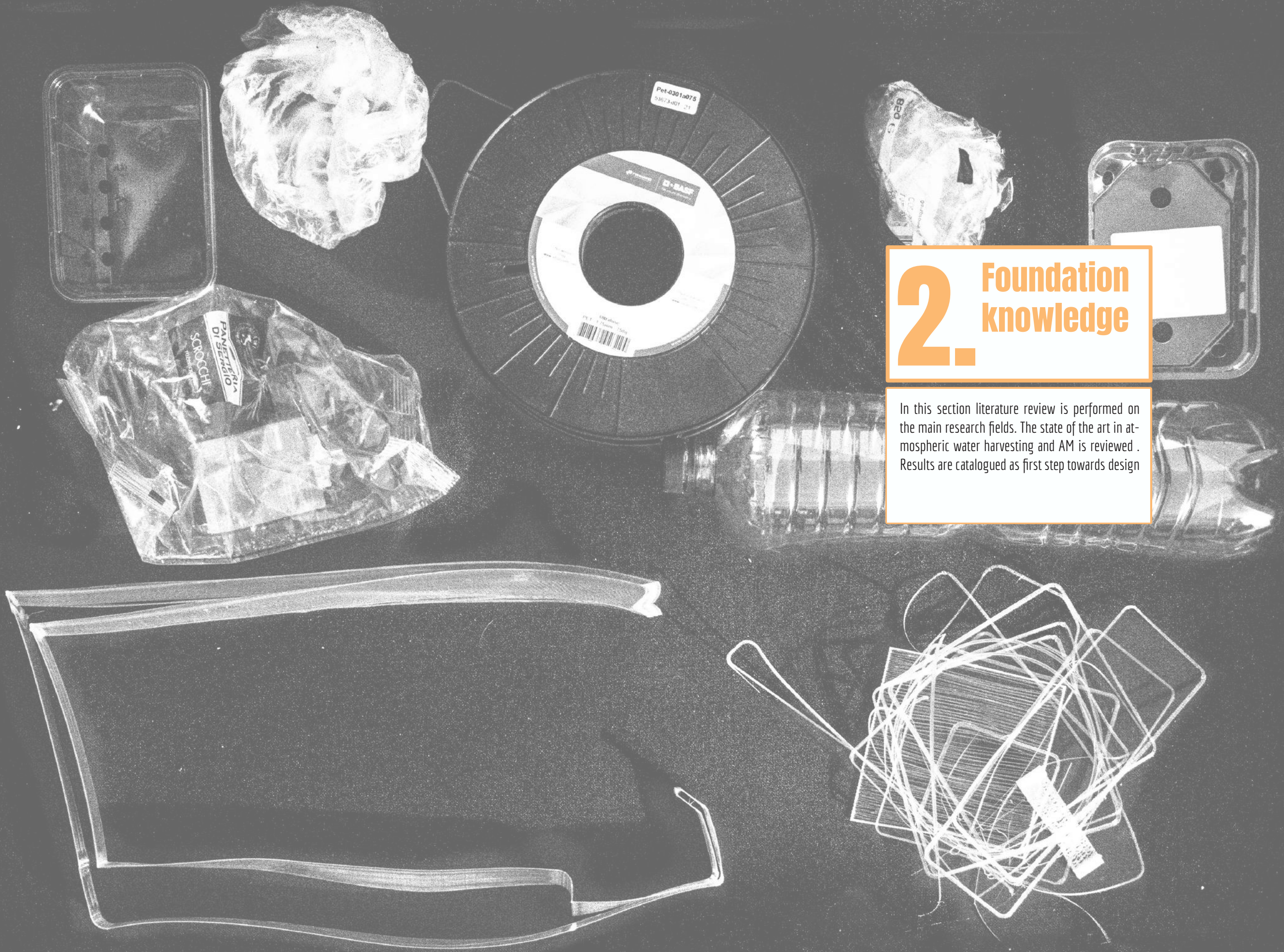
3) Pre-Design. This phase is still mainly related to literature review but in a more design-oriented way. The findings of the initial review are translated into manufacturing constraints and design parameters. The definition of a case study location leads to specific climate parameters that will be eventually used to evaluate the proposed design. The processes of dew and fog collection are analyzed in detail and simulative models are built and validated. Such models are used to analyze the impact of single parameters on the total performance. In this way it is possible to define a list of specifications and constraints that can be translated into design. Similar considerations are done regarding the process of 3d-printing. The main functions are identified and organized spatially through the use of graphs that highlight relations between different functions.

4) Design. In this phase, the design and prototyping of the part starts. The process is divided into three sub-design tasks: the condensing surface, the fog-catching surface and the overall building component. Different experiments and simulations are set up to evaluate the parameters involved in the water harvesting processes and how design through AM can influence them. The results of this research are integrated into the design of one component, that takes into account the combination of the different functions and their optimal design for 3d-printing. The method of research by design and design by prototyping are adopted. In this way the research progresses through a series of iterative loops that start from a performance target and goes through the evaluation of different options according to it.

5) Final evaluation. After the design phase, the design component is prototyped in 1:2 scale. Outdoor testing is performed on it and the results are analyzed. Its performance is simulated and analyzed also for the chosen case study location through the simulative models realized in the pre-design phase. The total amount of surface required to fulfill the water demand of one person is estimated and compared to existing solutions. The evaluation is performed also on the printability of the component and the economic feasibility of the overall design. The success of the research is measured both in its competitiveness in terms of water collection and cost.

An illustration of the main research inputs and outputs expected for each phase can be seen in Fig.9.





2. Foundation knowledge

In this section literature review is performed on the main research fields. The state of the art in atmospheric water harvesting and AM is reviewed. Results are catalogued as first step towards design

2.1 BIOMIMETIC INSPIRATIONS

Many examples of adaptations aimed to overcome shortages in the water supply can be found in both animals and plants populating extremely arid environments. To cope with the lack of precipitations, these living beings have developed systems to get water in alternative ways such as intercepting dew and fog, facilitating water condensation on their skin, or absorbing moisture from damp surfaces (Comanns, 2018)¹³. The collection process depends on different parameters, mainly related to the geometric and chemical properties of the exposed layer of the animal or plant. Different examples are catalogued in Fig.10.

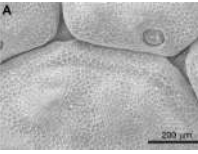
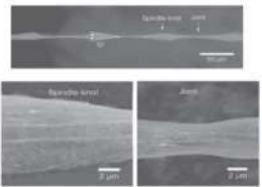
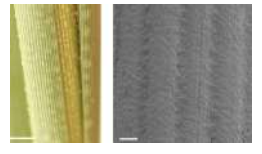
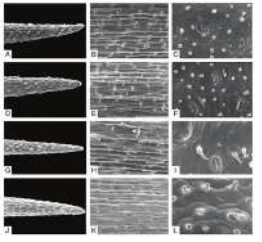
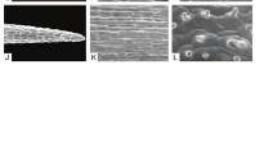
Name	Picture	Water source	Collection mechanism	Mechanism picture
Namid Desert Darking Beetle				
<i>Onymacris unguicularis</i>		Fog / Dew	Fog basking behavior. Insect elytra has grooves in the bottom part. All Hydrophobic. High emissivity, close to a black body.	
<i>Stenocara gracilipes</i>			Fog basking behavior. Insect elytra has irregular bumps. All Hydrophobic. For some literature, bumps are hydrophilic and valleys are hydrophobic. Different textures on peaks and valleys. High emissivity, close to black body.	
Thorny devil				
<i>Moloch horridus</i> ¹⁷		Moist substrate	Hydrophilic skin with hexagonal microstructures that when in contact get filled with water. Channels in between the scales transport the liquid.	
Spider web				
<i>Uloborus walckenaerius</i>		Fog	Combination of spindle knots and web joints. Joints are less rough than knots, so water moves towards the knots where it accumulates (for Laplace pressure gradient and structural anisotropy).	
Namib desert grass				
<i>Stipagrostis sabulicola</i> ¹⁸		Fog / Dew	Hydrophilic surface of leaves with irregular construction. Water is transported through grooves along the cone-shaped leaves.	
Cactus				
<i>Opuntia microdasys</i>		Fog / Dew	Hair-like needles instead of spines. Drops collect on tips of small barbs and then travel onto the needles towards the plant. (Laplace pressure gradient)	
Desert moss				
<i>Syntrichia caninervis</i> ¹⁹		Dew	Drops collect on tips of small barbs and then travel onto the needles towards the plant.	

Fig.10: Biomimetic inspirations table

The first and most famous example of atmospheric water harvesting is the Darkling Beetle from the Namib Desert. This insect is known to collect water on its skin through the so-called fog basking process. In fact, when exposed to humid winds, the beetle turns perpendicularly to the flow and then rotates its body at approximately 20 degrees (Nørgaard and Dacke, 2010)¹⁴. Fog drops stick to its shell and water starts to accumulate on it until the droplet becomes big enough to roll towards its head. According to literature, different types of desert beetles exist (Nørgaard and Dacke, 2010) and not all them show optimized features for fog-basking. The different species vary mainly in terms of size and integument structures. In some cases, a smooth surface with large grooves separated by small ridges is observed. The grooves appear to be more narrow close to the back of the insect and gradually wider towards its head. Other species are instead covered by irregular bumps alternated to valleys (Fig.11). Surface free energy gradients facilitate water flow from the bumps to the valleys. Even if the surface is covered in wax, such a difference in wettability results to be not due to chemical differences but rather to different degrees of surface roughness (Guadarrama-Cetina and others, 2014)¹⁵. The top of the bumps is in fact smooth, while the surface of the valleys presents a hexagonal microstructure that increases its roughness and therefore its hydrophobicity.

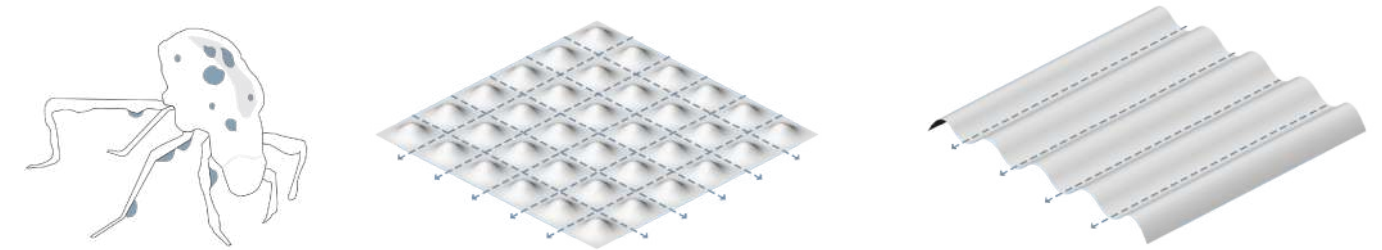


Fig.11: Namib beetle water harvesting principles

The geometric properties that facilitate water drop movements in spider webs or cactus spines are particularly interesting as well. In this case, the movement of the water drops is helped by the gradient of Laplace pressure, generated by different curvatures in various parts of the spine or of the web and gradients in surface free energy mostly due to variations in surface roughness. In both cases fibres are oriented in such a way that they facilitate the movement of water drops in a specific direction. In the particular case of the cactus, for example, the gradient pushes the drop to move towards the base of the conical spine (Jie, Hao and others, 2012)¹⁶. Different degrees of roughness and progressively wider grooves create also in this case a difference in surface free energy and make it more hydrophobic. With all these small adaptations and thanks to the hierarchical organization of the spines, the fog drops deposit on the smallest ones and then slowly coalesce and move towards its base (Fig.12). This has been proved experimentally by Jie (2012) as well and it has been observed that droplets would move in that direction independently of the orientation of the spine in space, showing how little is the influence of gravity and droplet selfweight in this specific process.



Fig.12: Cactus spine water harvesting principles

Biomimetic examples such as those presented above more in detail can give inspiration for the development of innovative solutions and their abstraction can lead to a better understanding of physical phenomena and of the parameters involved. The geometric considerations derived from the study of the adaptations of these living organisms will be later integrated into the design process.

2.2 RADIATIVE CONDENSERS

The amount of water in the air is estimated to be 14'000 km³, while freshwater on earth accounts only for 1200 km³ (Hamed and others, 2010). Dew water can therefore represent an unconventional and largely untapped solution to increase water availability in regions where supply or quality of freshwater is inadequate (Khalil and others, 2015)²⁰.

Dew formation is due to the condensation of water vapor on a surface that is below its dew temperature. This process is used by both passive and active systems to harvest water. However, this research will focus only on the first type and namely on radiative condensers. These devices are extremely simple and make use of the principle of radiative cooling to condense water during the night. Exposed to the night sky, the surface of the condenser radiates heat towards it and therefore cools to a temperature lower than the environment one. If the surface cools down enough it reaches dew point temperature, which means that the air hits its saturated vapor pressure and water vapor starts condensing on the device (Jarimi, Powell and Siffat, 2020)²¹.

The whole process relies significantly on specific climate conditions. Parameters like relative humidity, wind speed and cloudiness of the sky are only some of the additional variables that play a role in the condensation process. These parameters will be analyzed more into depth in the next section of the report. However, Khalil (2015), provides a clear schematization of the main factors that need to be kept in mind when designing a radiative condenser (Fig.13).

Passive Dew Collection				
Weather Conditions	Position	Material	Shape	Size
Sky emissivity	Inclination	Wettability		
Relative Humidity	Shading	Mass		
Wind speed	Exposure	Emittance		

Fig.13: Radiative condenser design principles [Elaboration of image from Khalil, 2015]

Up to now, radiative condensers have been realized with a smooth polyethylene foil insulated on the back (Fig.14). Different shapes such as funnels have been tested (Jacobs, 2008)²², but usually rectangular or square flat surfaces are preferred because easier and cheaper to realize. An inclination of around 30 degrees has been found to be a good compromise between sky exposure and water collection.

Depending on so many parameters, yields of radiative condensers are affected by a high degree of variability. Yields between 0.3 and 0.6 L/m²day have been indicated by previous studies and 0.8 L/m²day has been considered as upper dew yield limit (Khalil, 2015).



Fig.14 State of the art in radiative condensers

2.3 FOG COLLECTORS

If dew collection involves a thermodynamic process, fog collection is instead simply based on intercepting a flow of fog, which consists already of a mixture of microsize droplets (d=5-50micrometers), larger drops resulting from wind-driven rainfall and drizzle (Regalado, Ritter, 2016)²³. These collectors represent a viable solution for mountainous or coastal areas, where fog events are frequent.

A standard fog collector is composed of a mesh exposed to the fog flow and a collecting system at its base. Raschel polyethylene meshes usually produced to protect and shade crops, are often used, as their weave resolution ensure high collection rate and its triangular pattern facilitates water drainage (Rajaram, Heng and others, 2016)²⁴. These setups have proved in many scenarios their efficiency and their economic feasibility (Jarimi, Powell, Riffat, 2020) and many fog collection projects have been realized worldwide in the last 50 years (Klemm and others, 2012)²⁵ (Fig.14).



Fig.14: Previous fog collection experiences [Klemm, 2012]

Different configurations have been tested as well. Harp and Diagonal Harp collectors, made by parallel threads in various inclinations, and "Eiffel" tridimensional conical collectors for locations with no predominant wind direction have been tried out in Lima (Perù) by Lummerich and Tiedemann²⁶ (2010) (Fig.15). Multi-layered setups have also shown their potential in maximizing the water yield (Azeem and others, 2020)²⁷.

The parameters involved in the efficiency of a fog collector will be discussed in depth in the next section of the report. From a qualitative point of view, the liquid water content and the wind speed influence the total amount rate of water collection together with the collector's total efficiency. This value is the product between three different parameters:

- Drainage efficiency, meaning the amount of captured water that can efficiently be drained and stored.
- Capturing efficiency, which is the number of fog droplets that are trapped by the mesh.
- Aerodynamic efficiency, that quantifies the share of fog that flows through the collector.

If maximizing aerodynamic efficiency means increasing the overall water collection, basic aerodynamic principles need to be researched. In particular, the interaction of air flows with buildings could be relevant to design an efficient system.



Fig.15: State of the art in fog collection

2.4 ARCHITECTURAL AERODYNAMICS

Both the systems of atmospheric water harvesting described in the previous paragraphs interact with airflows. Radiative condensers face a decrease in efficiency when the wind speed close to the surface increases, while the water yield of fog collectors linearly depends on their aerodynamic efficiency and wind speed. The potential application of these technologies to a building component makes it therefore necessary to investigate the basic principles of aerodynamics and how air flows behave around built elements. In this research, wind is not analyzed in terms of horizontal load on a building, but more interest is given to the distribution and behavior of the streamlines around different volumes. Bluff bodies (bodies with flat surfaces and sharp edges) are considered, as supposed to be more similar to the final object of the research.

2.4.1 Reynolds number

The flow of a fluid depends on the intensity of the inertia forces and the cohesive forces due to the fluid viscosity. The ratio between these two values gives the Reynolds number. A Reynolds number below 2000 means that the viscous forces are dominant, the flow is laminar and the streamlines move parallel one to each other. A Reynolds number above 3000 means that the inertia forces are prevailing, generating wakes and a turbulent flow. Around a building and large objects in general, Reynolds numbers are usually on the turbulent side (Aynsley, 2011)²⁸.

$$Re = \frac{\rho V L}{\mu}$$

ρ : Fluid mass density
 V : Freestream fluid velocity
 L : Streamwise chord length
 μ : Fluid dynamic viscosity

Fluid inertia force: $\rho V L$
 Fluid viscous force: μ

2.4.2 Boundary layer

When the airflow moves past a solid surface, shear forces are generated between the fluid and the surface, slowing the flow down. The layer between the solid surface and the height where the particles reach 99% of the freestream velocity is known as boundary layer. The height of such a layer ultimately depends on the roughness coefficient of the ground (Aynsley, 2011) (Fig.16).

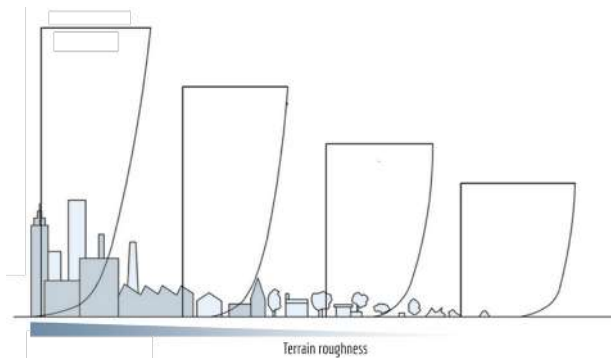


Fig.16: Boundary layer [Elaboration of image from Chochran, 2005]²⁹

2.4.3 Flow characteristics

Streamlines do not follow the surface of bluff bodies, but rather separate at their sharp corners when the momentum becomes higher than the fluid viscous forces. This separation creates turbulent wakes on the sides and on the leeward side of the body. On one point of the windward side, the dynamic pressure of the flow is completely converted into static pressure, meaning that the velocity of the flow there goes to zero. This is known as stagnation point (Simiu, 2019)³⁰.

When considering the wind around a building, two more flow behaviors are worth mentioning. The first is the lift force generated by sharp horizontal edges of the body, which cause separation of the fluid flow on the top face of the volume. This leads to the formation of a turbulent area and uplift forces above the roof. The last behavior is known as downwash, and it consists of descending flows with high velocity toward the base of the building. This is due to the pressure differences that the velocity gradient in the boundary layer creates (Stathopoulos, 2011)³¹ (Fig.17).

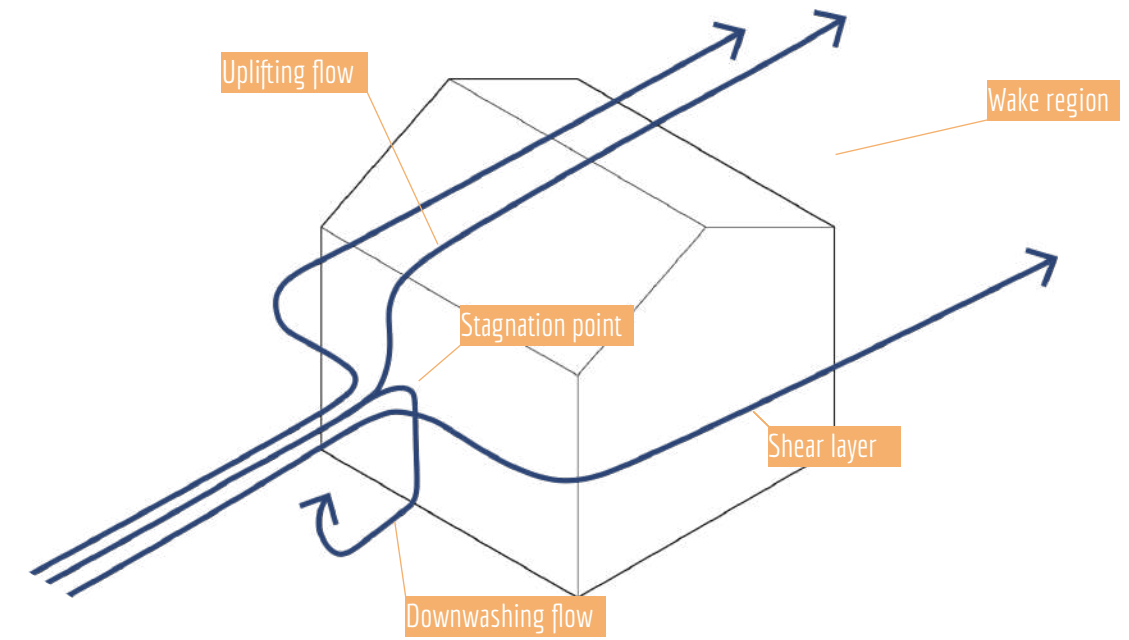


Fig.17: Flow characteristics

2.4.4 Fog collector aerodynamics

Despite the fact that the theory behind the performance and efficiency of fog collectors has not yet been discussed, it makes sense to anticipate in this section the correlation between these values and the aerodynamic behavior of the collector, that influences its wind catching capacity. Rivera³² (2011), provides an accurate analysis on this topic (Fig.18), that will later be used for detailed calculations. In this phase, it is important to mention that from his research the efficiency of the collector results to be inversely proportional to its drag coefficient. This coefficient measures the resistance of an object in a fluid.

This means that less aerodynamically efficient geometries are preferred when designing a fog collector, as they would catch more wind. Drag coefficients for standards shapes can be found in literature (Fig.19). Such an analysis is at this stage purely qualitative and useful to visualize how geometries could influence the efficiency of a collector.

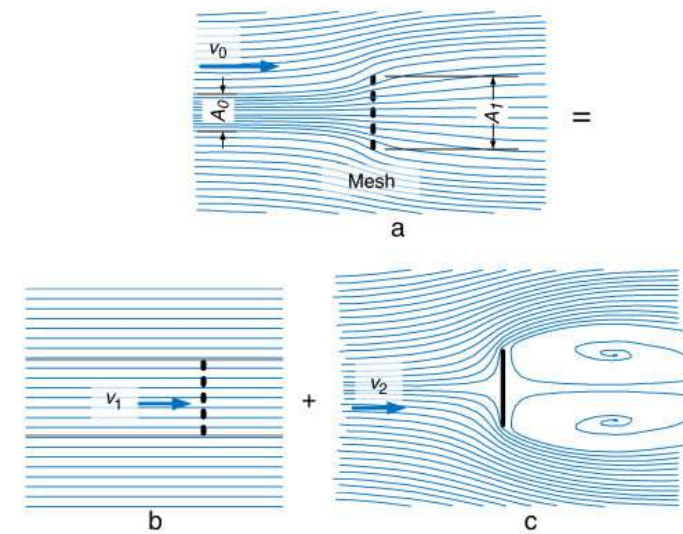


Fig.18: Fog collector's aerodynamics (Rivera, 2011)

SHAPE	REF.	C_D	SHAPE	REF.	C_D
	(a)	0.47 _g		—	1.17 _g
	(c)	0.38		(a)	1.20
	(c)	0.42		(g)	1.16
	(e)	0.59 _g		(d)	1.60 _g
	(f)	0.80 _g		(e)	1.55
	(d)	0.50		(a)	1.55
	(d)	1.17		VORTEX STREET	1.98
	(c)	1.17		(a)	2.00
	(b)	1.42		(a)	2.30
	(a)	1.38		(b)	2.20
	(f)	1.05 _g		(a)	2.05 _g

Fig.19: Basic shapes drag coefficient (Hoerner, 1906)³³

2.5 ADDITIVE MANUFACTURING

2.5.1 AM Techniques

Additive Manufacturing comprehends different techniques based on the layer-by-layer deposition of material in order to produce an object. This process is highly digitalized and considered to be usually convenient for the production of small size products, small batches, or particularly geometrically complicated or customized parts. Traditionally used for prototypes and parts that do not require a high level of performance, the unexplored opportunities that these techniques can give are gradually gaining the interest of the industry.

The International Standards Organization / American Society for Testing and Materials Standards (Daminabo and others, 2020)³⁴ classifies all the techniques into seven main categories of AM (Additive Manufacturing). These are:

- **Material extrusion (ME)**, consisting in the gradual deposition of layers of a fused material to form the object. Fused Deposition Modeling (FDM) is one of the best known examples of this technique.
- **Material Jetting (MJ)**, using an inkjet head to deposit droplet of a photopolymer to form layers that are let cure afterwards.
- **Binder Jetting (BJ)**, where a liquid is used to selectively bond material of a powder bed and produce the part.
- **Sheet Lamination (SL)**, consisting in producing the 3d part by bonding together different layers of material. Laminated Object Manufacturing (LOM) is one example of this technique.
- **Vat photo Polymerization (VP)** is a lithography-based approach that works by using uv-light to solidify and cure specific parts of a liquid photopolymer.
- **Powder Bed Fusion**, like selective laser sintering (SLS) and electron beam melting (EBM), in which heat is used to fuse and bond together different regions of a powder bed.
- **Directed Energy Deposition (DED)**, that uses a laser or plasma arc to melt metallic materials and depositing them layer by layer through a nozzle.

The processes included in these categories have different characteristics that need to be evaluated based on the specific element to be produced. The main variables from one technique to the other are the printing materials, the printing speed, the maximum printing resolution, the energy use and ultimately the affordability. However, the main common advantages of AM techniques are (Piccioni, 2019)³⁵:

- Possibility of having complex geometries and maximum design freedom, allowing for high degree of customization.
- Optimization of printing time and of volume and material consumption, therefore minimizing material waste.
- Reduction in material use resulting in overall cost reductions.
- Higher production efficiency.

The optimization processes involved in AM production methods can lead to a cost-effective production that at the same time addresses some of the main challenges related to sustainable development, reducing material and energy consumption (Daminabo, 2020).

On the other hand, some limitations still need to be overcome to enable AM processes to truly scale up. Especially with home-friendly techniques such as FDM, that find in their open source nature and in their easy replicability a great potential for innovation, the standardization of the process and its compliance to common mechanical and safety requirements is hard to achieve. The structural anisotropy of AM parts makes it even more challenging to ensure standard manufacturing standards (Daminabo, 2020).

2.5.2 Fused Deposition Modeling

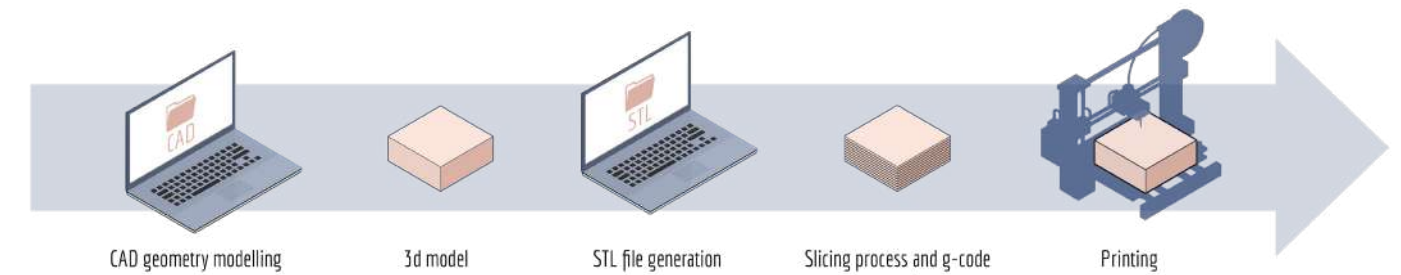


Fig.20: FDM workflow

Material Extrusion techniques can work with many different materials, including polymers and ceramics. Despite the fact that they are not the fastest procedures, the low energy consumption, the scalability of the process, and its limited cost make ME particularly appealing (Daminabo, 2020). Moreover, the availability on the market of affordable printers and printing filaments make FDM (Fused Deposition Modeling) an extrusion technique extremely home friendly and accessible. Mainly because of such open source, (such as the RepRap community) and democratic nature of the manufacturing process that can be easily replicated worldwide, FDM is chosen as main AM technique for this research.

Fused Deposition Modelling works by melting a filament of printing material and then slowly depositing it through a nozzle onto a platform. Layer by layer, the tridimensional object is produced. As in the other AM techniques, a specific workflow is required to obtain a 3d printed part (Daminabo, 2020) (Fig.20):

- Modelling of the 3d object into a CAD software.
- Translating the model into a STL file for production.
- Slicing process and g-code generation by CAM software.
- G-code is communicated to the machine, that can start production.

The final product is affected by different aspects related to the design and manufacturing process (Fig.21). Underestimating them could lead to different kinds of defects of the printed part.

Factors	Aspects	Affecting	Defects
CAM			
	Path planning	- Surface finish - Mechanical properties - Dimensional accuracy	- Overhang and bridging: absence of support may lead to structural instabilities - Stringing: leak of some plasticized filament when nozzle moves from one point to the other
	Part orientation	- Process efficiency and effectiveness	- Overhang and bridging: absence of support may lead to structural instabilities - Stringing: leak of some plasticized filament when nozzle moves from one point to the other
FDM Machine			
	Speed of 3D dispensing or filament feed	- Surface finish - Mechanical properties	- Stepped layers: visible trails of the deposited material - Warping: deflections due to uneven shrinkage of material - Structural inhomogeneity
	Pressure and temperature gradient	- Dimensional accuracy - Process efficiency and effectiveness	- Warping: deflections due to uneven shrinkage of material - Structural inhomogeneity
	Nozzle Design		- Stepped layers: visible trails of the deposited material - Stringing: leak of some plasticized filament when nozzle moves from one point to the other

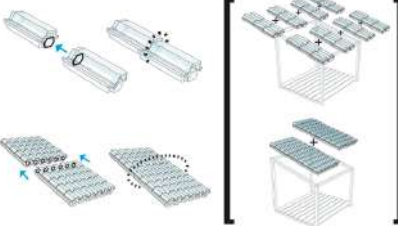
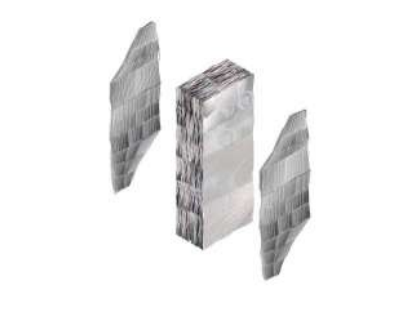
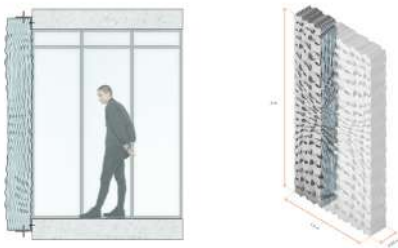
Fig.21: FDM design parameters and printing defect (Elaboration of image from [Daminabo, 2020])

2.5.3 rPET printing filament

When looking at polymers, different printing filaments for FDM are available on the market. Among them, PLA and ABS are the most common choices. More and more filaments produced with recycled polymers are becoming available. Recent studies (Little, Tanikella and others, 2020)³⁶ investigate an approach to circular economy and recycling called Distribute Recycling for Additive Manufacturing (DRAM), where users are pushed to recycle as they can use their plastic waste to 3d print different consumer products that they may need. In addition to the economic convenience, the use of recycled material would cut the embodied energy of 3d printing processes of around 90%. Despite the fact that PET, the polymer usually used for bottles and food packaging, is not the most produced plastic, it is highly recognizable for consumers and therefore more likely to be recycled. Moreover, its production is expected to keep a growth rate of 4.5% a year. Especially for these reasons, it is extremely interesting to explore the potentials of rPET filaments, as first examples of alternatives to simply downcycling plastic waste.

2.5.4 AM for building components

Many applications for AM into the built environment have been developed and tested. These examples show both the potentials and current limitations of the technology and could represent helpful inspirations for the development of new solutions. The most relevant precedents are catalogued in the following Fig.22.

Project	Authors	Function	Description	Picture
3d printed roofing ³⁷	RMS	Modular roof system for poorer regions of the world.	Inspired by roofing terracotta tiles, the modular elements are printed with recycled plastic and represent an inexpensive solution to replace the classic corrugated metal sheet roofing used in poor areas. The tiles are easy to produce locally and to replace, and represent an upgrade in the thermal and acoustic insulation of the dwellings.	
Fluid Morphology ³⁸	TU Munich	Building facades with tunable properties	Facade elements 60x100cm printed with plastic material, with high degree of customization depending on design requirements and climate conditions. Properties such as shading, thermal and acoustic insulation and ventilation can be tuned in the multifunctional integrated design procedure.	
Spong3D ³⁹	TU Delft	Adaptive 3d printed facade system	Realized with PETG, the technology consists in integrating in the 3d printed object two systems. Air pockets in the middle of the element ensure thermal insulation, while channels on the outer layers of it enable the flow of a liquid that works as thermal mass to guarantee indoor comfort.	
The AM Envelope	Piccioni, V. TU Delft MSc Thesis	Mono-material 3d printed facade	Design of a 3d printed facade system, optimized for thermal insulation and structural stiffness. Insights on the complete computational design and optimization workflow are given.	
Banyan EcoWall ⁴⁰	BigRep	Green wall	AM green wall designed to integrate in the printing process channels for the drainage and irrigation system of the plants.	
Cool Brick ⁴¹	Emerging Objects	Brick system for passive evaporative cooling	3d printed porous ceramic bricks designed to absorb water in its lattice structure, which is later used to cool down the air that passes through it. Bricks are interlocking but fixed with mortar.	

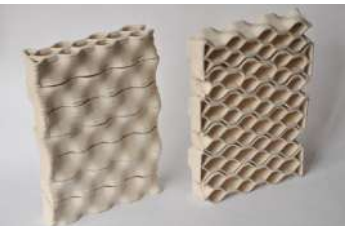
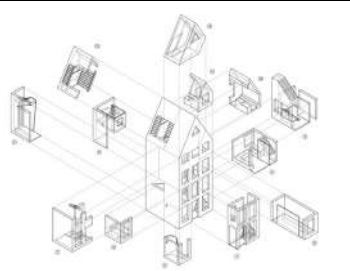
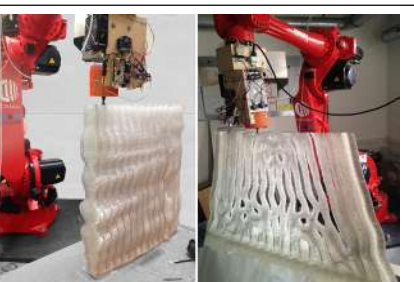
Building Bytes	Building Bytes	3d printed ceramic blocks	Ceramic modular elements printed individually. The technique allows for complex geometries and interlocking designs.	
3D printed canal house	DUS studio	3d printed components for a fully 3d printed house	The canal house is made of many printed elements and showcases the innovation related to 3d printing with polymers. The research focuses on the development of a global UI and of a smart parametric design tool.	
Double Face 2.0	TU Delft	3d printed solar wall	3d printed Trombre wall element, consisting of insulation material and PCM heat storage encapsulated in element, that can be optimized for different parameters such as shading	

Fig.22: AM for building components inspirations

All The projects presented share relevant features in terms of design approach to Additive Manufacturing and of its application to building components, such as roof or facade elements.

For example, the 3d printed roofing system designed by RMS (Resilient Modular System) shows many similarities with the objective of this research. The first one is the goal of the project, which is providing a solution to upgrade the living conditions in the poorest regions of the world. The roofing system aims to replace the corrugated metal roofing usually used in slums with a 3d printed tile. The product is therefore modular, easy and quick to interlock, and printable with a standard 3d printer. These principles are key for the design goal of this research as well and paramount to ensure the replicability of the process worldwide. Lastly, the modular system is produced through recycled plastic, making use of an important waste flow available worldwide.

The project Fluid Morphology developed at TU Munich represents another extremely relevant case study. This research looks at the possible applications of Additive Manufacturing in the building sector and push them beyond the design of structural elements. The focus is moved to facade components and to all the possible factors they could be optimized for. Shading, ventilation, thermal, and acoustic insulation are the main optimization parameters. This approach appears to be closer to the one adopted in this research, where the design of a structural element is moved a bit to the background, while the water collection potential becomes the decisive parameter in the design process. On the other hand, it is clear from the Fluid Morphology research as well how working with Additive Manufacturing necessarily implies designing multifunctional elements, so that the manufacturing freedom enabled by the process is used at its best.

3. PRE Design

The last step before moving to the actual design consists into quantitatively analyze the processes of atmospheric water harvesting that have been presented in the previous section. Design considerations for AM are presented, too.

3.1 PRE - DESIGN: RADIATIVE CONDENSER

After introducing the current technologies in the field of atmospheric water harvesting, the next step in order to design a new component is to understand the parameters that influence them and the laws that regulate the water collection process.

Looking at radiative condensers, two phenomena need to be investigated. The first one consists in the condensation and nucleation of water droplets on a surface, while the other refers to the collection of those droplets (Fig.23).

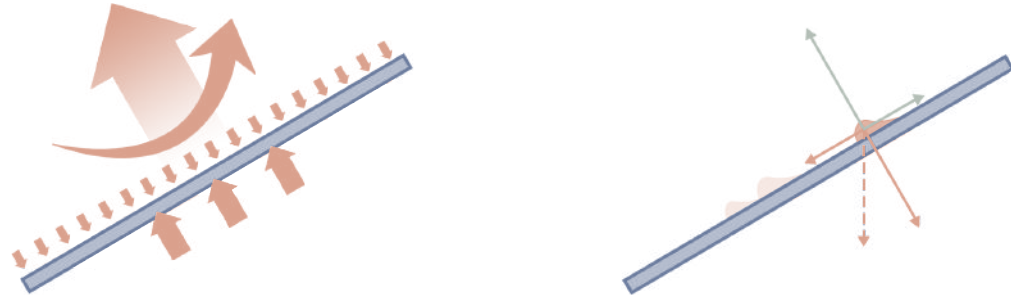


Fig.23: Water condensation and collection on a surface

3.1.1 Condensation

Condensation on a surface occurs when it cools below to the so-called dew point temperature, which is the required temperature to bring air with a certain relative humidity to its water saturation point. The air layer close to the surface therefore reaches its saturated vapor pressure and the excess condenses into water. In passive systems such as those considered in this research, the main way to cool down the condenser's surface is through radiative heat losses towards the night sky.

To model the process, the heat balance in the forms proposed by Nilsson⁴² (1996) and Gandhidasan⁴³ (2005), are considered and combined. The parameters involved in the process are listed in Fig.25. Considering a foil surface exposed to the night sky and insulated on the back, the total heat balance would be:

$$P = LE + Q_{cond} + Q_{conv}$$

P represents the thermal radiation towards the sky. In fact, due to their relatively low temperature and according to Wien's Law ($\lambda = \frac{b}{T}$), surfaces emit infra-red radiation towards the sky. The magnitude of this loss is equal to

$$P = \varepsilon_f \sigma (T_f^4 - T_{sky}^4)$$

It can be seen that this value depends on the infra-red emissivity of the foil and on the temperature of the sky. Its extensive calculations are provided in Appendix I, but it is relevant to mention that it increases with higher cloud coverage, as a bigger share of radiation is reflected towards the ground. Higher relative humidity reduces cooling potential as well, so dry clear nights theoretically maximize radiation losses.

The losses are balanced by different types of heat gains. The heat gain by convection with the surrounding air is given by the equation:

$$Q_{conv} = h_{conv} (T_e - T_f)$$

The convective heat transfer coefficient is evaluated depending on the type of flow but ultimately depends on the airflow velocity in the sense that higher values result in higher heat gains. Conduction heat gains occur through the backside of the plate. Their magnitude is calculated through:

$$Q_{cond} = \frac{k_f}{x_f} (T_e - T_f)$$

The last heat gain is the one involved in the condensation of vapor into water. This is defined as the product between the heat of vaporization of water and the mass rate of condensation. According to Nilsson (1996), this quantity is equal to:

$$LE = \frac{h_{conv} (e_{amb} - e_f)}{\xi}$$

These formulas are used to model the physical situation and understand the relation between the different parameters. Microsoft Excel is used to calculate the two main unknowns: the temperature of the surface and the mass rate of condensation. To solve this system of equations, iterative calculation is performed in Excel. In order to solve the equations, the heat transfer coefficient for radiation has to be calculated, too (Fig.24).

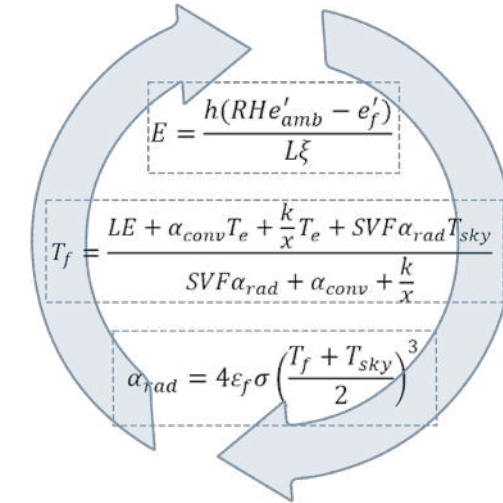


Fig.24: Condensation simulation iterative calculation

In the formulas above, the sky view factor (SVF) of the surface is introduced as a percentage reduction of the radiative cooling of the condenser. However, deeper research has to be done, in order to determine a more accurate relation between these parameters and other geometric variables of the surface such as inclination and curvature.

The Excel model shows that the gains for conduction are limited, while changes in the wind speed affect positively the mass rate condensation and at the same time produce relevant increases in conductive heat gains. As expected, higher cloud coverage reduces the radiative cooling. To better understand how each variable affects the process, a graph of the heat balance is built. Each variable is listed and their dependency is represented by a connection (Fig.26). Counting the number of connections would eventually give a better grasp of the most important parameters involved.

Symbol	Parameter	Unit
ε_f	Emissivity of the foil	
ε_0	Sky emissivity	
σ	Stefan-Boltzmann constant	$\frac{W}{m^2 K^4}$
T_e	Environment temperature	K
T_f	Foil temperature	K
T_{sky}	Sky temperature	K
T_{dew}	Dew point temperature	K
CC	Cloud coverage coefficient (0<<1)	
L	Latent heat of vaporization of water	$\frac{Wh}{kg}$
k_f	Thermal conductivity of the foil	$\frac{W}{mK}$
x_f	Thickness of the foil	m
h_{conv}	Convection heat transfer coefficient	$\frac{W}{m^2 K}$
ξ	Psychrometric constant	$\frac{Pa}{K}$
v_w	Wind velocity	$\frac{m}{s}$
e'_{amb}	Saturated vapor pressure (ambient temp.)	Pa
e'_f	Saturated vapor pressure (foil temp.)	Pa
SVF	Sky view Factor	
E	Mass condensation rate	$\frac{kg}{m^2 h}$
θ	Foil inclination	
κ	Foil curvature	

Fig.25: Condensation parameters

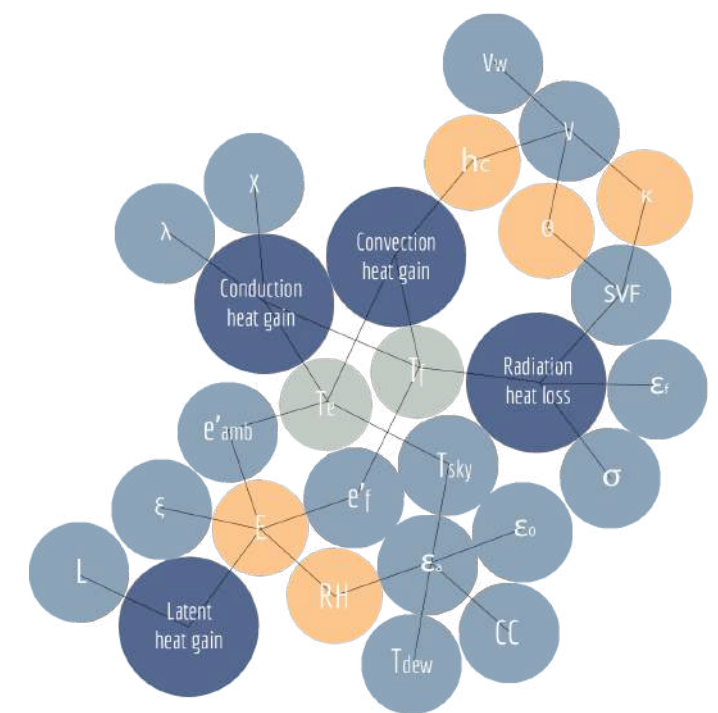


Fig.26: Condensation parameters graph

The graph presented above confirms how surface temperature and condensation mass rate represent the two main unknowns. Other variables appear to be significant for the process to work. These parameters are in particular the relative humidity, and the wind speed. However, to better understand their relevance, the Excel model is used to tweak all the variables and their different impact on the condensation mass rate is monitored. In order to do that, a standard situation is set as a starting point from which the different quantities are varied within an acceptable range. A case study presented from Nilsson (1996) has been considered for this. The initial values and results are listed in Fig.27-28.

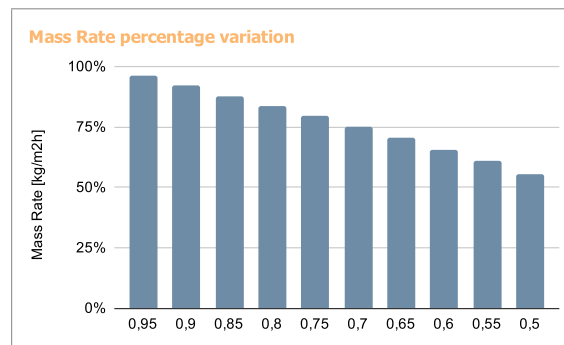
Symbol	Parameter	Value	Unit
ϵ_f	Emissivity of the foil	1	
T_e	Environment temperature	285	K
CC	Cloud coverage coefficient (0<cc<1)	0	
α_f	Conduction heat transfer coefficient	0,7	$\frac{W}{m^2K}$
v_w	Wind velocity	1	$\frac{m}{s}$
RH	Relative Humidity	100	%

Symbol	Parameter	Value	Unit
T_f	Foil temperature	283	K
E	Condensation mass rate	4,98E-02	$\frac{kg}{m^2h}$

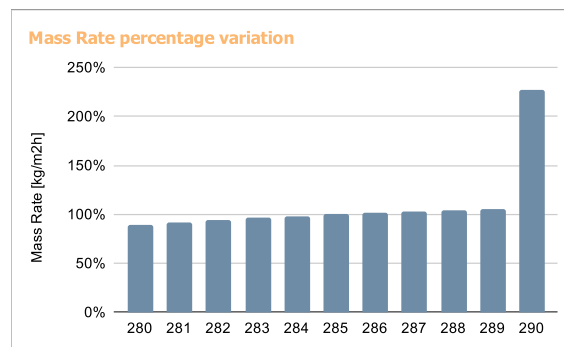
Fig.27-28: Condensation simulation input

Separately varying the value of the different variables, gives an idea of their impact on the final amount of collected condensed water. Fig.29-39 report the numerical data provided by the simulations and a graphical representation of the influence on the initial yield (considered in the graph to be 100% mass rate).

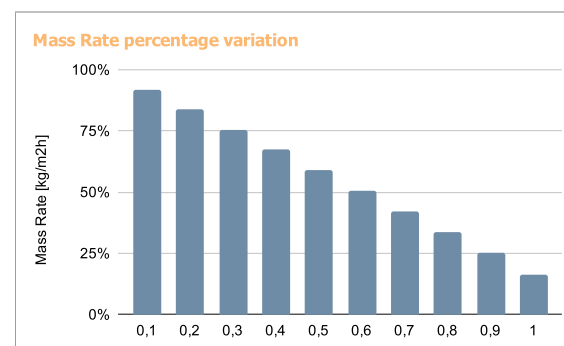
Foil Emissivity	Tf	Mass Rate	%
1	283	4,98E-02	100%
0,95	283	4,78E-02	96%
0,9	283	4,58E-02	92%
0,85	283	4,37E-02	88%
0,8	283	4,16E-02	84%
0,75	283	3,95E-02	79%
0,7	283	3,73E-02	75%
0,65	283	3,51E-02	70%
0,6	284	3,27E-02	66%
0,55	284	3,03E-02	61%
0,5	284	2,75E-02	55%



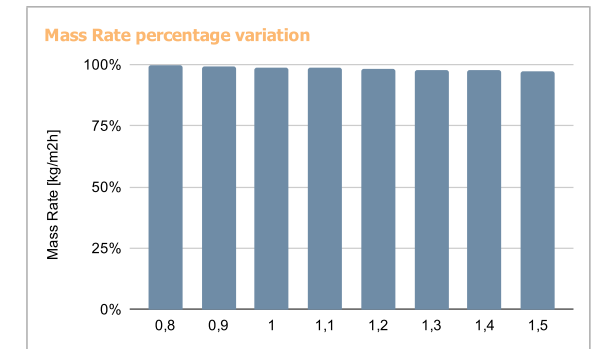
Te	Tf	Mass Rate	%
279	276	4,34E-02	87%
280	277	4,47E-02	90%
281	278	4,58E-02	92%
282	279	4,69E-02	94%
283	280	4,80E-02	96%
284	281	4,89E-02	98%
285	283	4,98E-02	100%
286	284	5,05E-02	101%
287	285	5,12E-02	103%
288	286	5,18E-02	104%
289	287	5,24E-02	105%
290	286	1,13E-01	227%



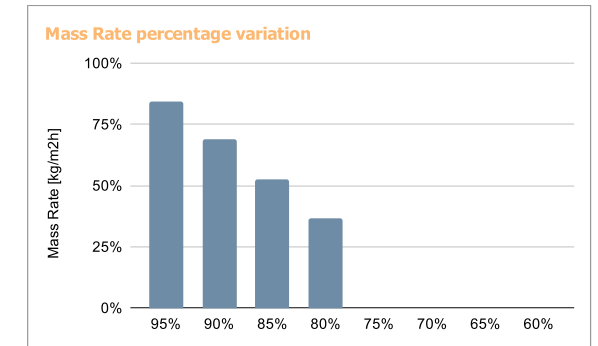
Cloud coverage	T surf	Mass Rate	%
0	283	4,98E-02	100%
0,1	283	4,57E-02	92%
0,2	283	4,17E-02	84%
0,3	283	3,76E-02	76%
0,4	283	3,35E-02	67%
0,5	284	2,93E-02	59%
0,6	284	2,52E-02	51%
0,7	284	2,10E-02	42%
0,8	284	1,68E-02	34%
0,9	285	1,25E-02	25%
1	285	8,22E-03	17%



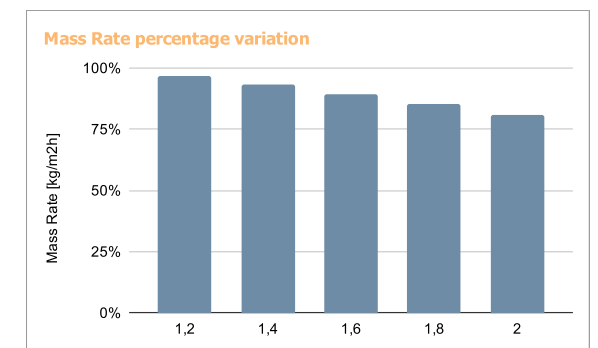
Conduction heat transfer coefficient	T surf	Mass Rate	%
0,7	283	4,98E-02	100%
0,8	283	4,96E-02	100%
0,9	283	4,94E-02	99%
1	283	4,93E-02	99%
1,1	283	4,91E-02	99%
1,2	283	4,89E-02	98%
1,3	283	4,87E-02	98%
1,4	283	4,86E-02	98%
1,5	283	4,84E-02	97%



Relative humidity	T surf	Mass Rate	%
100%	283	4,98E-02	100%
95%	282	4,21E-02	85%
90%	282	3,43E-02	69%
85%	281	2,63E-02	53%
80%	281	1,82E-02	37%
75%	280	0	0%
70%	280	0	0%
65%	279	0	0%
60%	279	0	0%



Wind velocity (RH100%)	T surf	Mass Rate	%
1	283	4,98E-02	100%
1,2	283	5,08E-02	102%
1,4	283	5,17E-02	104%
1,6	283	5,25E-02	105%
1,8	283	5,32E-02	107%
2	283	5,38E-02	108%



Wind velocity (RH85%)	T surf	Mass Rate	%
1	281	2,63E-02	100%
1,2	282	2,55E-02	97%
1,4	282	2,45E-02	93%
1,6	282	2,35E-02	89%
1,8	282	2,25E-02	86%
2	282	2,13E-02	81%

Fig.29- 39: Condensation simulation results and graphical representations

Two simulations have been performed for the wind velocity, with different levels of relative humidity. While with RH of 100%, faster winds bring more water vapour and are therefore beneficial, wind speed becomes detrimental with lower humidity levels. In this case, in fact, the airflow increases the heat gains by convection. The results provided for each variable by the model are combined in one graph (Fig.40). The illustration shows how fast, from the same starting point, the different parameters produce a reduction in dew yield.

As expected from the schematic graph representation of the process, relative humidity results to have the fastest effects on the condensed mass. Cloud Coverage, foil emissivity and wind speed produce as well fast reductions in efficiency, while it is clear from the graph how conduction heat transfer coefficient have minimum effects on the overall process. This shows how crucial radiation and convection heat transfers are for the process, whereas conduction plays a less vital role.

Mass Rate percentage variation: Comparison

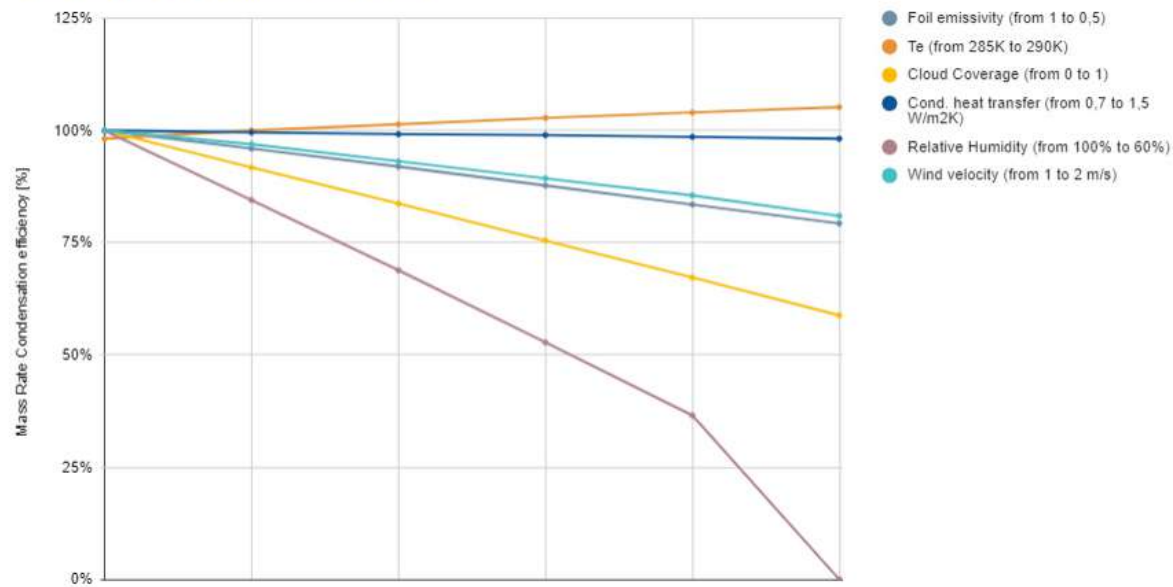


Fig.40: Comparison of the impact of different parameters on total mass rate

3.1.2 Collection

Once that condensation has started, collection efficiency has to be taken into account to obtain higher water yields. In fact, if a horizontal surface would theoretically maximize sky exposure and therefore radiative cooling, collecting dew would become challenging at the point of making the design inefficient. After nucleation, different strategies can be used to force the movement of drops towards a preferred direction.

The first and most obvious one is through the inclination of the surface. On an inclined plane, the static friction force balances out the horizontal component of the drop's weight. Both these forces depend on the angle of inclination of the plane (Fig.41).

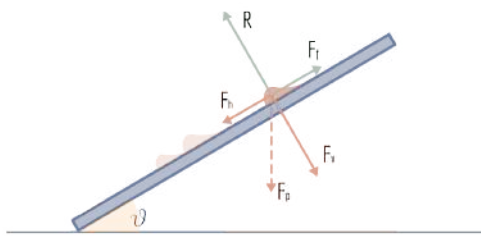


Fig.41: Inclined plane scheme

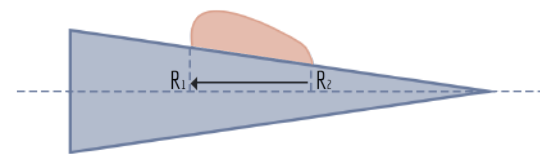


Fig.42: Laplace pressure scheme

Static friction is the main force interfering with the movement of the droplets towards the base of the condenser. Another strategy to overcome it uses shape curvature gradients to generate a Laplace pressure difference that develops a force towards the region with a bigger area of curvature (Jie, Hao and others, 2012) (Fig.42). Laplace pressure is defined as the pressure difference between the inside and outside of a droplet.

Finally, changes in the surface free energy of the condenser can develop a driving force towards the area with higher free energy. Wettability, or surface free energy, depends on both geometric and intrinsic material properties. If the material properties are taken as a constraint, not much can be done in tuning its contact angle and chemical wettability. On the other hand, roughness gradients can help in increasing the intrinsic hydrophilicity or hydrophobicity of the material (Wang, Wu and others, 2020)⁴⁴.

Looking back at the force balance on an inclined plane, in order for a droplet to move the sum of the three forces listed above has to be higher than the friction force. According to second Newton's law, the resultant of this force combination generates an acceleration parallel to

$$F_{horizontal} + F_{laplace} + F_{free\ energy} > F_{friction}$$

$$a_{tot} = \frac{F_{tot}}{m_{drop}}$$

3.2 PRE - DESIGN: FOG COLLECTOR

In the case of fog collection, no thermodynamic process is involved. Water is already in its liquid state and optimizing the performance of a fog collector means maximizing the amount of water that it can intercept and drain. As already explained in the previous section, traditional fog collectors consist of rectangular polyethylene porous meshes placed perpendicularly to the main wind direction. Sometimes two layers of mesh are placed in front of each other to increase the collection rate. Experiments have been made to test the efficiency of alternative and multi-layer setups. Compared to traditional collectors, multilayer harp setups (with vertical parallel threads) are found to be more efficient (Lummerich, 2011).

For this reason, the calculations by Azeem (2020) for multilayer harp collectors are used to model the behavior of a fog collector. When designing a fog collector, the unknown that has to be maximized is the flux of water coming out of it. This depends linearly on the collector's efficiency, the wind speed and the liquid water content of the specific fog.

$$\eta_{tot} = \frac{J}{LWCv_w}$$

While the other parameters depend exclusively on the climate conditions, the efficiency can be influenced by design strategies. According to Rivera (2011), the total efficiency can be formulated as:

$$\eta_{tot} = \eta_{ACE}\eta_{capt}\eta_{drain}$$

η_{ACE} is the aerodynamic collection efficiency, meaning the share of the total fog that flows through the collector. η_{capt} consists instead in the amount of that water that is intercepted and captured by the mesh, while η_{drain} equal to the captured amount that is ultimately drained by the mesh.

To simplify the calculations, some considerations are done. As the draining efficiency mainly deals with the possibility of re-entrainment of water droplets into the airstream, Azeem (2020) proposes two solutions: the use of multilayer collectors that can recapture re-entrained drops and the use of threads with the minimum diameter possible, as that would result in capturing smaller drops that are harder to be re-entrained. After accepting these design requirements, drainage efficiency is simplified to the value of 1. The design of a multilayer setup is therefore considered from now on. When the diameter of the drops tends to the diameter of the thread, the total efficiency results in

$$\lim_{d \rightarrow d_{\infty}} \eta_{tot} = \eta_{ACE} = \frac{A_{\infty}}{A} [(1 - (1 - s)^N)]$$

The equation above can be split into two parts. The aerodynamic efficiency depends on the fog fraction that is filtered by the collector and on the incident fraction, which depends on the solid fraction of the layers and on the number of layers. Further analytical steps on the formulation of the filtered fraction (Appendix II), lead to the equation

$$\varphi = \frac{A_{\infty}}{A} = \frac{v_w}{v} = \sqrt{\frac{c_d}{k}}$$

where the final value depends on the ratio between the drag coefficient of the collector and its pressure drop coefficient. In particular, the aerodynamic efficiency increases with higher drag coefficients, which correspond to less aerodynamically optimized shapes. On the other hand, efficiency also rises when minimizing pressure drops on the back of the collector. This apparent contradiction in defining the optimal aerodynamic behavior of a fog collector setup, shows the need of working on two different scales: the design of the collector geometry and the design of the surface porosity and texture. In this way, a meeting point in the maximization of drag and minimization of pressure loss can be found.

Implicit formulas are provided by Steiros⁴⁶ (2018) to calculate these values (Fig.4.3). Such formulas are used to perform iterative calculations in Excel and calculate different approximations of the aerodynamic efficiency. The model results helpful in evaluating the impact of each parameter on the total performance and on the best ways to reach the previously mentioned sweet aerodynamic spot. The results of the calculations are used to give an approximation of the total water yield and will be later implemented into the computational design workflow.

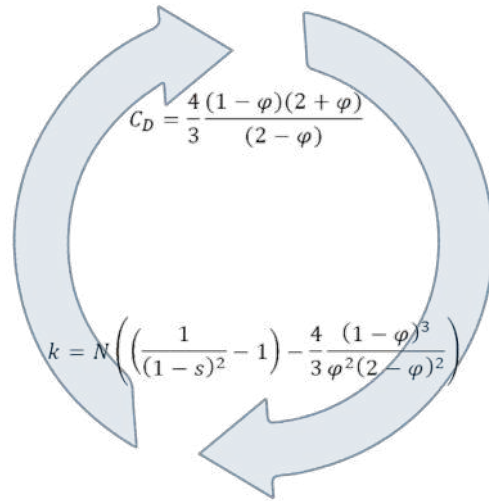


Fig.43: Fog collection simulation iterative calculation

As for the condensation presented in the previous paragraph, the main parameters involved in the fog collection process (Fig.44) have been listed and organized in a graph that clearly shows the relations and the hierarchy between different variables (Fig.45). This scheme is also used to find similarities between the two atmospheric water harvesting processes.

Symbol	Parameter	Unit
η_{ACE}	Aerodynamic efficiency	
η_{capt}	Capturing efficiency	
η_{drain}	Draining efficiency	
s	Solid fraction	
N	Number of layers	
φ	Filtered fog fraction	
χ	Incident fog fraction	
c_d	Drag coefficient	
k	Pressure drop coefficient	
d	Thread diameter	m
LWC	Fog liquid water content	$\frac{g}{m^3}$
v_w	Wind velocity	$\frac{m}{s}$
θ	Layer inclination	
κ	Layer curvature	
A	Collector area	m^2
<i>Pattern</i>	Specific surface texture	
J	Collected amount of water	$\frac{l}{hm^2}$

Fig.44: Fog collection parameters

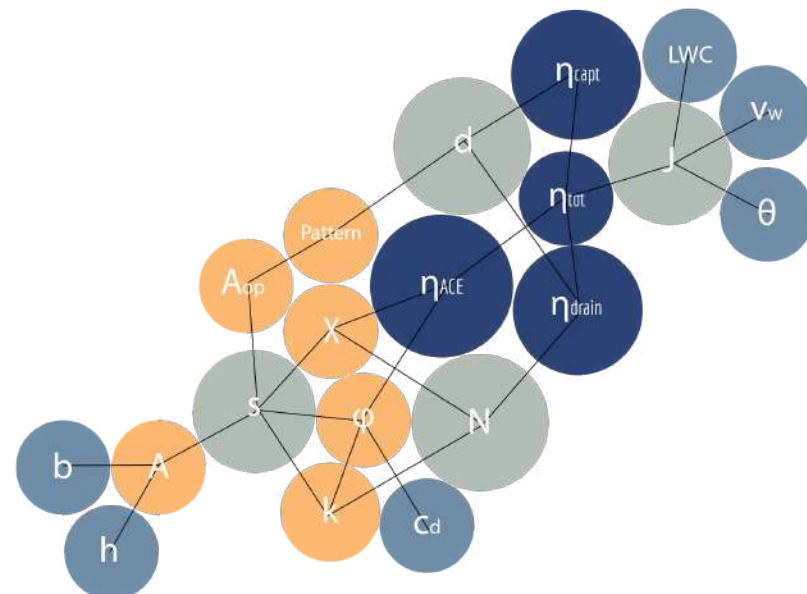


Fig.45: Fog collection graph

The green nodes highlight the variables with the highest number of connections to influence the efficiency. In the case of J (the collected mass of water), all the links mean that it ultimately depends on many parameters, including the fog collector efficiency. On the other hand, the diameter of the thread, the solid fraction (or shade coefficient) and the number of collecting layers represent three geometric variables that can be tuned during the design process. However, the calculation of the overall efficiency used as reference considers already from the start a minimization of the thread diameter.

Knowing this, what is still missing is an understanding of the impact that the solid fraction of the collector and the number of collecting surfaces have on the performance of the system. As for the condensation, a standard situation is set up in the Excel model compiled for fog collection and the values of the two parameters are gradually varied. The data are reported in tables and the percentage variation of the water yield compared to the one recorded for the starting point is calculated and used to plot a graph. The starting point takes a solid fraction (shade coefficient) of 0,3 and 1 layer of collecting surface. The wind velocity is set at 1 m/s for the all calculations, as it is already known that according to the considered formulas its increase would result in the linear growth of the collection rate of water. Inputs and results considered as starting point are reported in Fig.46.

Symbol	Parameter	Value	Unit
s	Solid fraction	0,3	
N	Number of layers	1	
v_w	Wind velocity	1	$\frac{m}{s}$

Symbol	Parameter	Value	Unit
φ	Filtered fog fraction	0,79	
χ	Incident fog fraction	0,30	
η_{ACE}	Aerodynamic efficiency	0,23	
J	Collected amount of water	0,42	$\frac{l}{hm^2}$

Fig.46: Fog collection simulation input

In Fig.47-50 the data collected for the variation of shade coefficient and number of layers are reported. For the solid fraction, it is interesting to notice how the collection rate initially grows but then decreases rapidly after a value of around 50%. This confirms the results found in literature, where a optimal shade coefficient between 0.5 and 0.6 is often reported (Azeem, 2020) and it is probably due to the fact that high solid fractions mean higher incident fog fraction levels and lower filtered fraction out of the total air stream.

The graph for different number of layers shows that adding a second collecting layer produces a 50% increase in yield, due to the highest incident fog fraction. Beneficial effects are still visible as the number of layers is increased even more, but after 5 collectors the collection rate seems to reach a plateau. This behavior leads to the conclusion that after one point, adding more and more layers does not become detrimental but rather useless. A comparative diagram between the two parameters can be seen in Fig.51.

Shade coefficient	Efficiency	J	%
0,3	0,23	0,427	100%
0,4	0,27	0,501	117%
0,5	0,29	0,532	125%
0,6	0,48	0,518	121%
0,7	0,25	0,46	108%
0,8	0,19	0,356	83%
0,9	0,11	0,204	48%

Number of layers	Efficiency	J	%
1	0,23	0,427	100%
2	0,34	0,615	144%
3	0,39	0,709	166%
4	0,42	0,757	177%
5	0,43	0,782	183%
6	0,44	0,793	186%
7	0,44	0,796	186%
8	0,44	0,794	186%

Fig.47-50: Fog collection simulation results and graphical representations

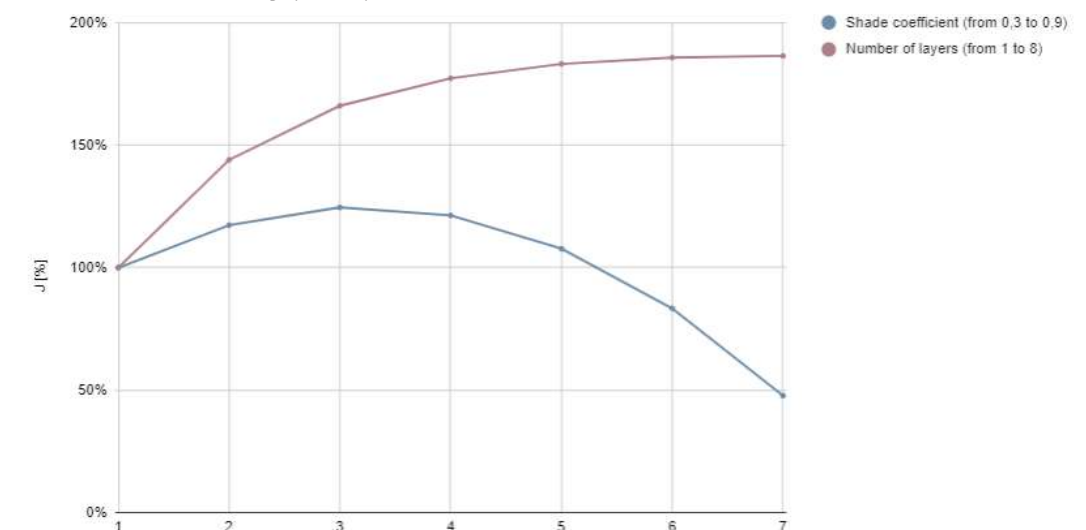
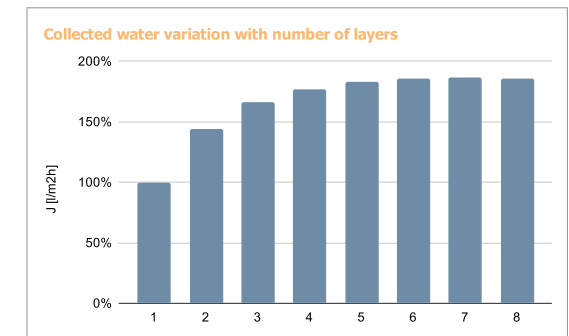
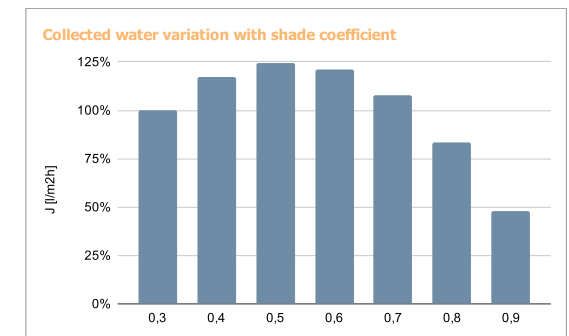


Fig.51: Comparison of the impact of different parameters on total collection rate

3.3 SPECIFIC CASE STUDY DEFINITION

How the main atmospheric water harvesting systems work has been analyzed and basic models to simulate them have been set up. This made clear how many climate parameters influence both these processes and therefore how important it is to choose a specific case study that could provide the research with the required weather data.

The process of choosing such a scenario starts from the definition of a climate area, gradually narrows it down to a specific country and eventually to a location that satisfies specific requirements (Fig.52). The chosen site does not represent the only possible location of the solution developed in this research, but rather an example of its possible applications. In fact, as stated in the first section of the report, the design should be flexible and adaptable enough to be tuned to the climate conditions of a broader region, where water scarcity and urban population growth are becoming pressing issues.

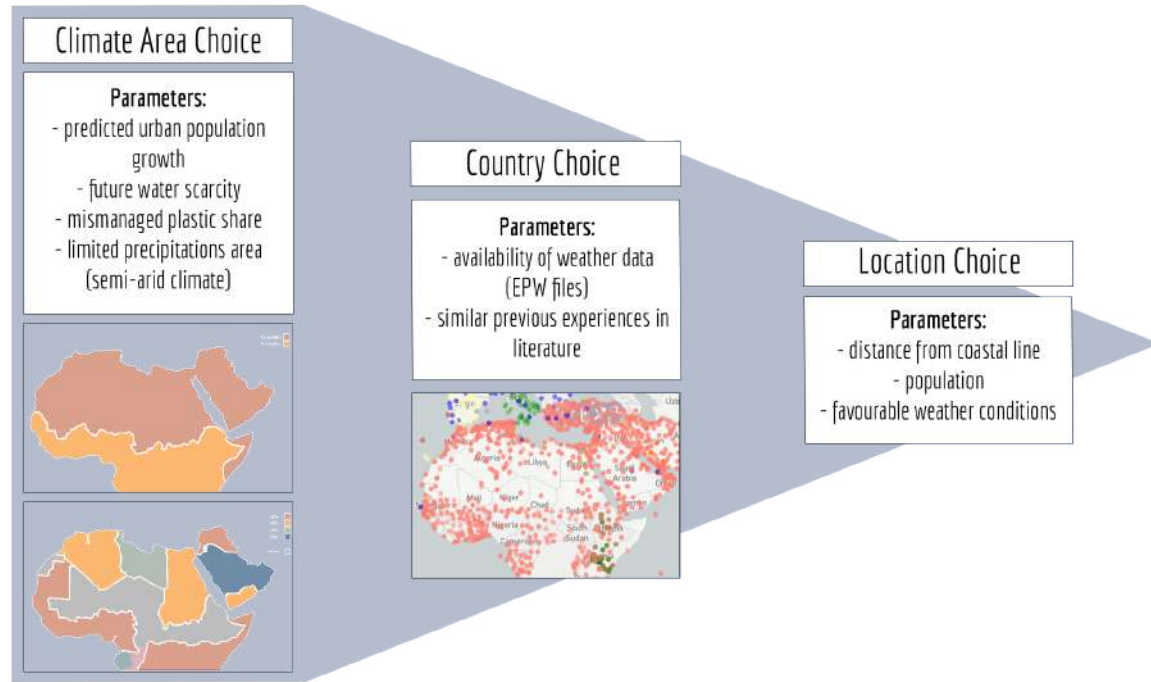


Fig.52: Specific case study definition scheme

The analysis of these emergencies presented in the first section of the report, combined with the data on mismanaged plastic waste has moved the focus of the research to the ECSWA countries, which consist of those situated in Northern Africa and South-Western Asia. The next step is to look more into the single countries. The parameters considered to make a choice are mainly related to the availability of complete data and on the existence in literature of similar water harvesting experiences, which could result useful in validating the accuracy of the models and design iterations in general. This means that the chosen country would not be necessarily the one more in need of such a solution, but rather the one with more complete information. In this evaluation, the EPW files availability has been considered when looking at weather data.

This research shows three potential candidates: Jordan, Morocco, and Yemen. All three of them present EPW files availability for multiple locations and previous literature on either fog or dew collection. However, the papers published by Lekouch⁴⁷ (2012) and Marzol⁴⁸ (2008) represent two extremely complete literature sources among those that have been studied. Data on rain and atmospheric water collection potential for the main cities of Morocco is reported, together with the main climate parameters and how they affect those potentials. Based on this, Morocco is considered to have the most complete set of data and is therefore chosen as main case study.

The last step in this decision process is that of choosing a specific weather station and therefore a location. Based on the predictions of urban population growth, the five most populous cities of Morocco are considered, as they would most likely be the ones to face slum growth as well. The cities are evaluated according to different parameters. When weather data are available, monthly data for RH, wind speed, cloud coverage and ambient temperature are combined to roughly estimate dew potential. The result are presented in Fig.53.

Code	City	Population	% Total	Distance from coast	EPW		1	2	3	4	5	6	7	8	9	10	11	12	
#1	Casablanca	3144909	8,50	0	☑	RH	83,83	82,97	79,59	73,82	78,71	80,08	80,36	78,29	81,72	80,5	82,12	83,46	
						vw	2,3	1,9	2,49	2,95	2,74	3,64	3,23	2,35	2,54	2,68	2,94	2,95	
						CC	7,6	7,15	5,32	5,51	7,01	7,17	7,25	6,84	7,2	7,29	7,47	7,37	
						T	13	14	15	16	18	21	23	23	20	16	14		
#2	Rabat	1655753	4,48	0	☑	RH	77,9	82,52	75,28	75,3	75,92	77,7	75,53	78,29	82,44	81,76	81,42	81,15	
						vw	2,8	2,52	3,23	2,72	2,99	3,04	3,03	2,48	3,17	3,14	2,12	2,17	
						CC	5,87	4,74	5,85	5,29	5,29	5,46	4,89	5,51	4,73	5,33	5,04	5,19	
						T	11	13	15	16	18	20	23	23	21	19	15	13	
#3	Fes	964891	2,61	2	☑	RH	71,9	71,38	75,25	69,73	61,31	48,38	37,79	45,79	54,93	52,41	61,88	67,26	
						vw	2,72	3,87	3,15	3,12	3,56	1,46	3,39	3,25	2,86	3	3,15	2,83	
						CC	6,09	5,93	6,24	6,08	5,4	4,28	2,6	2,7	4,81	5,12	4,9	5,1	
						T	10	10	13	15	19	24	28	27	23	20	13	10	
#4	Sale	903485	2,44	0	☐														
#5	Marrakesh	839296	2,27	2	☑	RH	68,77	61,46	65,77	58,94	54,38	51,02	45,87	44,46	46,76	59,48	65,74	61,94	
						vw	1,87	2,83	2,57	2,36	2,5	3,12	2,29	2,6	3,19	2,74	1,09	1,72	
						CC	4,17	5,07	5,17	4,58	4,23	3,85	2,68	2,67	3,42	5,26	4,63	4,31	
						T	12	14	16	18	21	24	28	29	26	21	16	13	
RH	Relative Humidity					RH	If Relative Humidity > 70%												
vw	Wind velocity					vw	If (wind velocity + cloud coverage) < 10												
CC	Cloud coverage					CC													

Fig.53: Moroccan cities weather data comparison

From this analysis, coastal cities such as Casablanca and Rabat seem to have the highest potential for dew collection, while cities in the inland such as Fes and Marrakech score lower. Before taking a decision on one city, the results of the evaluation are compared to the mapping of dew potential for Morocco provided by Lekouch (2012) (Fig.54), which confirms the results presented in the table above. Coastal cities result to have the highest potential, whereas cities in the inland show gradually lower values. According to these considerations, Rabat is chosen as example case study location.

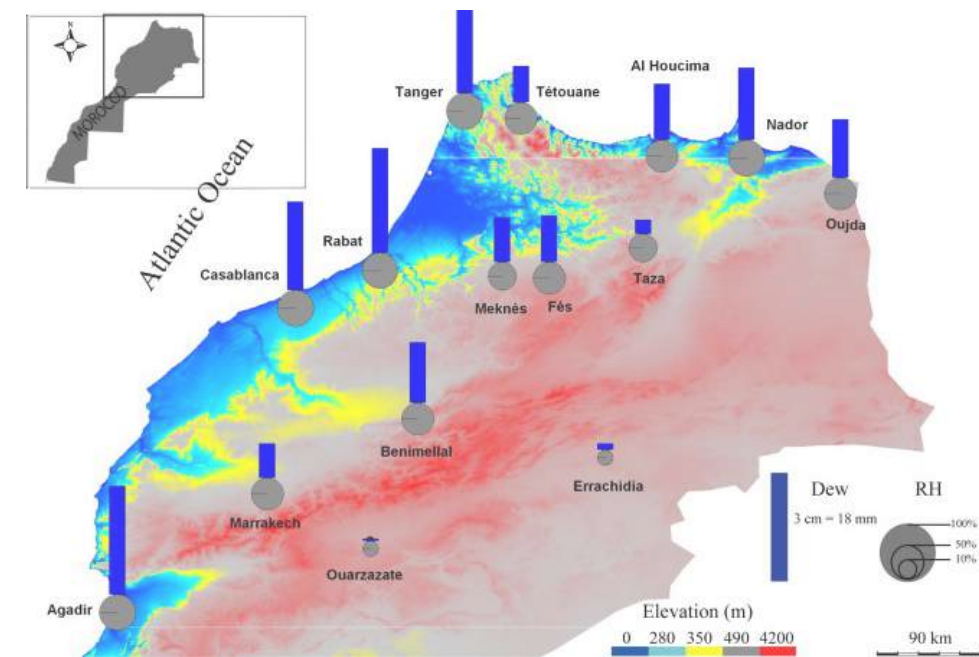


Fig.54: Moroccan cities dew water potential [Lekouch, 2012]

However, the design will be prototyped and tested in the city of Delft, in the Netherlands. For this reason, weather data for Rotterdam-The Hague (NL) will also be used further in the design evaluation process.

3.4 PRE - DESIGN FOR ADDITIVE MANUFACTURING

Up to this point, the problems that the research aims to address and the existing solutions to these have been analyzed. However, before diving into Additive Manufacturing, the definition of a general design workflow and the specification of a methodology that could guide the process are required in order not to compromise the innovative potential of a non-traditional approach such as design-through-prototyping.

As stated in the paragraph about methodology, the research is based on the concept of research by design and design by prototyping. In this way, the use of the potentials offered by AM is maximized, as the design process is performed in parallel to the actual printing and testing of specimens. Tripp and Bichelemyer⁴⁹ (1990) give a good overview of design by rapid prototyping, which compared to other design methodologies is not a linear problem-to-solution approach but rather a more holistic process dominated by a high degree of complexity and unpredictability. With this approach, the definition of functional requirements partially overlaps with the designing and prototyping of the part, which is then tested by the users and the designer. The execution of these steps in an early stage leads to a constant new understanding of the problems and to the determination of new design objectives in a circular loop process that ends only when all of them are met.

Due to this alternative approach to design and to the almost absence of manufacturing constraints with AM, the designer risks to limit the design focusing on more traditional solutions related to outdated constraints. A schematization of the design needs to be made and a method to be developed. In order to do so, the findings of Vayre⁵⁰ (2012) and Boyard⁵¹ (2015) are combined and used as reference.

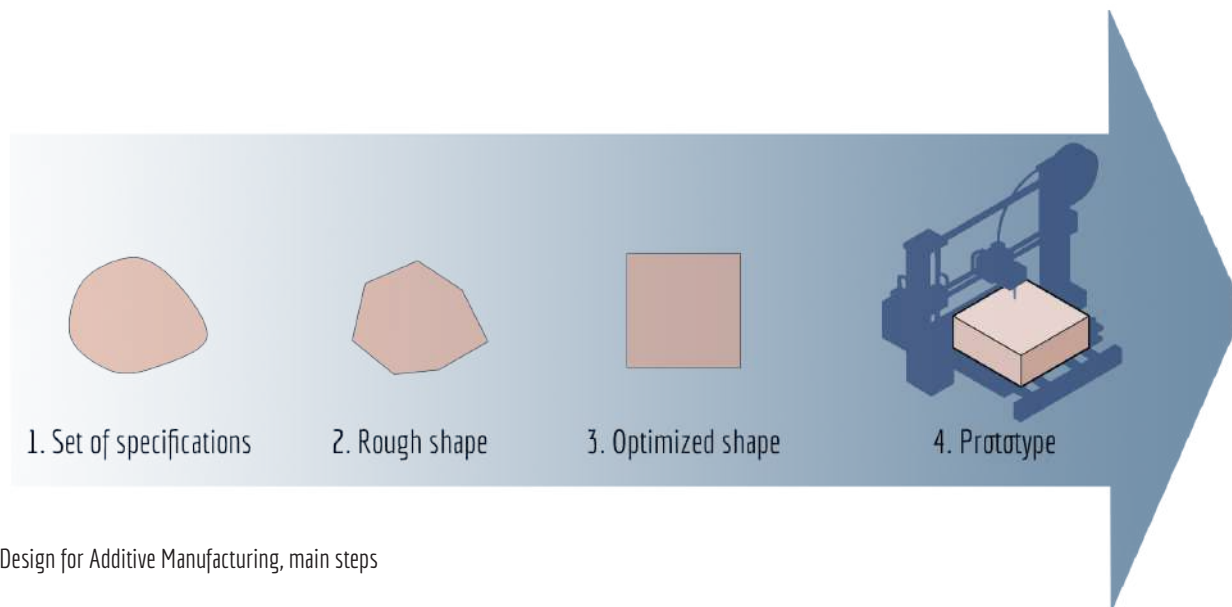


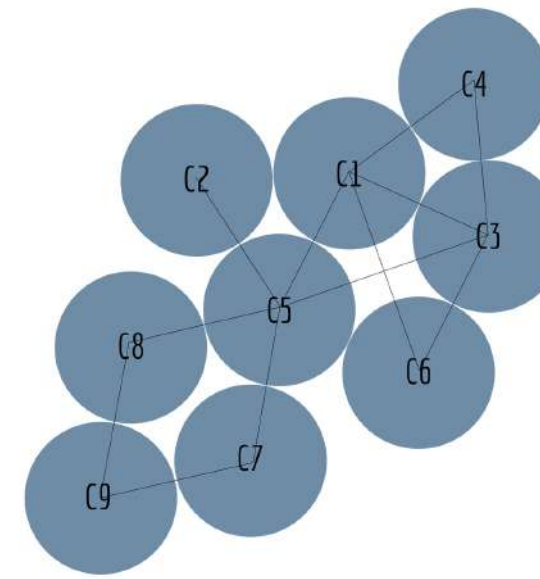
Fig.55: Design for Additive Manufacturing, main steps

According to Vayre (2012), the main steps are (Fig.55):

- analyze the requirements and constraints
- develop one or many rough initial designs
- optimize them for a certain amount of parameters
- validate them through prototyping.

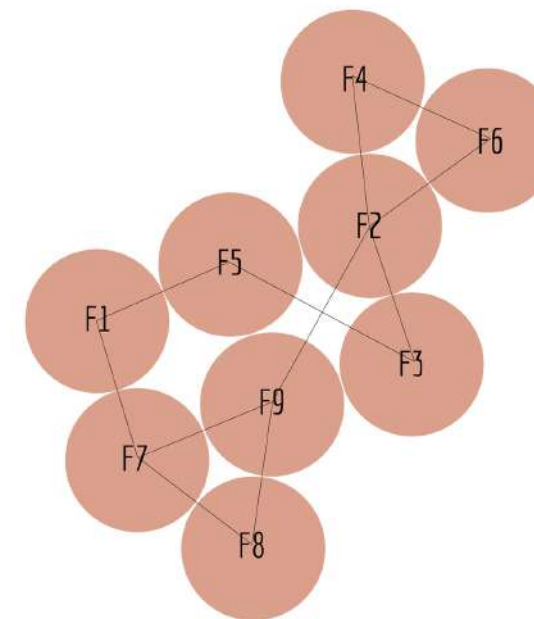
The first steps of this procedure are better detailed by Boyard (2015), who refers to the methodology proposed by Alexander⁵² (1964) of representing a design problem into a space and a set of interconnected points. Boyard suggests that the main functional requirements of the design have to be listed. The functions are then organized into a graph, where they are grouped based on their physical connections and proximity. Groups of functions separated from others form sets. This graph gives a first rough idea of the functional and spatial organization of the functions within the final product. Knowing this, the design task of this research has been detailed into functions. Such functions have been grouped into two sets: the condenser and the fog collector (Fig.56).

After this first representation, the function specification can take another step towards its representation as a tridimensional object. To Vayre (2012), a part consists of a set of functional surfaces, a general volume and a specified behavior. The sets identified previously are translated into surfaces. The general volume represents in this case the overall component that will integrate the two surfaces into a multifunctional component (Fig.57).



Radiative condenser set

- C1 - Has high exposure to the sky
- C2 - Has back insulation
- C3 - Has high surface area
- C4 - Reflects visible light
- C5 - Reduces wind speed close to the surface
- C6 - Has high IR emissivity
- C7 - Facilitates water drainage
- C8 - Directs water towards the ground
- C9 - Minimizes water losses



Fog collector set

- F1 - Has small threads diameter
- F2 - Has more than one intercepting layer
- F3 - Generates low pressure drops
- F4 - Has high drag coefficient
- F5 - Has optimal shade coefficient
- F6 - Intercepts high speeded air flows
- F7 - Does not clog with water
- F8 - Directs water towards the ground

Fig.56: Radiative condenser and fog collector sets

The identification of the two surfaces and the specification of their functions represents the last step of the pre-design process. It will also be the starting point and methodological guideline of the design phase that follows. The design is informed by the research performed in this stage, that will be considered as acquired knowledge.

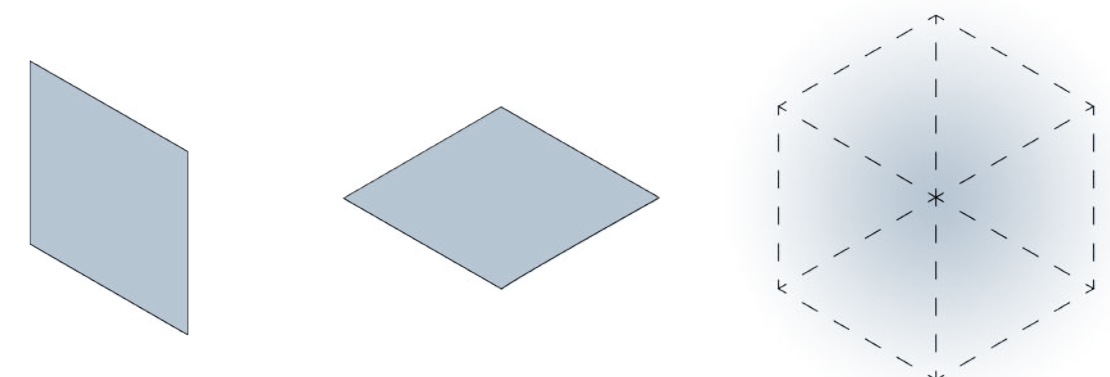
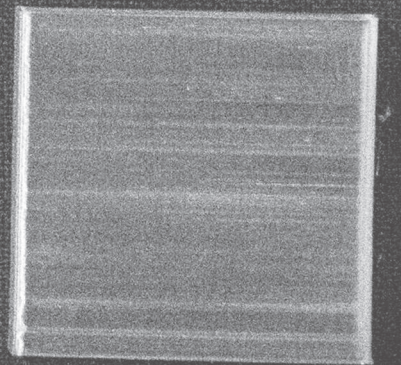
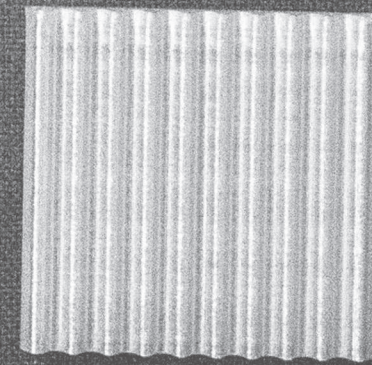
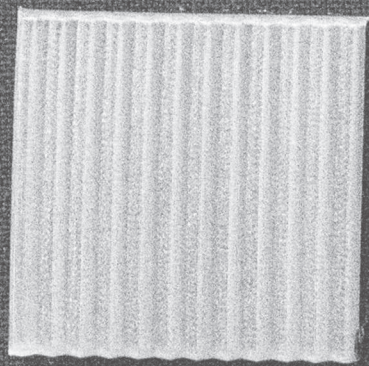
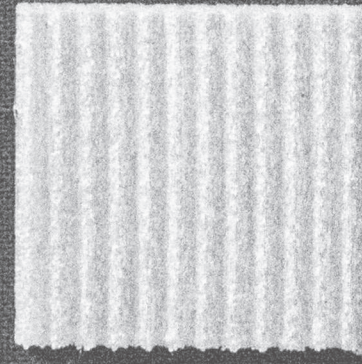
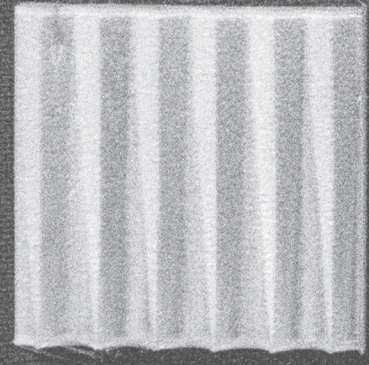
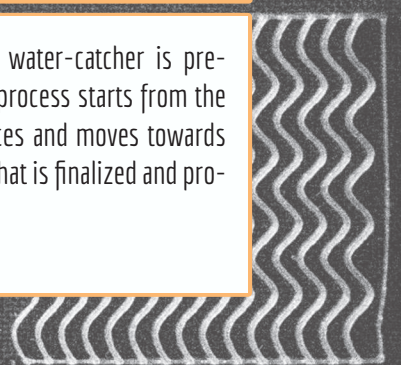
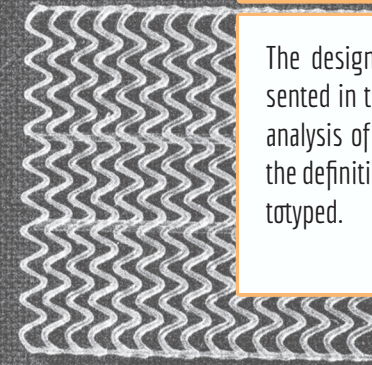
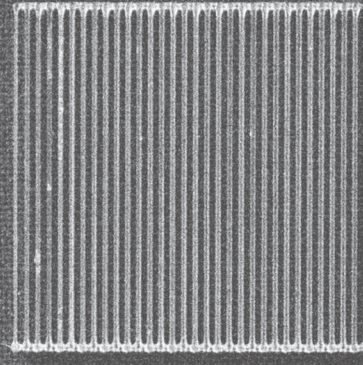
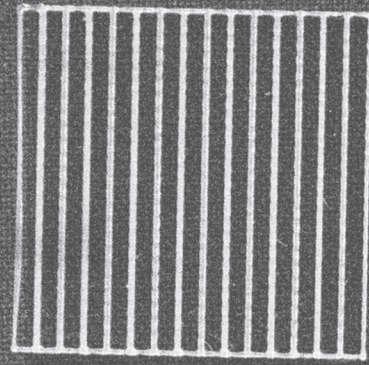
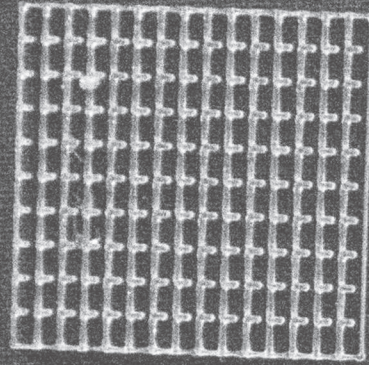
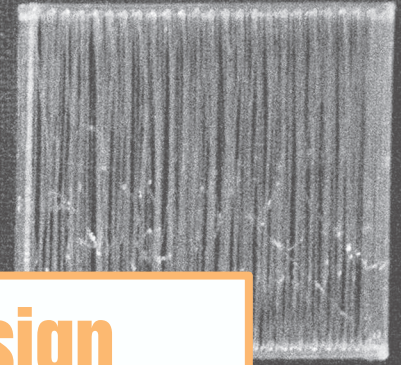
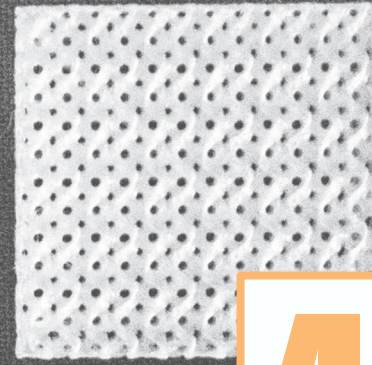
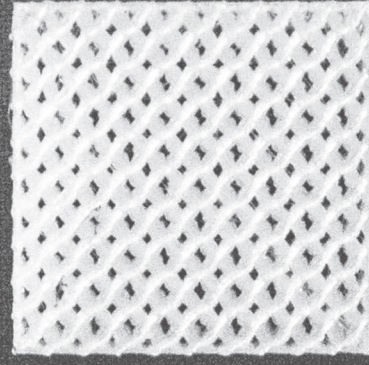
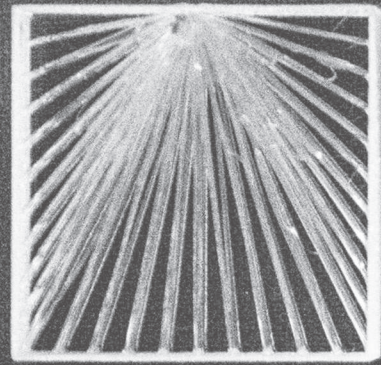
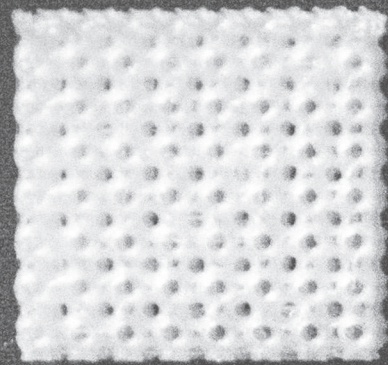


Fig.57: Functional surfaces and general volume definition



4. Design

The design process of the water-catcher is presented in this section. The process starts from the analysis of collecting surfaces and moves towards the definition of a solution that is finalized and prototyped.

4.1 DESIGN WORKFLOW AND TOOLS

In this section, the component's design process is described. As explained previously, the methodology of design through prototyping is adopted to perform this task. Physical and computational testing of different design iterations is therefore at the base of the research. Subdividing the main design problems into a series of smaller challenges represents another useful strategy that is used throughout the whole process and that will be used also to present the main results. In this way it was possible to follow a more holistic approach where all the intermediate results could contribute to the achievement of the final goal. The research aims to explore the potentials and limitations of 3d printing. The prototyping process is based on a series of physical and computational tools. Such tools are described below, as they haven't changed over time and represent necessary equipment to even start the research.

- FDM 3d printer Anycubic Chiron is used for prototyping, with a build size of 400x400x450mm.
- Transparent PETg filament is used throughout the whole process. Specifications from the producer can be found in Appendix III.
- Slicing software Cura (Ultimaker Cura 4.8.0) is used to process the geometries and translate them into g-code readable by the machine

4.2 CONDENSING SURFACE

The design of the condensing surface is the first challenge to be addressed. This is done according to the outcomes of the pre-design section and to the logic of breaking down the design problem into smaller pieces. The condensation process is divided into its different steps (Fig.58): radiative cooling, drop's nucleation, and water collection. For each step, the main variables that can be influenced by design are highlighted. They relate to geometrical properties since most of the environmental and material parameters have to be considered as constraints the design has to deal with.

The analysis of these properties relates to different scales of the device, which will be developed separately and then integrated into a strategy for an optimal 3d printed radiative condenser. The outcome of this section is not a final design, but rather an approach that will eventually inform the component design.

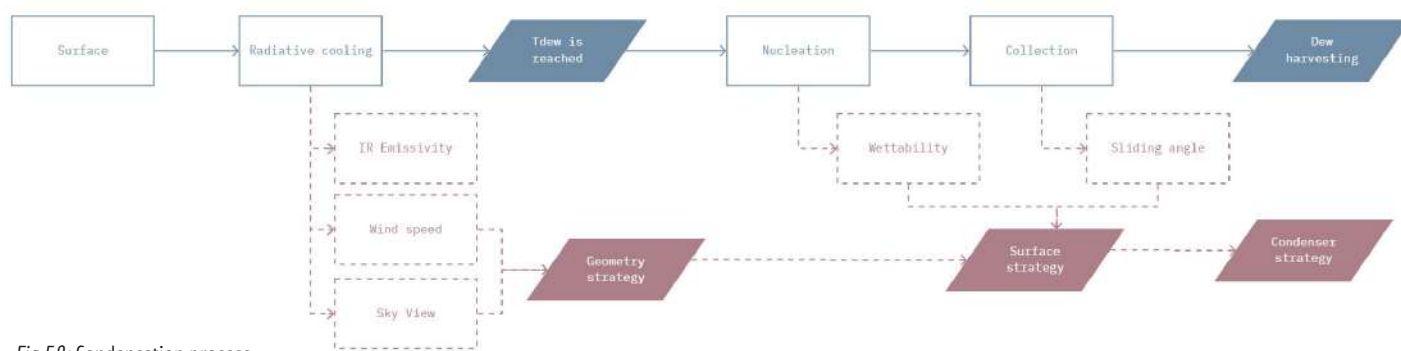


Fig.58: Condensation process

4.2.1 Temperature reduction

The overnight cooling of the surface is due to the heat losses by radiation of the surface towards the sky. The parameters involved in this process are the IR emissivity of the material, the radiating body's share of surface exposed to the sky and the wind speed close to it, that contributes to both heat gains by convection and continuous moist air flow.

The infrared emissivity it is mainly an intrinsic property of the material. Literature sources suggest that an increase in roughness can be used to enhance this value (Barrios, 2019). Since at this stage no significant change in roughness are applied, the average value of 0.92 (Terré, 2014) is considered for PETg. Later experiments will try to improve it, but effects will be analyzed exclusively from a qualitative point of view.

The sky view factor, which is the first necessary condition for condensation to happen, is introduced in the simulation model as a reduction factor of the heat transfer coefficient. The formula necessary to calculate is therefore:

$$\alpha_{rad} = SVF_4 \epsilon_f \sigma \left(\frac{T_f + T_{sky}}{2} \right)^3$$

In this stage, this factor is considered to be equal to 1 and no experiments are performed on it, as the design goal will always be that of maximizing the exposure to the sky of the condensing surface.

The simulations performed in the pre-design phase (see pag.28-29) have shown the effect of different parameters on the total water yield and how important it is to minimize the wind speed close to the condensing surface. Wind speed is also one of the few environmental factors that can be influenced by geometric properties and it is therefore considered worth studying it more in depth.

Wind speed analysis

To understand how much can geometrical changes affect the wind speed close to a surface, simple configurations have been modeled and tested through CFD analysis. CFD stands for Computational Fluid Dynamics, and it is a branch of fluid mechanics that utilizes computational power to solve problems about the flow of fluids. Fluid's motion is governed by the so-called Navier Stokes partial differential equations, that describe fluid's conservation of momentum and mass. However, in most cases, these equations cannot be solved analytically. What CFD does is to give an approximation of the solutions for such equations. To solve them numerically through a computer, the continuous domain is translated into a discrete one through a grid. Finite volume discretization method is applied, as it ensures that Navier-Stokes conservation laws are satisfied for the whole domain as long as they are satisfied in each single control volume. A grid is generated and solutions are calculated only at its nodes. The results for other positions in the volume are calculated through interpolations of the node's values. The grid can be built with different resolutions according to the complexity of the flow to analyze (Zuo, 2005)⁵³. The main steps behind a CFD analysis are illustrated in the diagram below (Fig.59).

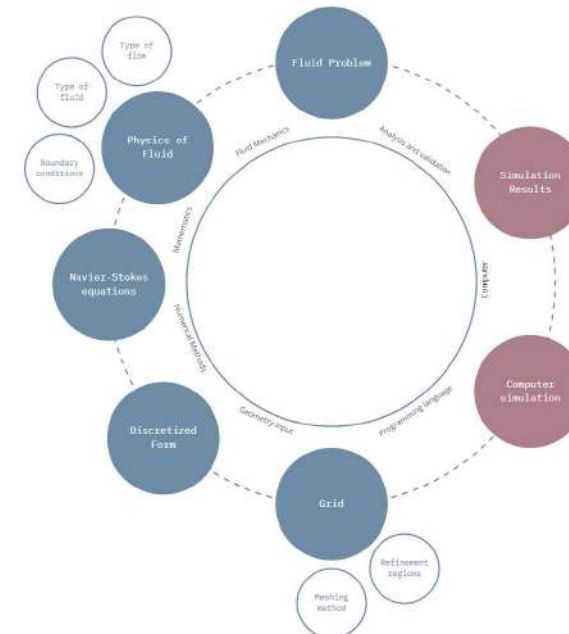


Fig.59: CFD process

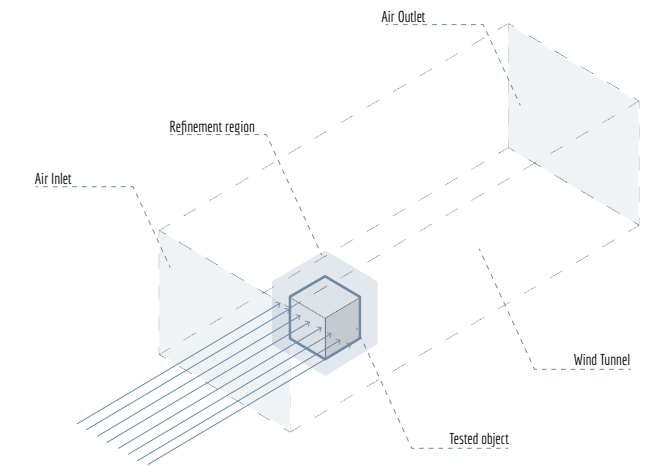


Fig.60: Wind tunnel simulation

Different simulations are possible thanks to CFD that therefore represents in many cases a reliable, faster, and cheaper alternative to physical experiments. This is true especially in the early design stages when an iterative process is applied and different testing conditions need to be evaluated. However, the simulations are extremely computational-intensive and therefore really depending on the machine that is used to perform them. This becomes the main constraint in terms of the geometric complexity of the tested object and the relative grid's resolution.

Throughout the research, standard wind tunnel simulations have been the main way with which CFD has been integrated into design workflow. However, also thermal parameters can be analyzed through this method. A wind tunnel simulation consists of an object contained in a bigger volume (Fig.60). One face of such volume is defined as the inlet and the flow of air at a specific velocity is set through it. Different boundary conditions and flow specifications can be set to better simulate specific scenarios. Then, the wind tunnel model is meshed and its faces are used as the grid and the discretized domain necessary for the simulations. Specific refinement regions can be applied close to the tested objects when a more complex behavior of the flow is expected to happen. Data about pressure and velocities distributions are usually the main results of the simulation.

In these first analyses, the engine *blue-CFD* is used through the interface offered by the plug-in *Butterfly* for Grasshopper. Steady incompressible airflow is chosen. This simplification assumes that the velocity of the fluid in a specific location does not change over time and that no significant changes in the fluid's density are present. The flow is set to be laminar at the inlet, with an initial speed of 3 m/s, which is found to be an acceptable approximation of average wind speeds in Rabat (see Fig.53). A pressure outlet is set at the back of the tunnel and a no-slip condition is applied to the rest of the walls. This means that no boundary layer is simulated.

The tested geometries represent different curved iterations of an initially flat surface, used as reference and control sample. Symmetric and asymmetric samples with different degrees of curvature are compared. The resulting velocities are measured in 3 points of the geometry. Measurements in those points are recorded at 2 different distances from the surface (2.5 and 5 cm) to understand the ability of specific geometries in minimizing wind speed. The geometries can be seen in the picture below (Fig.61).

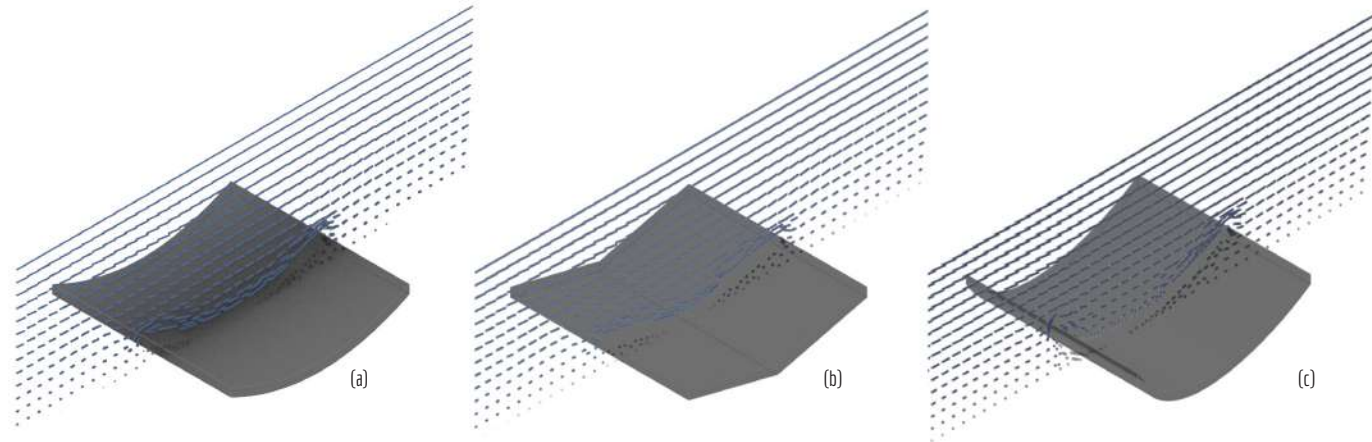


Fig.61: Basic surface wind tunnel simulations. U-shape (a), V-shape (b), asymmetric u-shape (c)

Compared to the initial flat surface, all the samples show significant reductions in the wind velocity close to the geometry. The recorded values for the different locations and distances can be seen in Fig.62. The highest reductions are recorded for the asymmetric U-shaped geometry. Close to the surface, the reduction of the velocity reaches 96% of the values recorded in the same location for the flat sample. The numbers show the effects of curvature on speed distribution. Between the different curved geometries, variations are instead less extreme. Differences in degrees of curvature do not seem to provoke particular behaviors in the airflow.

These results relate to the scale of the overall condenser. For this reason, they will be taken into considerations in a later stage of the research, when the overall design will be developed.

		Unit	#0 Flat_Surface	#1 V_Surface	#2 U_Surface	#3 U_Asymmetric_Surface
v_inlet		m/s	3,0	3,0	3,0	3,0
v_1	Left Corner	m/s	5,7	7,3	6,3	3,0
v_2	Face 1 Middle (d=2,5cm)	m/s	4,7	1,6	0,7	0,3
v_3	Face 1 middle (d=5cm)	m/s	7,6	2,6	1,4	0,2
v_4	Middle point (d=2,5cm)	m/s	8,4	0,2	0,1	0,5
v_5	Middle point (d=5cm)	m/s	8,8	0,9	1,1	0,1
v_6	Face 2 Middle (d=2,5cm)	m/s	8,3	1,6	0,7	0,3
v_7	Face 2 Middle (d=5cm)	m/s	8,5	2,6	1,4	0,7

Fig.62: Basic surface wind tunnel simulations. Velocity reductions.

Radiative cooling analysis

The analysis described above takes into account only geometries curved in one direction. This is acceptable when a prevalent wind direction is considered. Sky exposure, which is one of the main factors for radiative cooling, is instead omnidirectional. Terré⁵⁴ (2014), compares the cooling potential of different shapes, mainly inclined surfaces and funnels. The analysis is performed through a conjugate heat transfer analysis, that takes into account both convective and radiative heat exchange.

The results of the research presented by Terré (2014) show how geometrical modifications increase the cooling capacity of the surface. In particular, folded geometries perform better than smooth ones, and curved or funneled shapes generate higher cooling, due to the higher wind speed reduction (Fig.63).

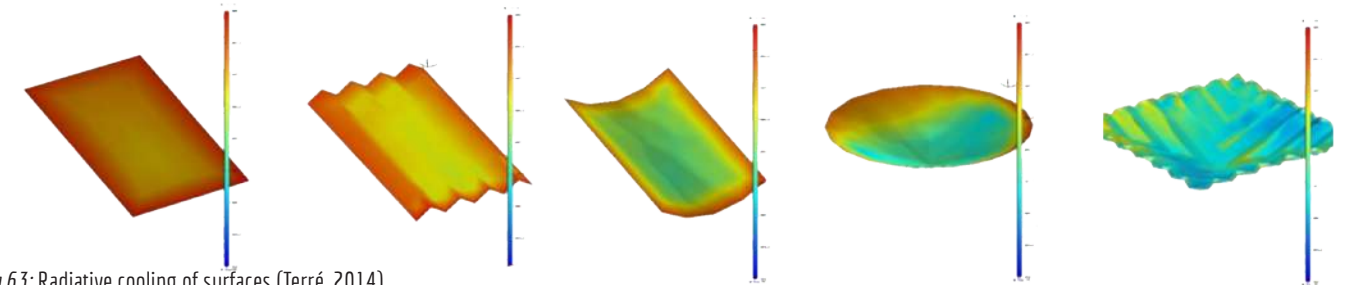


Fig.63: Radiative cooling of surfaces (Terré, 2014)

These two approaches are therefore considered to be promising for the design of an efficient condenser. However, single or double-curved surfaces behave differently when 3d printing is considered. In the case of funnels, the print layers have to be concentric and therefore perpendicular to the direction of the final slope. Single-curved surfaces, instead, allow for layers parallel to the slope (Fig.64).

The relevance of this property in the overall process is questioned and explored further in the next tests, to better inform the final geometry.

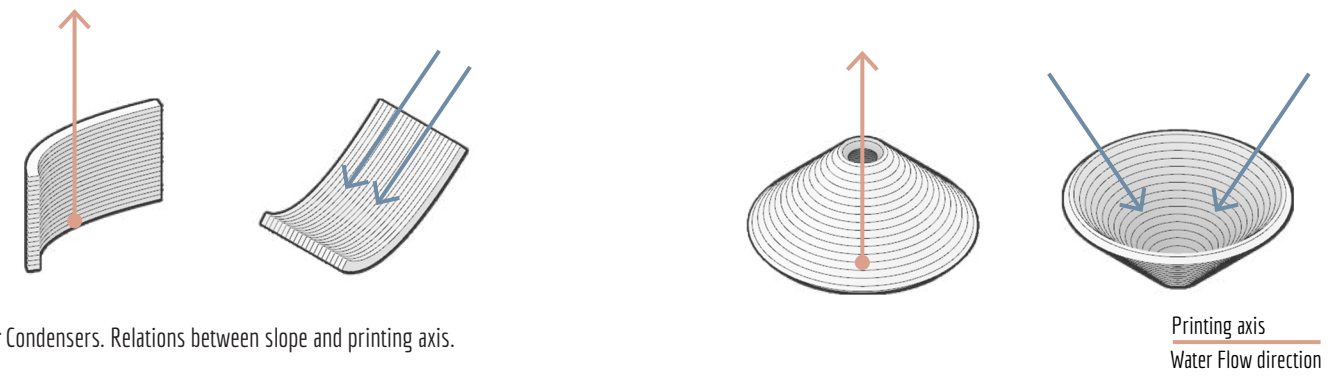


Fig.64: Condensers. Relations between slope and printing axis.

4.2.2 Droplet nucleation and collection

The geometrical properties involved in these phenomena are related to the properties of the surface itself. The following section researches how geometrical properties can affect the nucleation rate of droplets on the condenser and its collection efficiency. The relation between water collection and 3d-printing efficiency is introduced and used to evaluate the performance of the different design iterations developed for each experiment. Images of the samples used for the different experiments can be found in Appendix IV.

Sliding angle and water collection

To answer the question "does the orientation of the printing layers influence the nucleation and collection abilities of a 3d printed condenser?" the collection capabilities of different surfaces are tested. Similar to the surface characteristics reported in literature for cactuses (see pag.15), the print layers can be seen as a series of small grooves. These channels could play a role mainly in the collection efficiency of a surface.

For this reason, the critical sliding angle of different samples is tested. The sliding angle is defined as the minimum inclination for which a water droplet starts to slide downwards on it (Varagnolo, 2016)⁵⁵. Flat and undulated 5x5cm specimens are printed with different orientations so that the same configurations can be tested with the print layers both parallel and perpendicular to the slope.

Water droplets are placed with a syringe on the top part of the samples. A starting angle of 30 degrees is set, as it represents the most frequent inclination for radiative condensers reported in literature. The slope is then varied gradually until the minimum sliding angle is observed. The experimental setup is shown below (Fig.65).

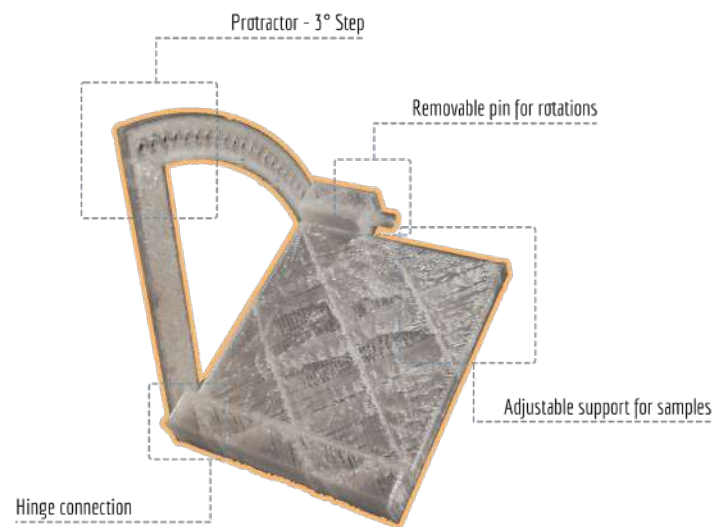


Fig.65: Sliding angle. Experimental setup

The importance of aligning the slope with the direction of the print layers is shown by the Fig.66 where all the results are cataloged. The sample with the lowest sliding angle is the flat one with parallel layers. Droplets tend to stick to the side walls of the undulated surfaces, increasing their sliding angle even when the slope is aligned with the printing layers. However, this limitation is considered to be promising in decreasing the water losses due to wind blowing close to the surface. Its directionality could also represent an interesting approach to maximize water collection in configurations with more complex curvature. Droplets on samples with layers perpendicular to the inclination do not slide even when their orientation is vertical. Angles bigger than 90° are not considered, as they would be excessively detrimental in terms of sky exposure.

#	Profile	Description	Layer direction to slope	Sliding Angle
#1		Flat	Perpendicular	>90
#2		Flat	Parallel	24
#3		Ondulated-Slight	Perpendicular	>90
#4		Ondulated-Slight	Parallel	33

Fig.66: Sliding angle. Results

Nucleation rate

The next experiment tries to answer the question: “do different geometrical configurations of the surface influence the nucleation efficiency of the condensing surface?”

For the experiment undulated and bumpy surfaces are studied. This is based not only on the previous experiment but also on the biomimetic examples presented in the early stages of the research. Both desert beetles or cactus’ external surfaces are characterized by either sets of bumps or grooves. Different 5x5 cm surfaces are generated by extruding different curved profiles. They are printed and tested in a closed chamber where a nebulizer is introduced. The experiment does not take into account the cooling of the surfaces, as the relative humidity is already brought to 100% by the nebulizer. In this way, only their “water catching” ability is tested. Samples are weighted before the experiment, placed flat in the chamber for 15 minutes, and weighted again to understand the collected mass of water.

The total surface area and the sky view factors are also measured, as more undulated tiles are expected to have a higher exposed area for the same amount of projected area. For what concerns the fabrication process, printed time and length are noted for each measurement and are later used in the comparative evaluation of the results.

The experimental setup is schematized on the next page (Fig.67).

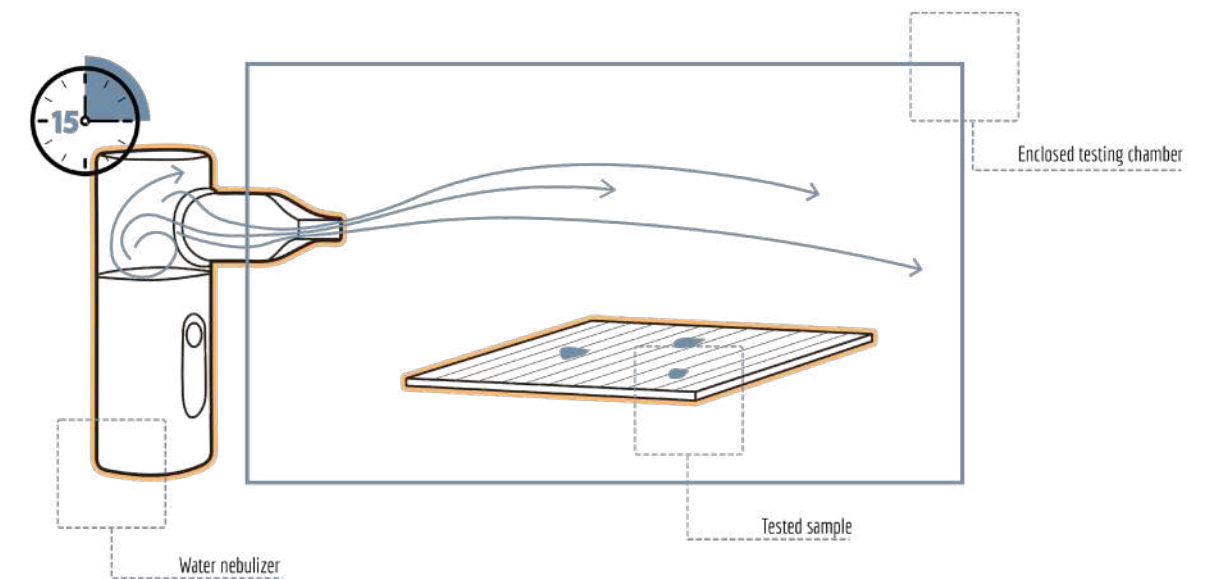


Fig.67: Droplets nucleation. Experimental setup

To compare the results, the absolute value of the collected mass of water observed for each sample is divided for its printing time, to measure it in comparison to the printing efficiency. The same thing is done for the sky view factor, which is divided by the printing time. The last coefficient that is compared is the one calculated through the ratio between the view factor and the surface area. High values of these coefficients mean better performance.

Results show (Fig.68) that compared to flat surfaces, undulated ones collect even three times more. The best scoring types are sharp surfaces. They score higher even when compared to the printing time. Only the squarish surface scores significantly worse, which is probably due to the high amount of sharp corners, that leads to a significantly longer time to print. In terms of the ratio between sky view and printing time, the flat surfaces perform better, since they are considered to have 100% view factor.

#	Profile	Description	Area [mm ²]	Average sky view (%)	Sample weight [g]	Printed length [m]	Printing time [min]	Collected water mass [g]	Collected mass/printing time	Sky view/Area	Sky view/Printing time
#1		Flat sample	2500	100	2,82	0,94	21	0,21	0,010	0,040	4,76
#2		Ondulated (Sharp)	3905,12	86	3,4	1,13	27	0,69	0,026	0,022	3,19
#3		Ondulated (Round)	4057,19	71,68	3,5	1,15	27	0,64	0,024	0,018	2,65
#4		Ondulated (Square)	5500	72	4,22	1,39	36	0,59	0,016	0,013	2,00
#5		Ondulated (Concave)	4103	84	3,41	1,14	27	0,7	0,026	0,020	3,11
#6		Bumpy	2500	100	3,84	1	23	0,30	0,013	0,040	4,35

Fig.68: Droplets nucleation. Results

The coefficients for all the samples are then mapped into a bar graph (Fig.69). It is possible to see how the flatter surfaces perform better in terms of sky view. However, the performance of undulated shapes shows a more balanced behavior and a significantly higher nucleation rate. As this value was the main focus of the experiment, undulated surfaces are researched more.

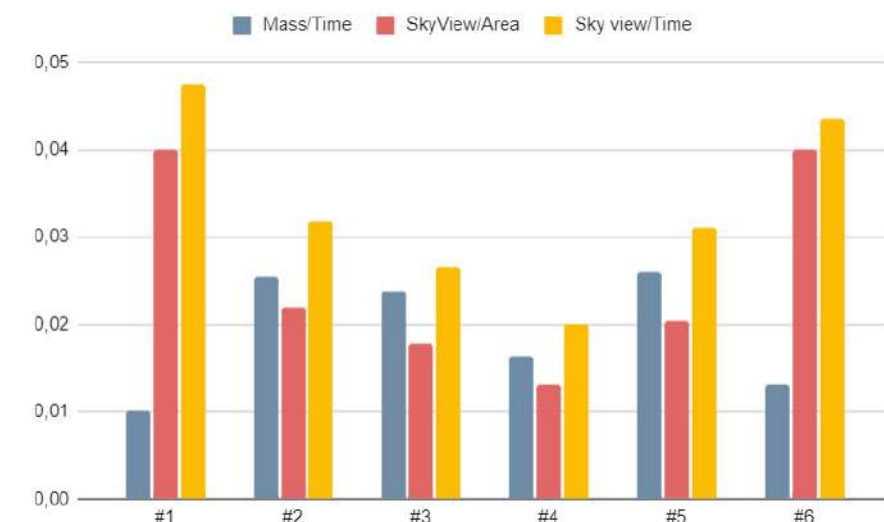


Fig.69: Droplets nucleation. Coefficient comparisons

Undulated surfaces nucleation rate

Undulated surfaces have higher directionality. The previous section has shown that more water nucleates on them compared to flat surfaces. As they don't have the lowest sliding angle, other approaches have to be explored. Laplace pressure gradients, induced by different curvatures, enhance water sliding in examples analyzed before such as cactus spines (Jie, 2012). The next experiment tries to answer the question: "How can Laplace pressure gradients affect the nucleation rate of surfaces?"

The experimental setup described above it is used again to test different 5x5 cm samples. Surfaces with different gradients of curvature in ridges and grooves are tested. The same gradient is applied to specimens with different amounts of ridges. Samples are laid flat so that only nucleation efficiency is tested. The collected mass and the sky view factor are measured. The ratio between these values and the printing time is used to compare the results.

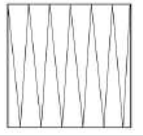
#	Pattern	Laplace Curvature		Number of ridges	Area [mm ²]	Average sky view [%]	Sample weight [g]	Printing time [min]	Collected water mass [g]	Collected mass/printing time	Sky view/Printing time
		Δr Ridges [mm]	Δr Grooves								
#1		2	0	12	3305	86	2,72	27	0,44	0,016	3,185
#2		2	0	6	2759	94	2,72	25	0,45	0,018	3,760
#3		2	2	12	3483	84	2,73	26	0,47	0,018	3,231
#4		2	2	6	2809	93	2,72	26	0,46	0,018	3,577
#5		2	4	12	3868	81	2,75	26	0,39	0,015	3,115
#6		2	4	6	3100	87	2,73	27	0,45	0,017	3,222

Fig.70: Nucleation on undulated surfaces. Results

The results show no particularly significant difference between the different configurations (Fig.70). This might be due to the limited dimensions of the experimenting setup. Complete understanding of the effect of Laplace pressure difference on nucleation rate is therefore not achieved. However, the specimens with the highest scores are two of those with a reduced amount of ridges. Since Laplace pressure gradients are considered to be beneficial for the collection of water (Jie, 2012), item #4 is considered for further research.

The chosen sample is 3d-printed again with different settings. The goal of the experiment is to finalize the optimal strategy for an undulated condensing surface. To do that, the results of the previous experiments are combined and analyzed together. The specimens are printed with layers both parallel and orthogonal to the slope. Additional roughness is added to the last specimen, as it could influence the wettability of the surface.

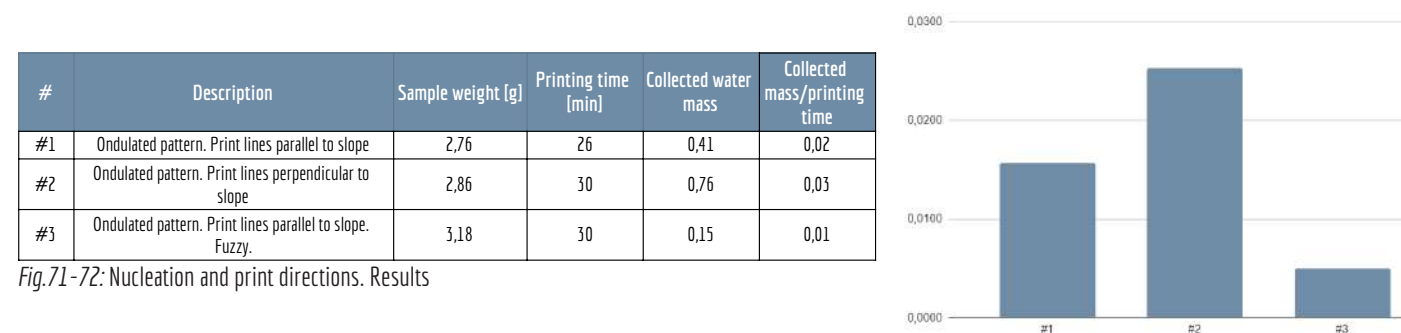


Fig.71-72: Nucleation and print directions. Results

Data (Fig.71-72) show that tiles with orthogonal layers catch more water than the others. The increased roughness does not bring any significant improvement in water collection. When compared to the printing time, this strategy results to be even less efficient in the design of an optimal condenser and it is therefore discarded.

4.2.3 Radar charts

The specimens presented in this final stage show different behaviors, that make them perform in peculiar ways in different fields. For this reason, the different approaches are evaluated qualitatively in terms of multiple efficiencies that relate both to water collection and 3d printability. Comparisons are visualized through radar charts (Fig.73). It is observed that the undulated condenser with the print layers parallel to the slope behaves well in terms of water collection. Its 3d-printing efficiency is fair, too. This approach is therefore considered to be the most promising for the design and will eventually be integrated into the final geometry. However, based on specific requirements, other approaches could also be chosen.

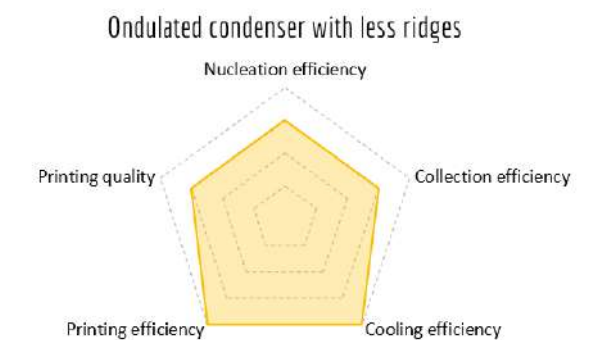
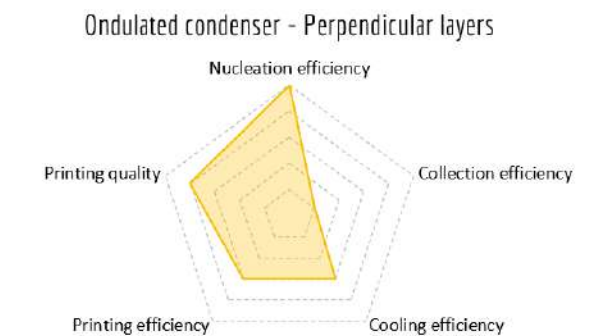
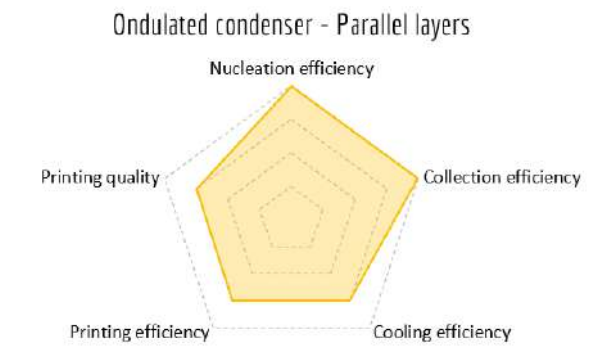
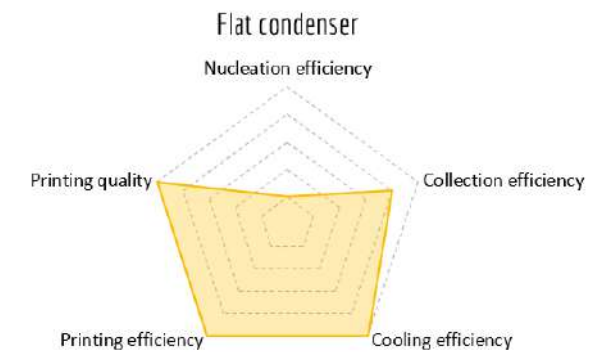


Fig.73: Radiative condenser's surface. Possible strategies

4.3 FOG CATCHING SURFACE

The design of the fog catcher is approached at this point. The pre-design research has shown how the efficiency of such a device is mainly related to its aerodynamic performance. This is measured through the product of two coefficients:

- *Filtered fog fraction*, which represents the share of fog that flows through the collector and depends on its geometry.
- *Incident fog fraction*, which is equal to the amount of that fog that hits and is intercepted by the device.

According to literature (Azeem, 2020), the incident fog fraction depends on the number of intercepting layers and on their solid coefficient. Since these parameters have been extensively researched and discussed in the previous sections of the report, the design process will investigate instead how different geometrical configurations can affect the efficiency of the device.

Two different strategies are investigated and compared from the beginning. The results of the analysis are used to eventually develop the optimal strategy for the design and fabrication of a 3d-printed fog collector. The first approach comes from literature and is that of using multilayer harp screens, which are considered to be the most efficient. On the other hand, the second option is based on the possibilities enabled by 3d printing and looks into generating a tridimensional collector. Following the principle of multifunctionality, the fog collector could in this way be integrated into the structural part of a component.

4.3.1 Multilayer Harp Collector

The experimental setup used in this section consists only of the water nebulizer already introduced for the previous tests. Specimens are placed vertically in front of it and 15 minutes cycles are performed. The mass of the sample is measured before and after the experiment so that the amount of collected water can be determined and the interception efficiency of each configuration can be estimated. As the main goal of this phase is determining if different geometries can improve efficiency, all the samples are designed and printed with the same shade coefficient.

Before proceeding towards the design of multilayer collectors, the first step is that of researching the behavior of different types of permeable screens. Since Additive Manufacturing allows for more complex geometries, different patterns are generated and prototyped into 5x5 cm tiles. The same shade coefficient and printing settings are used for all of them. In this way, it is possible to compare both the amount of collected water and the printing time, which represent the most interesting parameters involved in the fabrication system.

The efficiency of the different patterns is measured through the ratio between collected mass and printing time. Higher values of this coefficient mean higher efficiencies and are therefore preferred.

#	Pattern picture	Description	Area [mm ²]	Shade coefficient [%]	Sample weight [g]	Printing time [min, sec]	Collected water mass [g]	Collected mass/printing time
1		Straight lines	2500	15	1,13	4,26	0,11	0,026
2		Wavy lines, with 6 bumps	2500	15	1,32	5,15	0,11	0,021
3		Straight lines with protrusions on one side	2500	15	1,37	6,47	0,07	0,011
4		Radial pattern	2500	15	1,27	5,56	0,24	0,043
5		Wavy lines, with 12 bumps	2500	15	1,82	7,08	0,17	0,024
6		Straight lines with facing protrusions	2500	15	1,62	6,22	0,11	0,018

Fig.74: Single-layer fog collectors. Results

The data presented in the table above (Fig.74) show the best performing pattern to be the radial one. The amount of collected water is significantly higher than the one recorded for the other specimens. The two patterns with the highest score are considered for further research in multilayer collectors. This means that also the linear infill pattern is considered.

4.3.2 Three-dimensional Infill Collector

Infill patterns available on the Cura Slicer are considered to generate a three-dimensional collector. This is done because they represent a fast and efficient way of performing rapid prototyping, being already embedded in the slicing software. It means that highly computationally intensive 3d modeling of complex patterns can be avoided.

To be considered suitable for fog-catching purposes, infill patterns need to allow air and water flow in both directions. Without this property, water would not be able to move towards a storage area or wind would not be able to blow through the collector. Gyroid and unidirectional linear infill represent the only two options satisfying such requirements. In general, triply periodic minimal surfaces represent interesting options, since these infills have been proved to be efficient both structurally and thermally (Piccioni, 2019).

Cura offers three different infills based on different triply minimal surfaces. All of them have been used to prototype a block (5x5x1.5 cm) with the same infill percentage (12%). As for the previous experiments, the samples are exposed for 15 minutes to the fog flow generated by the nebulizer. The amount of collected water and its relation with the printing time are used to compare and evaluate the results.

The tested minimal surfaces are (Fig.76):

- Gyroid surface
- Schwarz P (Primitive) surface
- Schwarz D (Diamond) surface

#	Description	Solidity [%]	Print quality	Structural capacity	Shape flexibility	Print time [min]	Print length [m]	Mass [g]	Final mass [g]	Collected mass [g]	Collected mass/time
#1	Infill collector. Gyroid	12	++	++	++	34	2	8,76	9,33	0,57	0,017
#2	Infill collector. Primitive	12	-	++	+	38	1,89	8,67	9,23	0,56	0,015
#3	Infill collector. Diamond	12	+	++	++	35	1,95	8,39	8,91	0,52	0,015

Fig.75: Infill fog collectors. Results

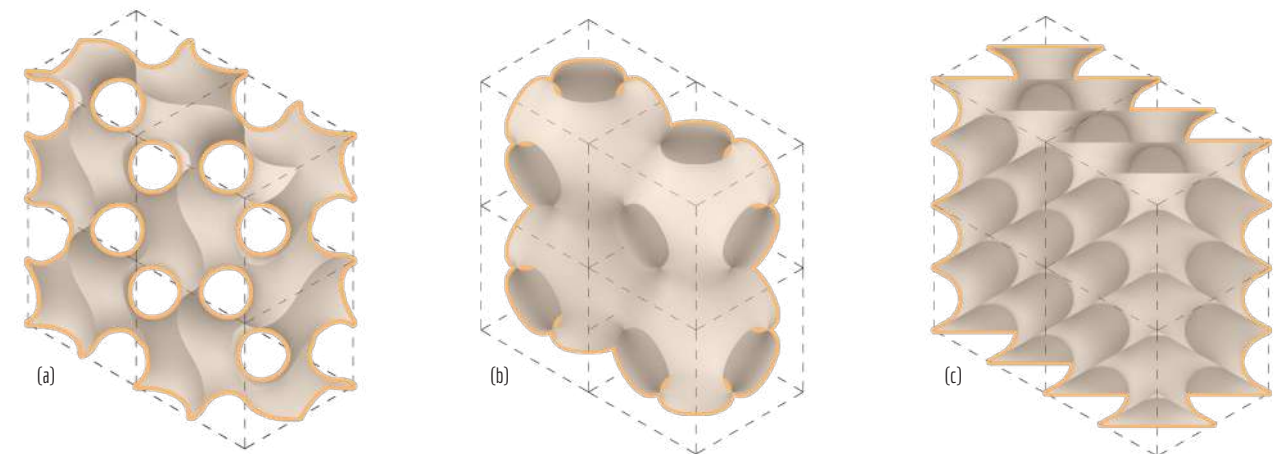


Fig.76: Triply minimal surfaces. Gyroid (a), Primitive (b) and Diamond (c)

The results of the analysis (Fig.75) show that there are no particular differences in the performance of the different samples for what concerns both printing time and water catching capacity. Qualitative analysis, based on visual inspection of the specimens, points out the lower print quality of the Schwarz Primitive pattern. This is due to the extreme fragmentation of each printing layer, which forces the extruder to stop and move a lot. Such behavior is usually not desired, as it leads to longer printing time and part defects such as stringing. On the other hand, the gyroid iteration shows the best results for both qualitative and quantitative parameters. For this reason, this pattern is taken into account for further comparison with the multilayered approach illustrated above.

4.3.3 Comparative analysis

The results from the previous sections are used to perform a final comparative experiment. In addition, a hollow 5x5x1.5 cm box is printed and used as an initial reference for the other specimens. A block with vertical linear infill is prototyped as well and tested as possible intermediate solutions between the two different approaches developed so far. For this experiment, all the samples are printed with a solid coefficient (equivalent to infill percentage) of 0.4. Multilayered collectors are printed with four collecting screens.

Qualitative and quantitative data are recorded for all the specimens. These include the structural capacity, the printing time, and the collected amount of water. As for the previous experiments, the efficiency of the sample is measured through the ratio between the water mass and the printing time.

#	Description	Solidity [%]	Print quality	Structural capacity	Shape flexibility	Print time [min]	Print length [m]	Mass [g]	Final mass [g]	Collected mass [g]	Collected mass/time
#0	Hollow specimen. Tested for reference	0	/	/	/	11	0,56	1,58	1,59	0,01	0,001
#1	Multilayer harp collector. 4 layers	40	+	-	+	16	0,82	2,39	2,77	0,38	0,024
#2	Multilayer radial collector. 4 layers	40	+	-	-	16	0,7	3,72	4	0,28	0,018
#3	Infill collector. Lines.	40	++	+	++	100	6,57	19,91	20	0,09	0,001
#4	Infill collector. Gyroid	40	++	++	++	86	3,23	12,83	13,66	0,83	0,010

Fig.77: Multi-layer fog collectors. Results

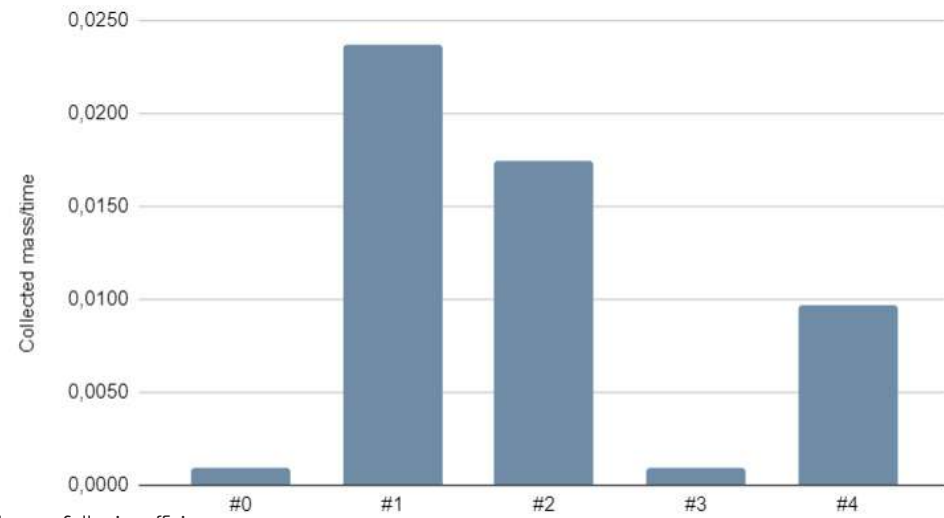


Fig.78: Multi-layer fog collectors. Collection efficiency

It is possible to see in the Fig.77 how the gyroid infill collector collects the highest mass of water. On the other hand, the difference in printing time and printed length between it and the multilayer harp collectors results in an overall worse performance.

As it can be seen also in the graph (Fig.78), the linear harp collector scores the highest result in terms of balance between fog-catching and printability performance. However, as the visual and qualitative analyses show, this approach cannot be considered suitable for applications where the structural capacity of the collector is needed.

4.3.4 Radar charts

The analysis presented in the previous section shows how differently the two different strategies behave. Depending on the application, both of them could represent a viable option. For this reason, they have been cataloged in a series of radar charts (Fig.79) that highlight their different performance and allow to easily choose the best option for a specific application.

This research focuses on developing a solution that could be as easy and fast to print as possible. Structural capacity is not necessarily a requirement in this case, as long as the component can withstand its weight. Therefore, the multilayer harp collector is considered to be the most promising strategy to integrate into the design of a final geometry.



Fig.79: Fog collectors. Possible strategies

4.4 COMPONENT DESIGN

4.4.1 Conclusions from previous sections

The sections above describe the research on the most efficient 3d printed surfaces for fog and dew collection. The results of this analysis are then integrated and combined into the design of one building component.

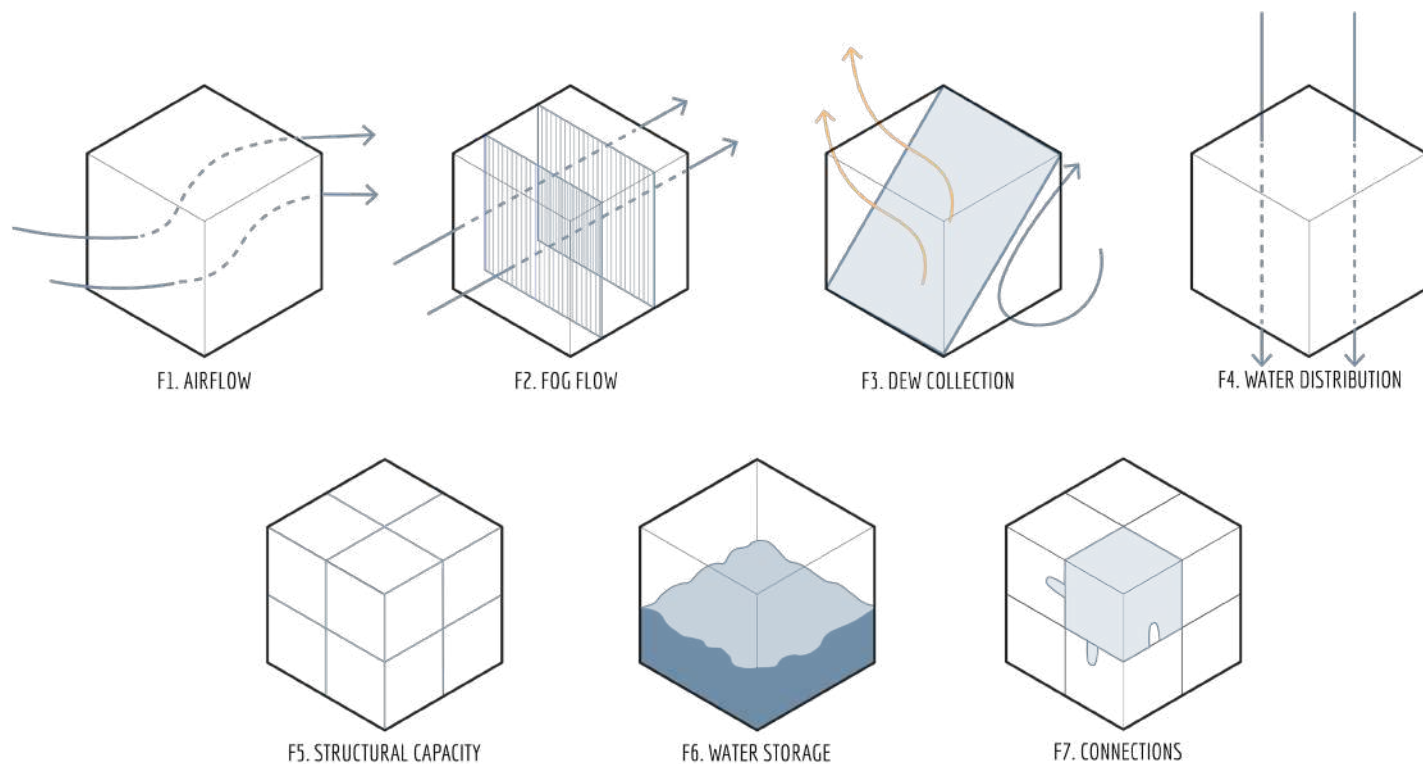
- *Dew*: the results show the importance of aligning slope and print layers. It is shown how an undulated surface is beneficial to increase water collection and the directionality of the surface. The dependency between nucleation rate and the number of ridges has been proven not to be relevant, so fewer ridges can be used to reduce printing time. Laplace pressure gradients do not lead to significant increases in printing time, so they can be implemented to improve the collection, even if they have not shown particular benefits in water nucleation.

- *Fog*: Multilayer collectors have shown higher interception efficiency when compared to the printing time. Single layers analysis has shown how harp or radial collectors collect more water than other configurations. According to literature, a shading coefficient between 0.4-0.6 is considered, for a maximum of 5-6 layers (Regalado, 2016).

4.4.2 Water-catcher Design Method

In this section, a method for designing a water-catcher is presented. Such methodology will then be applied to produce a specific geometry but could be applied as a general guideline for the design of different building components for different scenarios. The first necessary step for the design of a water-catcher is the clear definition of the functions that need to be integrated into the component. The main ones are those related to dew and fog collection, but more secondary ones need to be performed as well. Functions related to water distribution and storage are identified together with those related to structural stability and connections between modules.

The definition of the seven elements shown in the diagram below already suggests a specific orientation for some of them (Fig.80). This is based on physical parameters such as the flow of water or air, and the exposure to the sky. What is still not considered at this stage is the influence of the fabrication method, in which the part orientation has to be decided and can significantly influence the outcomes.



The analysis of the optimal condenser surface has also revealed the importance of aligning the print layers with the direction of the slope to improve the dew collection rate. Part orientation for 3d printing can then be introduced as a design variable and can become a useful guideline to orient and combine different functions. For this reason, the optimal print direction is determined for all the functions listed before (Fig.81).

The preferred print direction is identified through the desired orientation of the z-axis. To compare the results for different functions, the position of the axis is referred to the way a specific function has to relate with the environment. The result is an optimal orientation of the functions relatively to the sky and ground position. Different considerations can be derived from this representation.

- The fog-catching function does not have a specific orientation within this reference system. It is known that it should be perpendicular to the main wind direction. Since geometric changes can influence the airflow, this function does not represent particular limitations to the design.

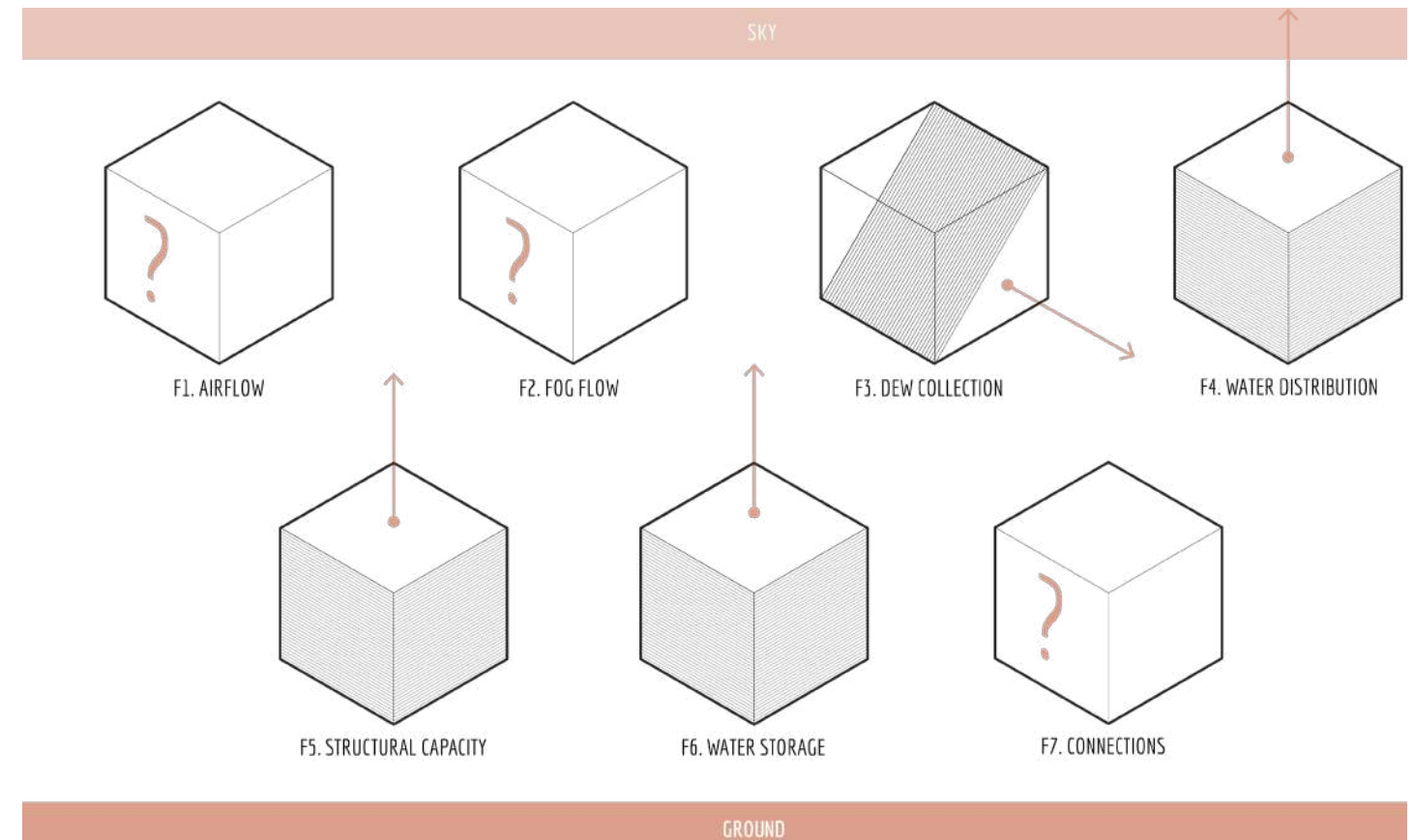
- It has been experimentally proven that in a condenser, the print layers should be aligned with the slope. An angle is desired to have both sky exposure and sufficient collection rate, but in this reference system, the printing axis can be considered horizontal.

- The water flow and storage systems present a vertical axis. This is because these processes are governed by gravity and the easiest flow would be a vertical one. For these reasons, a hollow vertical element would be preferred.

- Similarly, the structural function's optimal orientation would be vertical. This is because the main load the element needs to withstand is its weight, which is acting vertically towards the ground. Elements with print layers orthogonal to the direction of the load are considered to be stronger.

- No specific direction can be determined for the connections between modules. They will be designed in different ways according to the requirements of the design.

Knowing the optimal print direction describes another necessary step for the design of an efficient component. Functions with the same print direction can easily be combined, while the integration of the others plays an important role in the definition of the geometry. This analysis represents the starting point for the design of many different building components and in a conceptual phase ensures efficiency in 3d printing and water collection efficiencies.



4.4.3 Building component's orientation

The methodology described above can be applied to the design of different components. For a building envelope component, either a vertical or a horizontal orientation has to be defined (Fig.82). This choice can be related to different constraints such as the roof or facade surface available for the intervention and the local dew and fog events frequency.



Fig.82: Possible envelope component's orientations

The current research considers as a generic case study the Moroccan cityscape, which is generally characterized by low-rise buildings. For this reason, a 4x4x4m cube is analyzed in simulations to approximate a building. Looking at this scenario, both orientations are possible.

- *Vertical*: it is more exposed to fog than to dew. Depending on the density of the urban surroundings it might be harder to integrate in low-rise buildings.
- *Horizontal*: it has higher exposure to the sky, and therefore increased dew and rain collection potential. Wind flow might be limited because of reduced velocities close to the roof surface.

Since the building block considered for simulations is extremely schematic, the difference between horizontal and vertical orientation is analyzed further and quantified. To estimate water yields for the two options, the Excel-based predictive models presented in the pre-design phase are used.

The research in architectural aerodynamics has shown how both the windward facade and roof surfaces correspond to low-velocity areas. This has been tested through wind tunnel CFD (Computational Fluid Dynamics) simulations performed in the web-based software SimScale. Since a building component is supposed to adhere to the building surface, one of the design goals for both scenarios is to accelerate the airflow in the mentioned low-velocity areas. In this way, fog collection can be enhanced.

To compare the two situations, a simple geometry is modeled and tested in both orientations. It consists of a square pipe with a progressively reducing section. In this way, the wind velocity is increased at the outlet, and suction is created at the inlet. In the horizontal option, an overhang is added to induce air movement towards the inlet. The effect of these geometries is tested in a wind tunnel simulation in SimScale (Fig.83). The flow is assumed to be steady and incompressible. The velocity at the inlet of the tunnel is set to 6 m/s and a slip condition is set on the bottom face to simulate the wind boundary effect.

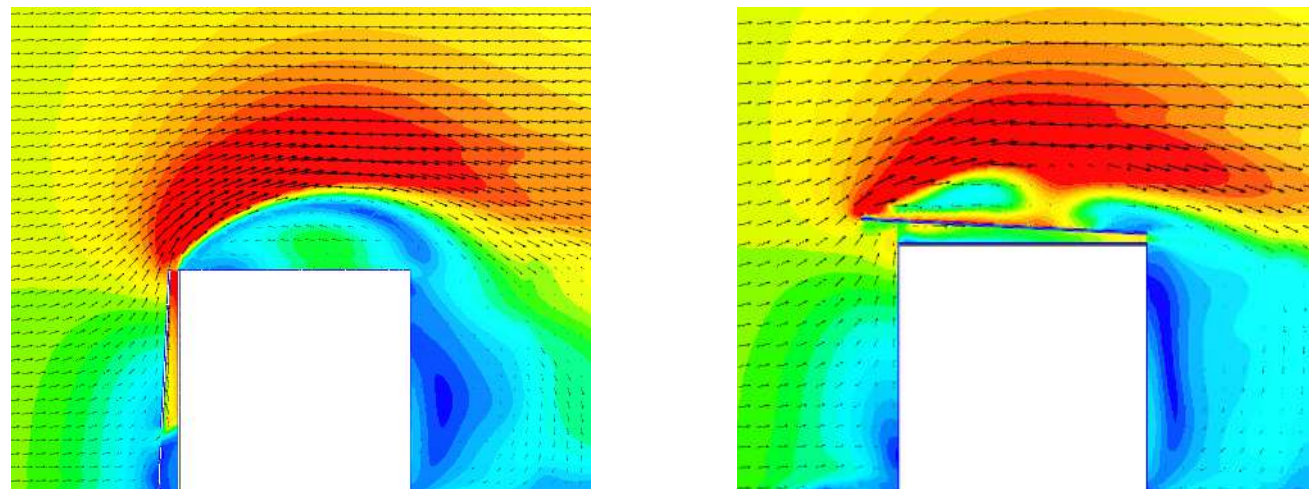
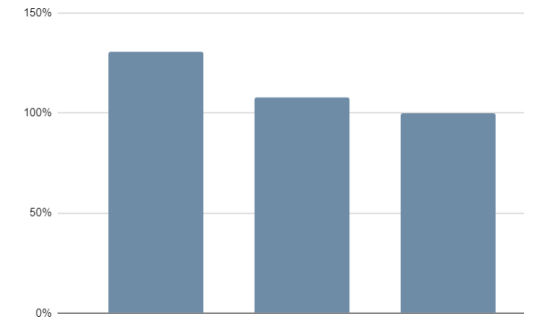


Fig.83: CFD simulation results for different orientations

The simulations are used to get an overview of the velocity's distribution over the building and through the geometry. The speed and the airflow in the middle section of it are measured and used to estimate the amount of water that could be collected during a fog event. Results are compared to those calculated for a standard single-layer collector exposed to wind with the same speed of that set in the wind tunnel simulation (6 m/s). A solid coefficient of 0.4 and a fog's liquid water content of 0.5 g/m³ are considered for all the calculations. Results are shown and compared in the table and graph below (Fig.84-85).

	V _{reference} [m/s]	A _{middle} [m ²]	Flow [m ³ /s]	J [g/sm ²]	J [l/hm ²]	%
Vertical	7,12	0,12	0,361	0,60	2,17	131
Horizontal	6,39	0,12	0,298	0,50	1,79	108
Standard	6,00	/	/	0,46	1,66	100

Fig.84-85: Fog collection yield. Results.



Since the airflow measured inside the geometries is forced through the collector, no filtered fog fraction coefficient is considered. This means that all the air that flows in the object collides with the fog-catching screens, generating a significant increase in water yield for both options. However, the vertical solution results to be the most effective, with a 31% increase in efficiency.

To have a complete overview of their behavior, the two orientations are compared also in terms of dew collection. To provide an estimation of the water yield, the first step has been determining the average sky view factor of the two options. The plug-in Ladybug for Grasshopper, is used to perform the calculation (Fig.86).



Fig.86: Sky View Factor simulations

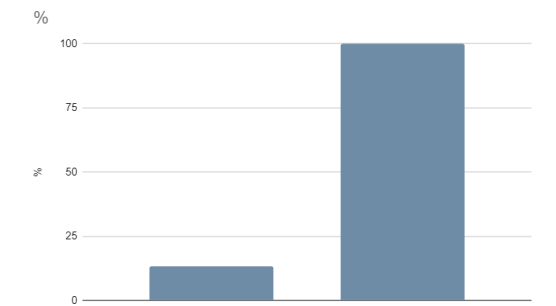
As predictable, the vertical orientation translates into a lower sky exposure (62%). This value is introduced into the Excel predictive model realized in the pre-design phase as a reduction factor of the radiative heat transfer coefficient. A value of 0.92 is considered as IR emissivity for PETg. Ideal conditions for condensation are set for the simulations (Fig.87).

IR Emissivity	0,92			
T _{air}	15	°C		
Cloud Coverage	0	%		
Wind Speed	1,5	m/s		
Relative Humidity	85	%		

	J [l/hm ²]	%
Vertical	1,94E-03	13
Horizontal	1,46E-02	100

Fig.87: Simulation input parameters

Fig.89: Dew collection yield. Results



The vertical orientation would generate a dew yield equal to 13% of the one that the horizontal option would achieve. The graph highlights how much sky exposure can affect water yield by condensation (Fig.89). The gap increases even more when considering the amount of surface exposed to rain and useful for rainwater collection. Since fog and dew happen with different frequencies, the data published by Lekouch (2012) are used to provide a weighted estimation of the total water yield. Further details can be found in Appendix V.

	Fog [l/hm ²]	Dew [l/hm ²]	Total [l/hm ²]	Weighted total [l/hm ²]
Vertical	2,2	1,9E-03	2,2	4,4E-02
Horizontal	1,8	1,5E-02	1,8	4,9E-02

Fig.90: Weighted results.

The result of this calculation for the case study in Morocco shows an higher water collection potential for horizontal orientations (Fig.90). For this specific scenario, a roof element is designed.

4.5 SCHEMATIC DESIGN

The design of the roof component starts from analyzing function by function the optimal orientation and print direction. According to the workflow described in the previous section, this helps in understanding the configuration of the geometry (Fig.91). The wind prevalent direction, which is parallel to the roof surface, is the main factor influencing the position of the fog and dew collectors. As it is possible to see from the image below, the water-catching functions share their optimal print direction. On the other hand, the best orientation for structural, water distribution, and storing functions would be perpendicular to it. This suggests that the distribution and storage of the collected water can be performed by a separate element that can be combined with the collector. For what it concerns structural performance the not optimal printing axis can be chosen as long as the part is still printable and the stability is ensured by geometry. However, the structural optimization of the component is not one of the objects of the research.

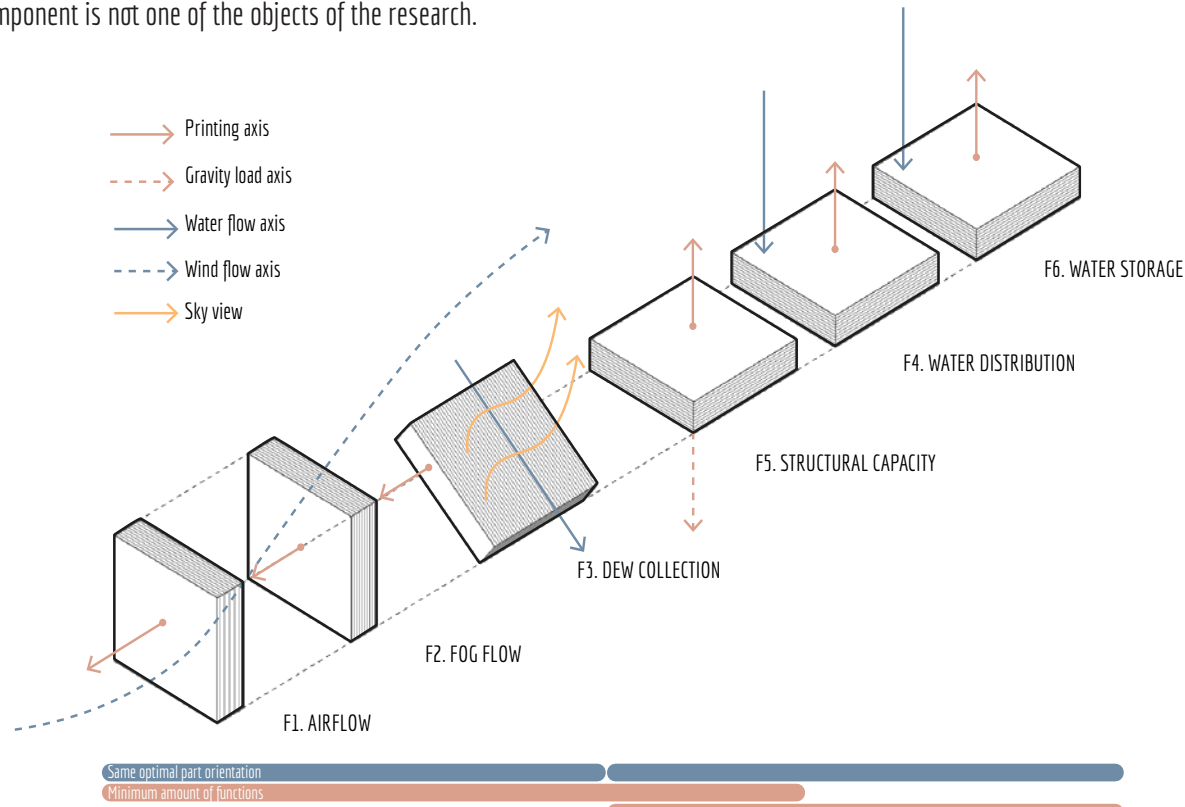


Fig.91: Roof component. Optimal orientation of functions

The previous considerations can be used to develop a first rough design (Fig.92). This version is then researched and optimized to achieve the desired performance. The relevant features that can be observed in the scheme are:

- Separate storage unit, with vertical printing axis (*Structural stability ensured by fabrication*)
- Collecting unit, with horizontal printing axis (*Structural stability ensured by geometry*)
- Inclined condenser surface, with print layers aligned with slope direction.
- Fog catching surfaces in an enclosed space, to increase wind velocity.

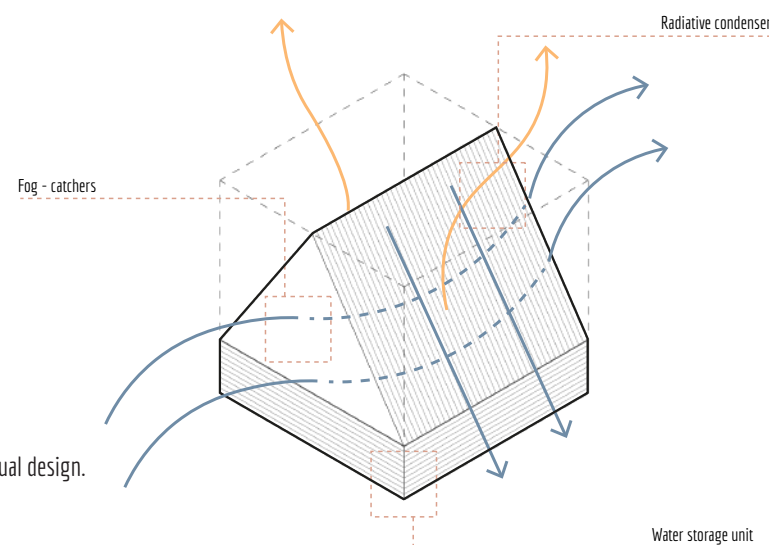


Fig.92: Roof component. Conceptual design.

Besides the importance of the part orientation, 3d printing fabrication presents other limitations that can be translated into design constraints. In this way, design iterations can be evaluated and possibly discarded during the process. The component has to fulfill three main requirements that can be summarized as (Fig.93):

- can fit in the printable bounding box allowed by the Anycubic Chiron (400x400x450mm) or has to be composed by a limited amount of modules that respect those maximum dimensions
- does not exceed the maximum printable overhang angle (45 degrees). This is done to ensure print quality while keeping standard settings easy to replicate
- does not exceed the maximum bridging span in the realization of the wind-catching surfaces. This distance is defined experimentally further in the research.

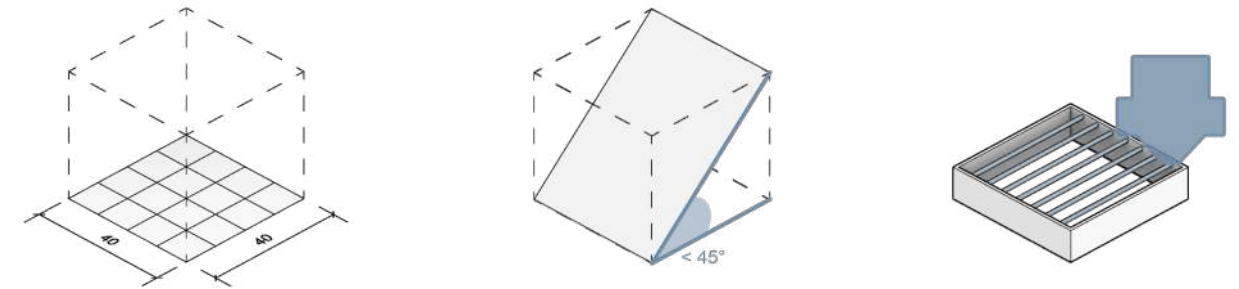


Fig.93: Fabrication constraints

Between these requirements, the maximum dimensions represent the most important one in the early stages of design. Since the atmospheric water collection rate grows proportionally to the surface area exposed either to the night sky or to a fog flow, the goal is to maximize the size of the component while keeping it printable.

For this reason, the printable bounding box is taken as the initial volume of the geometry. Within the water-catcher module, two regions are identified in this cube. They correspond to the front and lateral sections of the component. According to the principle that has been used so far, the two sections are approached separately to break down the design problem into smaller tasks. These tasks can be summarized as (Fig.94):

- Lateral section (*Fog Section*). Definition of inlet and outlet shape. Design of the geometry's profile to maximize wind flow.
- Frontal section (*Dew Section*). Definition of the inclined profile for dew collection.

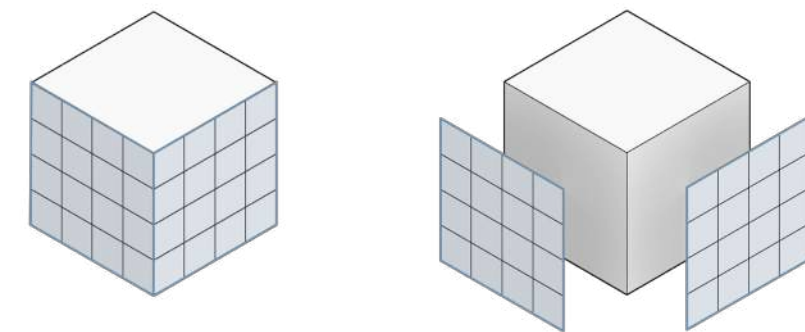


Fig.94: Module's design approach

4.5.1 Fog Section

As shown before, a roof component is placed on a low-velocity area around a building. The concept for the fog section is to force the flow into an enclosed space to accelerate it. With the simplification of considering an incompressible steady flow of air, the Bernoulli equation can be applied. It states that by reducing the height and the size of a channel, it is possible to create an acceleration in the flow and a reduction of pressure that helps sucking in more air. The most important parameter to maximize the fog collection performance is the total flow rate of air through the geometry. Different elements are considered to be important to increase this value. The main ones are the inlet design, the overall depth of the component, and the outlet size.

Such features are studied through computational fluid dynamics (CFD) wind tunnel simulations and then compared. Airflow pattern and velocities distribution through the component are analyzed. The design is defined step-by-step until a final optimal solution is achieved. The main phases of this process can be seen in the image below (Fig.95). The section is divided into a regular grid (a) and the maximum inlet's height is fixed to ensure maximum flow (b). The significant cells for the definition of the inlet's shape are identified (c) and different inclinations are compared (d). Once the inlet is defined (e), different options for the internal inclination of the component are compared (f).

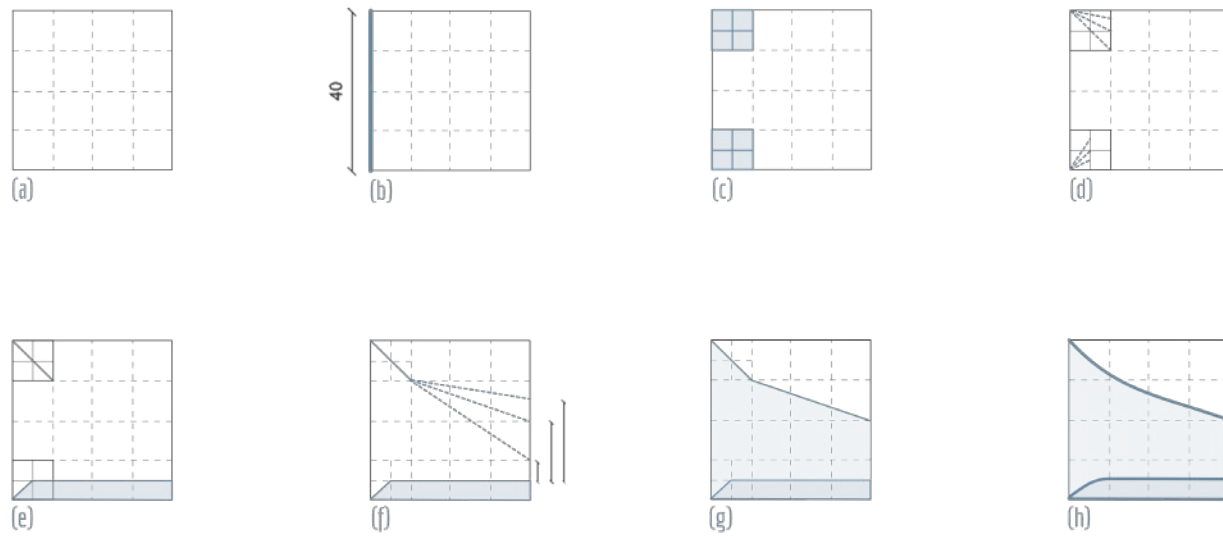


Fig.95: Fog section. Design steps

These inclinations affect the outlet height and have to take into account the maximum printing bridge for the wind-catchers. When one profile is chosen, the section is defined (g) and can be smoothed and tuned for better fabrication and aerodynamic behaviour (h).

To start this process, two preliminary actions have been performed. This is due to the need of defining an initial geometry to perform comparative CFD analysis. The first simulations look into understanding the optimal curvature approach for the section and its modular size so that an adequate grid system can be defined and used for the rest of the process.

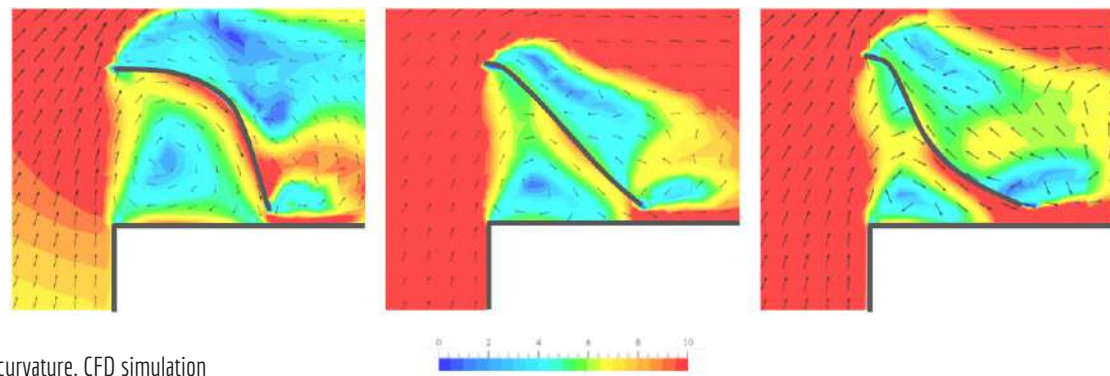


Fig.96: General curvature. CFD simulation

As it is possible to see from Fig.96, convex shapes generate circular motion of air that is not optimal for fog collection. A laminar flow is desired. This condition is already improved by straight or concave shapes. However, the last option shows the highest speeds at the outlet and the smallest recirculation area. For this reason, similar geometries are analyzed in successive steps.

The second simulation compares instead the behavior of a single and a double-module component. The results (Fig.97) show no particular differences in speed at the outlet. However, the length of the double-module option increases the laminarity of the flow in the final section of the module. In addition, a circular motion with reduced velocities can be observed in the low-pressure area outside the object. Even if this does not concern the fog collection, it is considered to be beneficial to increase the condensation rate. For this reason, a double module is considered more efficient and taken into account for future simulations.

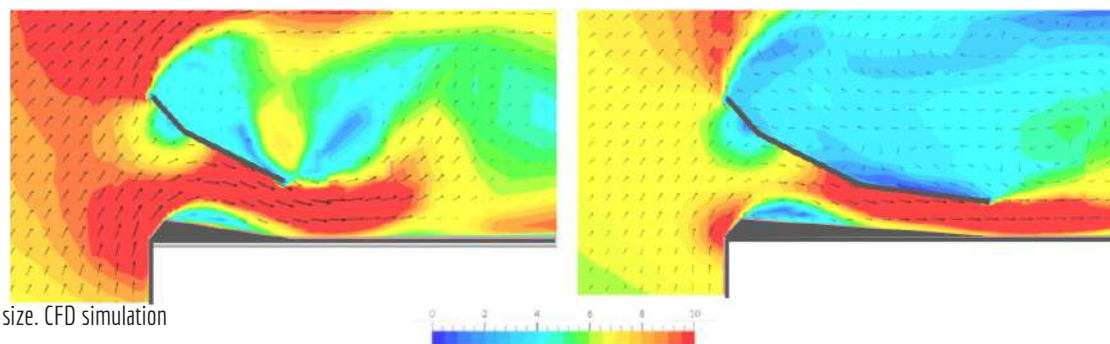


Fig.97: Modular size. CFD simulation

The previous experiments already show a defined geometry. However, this has been produced manually according to intuitive knowledge of a possible efficient option and represents just the first iteration of the step-by-step design workflow explained before. Different geometries are produced to analyze specific other parameters that influence the overall performance. The first ones to be researched are the best inclination of the inlet region and the best internal profile.

Three different inclinations are tested for the inlet (15°, 30° and 45°). No angles above 45 degrees are considered, as they would exceed the maximum printable overhang. The results of the wind tunnel simulations are qualitatively compared in terms of induced airflow through the geometry. Such an evaluation is performed in this stage by observing the airflow pattern and the velocities close to the inlet (Fig.98). A point where the speed decreases to almost zero can be observed in all the options: this location is where the wind direction is perpendicular to the surface and its kinetic energy is transformed into static pressure. A design is considered more efficient when this phenomenon occurs as close as possible to the outer edge of the component.

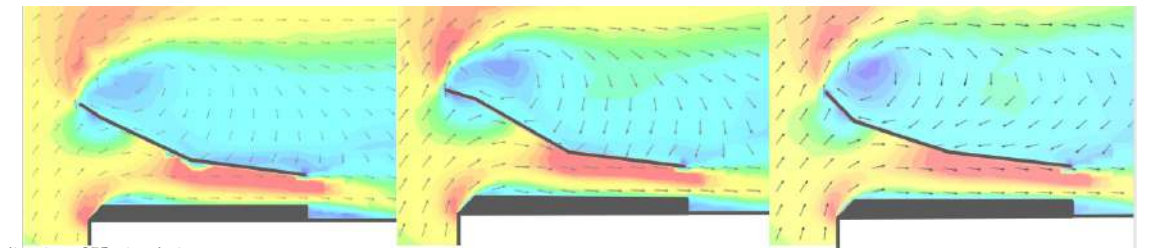


Fig.98: Inlet inclination. CFD simulation

The results show how smaller inclinations behave better in terms of moving outwards as much as possible the static pressure point, while still inducing the air to flow through the element. The inlet with an angle of 15° is considered the most promising option.

A further evaluation concerns the profile of the section from the end of the inlet region to the outlet. Different iterations with different intermediate and final heights are produced and tested. Heights from 5cm to 15cm are taken into account for the intermediate sections. Wind velocities are then observed and the flow rate at the inlet is measured. The option with the highest flow rate value is considered to be the most efficient.

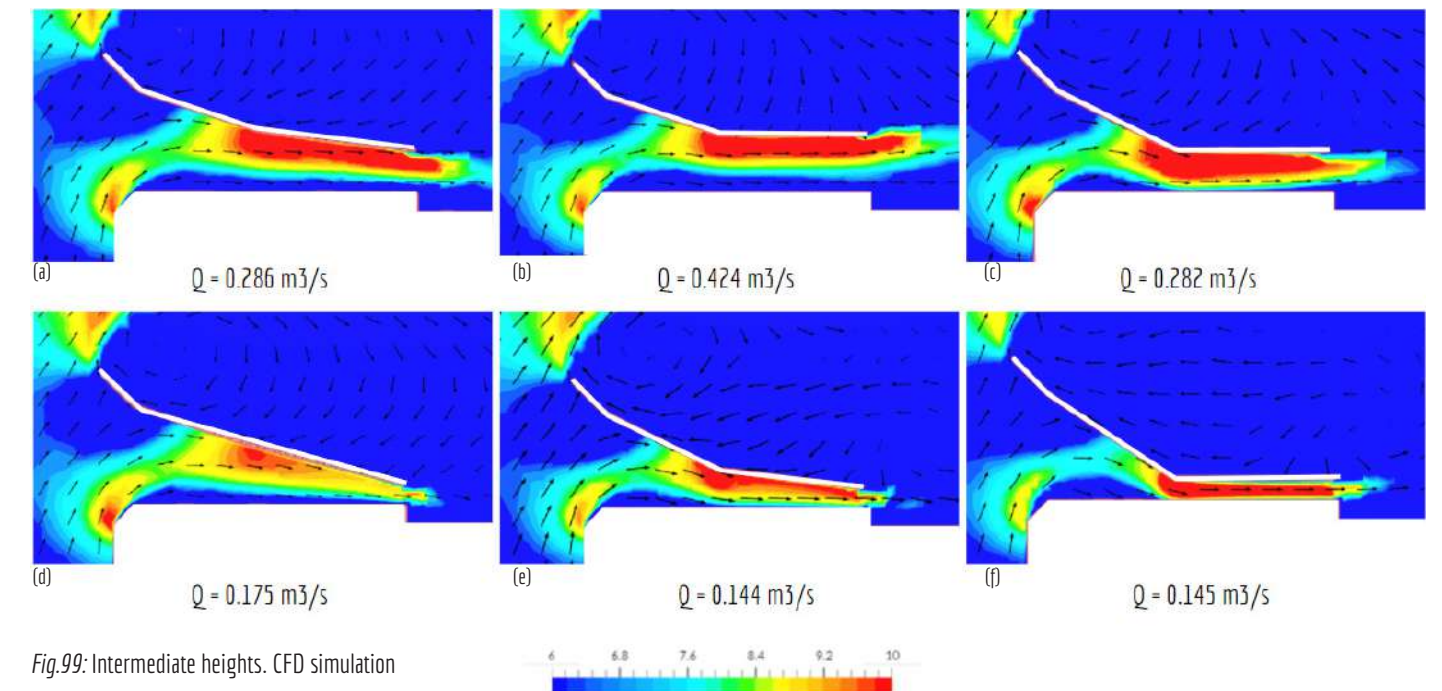


Fig.99: Intermediate heights. CFD simulation

Results of the simulations are color-coded to highlight only the velocities higher than the initial one set for the wind tunnel simulation (6 m/s). It is possible to see (Fig.99) how larger outlet heights produce more significant boundary layers on the bottom surface of the element. This means that the collection rate would be less in this region. On the other hand, such behavior could be beneficial to achieve an efficient flow of water from the collecting to the storage unit.

When looking at the flow rate, one of the options behaves particularly well (b). This alternative has a constant height of 15 cm throughout the whole second module. The absence of an overhang angle makes it also particularly suited for 3d printing. It has still to be tested if such a distance can be efficiently bridged to print the wind-catching screens. At this stage, the combination of this section and the optimal inlet inclination studied before is considered enough to move to the definition of the Dew Section.

4.5.2 Dew Section

Once the lateral section is defined, the definition of the frontal Dew Section can proceed faster. The features that need to be integrated in this process are the inclination and the profile of the condensation top surface and the definition of a system to store the collected water, which can be at the same time protected from the dirt and easy to access for inspection and cleaning.

As for the previous chapter, this process is articulated in a series of steps (Fig.100).

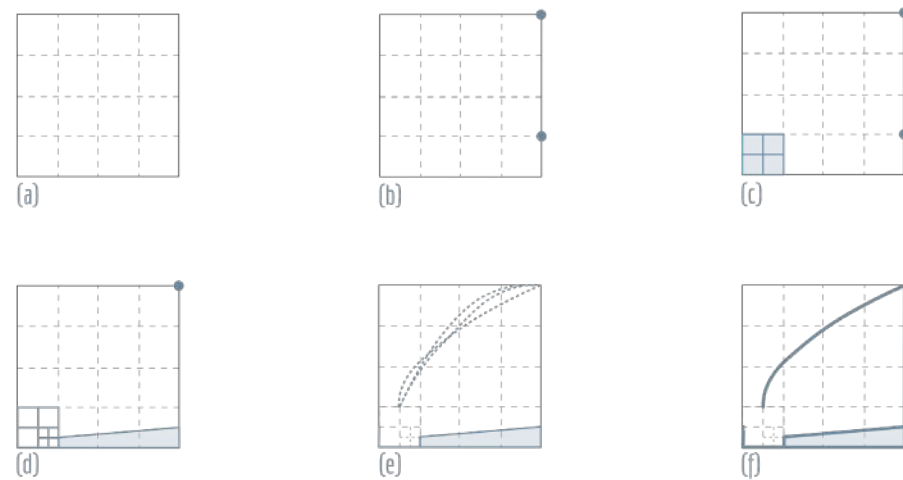


Fig.100: Dew section. Design steps

After the definition of a grid system (a), the relevant information of the fog section are reported (b). A region for the collection and storage of water is identified (c) and shaped so that constant slope is created to facilitate the movement of droplets (d). Finally, different profiles are evaluated (e) until one is chosen and the section can be finalized (f).

To evaluate the different profiles, the cooling capacity of the resulting surface is analyzed. The same reference profile at the outlet and the profile chosen in the previous section is used to generate different surfaces. A conjugate heat transfer analysis is performed on the simplified shapes through the SimScale engine. This analysis takes into account both wind-driven convection heat transfer and radiative heat losses. To perform the analysis, the properties of PET plastic are introduced in the simulator, and a wind speed of 1.5 m/s is set at the inlet. To simulate the night sky towards which radiation happens, the upper face of the domain has been set to a temperature of -2°C (Terré, 2014). All the other surfaces have been set as transparent to radiation.

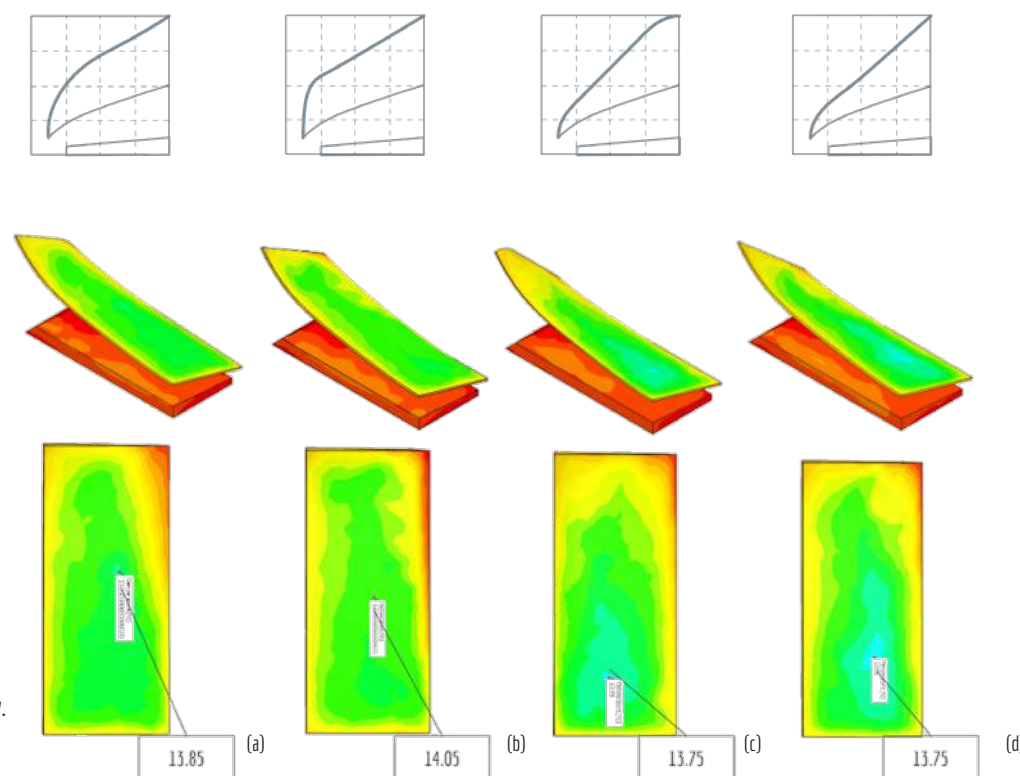


Fig.101: Cooling capacity. CHT simulation

Due to the relatively small geometrical variations between the surfaces, small temperature variations have been observed (Fig.101). As these differences could become more important with higher wind speeds, the analysis is used to choose the optimal profile. Two of the surfaces tested in the previous experiment, show the same cooling potential. Option (d) is preferred, as it has higher curvature at the top and this improves also water collection.

The definition of the condensation profile concludes the schematic design phase. The result is a primitive design (Fig.102), that embeds the main information about the dimensions and curvatures of the element. It is now possible to develop further each element, ensuring optimal performance and printability.

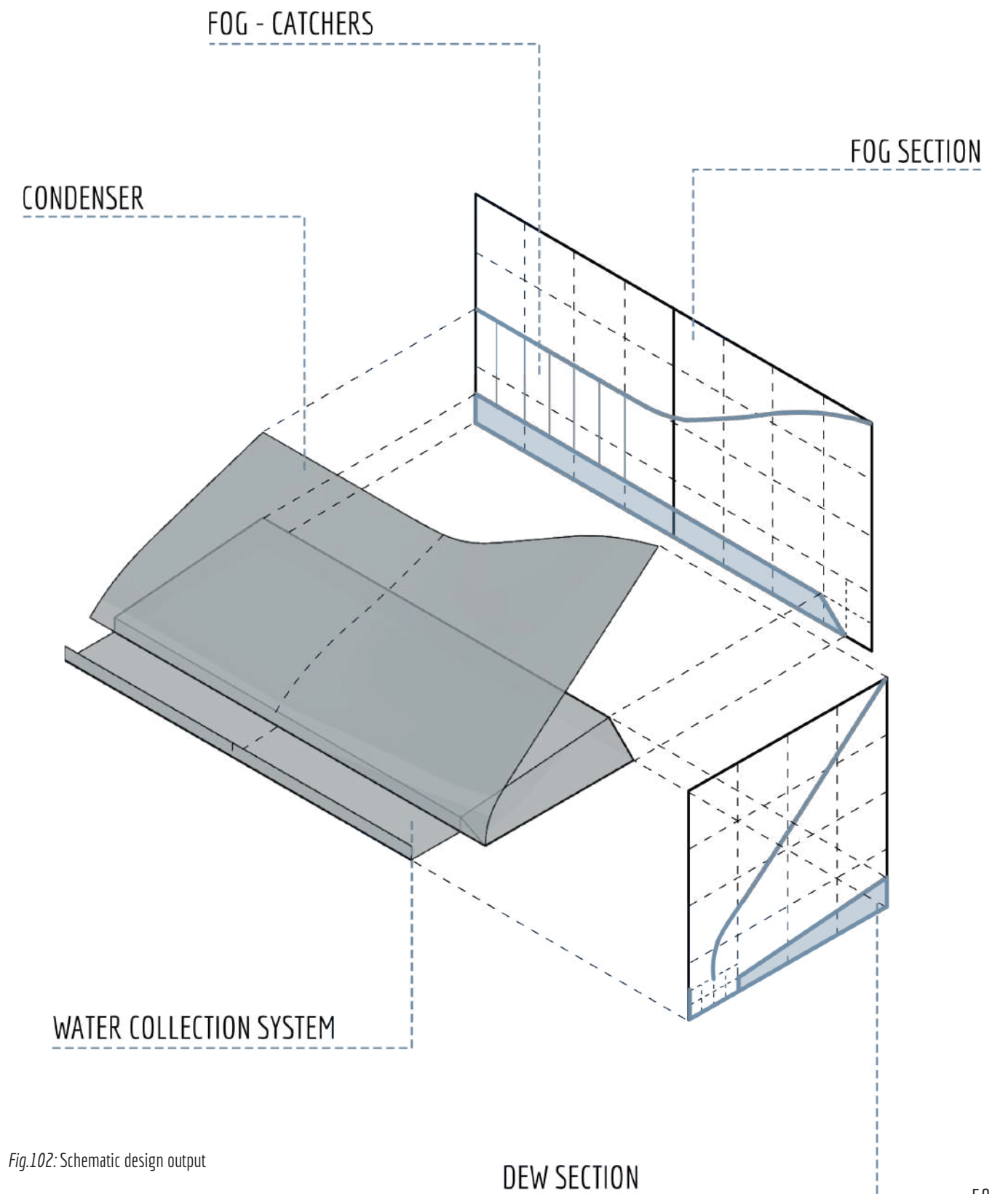


Fig.102: Schematic design output

4.6 DESIGN DEVELOPMENT

Different aspects of the design are progressively improved iteration after iteration. The goal of this process is to transform the schematic design into a printable product, that can be prototyped and tested. The main aspects that have been developed are presented in the following section.

Condenser surface

The shape of the condenser surface has been defined in the previous section. Thanks to the analysis of the print direction, the slope is aligned with the print layers. This property has been proven to be beneficial to reduce the sliding angle of a surface and to improve the water collection rate. The previous analysis showed also the benefits brought by undulated configurations to the water nucleation rate.

For this reason, a sinusoidal pattern is generated on the surface. The density and depth of the ridges are determined according to the results of the research on condensing surfaces. A reduced amount of ridges has shown better results in the ratio between water collection and printing rate. One ridge per cm is approximately modeled.

In the previous chapters, the concept of Laplace pressure gradients to improve water collection has been presented. Even if no significant benefits for water nucleation were found, the introduction of such gradients has no relevant impact on the printing time. For this reason, different degrees of curvature are introduced in the top and bottom sections of the surface (Fig.103). In this way, both ridges and grooves present gradients of curvature that should enhance collection capabilities.

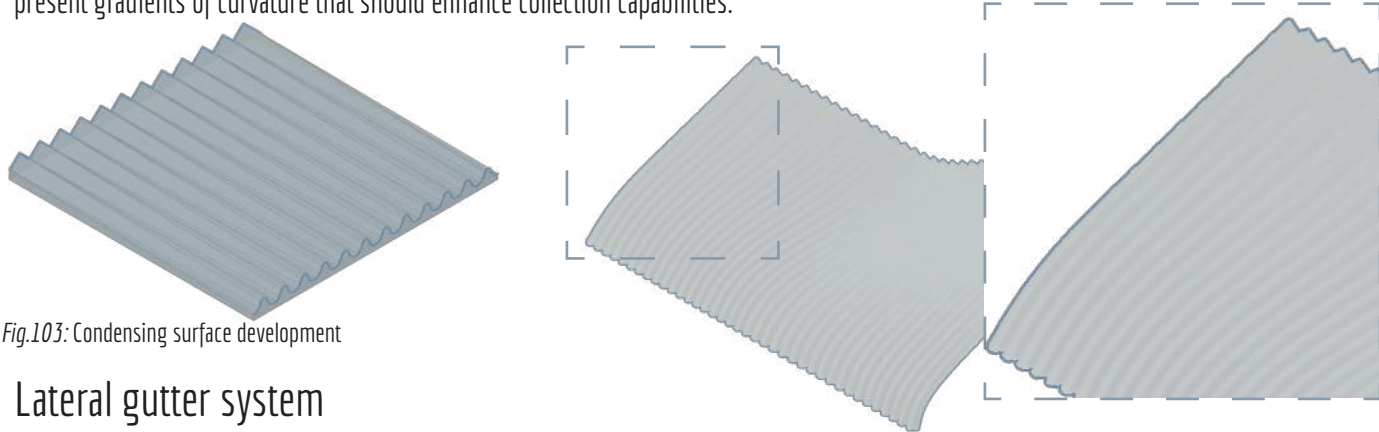


Fig.103: Condensing surface development

Lateral gutter system

The schematic design has introduced the need of having a water collection system on one side of the element so that the water collected through both dew and fog can easily be stored and measured (Fig.104). The design of this system takes into account that the prototyped design will be used and tested on an existing roof. It cannot be connected to a more sophisticated system, as it would be designed in a real-life scenario. Important features of this system are that it has to be fast to print, easy to inspect, and well protected from the incoming wind and dust.

The initial design (a), has a width of 10 cm and a depth 2.5 cm. A 5 cm wall on the side, protects the elements and offers possible support for the connection between neighboring units. Initial prototypes and printing tests with higher speeds show that sharp corners are more difficult to print. For this reason, an fillet version of the first version (b) is designed and tested. Printing quality improves significantly when corners are rounded. The final option (c) is eventually elaborated to provide higher protection to both the gutter and the wind-catching element.



Fig.104: Gutter system. Design iterations

Water tray

In the roof component that will be prototyped, the gutter system described above is combined with a water tray that can be removed. In this way, collected water can easily be measured daily and the system can be cleaned (Fig.105). The design of this tray, which was at the beginning extremely simple (a), evolved over time. The final shape (b), takes into account the maximum printable dimension and has therefore

a length of 40 cm. Two trays are therefore needed for the prototyped geometry. As it is possible to see from the section drawing, the geometry of the tray is slightly more elaborated. The shape is thought to both allow for droplets to slide and store higher amounts of water in a more protected way. In this way, morning water evaporation or dust contamination can be limited.

However, as the design of the prototype does not have to represent exactly the final product design, different variations can be imagined. For example, the presence of a base support for the part can provide enough room for water collection into bottles or small tanks. To facilitate this, modular trays with connectors for them can be designed (c).

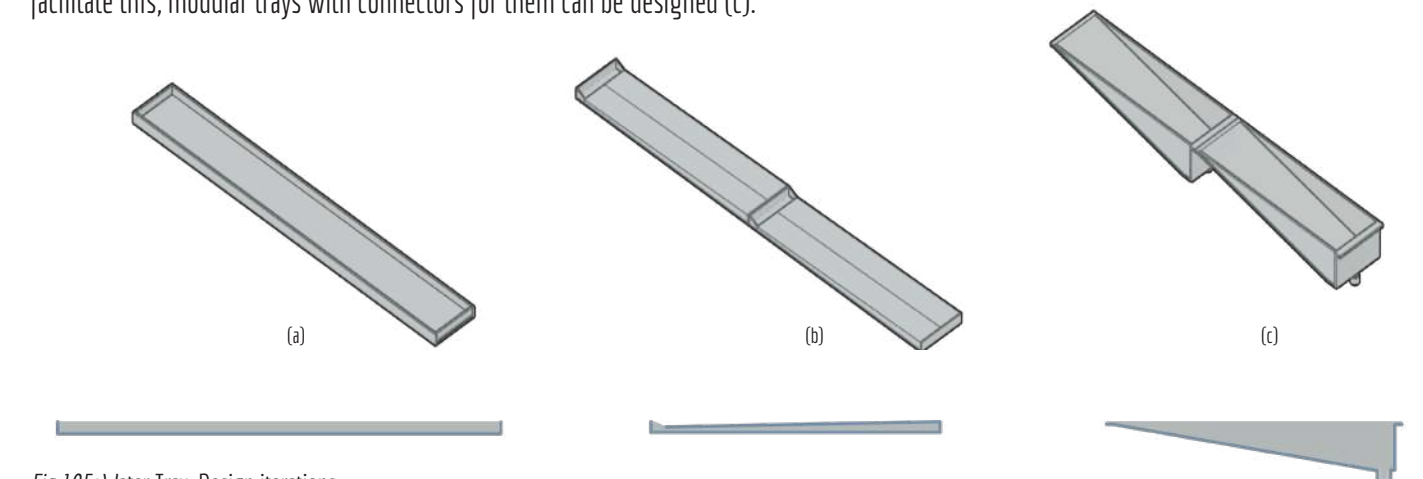


Fig.105: Water Tray. Design iterations

Connections

The decision of developing a component composed of two different modules generates the challenge of designing a connection between the two units. Such a joint has to happen on the backside of the first module. For this reason, it is decided to print each module vertically without a bottom layer, so that a positive-negative connection with the neighboring one is possible (Fig.106).

The front is instead shaped to fulfill both the role of connection and of an aerodynamically efficient inlet. Starting from an initial geometry (a), the connection is detailed to eliminate sharp angles hard to print and to obtain printable overhang angle, with a gradual curvature gradient (b).

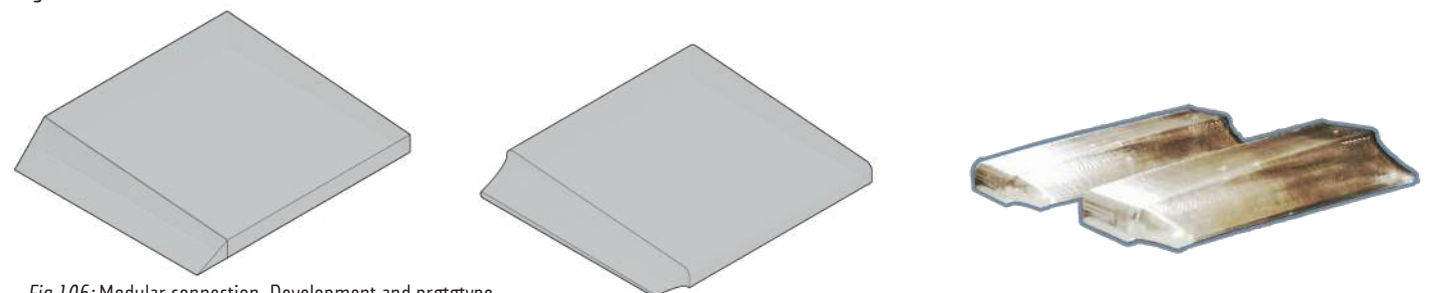


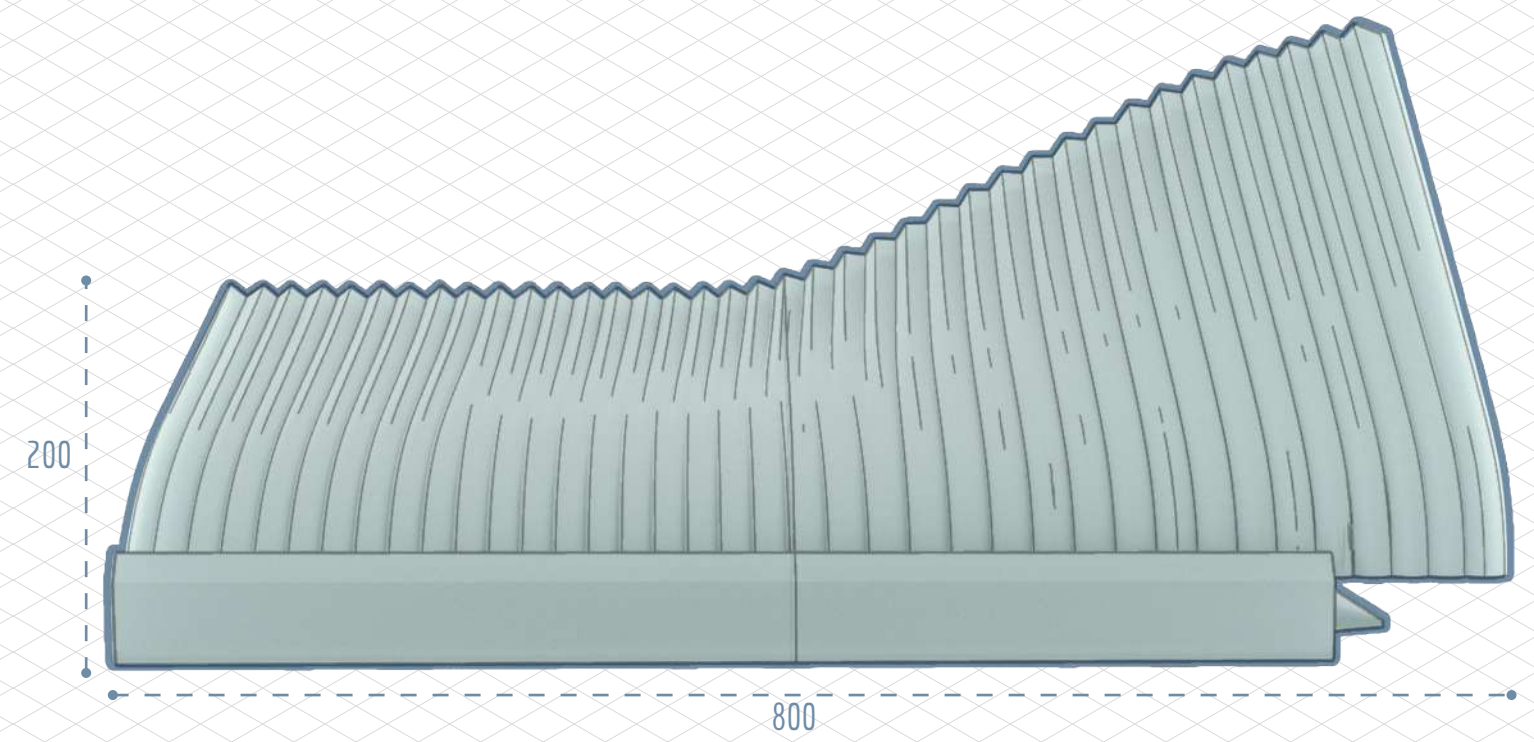
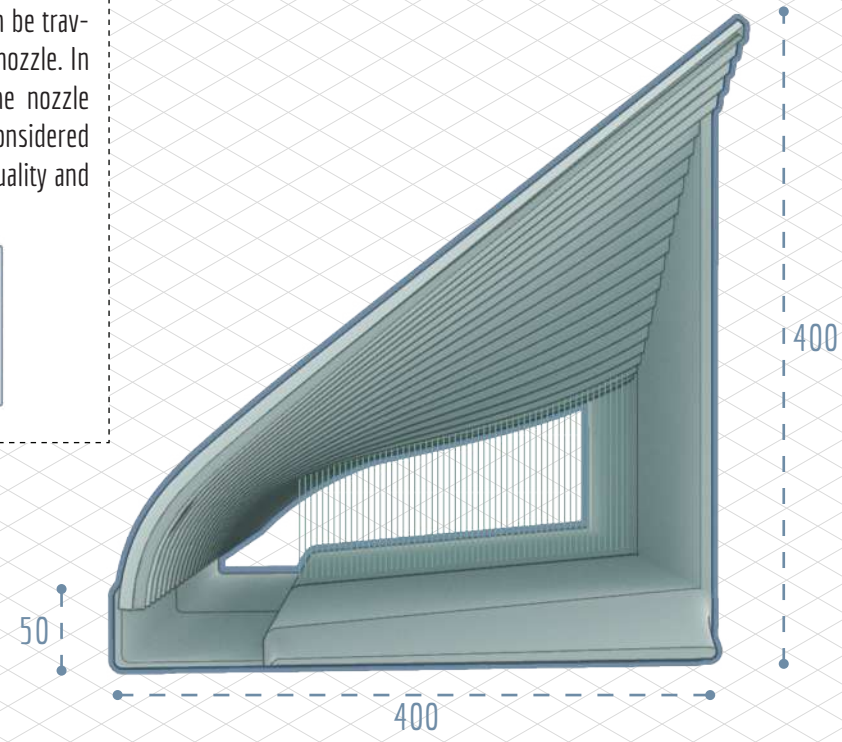
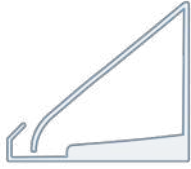
Fig.106: Modular connection. Development and prototype

4.7 FINAL DESIGN

The results from the schematic design and the more detailed design are combined into one final design. The flexibility of the design workflow is shown into the development of different design iterations with gradually higher degree of complexity. The water-catcher unit is designed first as a stand-alone unit that could be easily printed for testing reasons. More professional and controlled printing setup would allow to fabricate bigger and more complex geometries. For example, the use of nozzles or printer of bigger size would influence the maximum printable dimensions or the required printing time. Moreover, more controlled humidity and temperature levels could ensure consistent print quality and dimensional accuracy. The possible integration of a water-catcher unit into a structural module or into a complete 3d-printed facade system is presented in the following pages. Only initial design considerations have been performed on these solutions. The stand-alone component is considered further for the optimization of the printing process and for outdoor testing, and the printing efficiency of the fog-catchers.

Particular attention is given into modelling a geometry whose planar contour lines are continuous closed polylines, which is considered similar to a continuous spiral path and therefore the most efficient printing technique.

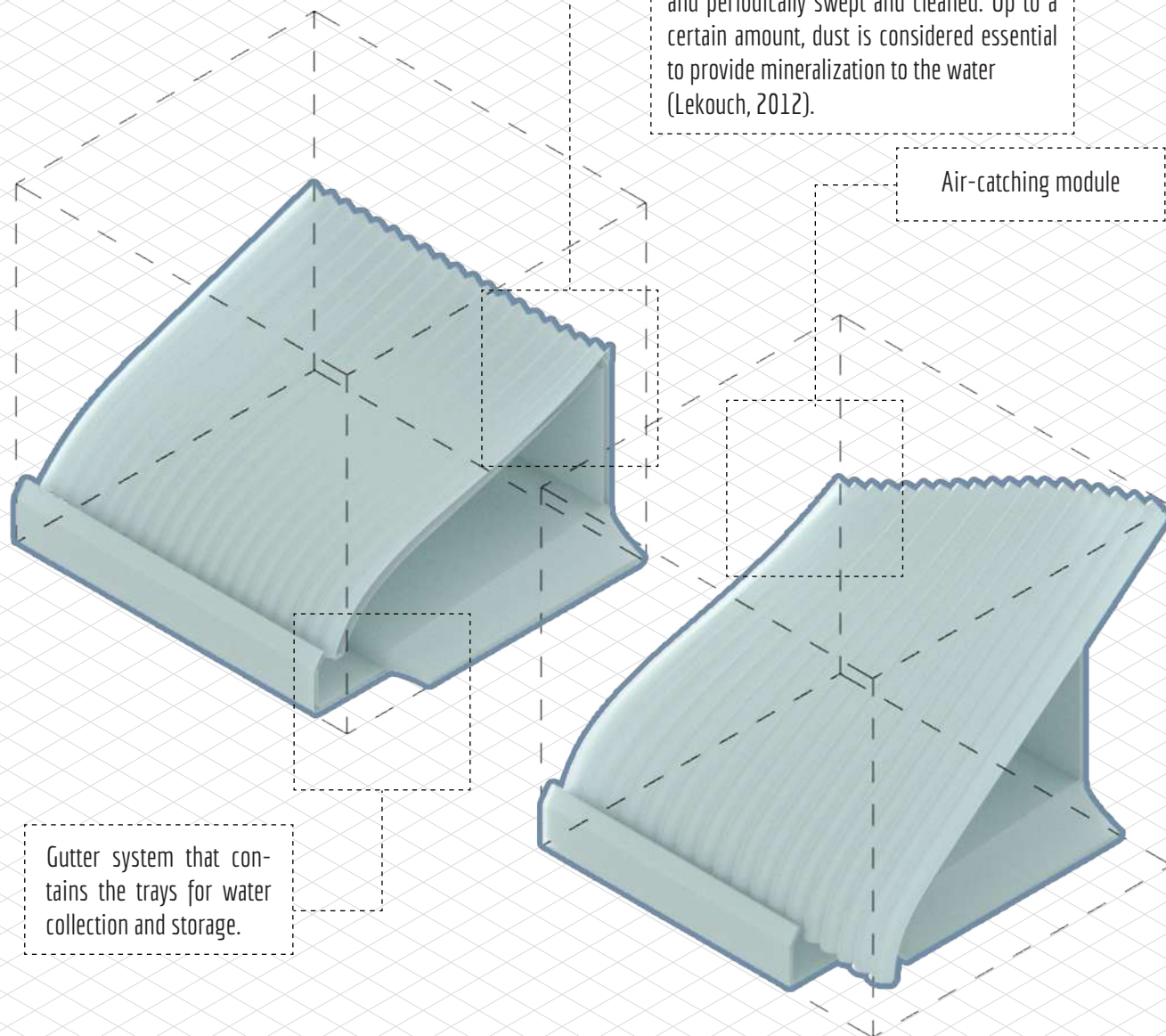
The geometry is refined so that a closed continuous path can be travelled layer by layer by the nozzle. In this way retractions of the nozzle are minimized. This is considered to be beneficial for print quality and reduced print time.



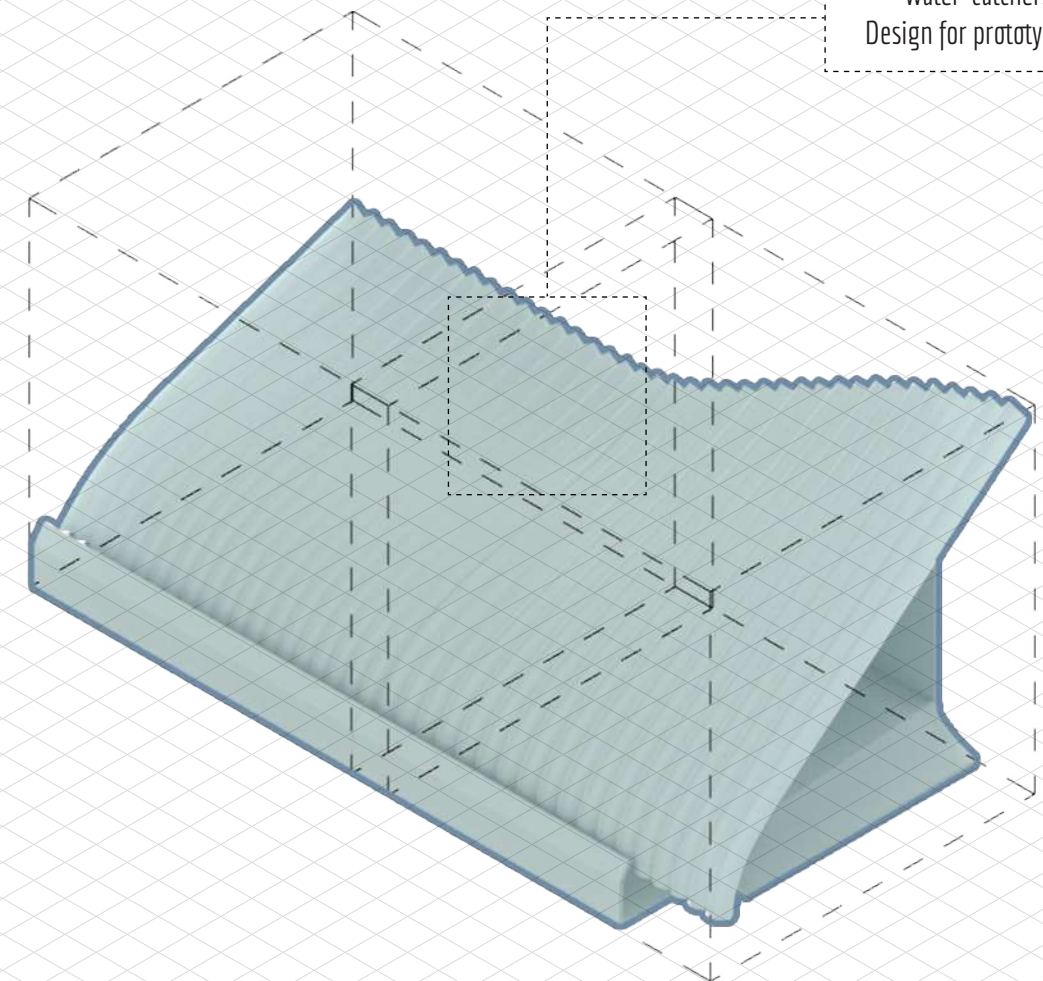
Fog-catching module. Can be easily removed and periodically swept and cleaned. Up to a certain amount, dust is considered essential to provide mineralization to the water (Lekouch, 2012).

Air-catching module

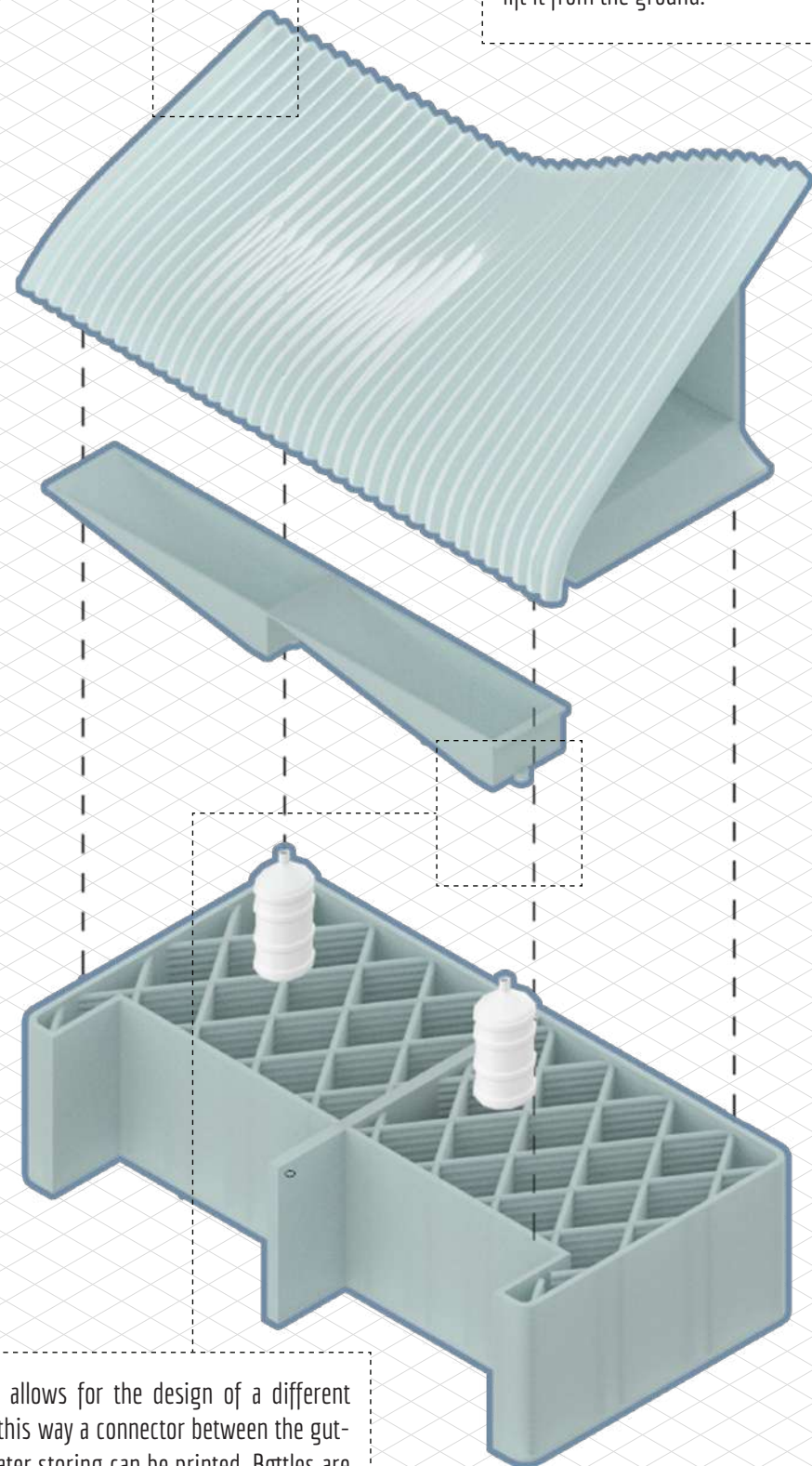
Water-catcher.
Design for prototyping



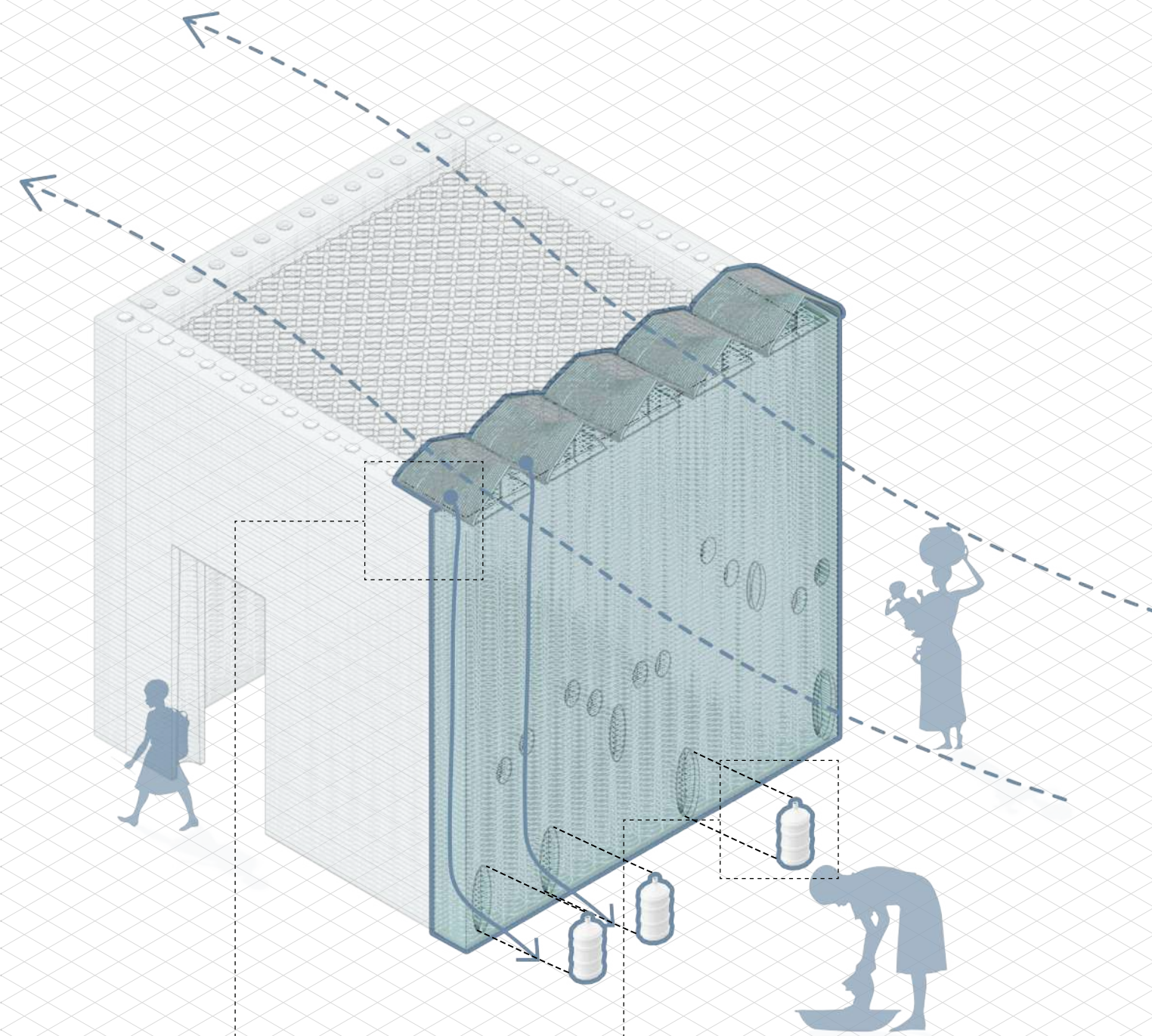
Gutter system that contains the trays for water collection and storage.



The design prepared for prototyping and testing represents the first and more simple solution. Different versions can fulfill different needs. An isolated water-catcher could be coupled with a 3d-printed base. In this way additional elevation is given to the unit to catch flows at higher velocities and to lift it from the ground.



The additional height allows for the design of a different water tray system. In this way a connector between the gutters and bottles for water storing can be printed. Bottles are easy to remove daily and could integrate water sanitation and filtering. The tray can also be connected through pipes to a more complex water management system.



The flexibility of the design allows to imagine its integration into 3d printed architectures of bigger scale. The water catchers placed on the rooftop can be collected to a facade system.

The water distribution and storage systems can be integrated into a series of vertical pipes into the facade. In this way water is efficiently brought to ground level where it can be collected in bottles and easily accessed by people.

4.8 OPTIMIZATION FOR 3D-PRINTING

The finalized geometry and the process followed to achieve it was shown above. The last step before prototyping is that of analyzing its printability and tune in the best way possible the printing settings. The goal of the process is to reduce as much as possible the time necessary for production, without compromising the structural stability of the component. However, the structural behavior does not represent the main focus of the research, and as long as the component can withstand its weight it is considered acceptable.

The analysis is performed by importing the 3d-models of the two modules in the slicer software (Ultimaker Cura 4.8.0) and progressively optimizing different settings. The fog-catching module (Fig.107) is used as a reference for the project, as it contains all the intercepting screens and it is therefore considered more complex to produce.

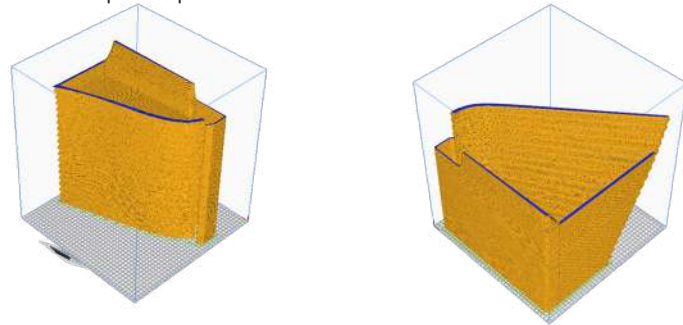


Fig.107: Final modules. Printable version

The steps of this analysis are summarized in the Fig.112. The properties that are finalized in each step are highlighted, while the options that are discarded are greyed out. The results are theoretically optimal settings that will be tested in the prototyping of the design.

The optimization process starts from average settings that have been used consistently in the production of smaller specimens for testing (#1). It is evident that the printing time in this initial option is too high and need to be reduced. The first setting to be changed is the wall count. The printing time appears to be linearly related to this parameter and a single wall options already reduces by 50% the initial required printing time (#2).

The next beneficial step is that of increasing the layer height, so that the total amount of necessary layers can be reduced. Using a 0.4mm nozzle, the maximum height considered is 0.3mm (#3). This brings an additional reduction to the initial time, but the consequences on the printing quality needs to be evaluated. Small 50x50mm samples are printed and compared. Samples are printed one after each other with the same spool of filament. A smoother surface is obtained with thinner layers, but at the same time a higher percentage of imperfections is observed. The quality of 0.3 layers is considered acceptable (Fig.108).

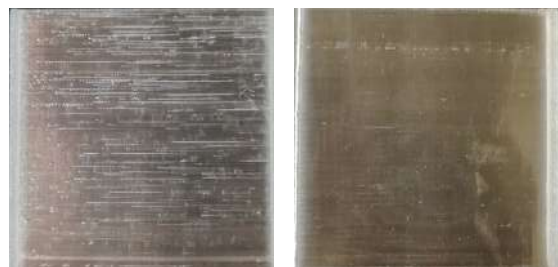


Fig.108: Layer height tests

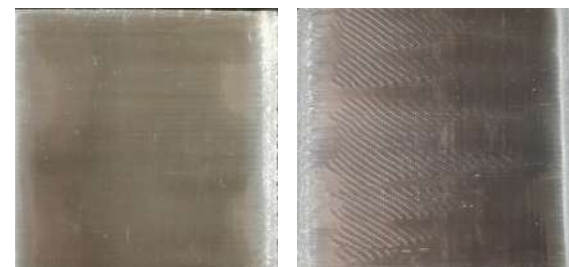


Fig.109: Printing speed tests

At this point, different wall printing speeds are tested to understand how fast the component can be printed without excessive losses in quality. The previous samples have been realized with a speed of 40mm/s, so iterations at 60 and 80mm/s are evaluated. The time reductions are proportional to the increase of velocity. It can be seen that the first speed increase does not impact the quality, while many more defects can be seen at 80mm/s. However, such defects appear to be mainly visual and do not reduce structural properties such as layer adhesion (Fig.109). The goal of the research is not to achieve the best visual quality as possible, but rather to produce a design easy and fast to produce. For this reason, the 80 mm/s can be considered a suitable speed (#5).

Besides the wall speed, also the infill speed with which the fog-catching screens are realized can impact significantly the printing time. Moreover, this part of the component has to be printed in mid-air, so the definition of these settings has to take into account the maximum achievable bridging length.

These properties are investigated through prototyping different samples with a bridging length of 15 cm, which is equal to the maximum one present in the final design (Fig.110). Along with the speed, also the flow of material and the printing temperature are progressively tuned. For all the samples, an infill percentage of 40% and a minimum speed of 40mm/s is considered.

Two different approaches are identified and tested. The first one is reducing the printing temperature and keep the speed relatively low (#2). In this way, the material needs less time to cool down, and at the same time the extruder moves slowly, offering support for the filament to solidify. The second strategy (#5 and #6) looks at the other end of the spectrum. Print temperature, speed, and flow rate are increased so that more material is melted and goes through the nozzle in the same amount of time. Being more liquid, the filament does not stick to the nozzle and is extruded more smoothly.

The data specifications of all the samples can be seen in the table below.

#	Dimension [mm]	Num. screens	Infill [%]	Speed [mm/s]	Flow Rate [%]	Temperature [C]	Printing time [min]
#1	5x15	2	40	40	100	235	18
#2	5x15	2	40	40	100	215	18
#3	5x15	2	40	60	100	235	16
#4	5x15	2	40	60	120	235	16
#5	5x15	2	40	80	120	250	14

Fig.110: Bridging length. Tested settings

The outcomes of the different strategies have then been assessed visually, considering general print quality and the frequency of defects (Fig.111). All options have shown the ability to bridge successfully the distance. Sagging of the wires is observed in all the specimens but is not been considered a defect, since to achieve efficient fog capturing sagged wires are not a problem as long as they are continuous over the span.

As it can be seen from the samples, low speeds generate a higher amount of defects (#1, #2). This is because the filament tends to curl on the extruder and stick to it for a certain length. After this distance the filament snaps, breaking the wire. This phenomenon is due to dirt accumulating on the nozzle. As the print proceeds it only gets worse, as more and more material sticks to it. This process appears to be enhanced by temperature reduction (#2).

On the other hand, higher speeds bring benefits to both print quality and necessary time. The highest reduction of defects is recorded when high speed is combined with higher temperature and flow rate (#5). The over-extrusion of material succeeds in obtaining a smoother flow of material, while reducing at the same time the printing time. For this reason, these settings are considered optimal for prototyping the component.



Fig.111: Bridging length prototypes

The last step in the definition of the properties of the fog-catching surfaces is the infill percentage, that corresponds to the solid coefficient of the collectors. The impact of this parameters on the overall efficiency of the system has been analyzed in the pre-design phase. For this reason, printing time and and collection efficiency are compared between different options (Fig.111). A shading percentage equal to 60% is considered a good compromise between the two variables.

#	Infill [%]	Printing time	Collection efficiency
#7	40	9h17min	0,95
#8	30	9h8min	0,88
#9	60	9h36min	0,99

Fig.111: Infill percentage. Tested settings



Fig.112: Printing settings optimization steps

As it can be seen from the graph below (Fig.113), the progressive tuning of all the main settings related to 3d-printing produces a significant reduction in the amount of time needed for fabrication. Moreover, reducing the wall count to one allows also to reduce the mass and length of filament required. This is particularly relevant when the size of filament spools are considered.

Spools are usually available on the market in sizes of 750 and 1000 g. Therefore, the initial option (#1) would need one whole roll to be printed. On the other hand, single-wall options would need half of it. In this way, both the modules the component is made of would be printable with one spool.

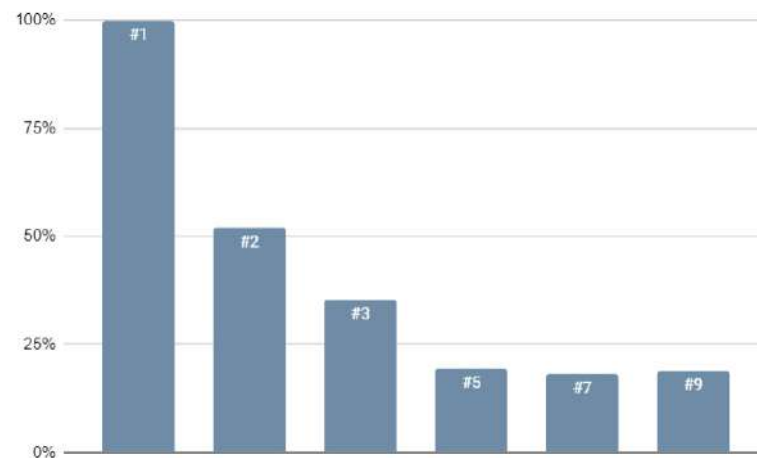


Fig.113: Printing settings optimization. Printing time reductions

Prototyping 1:1 segments of the design with the finalized settings (#9) results to be possible but hard to print. Layer adhesion to the printing bed and in-between layers is problematic after a certain height. This is due to the single wall count, that after one point becomes source of instability that leads to inefficient material deposition from the nozzle. Moreover, the single wall count generates a highly flexible result that might not be structurally strong enough to resist outdoors. Based on this, further improvements can be applied to the settings to minimize these issues.

Based on these observations, two improvements points are researched. The first one is to improve the pressure with which material is deposited so that layer adhesion can be enhanced. The second concerns structural stability and looks into the effects of increasing the wall thickness. Increase the pressure means raising the amount of material that in the unit of time flows through the nozzle. If the speed is kept constant, this means that an higher volume of material has to be squeezed in the same surface area.

A setting in the slicer (Ultimaker Cura) allows for flow rate increases while all the other variables are fixed. A flow equal to 120% is tested, but the effects of more significant changes in this settings is simulated and analyzed. It can be seen (Fig.114) that it has no impact on the print time, since no speed modifications are done. On the other hand, the printed mass of material grows almost linearly with the the flow rate. No considerations are done about the maximum flow allowed by the extruder. It should be tested in order to set an upper limit in the tuning of such setting.

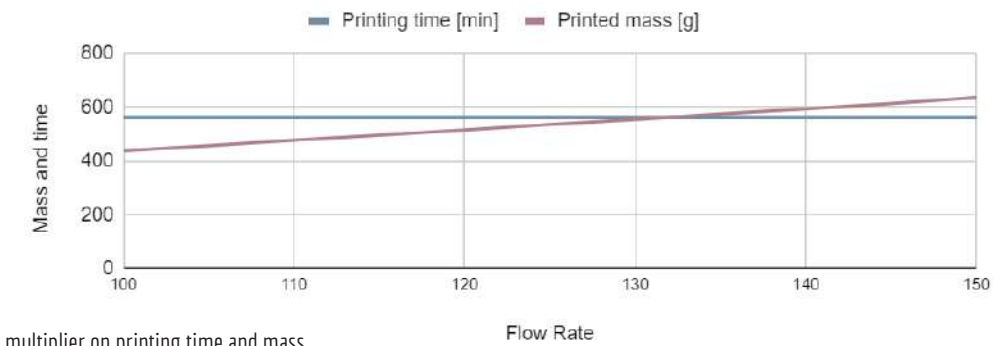


Fig.114: Effect of flow multiplier on printing time and mass

Two different approaches can be followed to increase the wall thickness and therefore the component's strength. The first one is to keep the wall width constant and just increase the wall count. As it can be easily imagined, when the speed is kept fixed this leads to a linear growth of both print time and mass and it is therefore not desired. However, some printing tests are done with double wall count and the performance is simulated for a count up to four. The results are plotted below (Fig.115).

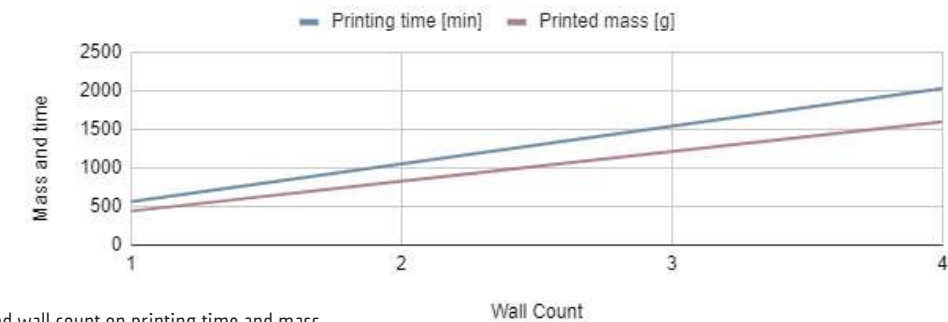


Fig.115: Effect of increased wall count on printing time and mass

The second strategy is instead based on a concept similar to that taken into account for the flow rate multiplier. The wall width is set at the beginning to 0.4mm, which is equal to the nozzle diameter. However, wider walls could be potentially be printed. The way to do that is by increasing the amount of material which is deposited per unit of time on a linear unit of space. The quantity of material to melt is measured by the extruder as volume to deposit. If the layer height and the wall speed are fixed, higher flow has to be translated into bigger layer widths.

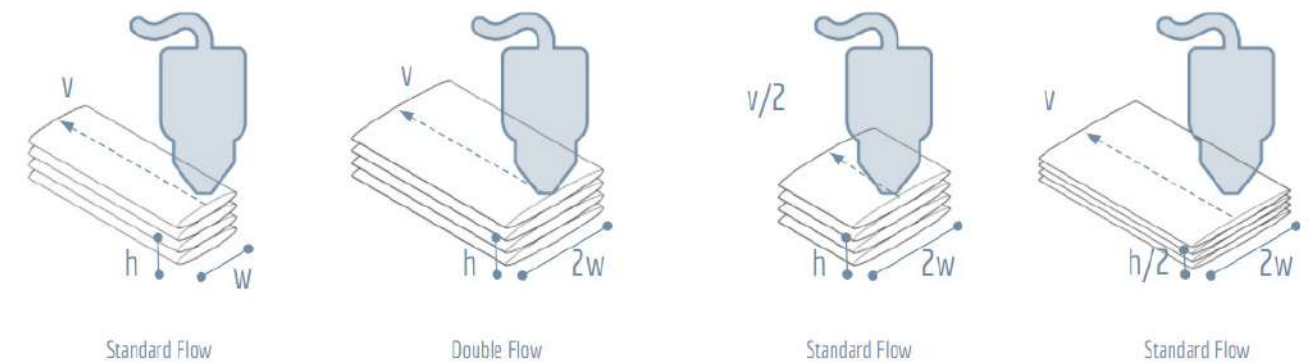


Fig.116: Flow rate. Variables involved

As it can be seen from the diagram above (Fig.116), doubling the layer width doubles the volume of the elliptical cylinder that is printed by the extruder in a unit of time. This means that the flow rate, which is equal to that volume, doubles too. If instead a particular layer width is required, the other parameters influencing the volume of material can be tuned so that the maximum flow is not exceeded. These variables are either the printing speed or the later height. If the increase of only the wall width does not impact the print time but only the consumed material, reducing one of the other factors leads inevitably to an increase in time. Assuming that the extruder can handle high flow rates, different wall widths are simulated keeping constant speed and height. The impact on the time and mass is plotted and shown below.

The width is varied from 0,4mm to 0,8mm, which is equal to a double wall count. As it was predicted, it is shown (Fig.117) that the printing mass increases linearly with the width. However, an unexpected decrease of the time is observed. This is probably due to the increase in width of the infill lines. Keeping the same solid percentage, higher widths means that less lines have to be traced.

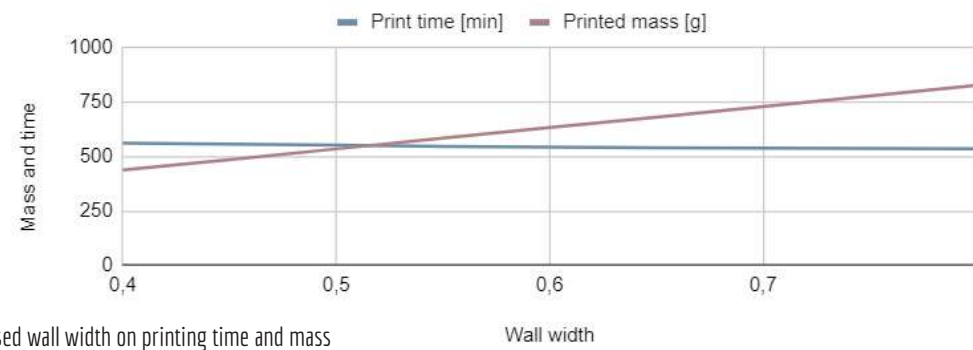


Fig.117: Effect of increased wall width on printing time and mass

Comparing the two approaches, doubling the wall count would lead to the doubling of the component's printing time. On the other hand, increasing the flow rate would even produce a time reduction. However, not enough testing has been done to understand the maximum printing rate of the extruder mounted on the printer which is used for prototyping. An additional 20% has to be added to it, since 120% flow rate has been considered necessary to increase the pressure and adhesion between layers. A 220% flow rate is therefore considered too high for the current extruder. For prototyping, the wall width is doubled and the printing speed is set to 40mm/s, which is equal to half of the initial one. The layer height is kept to 0.3 mm, so that in the end the total flow of rate is kept constant.

The previous analysis showed the benefits that increasing the flow rate would have. Printing with a more powerful extruder and a bigger nozzle could enable to design with higher and wider layers, keeping the wall count and the printing time low. However, it has to be said that more material would need to be used and more energy to be consumed. Specificities of fabrication locations could influence the availability or cost of one or more of these parameters. The settings could then be tuned to optimize the printing process for the specific variable.

The options considered so far take into account that a 0.4mm nozzle. This is one of the most common diameters of nozzles for home 3d-printers. However, bigger nozzles and more powerful extruders are available for professional setups. The option of printing the module with a 1.2mm nozzle is considered and average printing values are used to estimate the printing time. As predicted, it can be seen that required time can in this way be drastically reduced.



Fig.118: Final printing settings based on nozzle diameter

The analysis and optimization of the printing settings has shown the different impact of different parameters. Both the options presented above (Fig.118) lead to a functioning module. However, different settings lead to elements with different properties. Choosing between one printing option rather than the other can depend on many factors. As said above, this can be related to particular requirements related to the performance of the object or to specificities of the printing setups.

If only a 0.4mm nozzle is available, either time or printing ease can be prioritized. If material availability is not a limitation, a bigger nozzle can be chosen. This would lead to an extremely high printing time efficiency and structural stability.

The behaviour of these different approaches is analyzed qualitatively and compared in a series of radar charts (Fig.119). In this way a clear overview of their properties is provided and they can be analyzed in a case-by-case approach based on specific requirements.

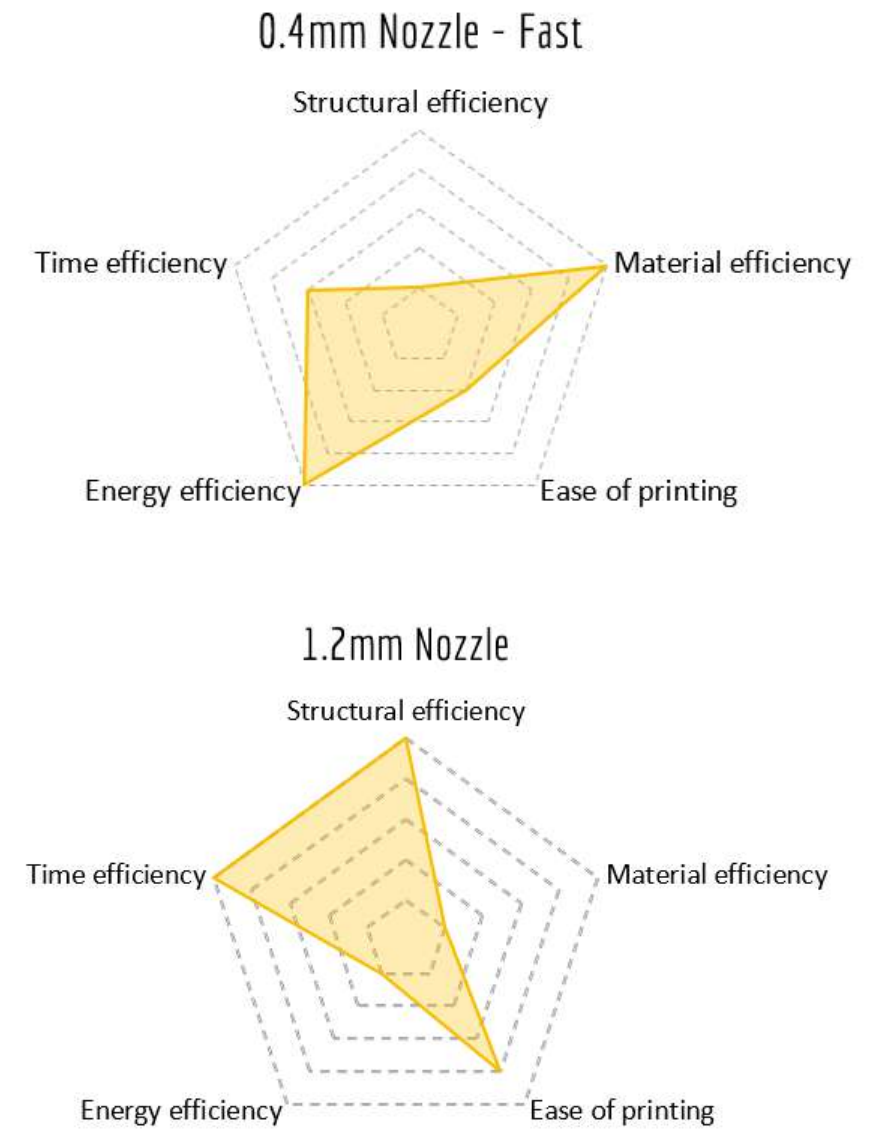


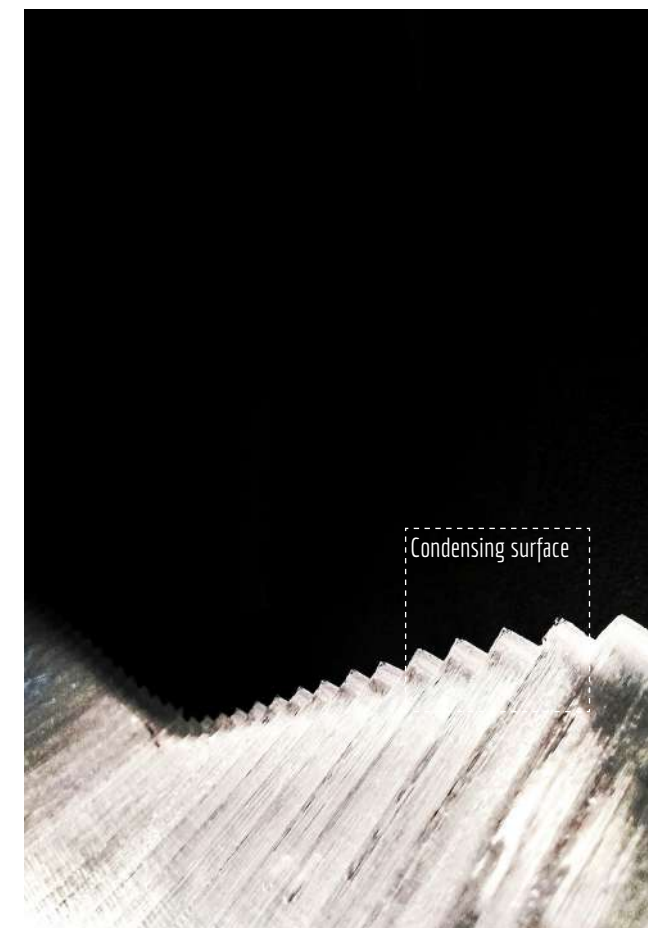
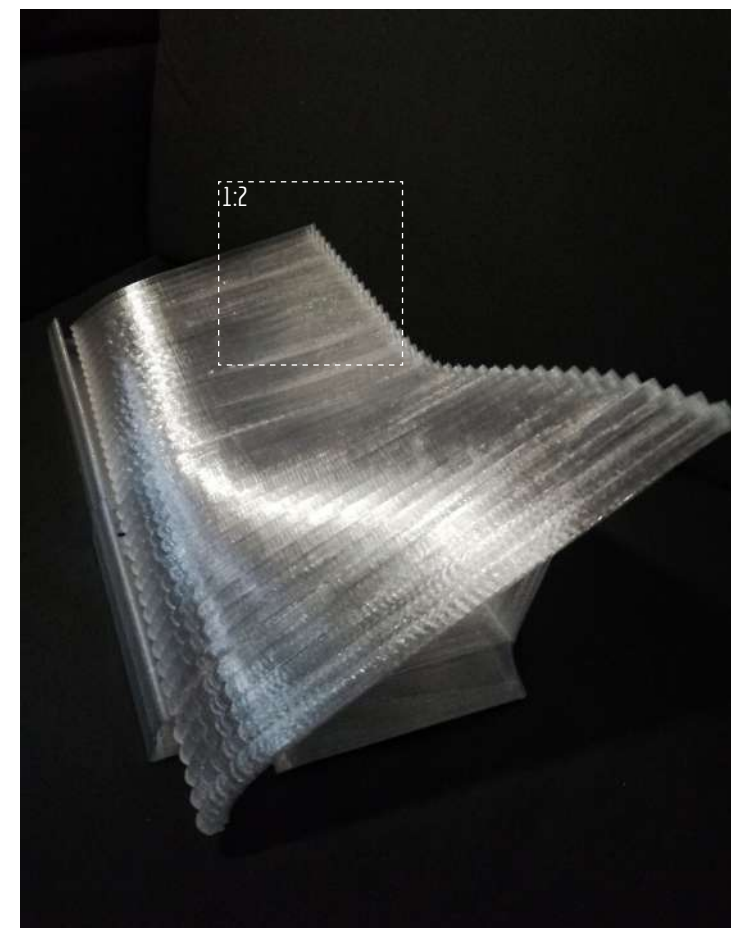
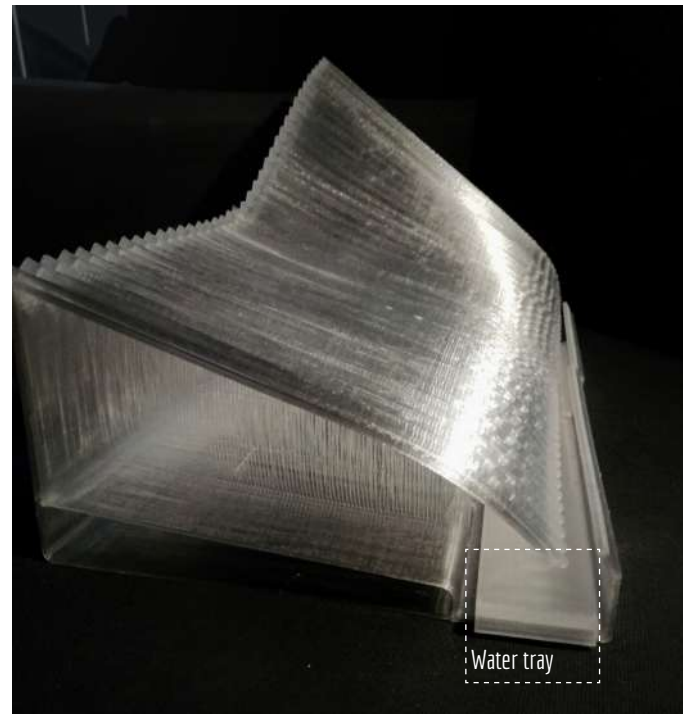
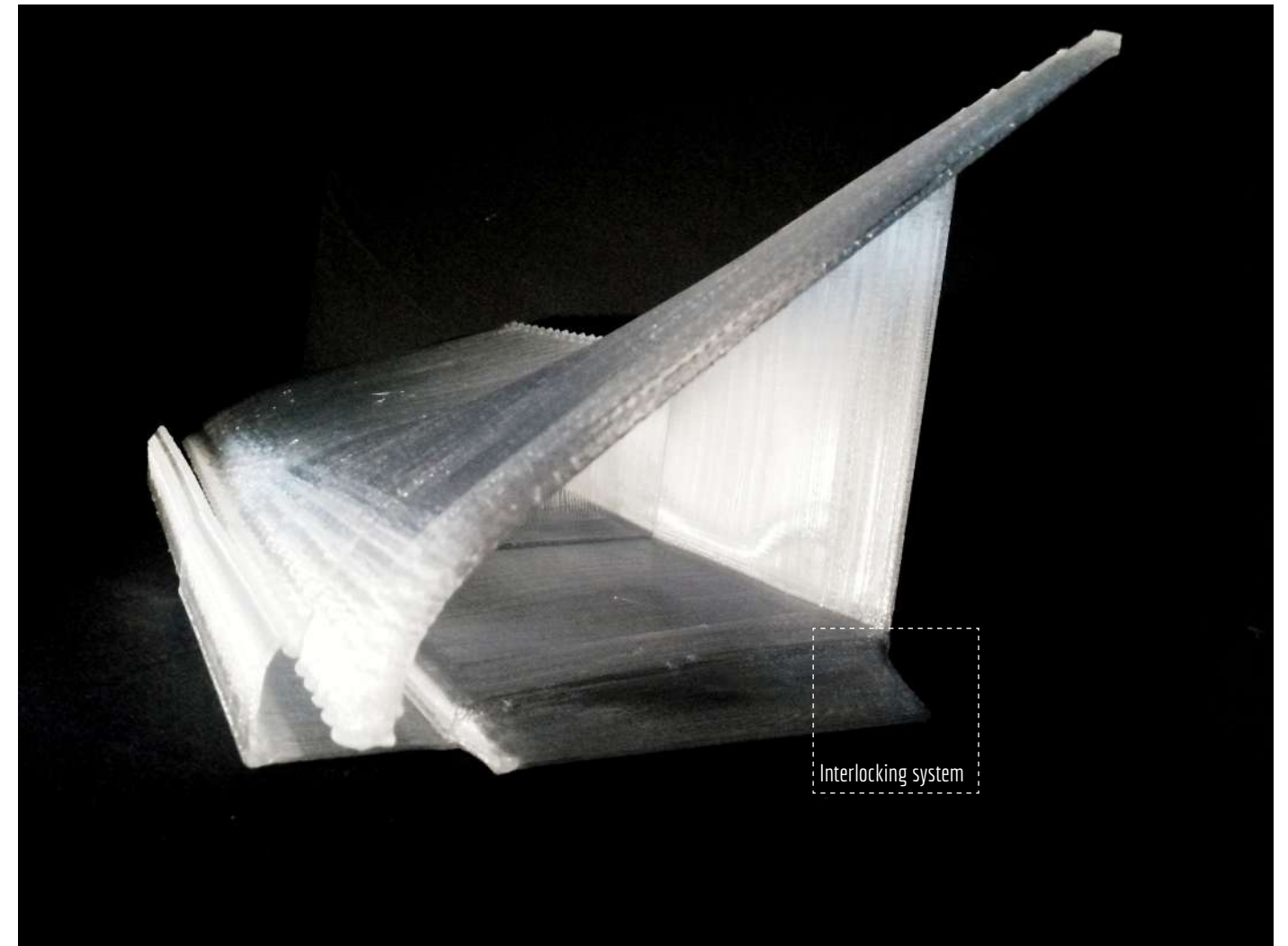
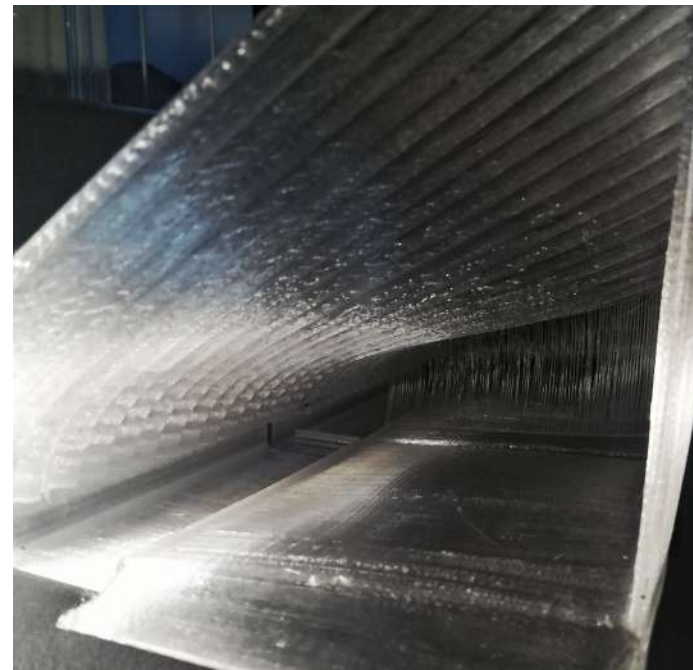
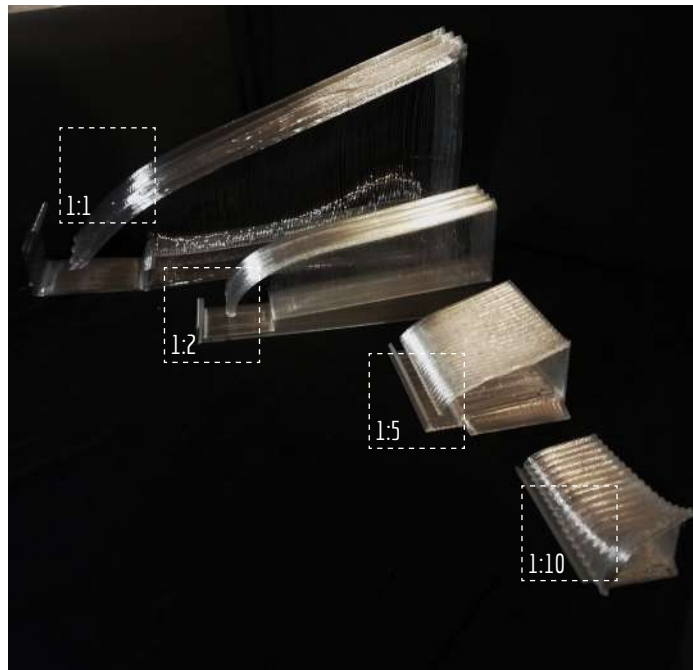
Fig.119: Printing settings. Possible strategies

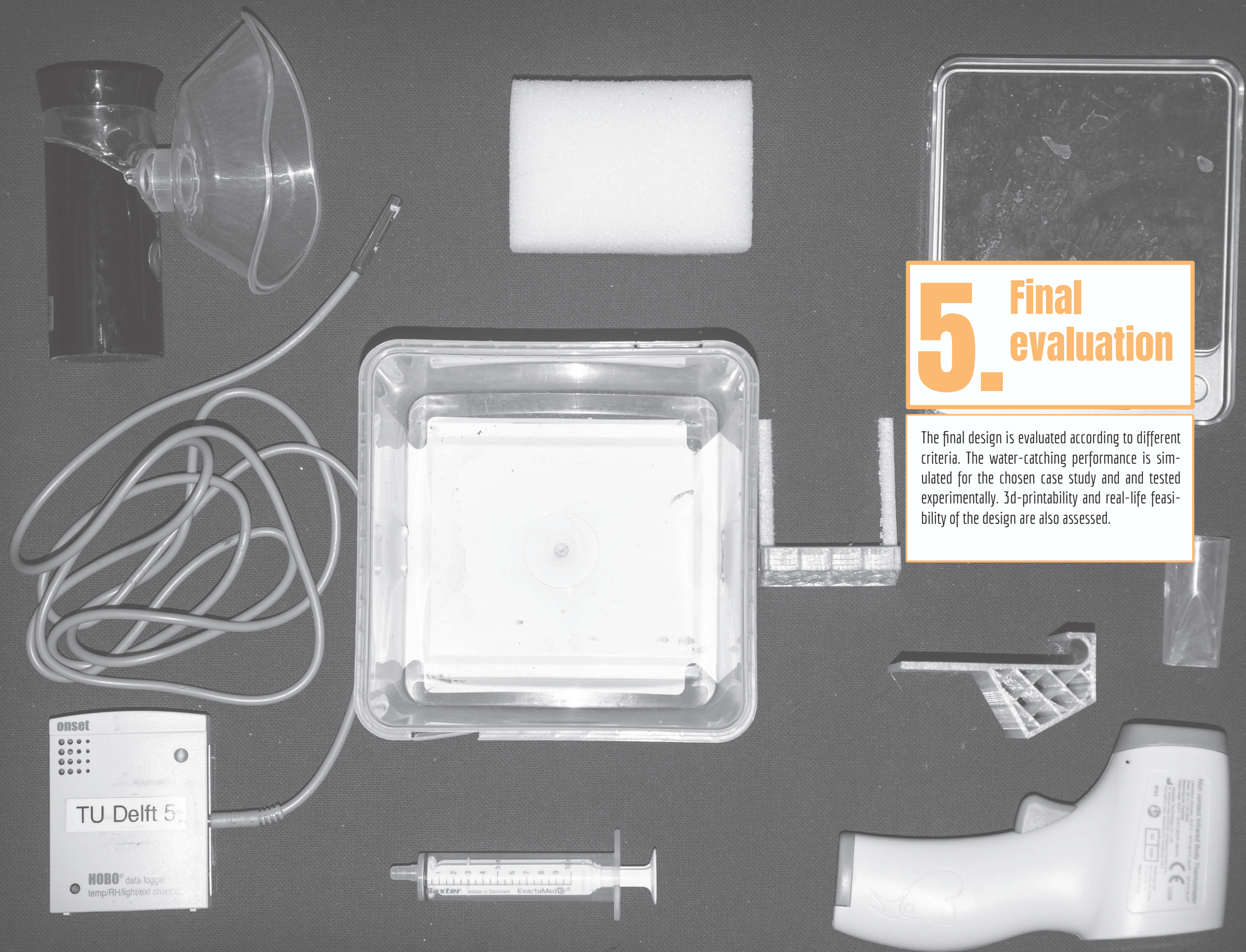
4.9 FINAL PROTOTYPING

The development of the design and its printability have been presented so far. The goal was to move from small scale prototyping up to 1:2 and 1:1 scale. In this way, both 3d printing efficiency and water-catching abilities could be tested. A prototype for outdoor testing is therefore produced.

It is decided to print a complete 1:2 water-catcher, to be able to print it with a 0.4 mm and a double wall width within a reasonable amount of time. Overheating problems had been experienced before, so minimizing printing time in this setup is considered paramount. The component is printed in two different modules so that also their connection could be tested. Four fog-catching screens are printed in the fog-catching module with a shade coefficient of 0.6.

In the following pages, an overview of the results is presented. It is possible to see both the patterning of the condensing surface and the printing efficiency of the fog-catchers. Some defects are still visible in the printing of the screens, but their quality is still considered sufficient to fulfill their purpose.





5. Final evaluation

The final design is evaluated according to different criteria. The water-catching performance is simulated for the chosen case study and tested experimentally. 3d-printability and real-life feasibility of the design are also assessed.

5.1 WORKFLOW'S FLEXIBILITY

A design workflow for water-catching components has been presented previously. Such workflow takes into account the main functions that each design should fulfill and the optimal print orientation for each of such tasks. After defining the position and preferred orientation of the component, the functions are combined so that only one printing axis is obtained. If this is not possible, other strategies need to be pursued to accommodate those that do not share the same optimal axis.

The workflow has been tested on the design of the roof component, whose design and fabrication process is presented above. However, many other design iterations can be produced when different scenarios are imagined. Additionally, the maximum printable dimension has to be seen as a constraint related not to a functional need but rather to a fabrication limitation. When the printing equipment is scaled up or down, different components can be designed (Fig.120).

The designs that are presented in the next pages have been developed exclusively on a conceptual level. Small scale prototyping is performed to analyze their printability (Appendix VI). Computational or experimental testing has not been performed on them, and their water-catching performance has not been estimated. The goal is instead to show the potential and flexibility of the proposed design workflow. For what it concerns the scale, three different printing setups have been considered:

- Standard home 3d-printer

A standard FDM printer is considered (Anycubic i3 Mega S), with a maximum printing volume of 210x210x205 mm and a 0.4 mm nozzle. The device is suitable only for the production of small items.

- Big-scale 3d printer

The printer used throughout the research is considered (Anycubic Chiron). The build volume is equal to 400x400x450 mm and both 0.4 and 1.2 mm nozzles are thought as possible options to produce mid-size elements.

- Robotic Arm

A standard Kuka robotic arm is taken into account (KR 360 R2830). The arm can reach a maximum horizontal distance of 2826mm and a vertical span of 3798mm.

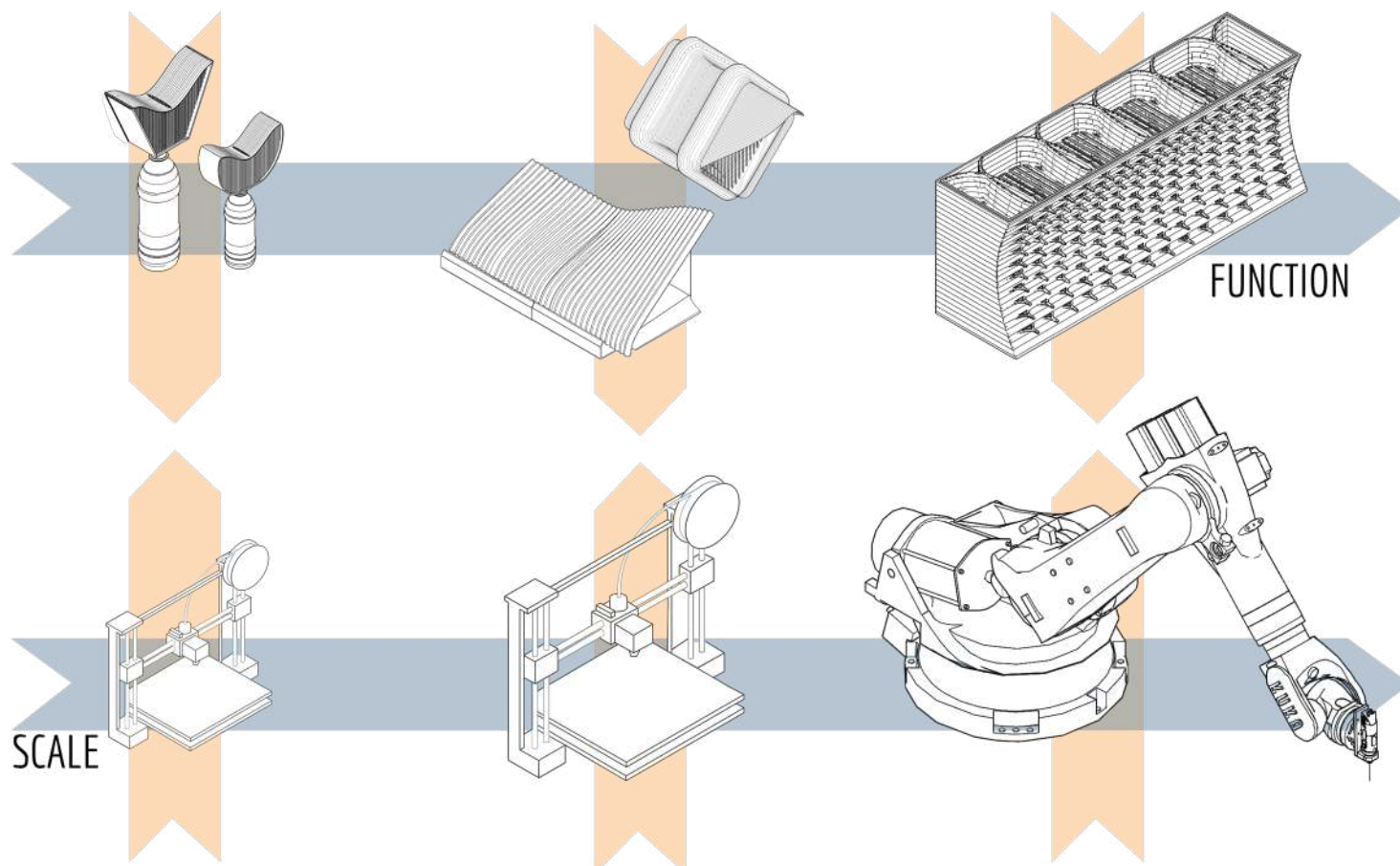


Fig.120: Workflow flexibility in function and scale

5.1.1 Standalone component

When a small printer is available, small water-catchers can be designed. This standalone version is thought to be placed outside or on a balcony and to be connected directly to a bottle. Sanitation or filtration systems could be later integrated into the bottle. Looking at the two schemes it is possible to make various considerations (Fig.121):

- The fog flow is considered to be horizontal, as the collector is designed to be an independent unit and not a building component.
- Dew and rain collection happen on an horizontal plane parallel to the sky. To align the slope to the print layers, the orientation has to be equal to the one used to realize the fog screens.
- Structural stability and water distribution and storage are functions governed by gravity. Their print axis is therefore vertical.

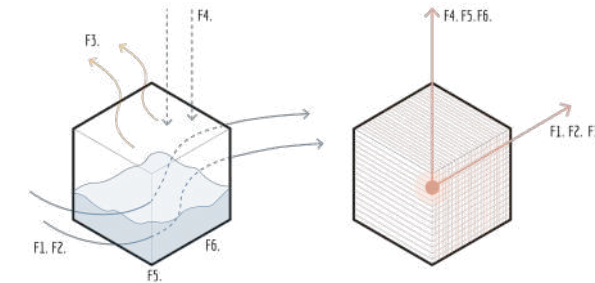


Fig.121: Standalone component. Functional configuration

The design is informed by these considerations. Multiple optimal printing axis are found, so different strategies have to be applied. Since the water-catching functions share the same axis, this is chosen as optimal orientation for printing.

For what concerns the other functions, structural stability can be achieved also when a non-optimal axis is used. This represents a viable solution when the structural capacity of the component is not vital. Water storage is in this case provided through the use of an external element to which the component is connected. The final part of the object is in fact shaped to fit into a standard 1.5 litres plastic bottle (Fig.122).

Finally, the optimal strategies previously discussed for the design of 3d printed dew and fog catching surfaces are applied to design. The parametric approach used to design the whole component, allows for high adaptability when more detailed analysis are performed.

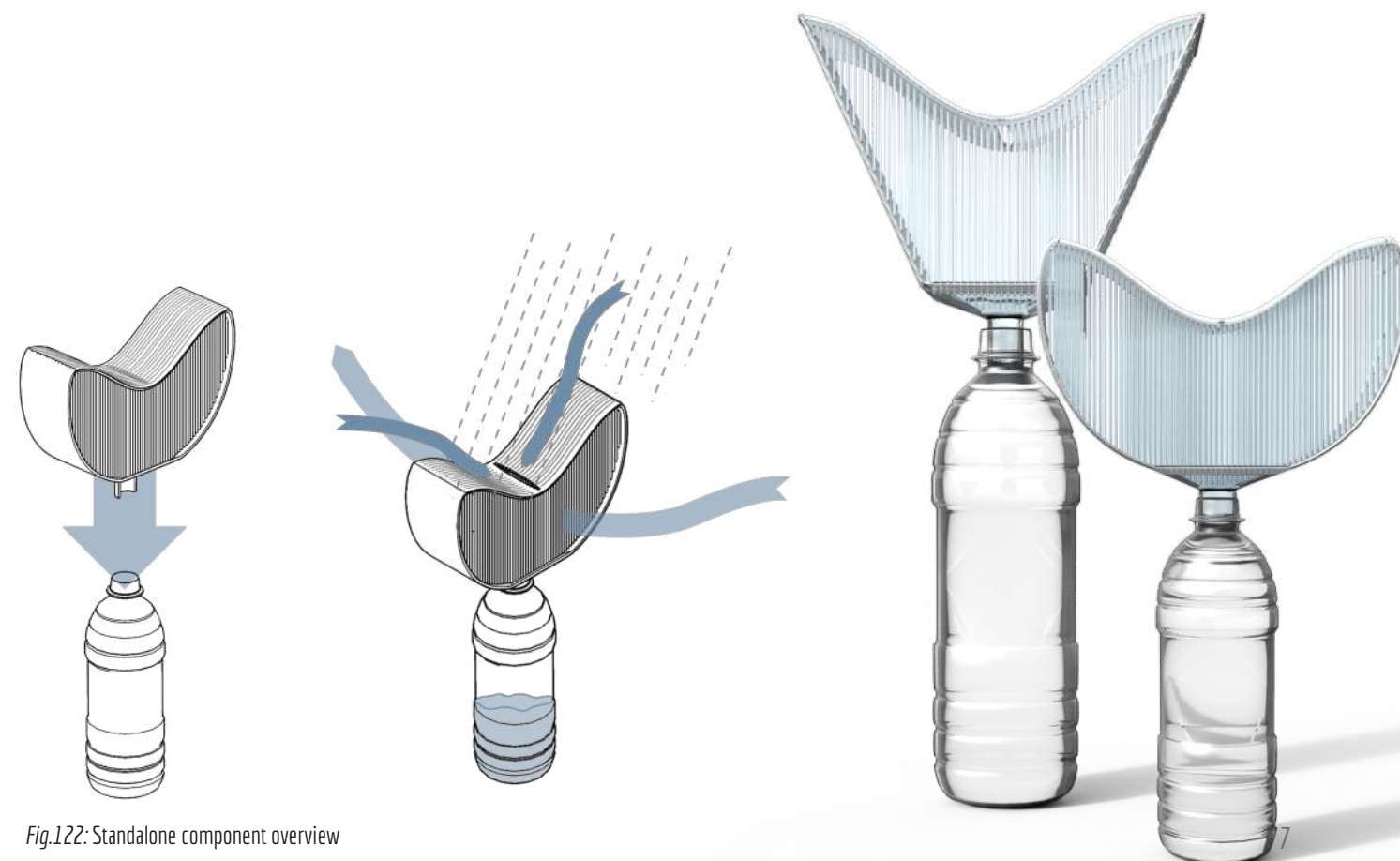


Fig.122: Standalone component overview

5.1.2 Modular wall system

When a big-size printer is available, modular building components can be more easily designed and fabricated. This is for example the case of the roof component that has been presented so far and used for performance evaluation. If a vertical orientation is chosen, different considerations can be made. In this iteration, a modular component that can be assembled into vertical elements is presented. The possible uses for such a design are fences, interventions of landscaping or realization of urban furnitures for the community.

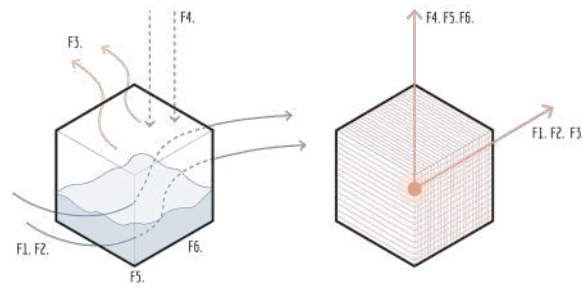


Fig.123: Wall system. Functional configuration

Similarly to what presented for the previous options, the schematic diagrams are useful to guide the design and to highlight which challenges need to be solved (Fig.123). The diagrams the same discussed for the standalone component. Also in this case, the element is thought not to be attached to a building but rather to be more isolated in an outdoor urban space. For this reason, the wind flow can be considered to be horizontal. Because of this, the optimal print axis for dew and fog-catching functions is the same. Special components are designed at the base so that water bottles or jerry cans can be fit in them and used for water storage. As the diagram suggests, an opposite print axis is used to accommodate these functions in the base modules.

The modular elements have a rotated square shape. An inclined surface on their upper edges works as radiative condenser, while intercepting screens within the block collect fog-water. The modules are designed to interlock on the edges, while leaving an open u-channel in the middle part. When two modules are stacked on top or next to each other, the two channels generate a closed cavity where water can flow towards the ground and be stored (Fig.124).

The design is developed with a fully parametric approach, so that it could be easily adapted to approximate different surfaces. Its modularity makes it easier to replace defecting items or to periodically maintain them.

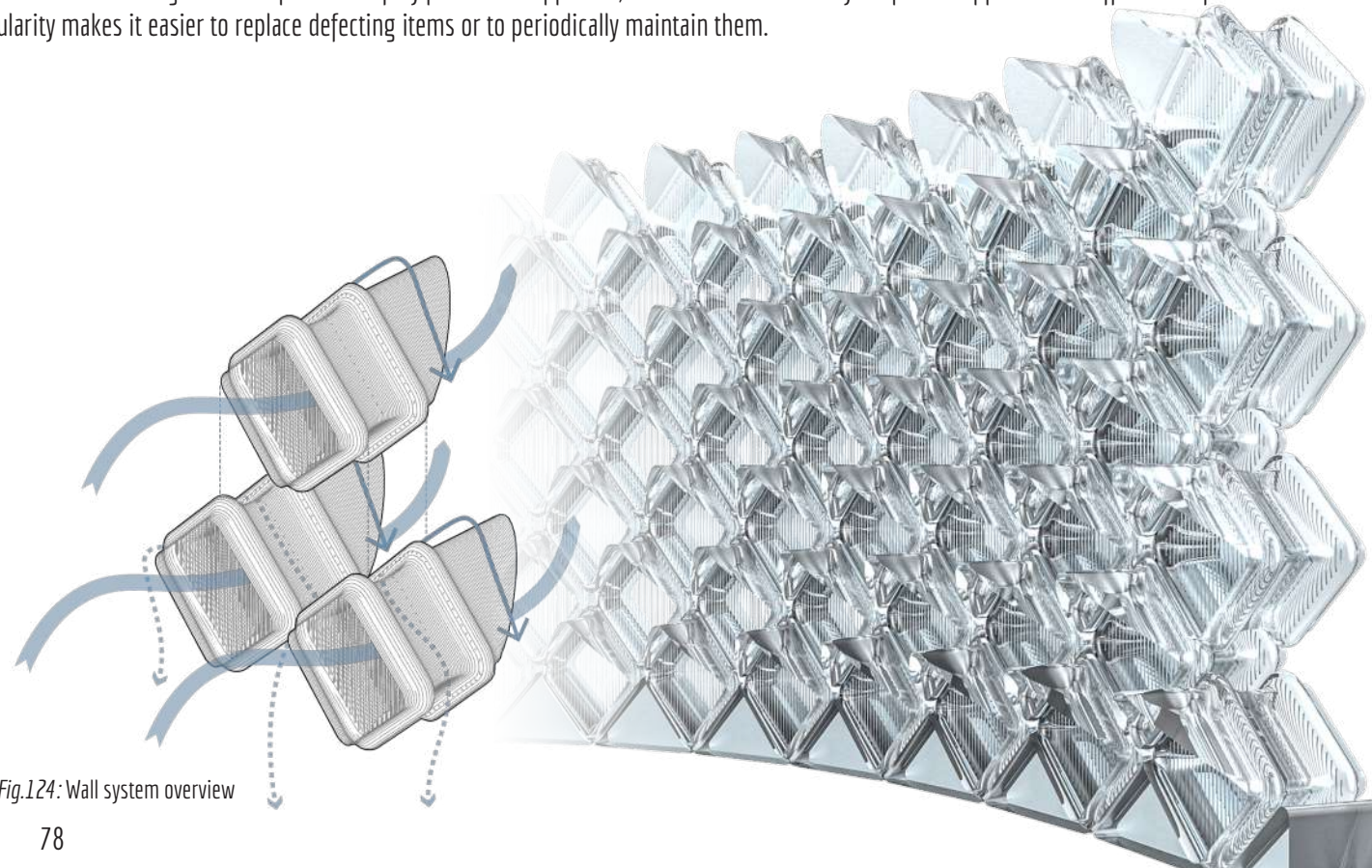


Fig.124: Wall system overview

5.1.3 Facade system

The last solution explores the design and production of bigger façade elements. The fabrication is performed by a robotic arm that can be used to produce either full-elements or smaller modular components. Looking at the diagrams, new considerations are formulated (Fig.125):

- Next to the façade of a building, airflow is vertical. Fog-catching layers have therefore to be parallel to the ground plane.
- Dew-catching surfaces need to be parallel to the sky plane.
- As usual, water storage and structural functions share a vertical optimal printing axis.

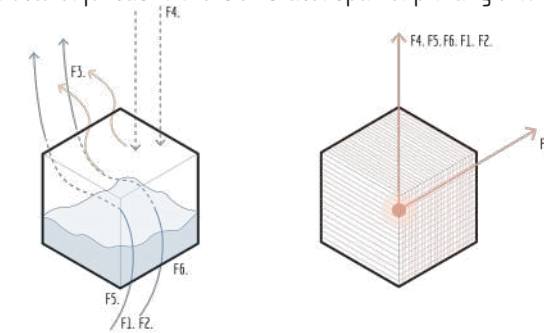


Fig.125: Facade system. Functional configuration

It results that the water-catching functions do not share the best printing orientation. As the horizontal surface for dew-collection would still be limited on a vertical façade element, fog collection is considered to be the priority. A vertical axis is chosen.

The façade panel presented in this section is composed of two different prints: a foundation block, which is used as main air inlet inside the component and water access, as it can host jerry cans or other plastic containers. The upper element is a hollow block composed of different channels. Fog is expected to flow within it and be accelerated by the progressively reduced section. Multiple intercepting harp screens placed at specific layers intercept water, then then flows by gravity towards the base of the panel. A different dew collection strategy is developed to remedy to its not optimal orientation.

Research and tests on bumpy surfaces similar to cactus spines were presented in the design chapter. A similar strategy is used to model the front surface of the panel. Bumps offer a reduced surface that cools down easily overnight and can facilitate condensation. Openings at the back side of the bumps allow for water flow into a frontal cavity. The water can then flow towards the base of the panel (Fig.126).

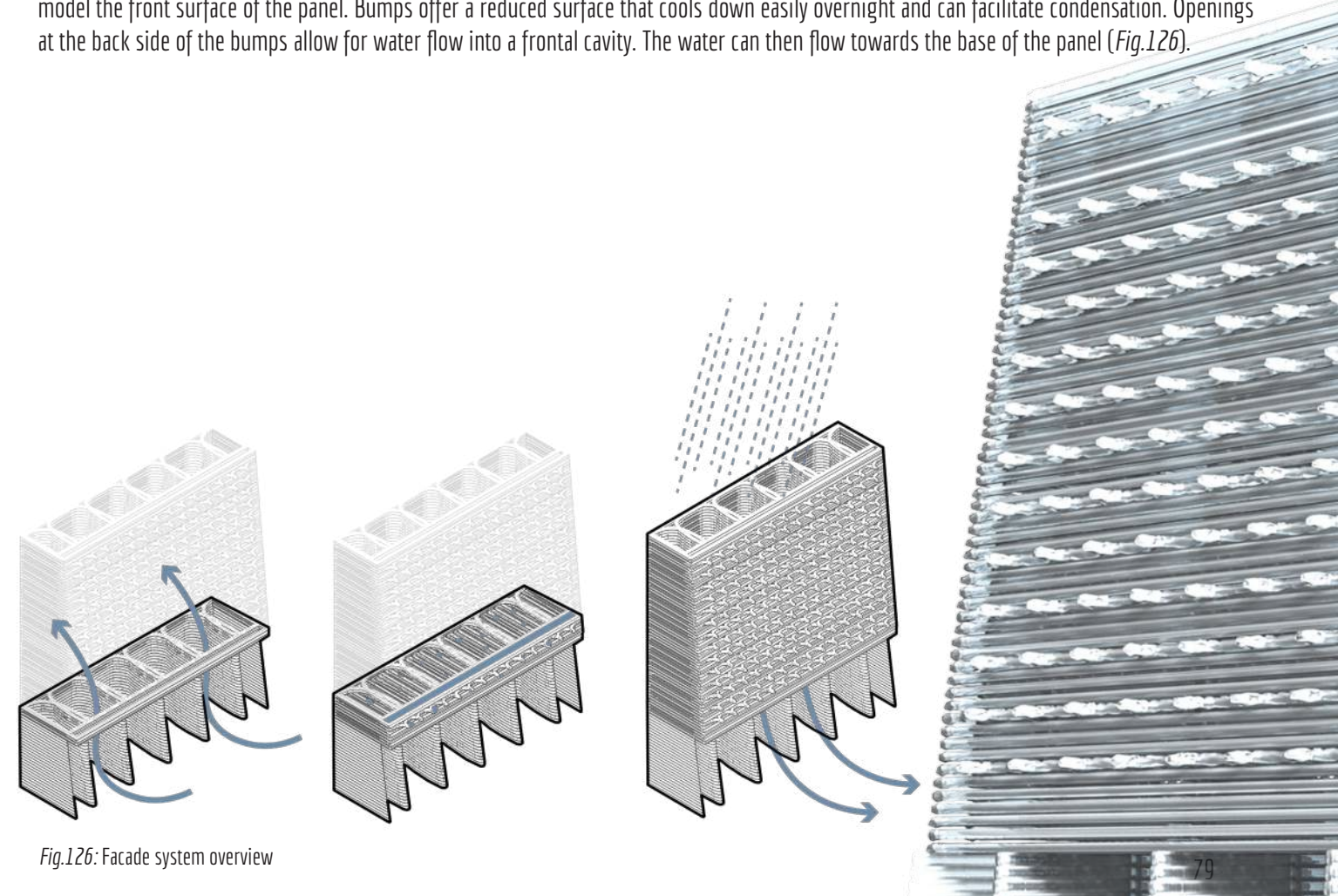


Fig.126: Facade system overview

5.2 WATER COLLECTION EFFICIENCY

The performance of the component is estimated both theoretically and experimentally. The 1:2 prototype is tested outdoors and its behavior is compared to that of standard fog and dew collectors. Ideally, the percentage difference between the new and the traditional systems is used to correct the dew and fog estimations for the chosen case study location. In this way, an estimation of the total number of modules necessary to fulfill the basic needs of one person is calculated.

5.2.1 Experimental setup

A 1:2 prototype of the component is tested outdoors for two weeks. The location of experiment is the roof terrace of a building located in Barbarasteeg 2, in Delft (Fig.127-128). The terrace is placed at an height of approximately 6m from the ground and it is therefore close to the 4m height used for the previous simulations. Taller buildings surround the chosen roof, influencing both its sky exposure and wind direction.



Fig.127-128: Experiment location

The sky view factor is a significant correction coefficient in the calculation of dew water yield. For this reason, the urban surroundings and the roof are schematically modelled and used to perform a view factor simulation in Ladybug for Grasshopper (Fig.129-130). The results can be seen below. The highest view factor is recorded for the middle part of the surface, where it is equal to approximately 60%. However, for safety and accessibility reasons it has been decided to place the object far from roof edges and as close as possible to the main building. The position of the object is highlighted in the images above.

Such position corresponds to the area with less sky exposure. A factor of 0,45 is therefore considered for the simulations. Due to the position in between other volumes, the orientation of the component is also forced to be perpendicular to the main wind direction. This is known to be detrimental for the overall performance, but it is accepted to minimize safety risks related mainly to possible unexpected strong winds that could make the prototype fall.

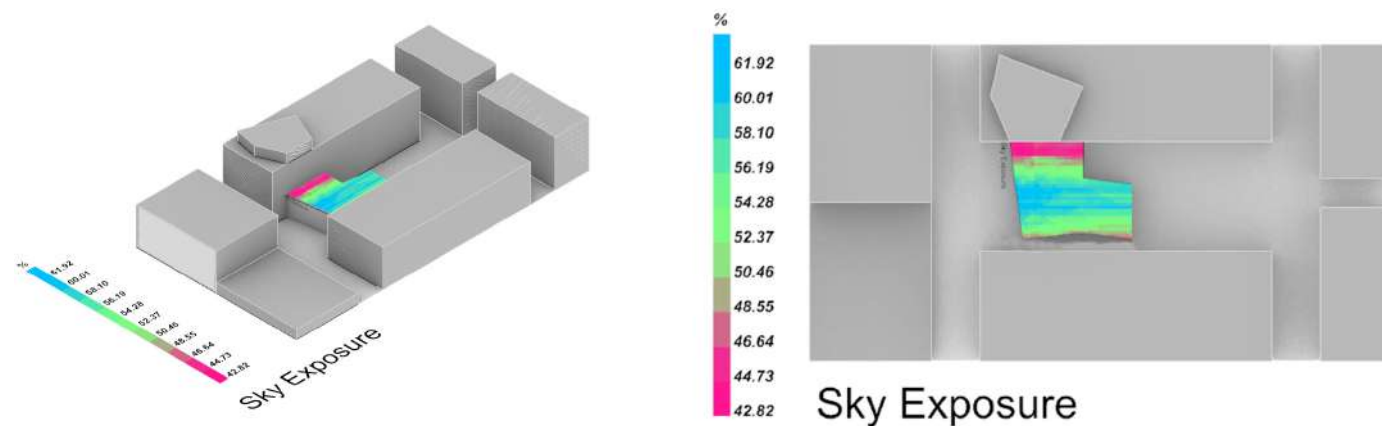


Fig.129-130: Experiment location. Sky view factor calculation

The prototype has been presented in the previous section of the research. Some additional operations have been necessary to prepare it for the experiment. The overall experimental setup can be seen below (Fig.131-132).

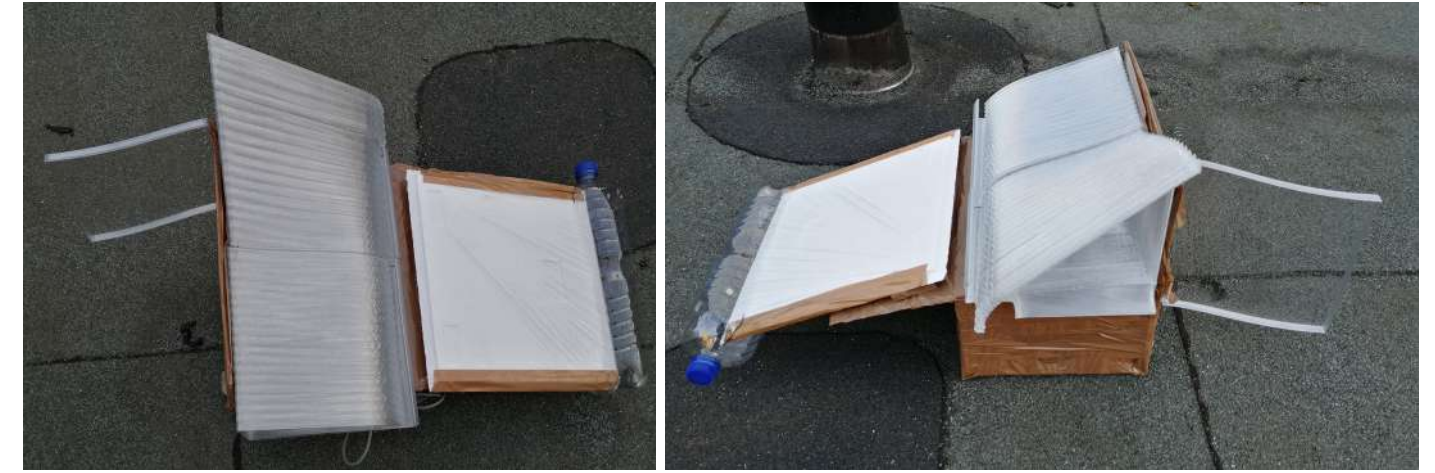


Fig.131-132: Experimental setup

The water-catcher has been fixed to a base which gives an additional height of 15cm to the object, simulating slightly more the roof edge condition in which the component would normally be placed. The base gives also extra weight to stabilize the component and offers support for all the other devices. To understand the benefits provided by the design, a standard water catching surfaces are fixed on the side of the condenser. The condensing surface is realized with a 25x25cm polystyrene board wrapped in plastic foil. In this way the back insulation of standard radiative condensers is simulated as well. A plastic bottle is fixed to its lower edge, so that water can easily be connected and measured. A flat fog-catching harp collector has been 3d printed. It consists of a 20x20cm single layer screen printed with the same shade coefficient used for the water catcher.

The goal of the object is not only comparing the behaviour of the different designs, but also that of monitoring the climatic conditions under which dew and fog events can occur. To do that, a data logger is fixed to one side of the prototype. In this way temperature, dew point temperature and relative humidity can be measured and recorded. An external temperature sensor is added to the logger and placed within the component to provide an estimation of surface temperature. The time interval for recording data is set to 30 minutes.

To simulate condensation, cloud coverage and wind speed values are also needed. As it has not been possible to measure them directly on the object, average weather data for the city of Delft are used.

The prototype is checked twice a day. At 7:00 am in the morning, to collect atmospheric water. The trays are emptied into a jar that is then weighted. A sponge is used to scrape the surface and collect as much water as possible. In case of precipitations during the day, the surface is dried at 8:00 pm, so that dew measurements are still possible overnight.

5.2.2 Experimental results

The prototype is tested for seven weeks, from the 26th of April to the 13th of June 2021. The data collected are presented in the pages below. However, the ideal scenario would have been to perform the experiment for a longer period of time, so that more reliable and insightful information could be gathered regarding the fog and dew collection efficiency of the water-catcher.

The period in which the object has been tested was characterized in the first half by frequent precipitations and by isolated strong wind events. On the other hand, the second half recorded almost null precipitations and much lower humidity levels. The prototype resisted to the atmospheric agents, showing promising results in terms of stability. However, when a 1:1 sample will be tested, reducing its flexibility could be beneficial to obtain a stronger element. Visual analysis of the component showed quick accumulation of dirt particles in the gutter systems and on its inner side. While cleaning the condenser is extremely easy, accessing those areas has been more difficult and should be object of future

improvements of the design. No significant change in colour or visual quality are observed on the plastic component despite the exposition to both rain and intense sunlight.

For what concerns the collection of data, different observations can be made. Firstly, the values recorded for the surface temperature are considered not accurate enough. This is because the sensor was placed on the bottom part of the component, as no other way was found to locate it close to the surface and at the same time protect it from water. Secondly, another problem was related to rainwater. Being able to access the roof only in specific moments, it has not been possible to monitor constantly dew formation. If precipitations are recorded for a night, no condensation can be measured regarding that same night.

The data collected by the logger are plotted in Fig.135. In the first graph it is possible to observe the relationship between external temperature, and dew point temperature. On the bottom graph, relative humidity is plotted, too. The first thing that is noticed is that the relative humidity never reached 100% close to the specimen. This means that in the considered seven weeks, no fog events occurred in proximity of the object. The water yield related to this phenomenon is therefore null and no experimental validation can be yet provided for it.

The bars visualized in the second graph (Fig.135-b) show the precipitations recorded for this period and the water mass collected from condensation. Rainwater collection is not measured on site, as it does not represent the main focus of the experiment. Weather data for the city of Delft are plotted and no speculations on the efficiency of the device in its collection is presented.

In the tested period, the frequency of dew events has been extremely low. During seven weeks, measurable condensation is recorded only on three days. The amount of water collected for each of these events can be seen in Fig.133.

Date	Time	Te [C]	RH [%]	DewPT [C]	vwind [m/s]	Rain [l/m2]	Dew [l/m2]	Cloud coverage	Theoretical value [l/m2]
01/05/2021	07:00	3,5	91,8	2,0	1,9	0	0,034	0,12	4,27E-03
13/05/2021	07:00	8,4	93,8	7,2	0,0	0	0,002	0,25	4,98E-03
20/05/2021	07:00	7,7	96,6	7,0	0,0	0	0,010	1	7,36E-05

Fig.133: Recorded data for condensation event

The measurements are normalized for one unit of area and compared to the theoretical nucleated mass. The values recorded by the logger at 07:00 of the mornings when condensation happened, are used as inputs for the model to calculate the theoretical mass of water. The reason why this particular time is chosen as reference can be observed in the graphs. Condensation is estimated to take place when the difference between the dew point temperature and the external temperature is the lowest. In this way, the energy barrier that vapour has to overcome to start condensing is minimized. In Fig.135-a, it can be seen that external and dew point temperature are closest in the early morning. For this reason, the data recorded at 07:00 are used as reference.

If condensation happened those three mornings, the surface temperature in that moment had to be at least equal to the dew point temperature. To calculate the theoretical water mass the formula previously introduced (see page 24) is used:

$$E = \frac{h(RHe'_{amb} - e'_f)}{L\xi}$$

As it can be seen in the table above, theoretical and measured values approximately share the same order of magnitude. However, also because of the limited amount of data, no specific consideration on the accuracy of the model can be derived. Significant difference is noticed between the measurements and the corresponding predictions. The exact reason for it cannot be said with complete certainty, but one possible explanation could be the effective duration of the overall process. Experimentally, yield is measured daily and no clear information about the nucleation time can be collected. On the other hand, the water yield is calculated theoretically on an hourly base. The nights in which the difference is more considerable, dew formation lasted probably more than one hour.

Even when experimental results are higher than the calculated ones, the magnitude of such difference is not constant so it is not possible to develop a correction coefficient. However, the model used to simulate the process seems to be conservative in its predictions. To have a better insight on this, more data are needed. Such data could be obtained by performing a similar experiment for a longer period of time and by choosing a more suitable location. On the other hand, the importance of accessing more complete weather data or increasing the number of parameters measured on site is considered paramount to validate predictive computational models.

As final check of the reliability of the data recorded, the radiative heat exchange coefficient is calculated for those specific moments. A null cloud coverage is in this case considered. To calculate this value the heat balance needs to be solved.

$$P = LE + Q_{cond} + Q_{conv}$$

The radiative heat exchange is calculated assuming as done previously a surface emissivity of 0,92 for the condenser. The results are then compared to the Unsworth approximation, which has been introduced and adopted in the pre-design phase. The comparison between the results for each dew event can be seen in Fig.134.

Date	α_{rad} [W/m2K]	α_{rad} theory [W/m2K]	%
01/05/2021	4,3	4,0	108%
13/05/2021	4,5	4,2	107%
20/05/2021	4,5	4,2	108%

Fig.134: Radiative heat exchange coefficients

The initial results appear to be encouraging towards the calculation of a correction coefficient to eventually apply to the simulative models that are used to approximate the yearly performance of the water-catcher for various locations. However, the experimental setup should be updated and a longer testing period should be considered, so that more data are collected. For the moment, it is not possible to integrate this result into further calculations. The scarcity of dew events should be critically evaluated, but the climatic difference with the case study location and rainwater should also be considered. During the timeframe of the experiment, in fact, 125mm of rain were recorded.

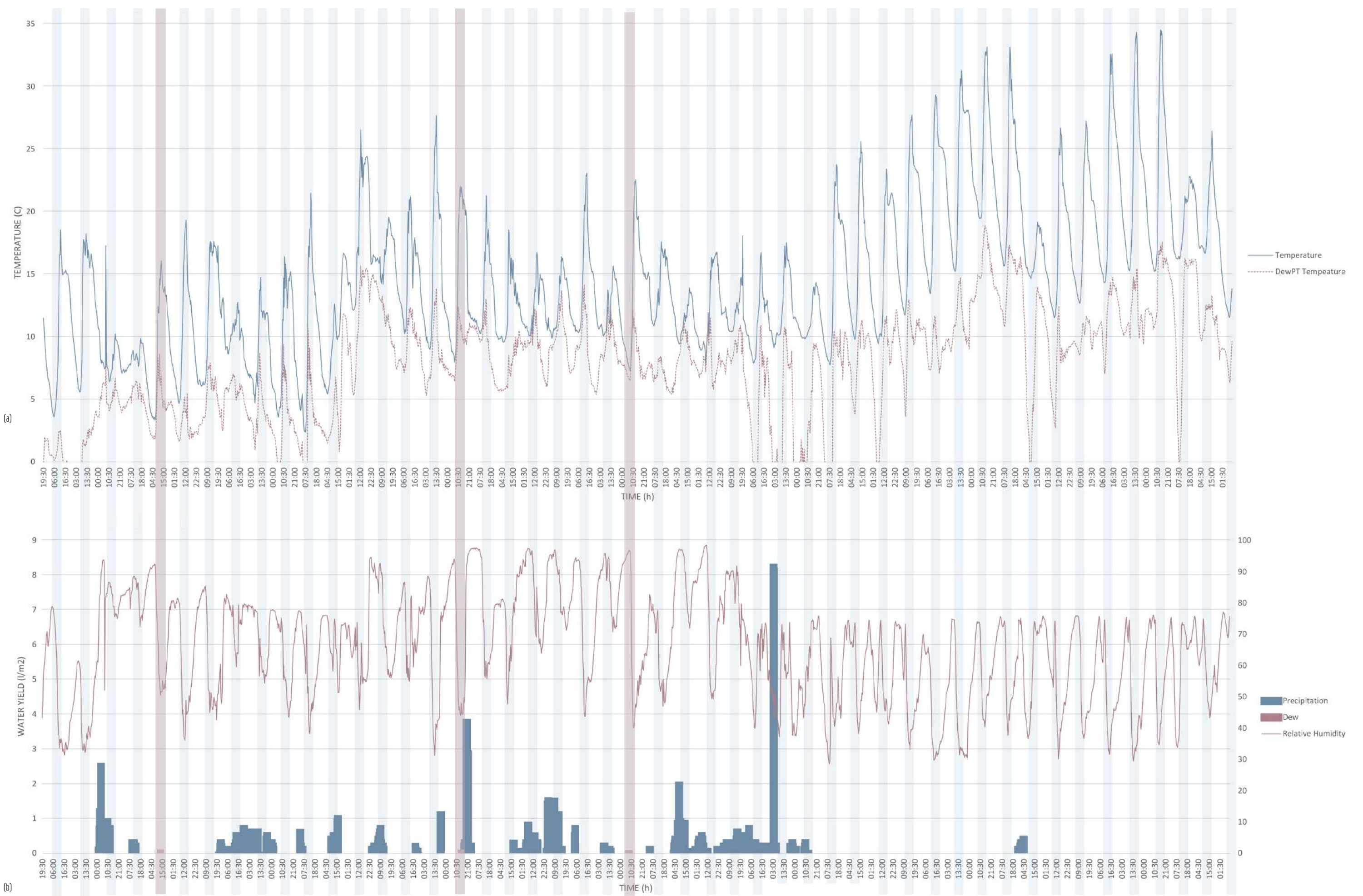


Fig.135: Recorded experimental data

5.2.3 Water collection potential

The predictive Excel models developed in the Pre-Design phase and used to analyze and explain the processes of both dew and fog collection, are used in this stage to calculate the total water collection potential of the designed component. The calculation is performed on the weather data recorded for the city of Rabat, which has previously been chosen as case study for the research.

Hourly weather data are extracted from the specific .epw data file and converted into .xls format, easier to process and analyze in Excel. The values related to ambient temperature, dew point temperature, relative humidity, wind speed and cloud coverage are used as variable inputs for the calculations. Additional parameters are defined as constants to use throughout the whole calculation. The chosen values are shown in the table below (Fig.136).

Symbol	Description	Value	Units
ϵ_{surf}	Infra-red emissivity of condenser	0,92	/
σ	Stefan-Boltzmann constant	5,67E-08	W/m ² K ⁻⁴
L	Heat of vaporization of water	628	Wh/kg
h_{cond}	Conductance coefficient	0,2	W/m ² K
ξ	Psychrometric constant	66	Pa/K
SVF	Sky view factor	1	/

Fig.136: Input parameters for dew simulation

Iterative calculations is performed on the hourly data to predict the surface temperature reduction due to radiative cooling and the related collected mass of condensed water. The calculations are performed relatively to a surface of 1m² and the water yield is calculated monthly. In this way it is possible not only to analyze the yearly results but also to understand the efficiency of such technology in different parts of the year. The results are organized in a table (Fig.137) and plotted (Fig.138) to get a more intuitive visual understanding of their reciprocal relations.

	January	February	March	April	May	June	July	August	September	October	November	December	Total
Dew yield [l/m ²]	0,67	0,93	0,70	0,64	8,22	15,67	9,38	14,18	18,54	10,21	1,59	1,46	82,19
Dew yield [l/module]	0,23	0,32	0,24	0,22	2,79	5,33	3,19	4,82	6,30	3,47	0,54	0,50	27,95

Fig.137: Collected dew monthly predictions

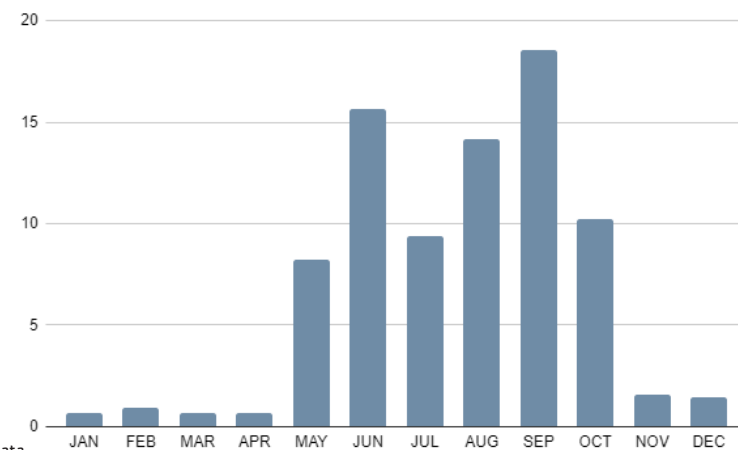


Fig.138: Collected dew water. Monthly data

A significant gap between potential water collection is clearly visible between cold and warm seasons. Almost 93% of the total amount of water is in fact collected between May and October, while in the other months the condenser's yield is almost negligible. The highest value is recorded for September, with a daily average of 0,61 l/m². This value is aligned with those found in literature, that are between 0,4 and 0,8 l/m² (Khalil, 2015).

The results are translated into the water yield that a single 3d printed module can achieve. For this reason, its surface area exposed to the sky is measured and used to adjust the monthly data. An area of 0,34m² per module is considered. As it possible to see in the second row of the table presented above, the total amount of water that a single component could collect yearly on a roof in Rabat is 27,95 litres.

Knowing this data, it is then possible to calculate the total surface area necessary to satisfy a specific water demand. According to the research, the basic daily water need of a person is equal to 50 litres. By fulfilling particular recommendations in terms of efficient use, this quantity can be reduced to 32 litres (Zielinski, 2020). Starting from both these quantities, different scenarios are analyzed and calculated.

The first one is calculated by dividing the total water yield for the whole year. This could be possible if a long-term storage system is combined to the water collecting system. Issues and recommendations related to sanitation and hygiene of such solutions are not explored in this research. The second solution considers instead that other water sources are available and integrated to the atmospheric water harvesting system. For this reason, dew water could be considered as a supply for the summer season. In this period not only the collection rate is exponentially higher, but the climate is more dry and droughts are more frequent. With this approach the total water yield has to be divided by a reduced amount of days, increasing the daily supply.

Dew yield [l/m ²]		Water demand = 50 litres		Water demand = 32 litres	
		Required area [m ²]	Required modules	Required area [m ²]	Required modules
Yearly supply scenario	0,23	222	653	142	418
Summer supply scenario	0,38	130	383	83	245

Fig.139: Required surface and modules for dew collection

As it can be seen from the table above (Fig.139), considering a reduced water demand and a short-term summer storage, approximately 83m² of condensing surface would be required, which is equal to 245 of the designed water-catchers. 142m² would be needed otherwise.

However, different considerations need to be made regarding these results. The data have been calculated theoretically and do not take into account the specificities of different locations such as surrounding buildings or roof height. In this sense, the wind speed used for the calculations and recorded in the weather data represents a reference value that would change according to specific conditions. Moreover, the water yield considers only the nucleation efficiency of the surface. The collection efficiency should be estimated as well.

On the other hand, the estimation presented above refers only to dew potential and does not include other atmospheric water sources such as rain and fog. The number of required modules is expected to decrease significantly when these events are taken into account.

To consider fog flow, the efficiency of the component needs to be calculated. Due to its geometry, different considerations are made the predictive model presented in the Pre-Design phase for standard collectors is slightly modified. The aerodynamic efficiency of fog collector has been defined as the product between the filtered and the incident fog fraction:

$$\eta_{ACE} = \varphi\chi$$

The incident fog fraction depend on the number of intercepting layers and on their solid coefficient. The filtered fraction instead is related to the magnitude of the flow flowing through the screens. Since the flow is forced to go through an enclosed space, the filtered fraction can in this case be considered 100% of it. The efficiency is then reduced to the incident fog fraction, that determines the amount of collected water.

As it has been shown in the previous sections, the calculation of the flow rate through the component is performed through a CFD wind tunnel simulation (Fig.140). A velocity of 3 m/s is set at the inlet and a collector with 4 layers with a shade coefficient of 0,6 is tested. Assuming a fog liquid water content of 0,5 g/m³ (Azeem, 2020), the flow is then used to calculate the total amount of collected water.

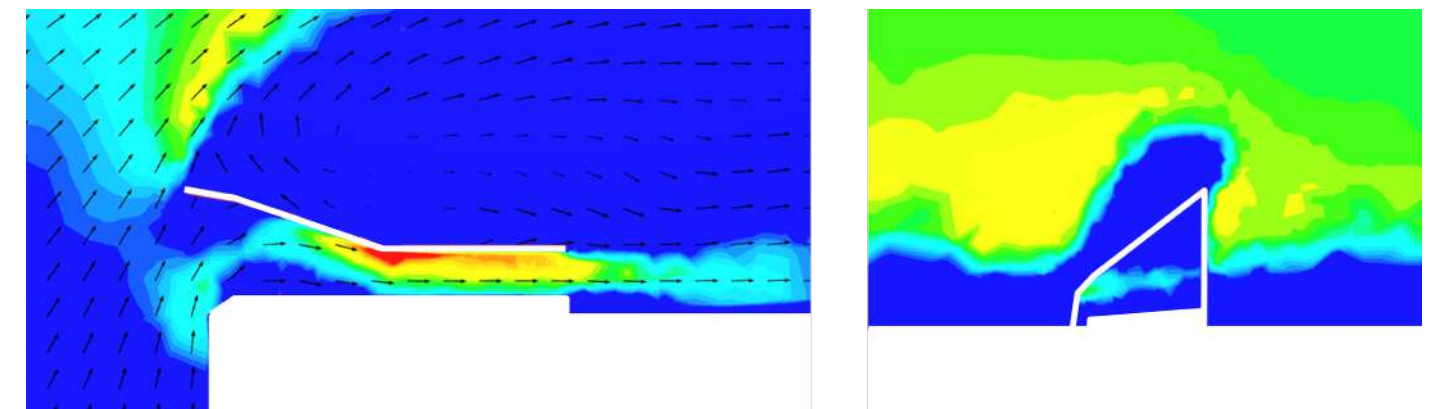


Fig.140: Water-catcher. Wind tunnel simulation

The same value is calculated then for a standard collector with the same shade coefficient and amount of intercepting screens. The comparison between the two values is used to provide an estimation of the efficiency improvement achieved thanks to the component's design. Results are summarized in the Fig.141.

	Num. screens	Shade coefficient	Area [m ²]	Flow [m ³ /s]	v _{ref} [m/s]	Total efficiency	J [l/hm ²]	%
Standard collector	4	0,6	0,08	/	3	0,29	1,58	100%
Water-catcher	4	0,6	0,08	0,106	1,325	0,97	2,31	146%

Fig.141: Fog collection yield. Simulation for water-catcher and standard harp

Even if the average speed within the component is lower than the initial outdoor one, all the air that flows in the component goes through the screens and the efficiency rises significantly. In terms of yield, the water catcher appears to collect 46% more water than a standard screen with similar properties.

As it is not possible to perform CFD simulations for all the hourly weather data related to the city of Rabat, the recorded wind velocities are used as variable input for the Excel predictive models. According to the findings just presented, 146% of the total water yield is considered as estimation of the component's performance. The same settings in terms of liquid water content, solid coefficient and number of screens are used for the analysis.

	January	February	March	April	May	June	July	August	September	October	November	December	Total
Fog yield [l/m ²]	38,93	12,62	93,94	3,92	11,08	4,77	8,69	6,39	21,23	66,09	38,24	31,93	337,81
Fog yield [l/module]	3,11	1,01	7,51	0,31	0,89	0,38	0,70	0,51	1,70	5,29	3,06	2,55	27,02

Fig.142: Fog collection monthly simulation data

Data show that fog events, despite being less frequent than dew, can still represent a consistent supply throughout the whole year (Fig.142). Results have been calculated based on 1m² surface and then normalized to 0,08m² area that corresponds to the inlet opening of the component.

As for the condensation, results are plotted (Fig.143). March and October have the highest amount of collected fog, but as it is highlighted in the table above, higher water collection rates are generally recorded for the period between September and March.

If compared with the data recorded for condensation, this suggests one of the possible benefits related to integrate the two collecting systems. In fact, the periods of maximum efficiency correspond to the different parts of the year. In this way a more consistent supply could be produced throughout the whole year by the component.

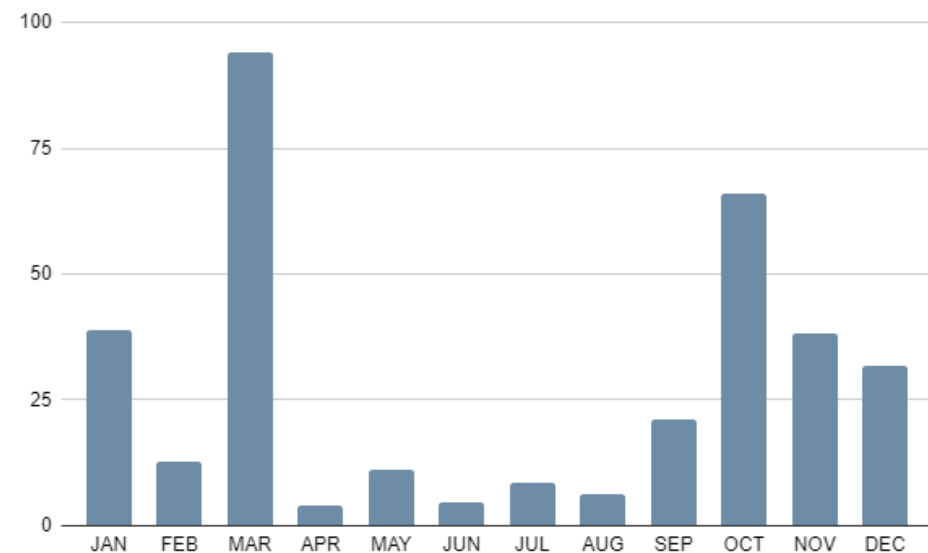


Fig.143: Fog collection monthly simulation data. Graph

The normalized results for the performance of the component for both fog and dew collection can be combined to calculate an estimation of its total water potential. The total yearly yield of one module is equal to 55 litres, which corresponds to a daily output of approximately 0,15 litres.

Water yield [l/module]	Water demand = 50 litres		Water demand = 32 litres	
	Required area [m ²]	Required modules	Required area [m ²]	Required modules
Yearly supply scenario	0,15	113	332	212
Summer supply scenario	0,26	66	195	125

Fig.144: Required surface and module. Dew and Fog scenario

The calculation for the required surface area and amount of modules necessary to fulfill the water demand of a single person is performed again taking into account the combination between fog and dew collection (Fig.144). Compared to the results for only condensation, the introduction of fog catchers allows for a 40% reduction of the number of required modules. The beneficial effects of combining the two technologies is therefore clearly noticeable.

The necessary surface to provide the minimum quantity of water it is equal to 42m². However, rainwater is still not considered into the calculation. Despite the fact that the current research does not focus on it, providing an estimation of its impact is useful to get a more realistic insight on the performance of the water condenser. For this reason, cumulative precipitation data for the year 2020 are considered. 382mm of rain have been recorded for Rabat in 2020 (meteostat.net). Considering the surface area of the water catcher, this would mean that approximately 130 l/m² of rain would it. A collection efficiency of 80% is considered for rainwater and the resulting value is added to the previously calculated water yield. The data are shown in the table below (Fig.145).

Water yield [l/module]	Water demand = 50 litres		Water demand = 32 litres	
	Required area [m ²]	Required modules	Required area [m ²]	Required modules
Yearly supply scenario	0,51	34	99	21

Fig.145: Required surface and module. Dew, Fog, and Rain scenario

Since the precipitations data are considered for the whole year, only the yearly supply scenario is calculated in this stage. The results show that when also rain is considered, the water-catcher could reach an average daily yield of approximately 0,5 litres of water. This means that to reach the threshold of the minimum necessary water supply 22m² would be required. This surface is equal to approximately 63 water-catchers (Fig.146).

When an household of four people is considered, the total surface would rise to 88m². Despite being a large area, it could still be met partially or totally by the flat roofs of the low-rise buildings that populate the cityscape of cities like Rabat. However, this does not take into account that fog collection happens mainly when the water catchers are placed on the roof's edges. This would cause a decrease in efficiency and an higher minimum surface.

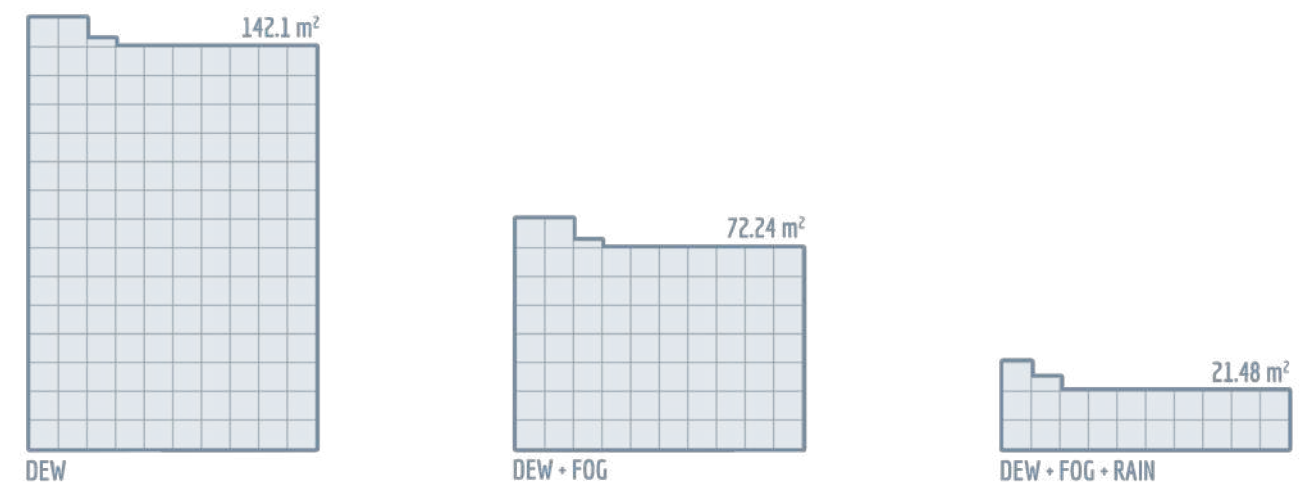


Fig.146: Required surface for different scenarios

5.3 FABRICATION EFFICIENCY

Realizing a 1:2 prototype and segments in a 1:1 to scale, allows not only to test the performance of the component, but also the efficiency of the printing process and the quality of the results. Issues and part's defects can be due to either design flaws or inaccurate printing settings. Such visual analysis has allowed the research to proceed and it has represented active part of the design development phase. Performing the same observations at this stage can give useful insights on the limitations of the research and suggestions for its further development.

The analysis of data such as printing time and mass has been useful to progressively optimize the fabrication process. One further step is taken in this direction, trying to estimate the economic feasibility of the project. In this way, time and material use can be translated into a rough monetary equivalent, that represents a more understandable indicator of the feasibility of such projects in developing countries.

5.3.1 Printing quality

As it has been shown in the dedicated section, the complete component is prototyped for experimental reasons to a 1:2 scale. A double wall count is used to increase the stability of the component and minimize layer adhesion problems. 1:1 sections are prototyped to test the different printing settings developed previously. Only a 0.4mm nozzle is used, so the settings assumed for a larger 1.2mm nozzle have not been tested yet. The images below show a section printed with double 0.4mm wall count (Fig.147) and one printed with 0.8mm wall width and half speed (Fig.148). The flow of material in the unit of time is therefore the same. No settings are changed for the linear infill pattern that generates the fog-catchers. For this reason it has not been considered paramount to print in option from Fig.148.

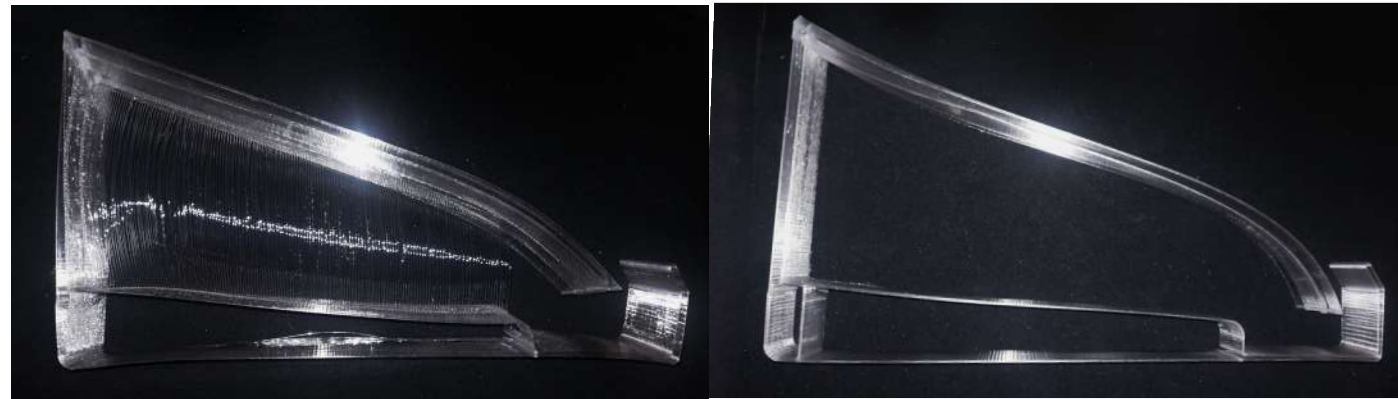


Fig.147: Double wall 1:1 section

Fig.148: Single wall 1:1 section

It is possible to notice from a qualitative inspection that the specimen printed with a single wall count appears to have a higher visual quality. Less bending is also noticeable in the middle part of the component, meaning that it is stiffer than the previous version. Reducing the wall count and the speed is considered beneficial for the overall end result. This needs to be evaluated in terms of economic feasibility, as it can impact significantly the material and energy use related to the fabrication of a single water-catcher.

Zooming in, it also possible to analyze the print quality more in detail. Particular attention is given to the fog-catching screens, as they have been a delicate part of the design process (Fig.149-150). Significant sagging is observed in the screen layer. However, this does not impact negatively the collection efficiency as long as the wires are continuous from top to bottom. From this point of view, no major defects are observed in the 1:1 prototype. Also the maximum span, which is equal to 15cm, is bridged successfully.

The sagging needs to be taken into account into the correct spacing of the screens within the module. In fact, if they are too close the wires of the upper screen might stick to those below, leading to print failure.

For this reason, the settings related to the fog-catching screens can be considered validated. Overall part settings still need to be tested into the print of one complete component and more tuning might still be necessary. The maximum flow rate bearable by the current extruder will be tested and the possibility of switching to a bigger nozzle can be taken into consideration.



Fig.149-150: 1:1 section details

5.3.2 Local production's feasibility

The research objective set at the beginning aims to propose a solution for developing countries through recycled plastic waste. However, the design by prototyping process has been performed throughout the year using only commercially available PETg and PET filament. The price of a 1 kg spool of filament is around 30 euros. It is clear that such initial cost would already compromise the feasibility of an application of the research in developing countries such as Morocco. In fact, according to literature (WorldBankGroup, 2016)⁵⁶ the price of a spool there could rise to 50-65 euros due to shipping expenses.

Considering an alternative scenario becomes therefore paramount. Locally collect and process waste plastic into 3d printing filament is in fact expected to drastically reduce its cost. Such filament becomes then the raw material for the production of the designed building components, that represent the final step of the upcycling process of waste plastic. Analyzing this flow helps not only determining the cost of the water-catcher, but also understanding the social and economic impact that this could have on local communities.

In order to transform waste into a 3d printed roof component, a production facility should take care of a series of different steps (Gall, 2020)⁵⁷. These could either be located in the same facility or give the opportunity to develop different small businesses. The main actions are:

- Collection of waste plastic
- Cleaning of the plastic
- Shredding into flakes of similar size
- Extrusion of the flakes into filament
- Printing of the roof components

These steps are composed of many more smaller processes, that are listed in the diagram below (Fig.151). Moreover, during the process the material itself changes shape and state. The different products are for each state are shown in the diagram.



Fig.151: Recycled plastic filament's production process

To estimate the cost of the final component one needs to get an overview on all the phases. According to literature, waste collection and management in developing countries is vastly informal and performed by waste pickers that represent the least rewarded working force in the whole waste recycling process (Gall, 2020). Virtuous realities such as the Kenyan startup Mr. Green Africa represent alternatives to this system, where the pickers are seen as "invisible heroes". This company produces granulate from different kind of plastic collected locally. To do so, it buys waste for a fair fixed price from the pickers, that are in this way encouraged to keep collecting. The price is fixed to 19 Kenyan Shillings per kg of plastic (approximately 0,15 euros). The company produces then different products that are commercially available for various applications.

However, without considering the profit of the company the price for the granulate is still low. The feasibility of filament's production from plastic waste buy-in for a case study in Tanzania has been researched (WorldBankGroup, 2016). Information on the energy and labour cost is provided, together with estimations on the durability of the extruder. An expected cost of 2,84\$/kg (2,35 euro/kg) is calculated, considering a lifespan of 3 years of the extruder. In this case plastic flakes are used for the production of the filament and not more processed granulate.

An initial extruder cost of 1500\$ is considered. However, not commercially available solutions are widely known among the 3d printing community and have been tested and proved their efficiency in the recycling of polymer waste. It is the case of the RepRapable Recyclebot extruder, which is almost full 3d printable within 24 hours and for a cost of less than 700\$ (579,37 euro) (Woern, 2018)⁵⁸. Considering this value and without any profit margin, the cost of the filament can be brought down to 1,77\$/kg (1,46 euro/kg). This price is equal to 5% of that of the filament that has been used for the research.

The costs resulting from the first phases of the reprocessing of plastic are estimated and summarized in the diagram below (Fig.152). The filament cost can be used as input for the calculation of the building component's price.

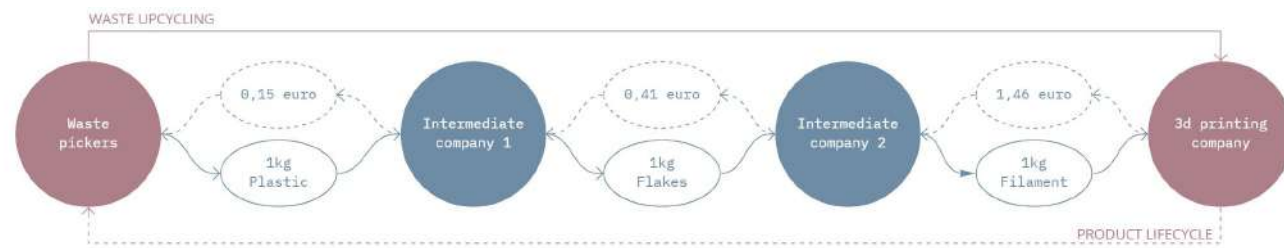


Fig.152: Intermediate production steps. Cost estimation

The diagram highlights also how the two most important links of the production chain are the waste pickers that start the upcycling process and the 3d printing company that develops a products out of it. Cyclically, the product turns into waste after a certain period of time and can be reintroduced into the loop as waste. Moreover, the printing facility could implement more advanced tools such as granulate extruders to print directly from waste plastic flakes. In this way one intermediate processing step could be skipped, resulting in lower costs.

To perform the calculation for the last production step, some assumptions need to be made. In particular, a 3d printer needs to be chosen as reference and some estimations on the required labour are necessary. As the research has been performed with a Anycubic Chiron and the prototype has been tested only through it, the same printer is considered for calculations. A durability of 3 years with an average of 50 working hours per week are considered. As mentioned above, more sophisticated machines could be used, but they would require a considerable initial investment that is not considered feasible in the early phases of developments of a local business.

The variables that influence the total cost are:

- Material: the filament cost is based on literature research and set to 1,46 euros/kg.
- Tools: the cost published on the producer's website is taken as reference (372 euros).
- Energy: an energy cost of 0,41 euros/kWh is found in literature (WorldBankGroup, 2016) and an average energy consumption of approximately 400 W is considered for the printing setup
- Labour: a labour cost of 1,66 euros/h is considered (WorldBankGroup, 2016). One worker is considered enough to operate multiple printers. No training is taken into account
- A total of 6 is printers is considered manageable by one person and it is therefore considered.

The goal of the calculation is to understand a realistic possible price for the designed building component. No speculations on the magnitude of the initial investment is done. To compare the costs, the different values are initially calculated for one kg of material. To get the right proportion about the material flow and energy consumption, the data simulated in the section related to the optimization of the printing process are considered. For a 1.2 mm nozzle, the smaller module of the component would weight 1,3 kg and take approximately 4,5 hours to print. Based on these values, the following results are obtained:

- Printer write-off [euros/h] = 0,047
- Printer write-off [euros/kg] = 0,16
- Energy cost [euros/kg] = 0,69
- Labour cost [euros/kg] = 0,30

These values can be added to the filament's cost to understand a price per kg of printer materials. Knowing the total weight and printing time of the building component can be estimated. A printing time of 9 hours and a mass of 2,5 kg is considered for the overall water-catcher.

A total cost of 6,52 euro is calculated for one complete water-catcher (Fig.153). Looking at the cost breakdown illustrated in the diagram below, future possible optimizations could be thought. In this process, different design features of the component could influence the total cost. In one scenario, the printing time could be reduced as much as possible. This would reduce the labour cost but would most probably lead to the use of bigger nozzles and more powerful extruders. In this way, more material and energy would be spent to produce the same component in a shorter time. On the other hand, material use could be better optimized to minimize the required filament. A similar decision would probably result in thinner but denser wall, impacting negatively the printing and labour time.

However, from this estimation the filament results still to be the highest expense to face. Minimizing the intermediate steps in between raw material and final product, and improve the design towards optimal use of material would have the greatest impact on the overall cost of the component.

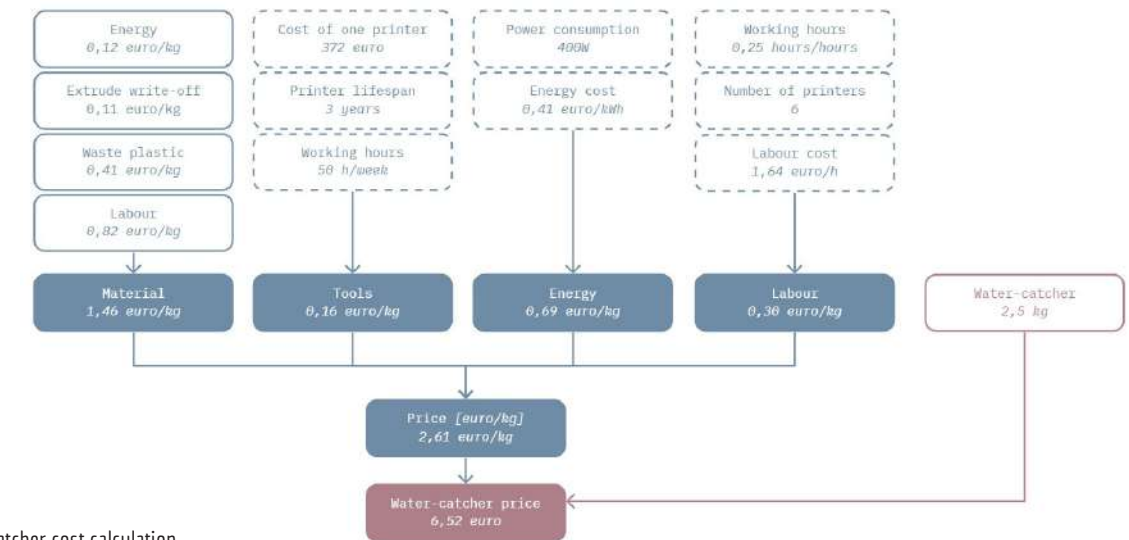


Fig.153: Water-catcher cost calculation

The price per component could still seem too high to be easily purchased in local communities. However, in order to get a realistic image it has to be compared to the current cost of drinkable water. Water in Morocco is usually provided by private institutions, and usually a bottle of fresh water costs 1 euro/litre (Lekouch, 2012). The predicted results can be compared to this value, providing an overview of possible savings. Economic savings would generate wealth in local communities that would be able to invest to fulfill other needs. At the same time, due to the local collection of water, especially women, would not have to daily long walks to fetch water. This generates time savings and feeds the positive loop generated in the community by the water-catchers.

Lekouch (2012) provides interesting estimations of the cost of installing different kinds of radiative condensers on existing roof slopes. The calculated values take also into account rainwater collection. For this reasons, the performance of the water catcher is calculated also in a scenario that does not consider fog collection, but only rain and dew. In this way the benefit provided by integrating the third collection system can be more easily understood. A durability of 4 years is estimated for the water-catchers.

	Water Yield (l/module)	Durability (years)	Component Price (euros)	Water price (euro/m ³)	Water price (euro/l)
Bottle Water	/	/	/		1
Rain and dew collector					
Hydrophilic paint	/	10	/	5,7	0,006
Hydrophilic foil	/	4	/	10	0,010
Water catcher					
Rain + Dew	157,83	4	6,15	/	0,010
Rain + Dew + Fog	184,85	4	6,15	/	0,008

Fig.154: Atmospheric water harvester cost comparison

The results show that the cost for one water-catcher could be compete with that of more traditional solutions (Fig.154). Additionally, the design is thought for flat roofs, which would increase its convenience compared to other methods. However, the durability of the product should be tested to understand the reliability of the calculations.

Compared to bottled spring water, the price per litre is extremely low (Fig.155). This should ensure enough margin for filtering and sanitizing the water, while still keeping it below that threshold. This could also generate interesting consequences in the pricing of water from privates, since they would need to remain competitive on the market.

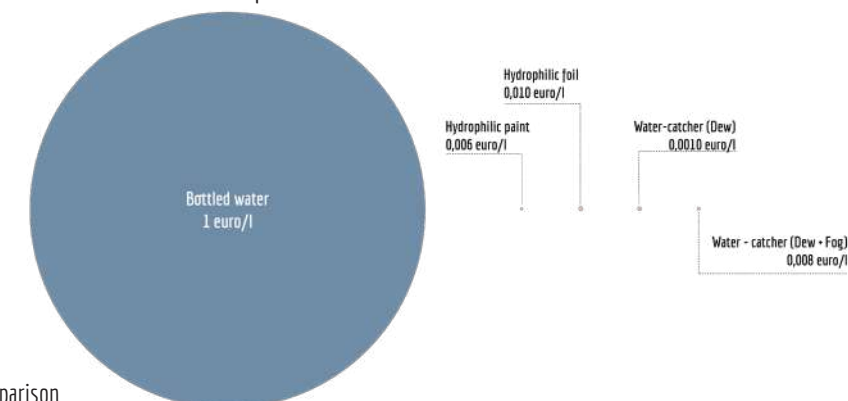


Fig.155: Water cost comparison

A more realistic cost estimate can be provided when also water disinfection costs are taken into account. Thanks to the water-catcher technology, water collection happens extremely close to its point of use. For this reason, HWTS (*Household water treatment and storage*) methods are considered (Lantagne, 2006)⁵⁹.

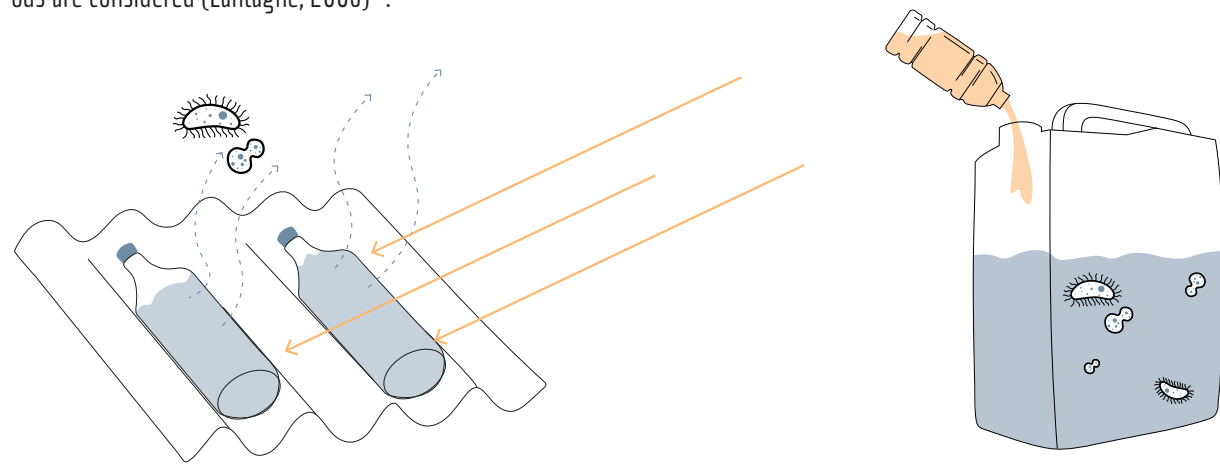


Fig.156: Water sanitation methods

In particular two methods are considered due to their extremely low cost or worldwide availability (Fig.156):

- *Solar Disinfection*

Plastic bottles are filled with low-turbidity water. The bottles are shaken to oxygenate the water and placed in the sun for six hours. The method has been proven to eliminate bacteria and viruses (Lantagne, 2006), and has no additional cost.

- *Chlorination*

A solution with water and sodium hypochlorite is created. The solution is widely available in bottles, thanks to the interventions of NGOs such as PSI (Population Services International). The bottle comes with instructions that make it easy to use (Lantagne, 2006). The cost of a 150 ml bottle is around 0,21 US dollars (0,17 euro) and can sanitize up to 1000 litres of water (Blum, 2014)⁶⁰.

The cost estimate of one litre of water can be adjusted according to the new findings (Fig.157).

Sanitation method	Equipment		Basic water cost [euro/l]	Sanitation additional cost [euro/l]	Total cost [euro/l]
	Cost	Units			
Solar disinfection	0	euros	0,008	0	0,008
Chlorination	0,17	euros/bottle	0,008	0,0002	0,0082

Fig.157: Adjusted water cost from water-catcher

As the experimental results do not yet give a fully reliable overview on the water-catching performance of the component, it is interesting to compare the impact that a reduced water yield could have on the overall cost. The water yield is progressively reduced from the calculated theoretical value (Fig.158). It is found, that even a 95% reduction would lead to a cost per litre equal to 0,16 euros, which is approximately six times less than the price of bottled water (1 euro/bottle). However, this corresponds to an increase of around 2000% when the cost is compared to the initial one. It is noticed that 85% of the initial yield represents the threshold below which the application of the water-catcher becomes less competitive with existing technologies in the field of atmospheric water harvesting.

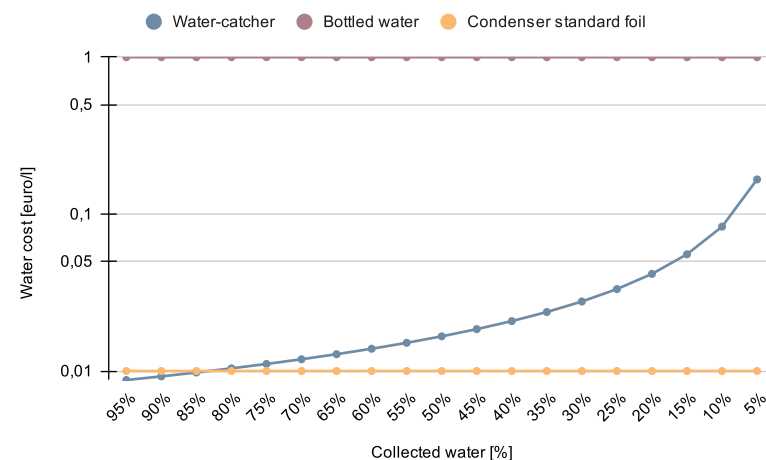


Fig.158: Yield-to-cost comparison

5.4 NEXT STEPS

5.4.1 Design improvements

Prototyping and testing the first design of the water-catcher showed some flaws that can become the object of future research and design development. In the last phase of the research, some of the possible improvements are analyzed and integrated into the final prototype. The modifications concern various aspects of the geometry:

- Storage into water trays

The initial design shows problems achieving an efficient flow of water from its main body towards the side where the trays are placed. This is because of the additional thickness of its edge that represents a flat surface where droplets can stagnate and slide away when the tray is inspected. For this reason, this detail is improved through the modelling of a slot for the tray within the main part. In this way, the two elements overlap and water losses are reduced (Fig.159).

- Connection between modules

The 1:2 modules prototyped for testing were designed to connect only on their lower part. However, the condensers were in this way able to move independently, leading to air losses through the gap and risks for the structural integrity of the overall component. Before starting the experiment, two nails are fixed on the upper and lower corners of the condensers and used to better fix the two modules. In a later stage, two connectors are modelled in the same position and integrated into the 3d printed geometry. Due to their conical shape and to the absence of bottom layers in the front module, the connectors can slot into it and connect the parts (Fig.160).

- Back insulation of the condenser

To reduce printing time, the modules have been printed at first without any bottom layer. In this way, the condenser surface presents an open cavity that could reduce its cooling potential. The design explores the possibilities of mono-material fabrication, so additional insulation material on the back of the plate are not at first considered. Since a closed air cavity provides thermal insulation as well, the element design is modified through the introduction of bottom layers in the back module. This leads to a slight increase in printing time but it is considered beneficial for both water-catching performance and structural stability of the design.

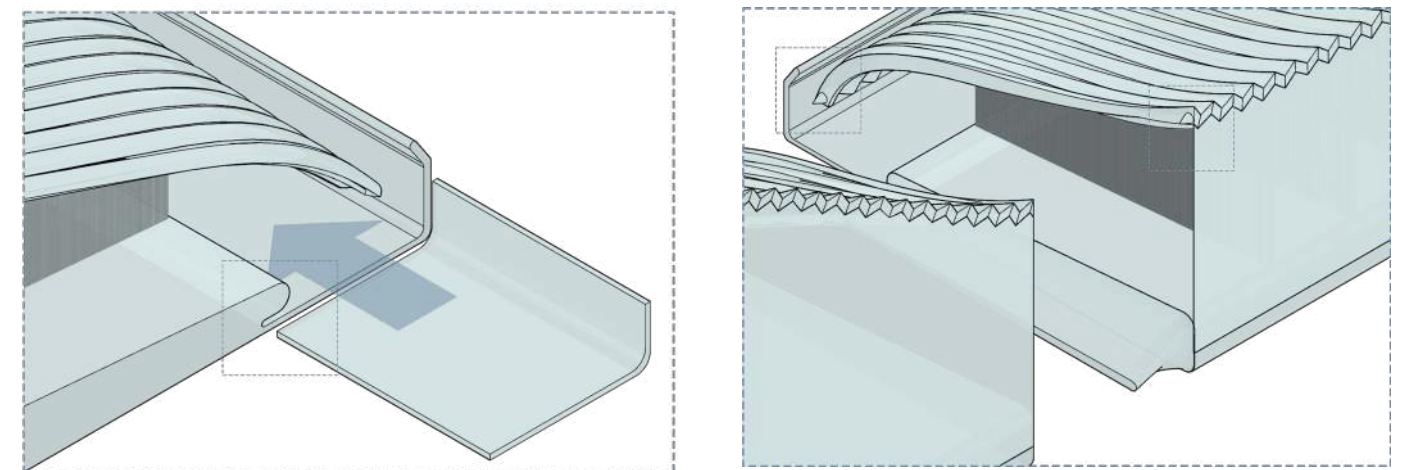


Fig.159-160: Design improvements

5.4.2 Water-catching performance

The water-catcher has been tested for almost two month in the city of Delft. Limitations related to the location, urban surroundings, and nature of the experiment were known from the start. However, the performance of the component has been worse than expected. The reasons for that can be multiple:

- the sky view factor of the condenser was too low due to the specific positioning of the specimen on the rooftop.
- the measurements and control of the experiment was rudimental, due to the limited access to the rooftop and to the domestic resources available.
- the weather conditions were not ideal and did not resemble those for which the design is thought.

However, the standard control surfaces for fog and dew collection did not show any improved behaviour compared to that of the water-catcher. Moreover, no fog event has been recorded by the data logger during the whole experiment. This does not coincide with the information provided by past weather data used as reference for the rest of the research. In fact, for the city of Delft, 5 fog events are recorded for the month of May 2021 (<https://www.timeanddate.com>). This highlights the limitations of using standard data for atmospheric water potential studies, and the need to collect local data. Based on these considerations, a second evaluation of the water-catcher's performance could be improved in different ways:

- Location

The experiment should be performed as close as possible to the case study location. The climate should at least be comparable. A rooftop in a more homogeneous urban height context should be chosen, so that higher sky view factors could be achieved. As for the positioning of the specimen on it, the element should be safely placed on the edge of the roof, so that wind intake is maximized.

- Duration

The experiment should be performed for a longer period. In this way, more reliable and complete information on the overall yearly performance of the component can be obtained.

For example, Lekouch (2012), which has been used as main reference for the experimental aspect of the research, reports data for one year in the city of Mirleft (Marocco).

- Data

Wind speed, surface temperature, cloud coverage and amount of precipitations need to be measured together with the other parameters (ambient temperature and relative humidity). In this way, the dependency from external weather data is minimized and higher control can be achieved in maximizing accuracy and reliability of data.

5.4.3 3d-printability

The design improvements discussed above take into account 3dprinting constraints and are thought to facilitate the fabrication process. Next to it, other aspects of the printability of the design can be investigated in future research and represent useful developments of the design. In particular:

- Printing equipment

A mid-size FDM printer was used for the research. The constraints this brought to the design concern mainly the maximum print dimension and the extrusion rate of the 0.4 nozzle which is mounted on it. As shown in the previous sections, different AM tools allow for the design and fabrications of different components at different scales. It would be relevant to study the impact of bigger nozzles or more advanced tools such as robotic arms on the fabrication efficiency and quality of the end product. To increase the affordability of the process, a customized printer could also be designed with off-the-shelf components. In this way not only the equipment costs would drastically be reduced, but the control on the manufacturing process could increase and be optimized for parameters such as dimensions, extrusion rate or material cooling.

- Printing material

The research focuses on exploring the potentials of processing waste plastic for additive manufacturing applications. rPET is considered as main material from the beginning, as its application for the production of commercially available filament is more common. As said before, this type of plastic is also extremely diffuse and easy to recognize. All these reasons, make it a suitable option for 3d printing. However, plastic waste is composed of different polymers. Specifically, seven groups are usually identified⁶¹. When their recycling is possible, the process is often different from polymer to polymer. Data about polymer classification and recyclability is presented in Fig.161.

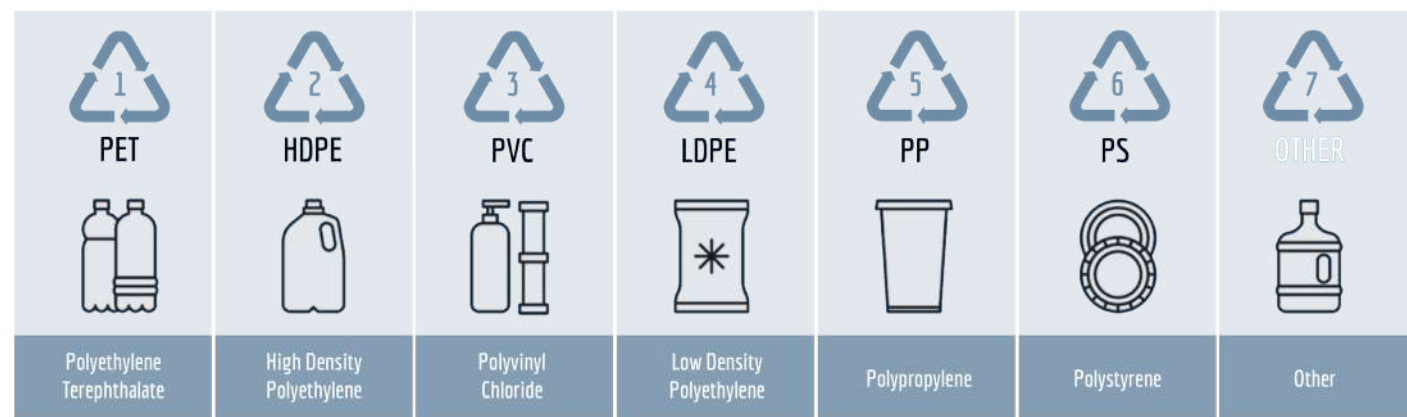


Fig.161: Types of plastic polymers

According to the data presented by Geyer (2017)⁶¹ about waste production by polymer for 2015, PET comes in fourth position after LDPE, PP, and HDPE (Fig.162). Even if all these polymers are recyclable, the process for flexible LDPE products is challenging and might require specific blades for shredding.

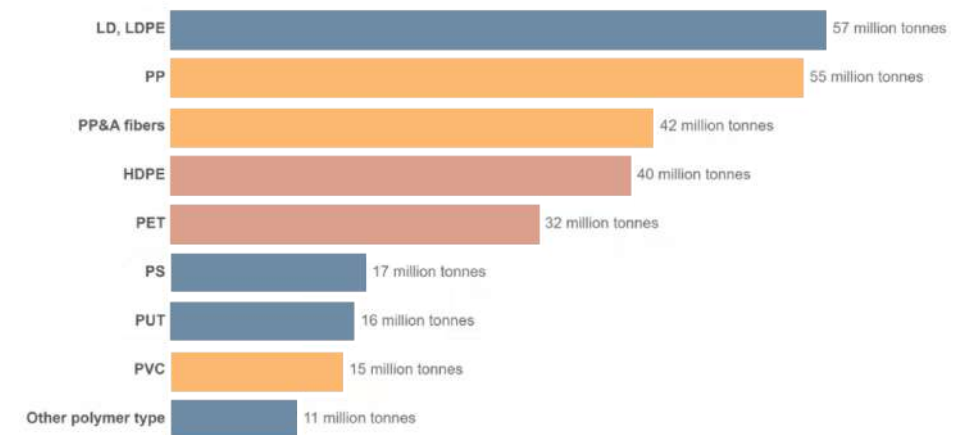


Fig.162: Plastic waste by polymer (elaboration of chart from Geyer (2017))

Recycling companies in developing countries such as *Mr. Green Africa*, already presented during the feasibility analysis, already sell granulate made of different types of plastics (rHDPE, rPP, rPET) that are therefore suitable for the production of 3dprinting filament. Despite being less common, examples of LDPE are found in literature. In particular, Hart (2018)⁶² studies possible small-scale military applications of LDPE filament obtained from Meal-ready-to-eat (MRE) bags.

Different plastic wastes can be used to produce filaments. Choosing one polymer rather than another could be related to local availability or, in the case of LDPE, to the type of available recycling equipment. According to makers community forums⁶³, different aspects of printing with particular materials can result challenging and need therefore to be investigated (Fig.163). Specimens produced with different filaments should be also tested in terms of radiative cooling potential and water-nucleation efficiency. In particular, LDPE could represent a particularly interesting solution, as it is the same polymer from which the OPUR (international organization for dew utilization) standard condenser sheet

	Suitable for extrusion	Melting Temperature [C]	Bed Temperature [C]	Pros	Cons
LDPE	☑	121-232	?	- high tensile strength - Impact resistant - Weather resistant - Flexible	- low stiffness - poor adhesion - high shrinkage
PP	☑	208-251	85-100	- fatigue resistance - chemical resistance - durable	- heavy warping - poor adhesion - low strength
HDPE	☑	177-274	100-130	- watertight - lightweight and strong - food safe	- heavy warping - poor adhesion - high shrinkage
PET	☑	260-280	75-90	- good adhesion - low warping	- stringing - hygroscopic - poor bridging

Fig.163: Polymers printability

These considerations represent the main directions of research that have to be investigated further in order to design a more functional product that could represent a profitable and efficient solution for an hypothetical company in developing countries to propose. It is clear that certain aspects would have to be analyzed case-by-case before setting up such a business. These relate to the local atmospheric water collection potential, the available resources and the possible additional needs that the water-catching products could satisfy in the local urban scenario. When the initial analysis shows potential for a specific location, different target groups can be identified and a variety of different components could be developed. In fact, the flexibility of the proposed workflow has been previously shown through the development of different design iterations and use of various equipment. Based on this, a preliminary roadmap for the development and management of such a company can be imagined and used as starting point for future applications (Fig.164).

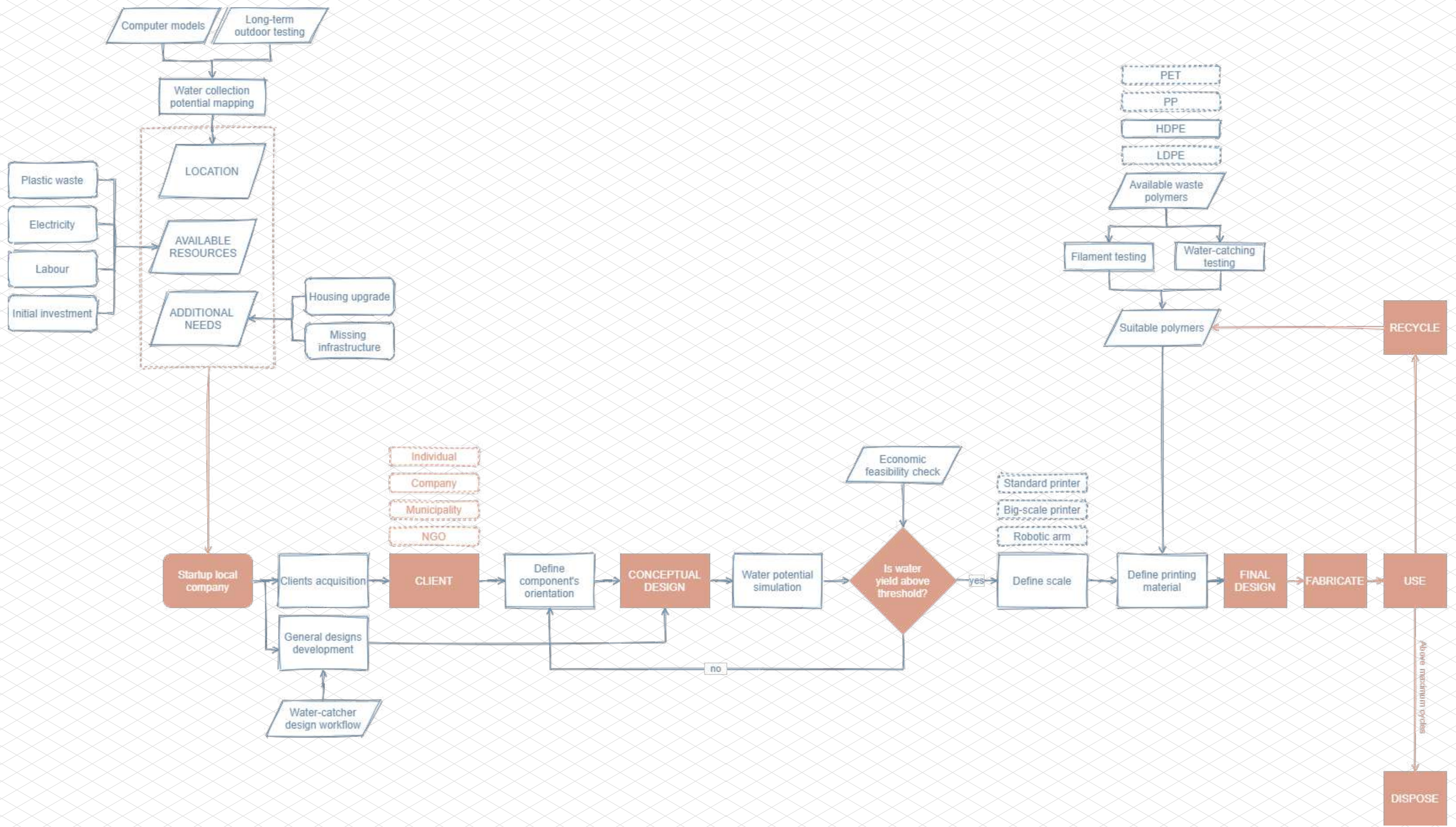


Fig.164: Roadmap for the development of water-catchers as business

5.5 DISCUSSION

The goal of the study was to investigate how 3d printing could contribute in the design of a building component for the mitigation of water stress in developing countries. The challenge has been approached systematically and a solution for a roof component is proposed and evaluated according to different criteria that range from its water-catching efficiency to its economic feasibility.

It is found that 3d printing allows for fine surface tuning that can be configured to fulfill specific requirements. The printing variables involved in this process are evaluated and compared, so that the same logic used in this research could be applied to a different printer. Condensers with higher directionality and tunable pressure gradients are generated. On the other hand, vertical harp collectors are confirmed to be the most efficient solution in fog-catching. A technique to successfully 3d print multilayer harp collectors on variable bridging distances is proposed. A flexible design workflow is then designed so that both physical and fabrication requirements are properly taken into account into the combination of these surfaces. Thanks to this, many design iterations are generated and a roof component is further developed and tested.

The evaluation process of the proposed design starts from its water-collection performance for the location of Rabat, chosen as case study. The study demonstrates that the integration of fog collection into a condensing roof setup reduces of around 50% the surface required to meet the minimal water supply prescribed by the UN. When rain water is considered, this surface decreases even more reaching 21m². This area per person could be met on an average flat roof. The water-catching ability is also tested in Delft (Netherlands) through a physical experiment and data about its performance are gathered and used to correct the simulations performed for the real case study.

Economic feasibility is researched, too. Assuming average energy and labour costs found in literature, a price of 6,52 euro is calculated for each component. This value is then used to calculate an estimation of the price per liter of water. The result of this calculation is of around 0,01 euro/l. This price rises slightly when sanitation costs are considered. This result is comparable with the cost of standard atmospheric water collection systems and much lower than the average cost of bottled water in these countries. Therefore the proposed solution is considered competitive with already existing devices and useful in challenging the pricing of water from private suppliers.

These findings provide new insights on the future potentials of AM in challenging existing technology while making use of waste flows. The end result is in fact not only about collecting water but also about exploring the societal impact that the development of such product could have on small communities. Work and learning opportunities are created through it, while at the same mitigating the waste and water scarcity pressing issues.

However, some limitations need to be done due to the particular situation in which the research was performed. Domestic printing and experimental setups have been used in the design process. For this reason, variations in the fabrication tools such as bigger nozzles or more powerful extruders have not been tested yet. Their beneficial effects are therefore only theorized. Moreover, only PET plastic has been used for prototyping, while many more waste plastic polymers could be tested and compared in terms of printability and water harvesting abilities. The possibility of designing more advanced experimented setups should also be evaluated in case of further or more specific studies. Lastly, a consideration about time needs to be done. Testing is a really important step into the design of new products and it would have been beneficial also in this case to gather more data regarding water yields and durability of the component. However, due to the limited timeframe this has not been possible.

Despite the limitations, that regard the most practical aspects of the research, the methodology used can be considered valid and applicable also for the development of different solutions in this field. The systematic approach used provides a linear storyline to follow and shows in each step different design directions that can be explored based on specific requirements or desires. Aware of the challenges related to the design of a complete and working product in a limited amount of time, this research aims to show the potentials of this application and an efficient workflow to investigate them.

5.6 CONCLUSION

To summarize the results of this thesis and to which degree it met the initial ambitions, the research questions formulated in its early stages are presented again and answered. The main sub-questions are answered first.

- What is the current state of the art in passive atmospheric water harvesting?

Different technologies exist for dew and fog collection. Flat radiative condensers are usually realized with a white hydrophilic polyethylene foil and inclined so that they achieve both high sky exposure and collection rate. Stand-alone applications and integrations of such foils on roof slopes have been investigated. Fog collectors are traditionally composed by single or multiple polyethylene nets placed perpendicularly to the main wind direction. Experiments have compared standard meshes to harp collectors composed by vertical wires and demonstrated their higher efficiency. However, the most common limitation in the real life application of more sophisticated application is their economic competitiveness as they are usually needed in less wealthy scenarios (Lummerich, 2011).

- Which physical parameters are involved in passive atmospheric water harvesting and how do they affect the collection yield?

Dew collection is based on the principle of radiative overnight cooling of a surface. Different parameters are involved in this process, such the infrared emissivity of the condenser, its exposure to the sky and environmental variables such as cloud coverage, relative humidity and wind speed close to the surface. A simulative model of the physical situation has shown that humidity and cloud coverage have the highest impact on the water nucleation rate. Among the variables that can be controlled by design, wind speed has the highest effect on it by increasing convective heat gains. This can be affected through geometrical configurations that reduce this value close to the condenser. For what concerns fog collection, multilayer collectors have been proved to be more efficient (Azeem, 2020). In their design, the shade coefficient of the intercepting screens and their number are the most relevant parameters affecting the overall performance.

- What are the main fabrication constraints involved in the 3d printing process and how would they influence the design of a building component?

Different fabrication constraints have been derived mainly from the prototyping and testing process. The first one is the maximum printable dimension which varies from printer to printer and has to be taken into account into the preliminary design stages. The testing of water catching surfaces has highlighted the dependency between collection efficiency and print layer orientations. This needs to be considered in the combination of the different functions that a building component needs to perform. For this reason, an adaptable workflow is developed and used to produce the final design. The development of the final design uses as fabrication constraints the maximum overhang angle that influences the inclination and curvature of each surface and the maximum bridging length. These parameters are important in the definition of the maximum printable fog collector's size. Lastly, particular attention needs to be given to the balance between required printing time, material use and print quality. Different compromises can be made between the three parameters based on the requirements of a specific location or project. Continuous print layers and single wall count are usually considered beneficial to reduce printing time, even if this might lead to higher material consumption.

- What is most efficient building envelope component type to be designed as an atmospheric water harvester?

The water collection potential of different options is tested in the early design stages to estimate the best orientation for water harvester. In particular, facade and roof integration are compared. Two similar scenarios, based on the initial design concept of forcing the fog flow into an enclosed space are simulated and their potential is used through simulation models built in Excel. The results show that a vertical orientation would experience an higher fog flow. On the other hand, the horizontal orientation allows for a higher exposure to the sky and rainwater. When this information are weighted according to the frequency of the different event recorded for the case study location (Rabat), the horizontal orientation shows higher potential. However, this might change based on specific requirements or features of the urban surroundings.

- How can the performance of an atmospheric water harvester be assessed and evaluated?

Different evaluations can be performed on the final design. The main one regards its water-collection abilities. Simulative models are built to simulate both radiative cooling and fog collection. Such calculations can then be implemented on weather data files of specific location, to estimate the total yearly water yield. Nowadays such files are available for many locations worldwide. Precipitation data can be added in order to get a more complete estimate of the performance of one component. Physical testing is also considered as evaluative method and performed. As for the simulation, the best option would be to run it for a long period of time and on the specific location so that reliable data can be collected. This has not been possible, so the element is tested in the Netherlands and results are compared to local weather data. Even if a limited amount of data is collected, a comparison with standard solutions is performed. Lastly, a fabrication and feasibility evaluation can be performed to assess the performance of the design from a social point of view. The cost that it would have and the consequences that it would generate in a community can be estimated.

Now, the main research question can be answered. It was formulated at the beginning of the research as:

“How can AM (Additive Manufacturing) with rPET be used to design a building envelope component optimized for maximum passive atmospheric water harvesting and therefore mitigate water stress in semi-arid regions of developing countries?”

The aim of the thesis was to explore the potentials and limitations of using Additive Manufacturing for the design and fabrication of a water-catcher. Specifically, a roof component has been designed as estimated to have higher water collection potential.

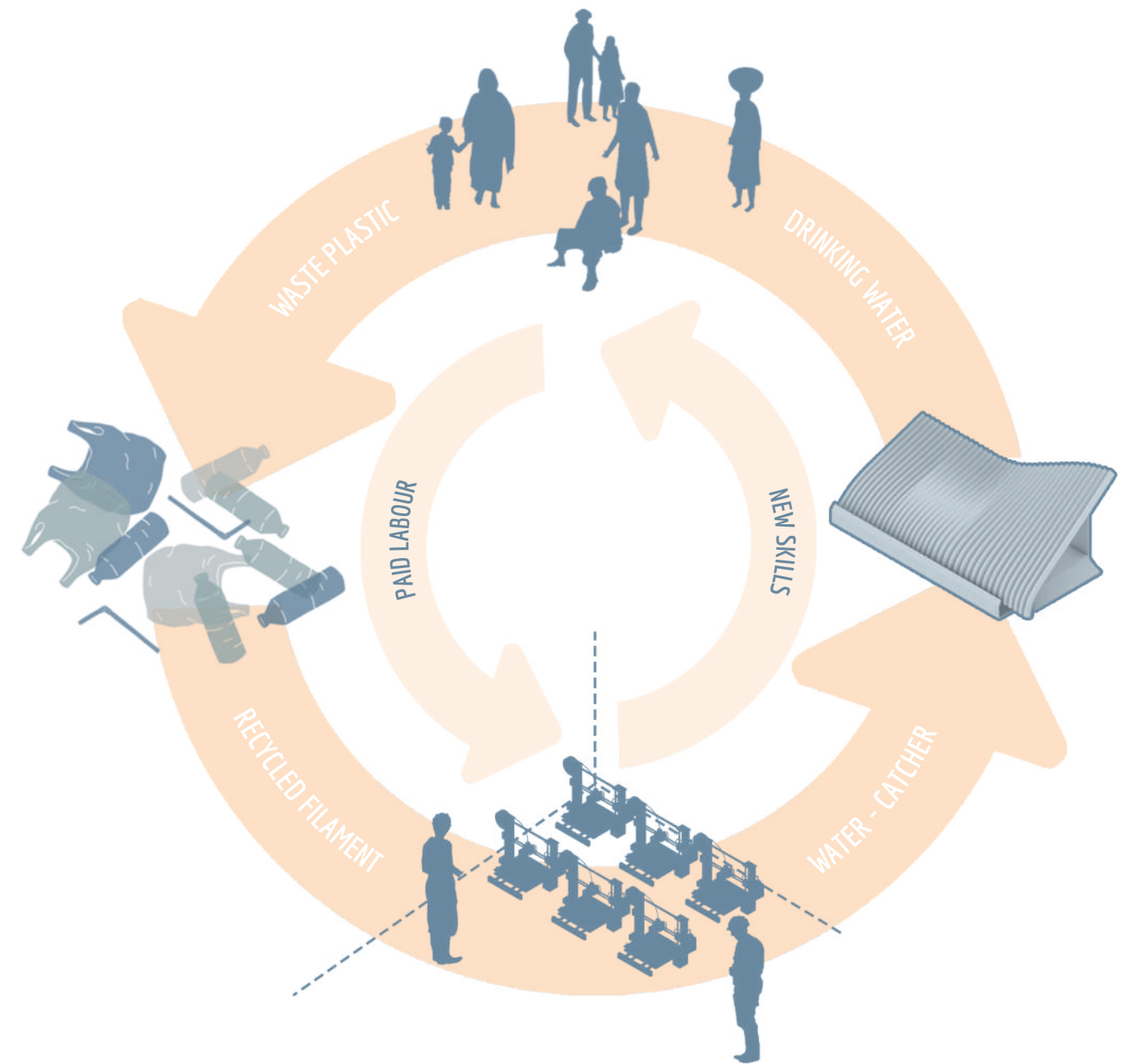
The definition of this goal is radicated into the societal problems that this research aims to address. In particular, increasing water scarcity in developing countries and plastic waste are considered the challenges to face. In these scenarios, such issues have a significant societal impact and new solutions should be evaluated in order to mitigate them. To answer the research question, it has been not only important to design an efficient water collector, but also to analyze its feasibility and the impact that this could have on communities.

After analyzing the state of the art in atmospheric water collection, the basic principles and constraints of 3d printing are studied. One of the benefits of this technology is the possibility of designing multifunctional elements and realize them with just one material. This feature is considered interesting to integrate both the main atmospheric water harvesting systems into a single component. Based on this principle, the systems are studied separately at first. After several prototyping and testing sessions, an optimal strategy is developed for both of them. Such strategies are then integrated into one component that is schematically designed taking into account the optimal part orientations for both water harvesting and digital fabrication. The design is then progressively developed until a final prototype can be realized and evaluated.

The simulations performed on the final design show that the integration of fog and rainwater collection into the calculations for dew water yield enable to reduce significantly the roof surface required to provide a minimum acceptable supply of water for one person living in Rabat, Morocco. Moreover, the feasibility check shows that when a minimum durability is ensured and some basic assumptions are done on energy and cost labour, one component would have a reasonable cost. When the cost for one liter of water is calculated, the result is extremely close to those calculated for standard existing solutions. It can be concluded that it is possible to design and manufacture a 3d printed component that is able to compete with already established technologies in the field of atmospheric water harvesting.

Contrary to solutions like hydrophilic foils or fog catching nets, 3d printing brings also a different potential to the community (Fig.165). The design and realization of an element like the water-catcher not only reuses waste materials and offers job opportunities to members of the local community. More interestingly, it gives the chance to learn and practice new skills that can be later applied to the production of many other different products to address various problems. This would not be so easy with traditional production methods that require more specific tools, but is enabled by the flexibility of 3d printing. The ability of the water-catcher research is not only that of mitigating water stress, but also to teach a set of values and a methods that can be applied again. The flexibility of the proposed design workflow enables users to design a variety of components that could address in different ways the issues of water scarcity and plastic waste, ranging from public sensibilization to urban installations or housing upgrade. Additionally, the multifunctional nature of the design gives a new architectural value to the technology of atmospheric water harvesting. In parallel to catching water, the developed solutions can solve other issues of the local built environment such as increasing the thermal insulation of a facade, improving the acoustic performance of a roof during rain events or create new spaces on a urban level. However, such potential have not been yet quantified and would need additional studies.

Despite this initial results, more research needs to be performed in order to get to a final working product. Multiple aspects of the project could be developed further. On one end, fabrication efficiency could be investigated more and the impact of using more customized printing equipment should be taken into account and tested. The performance obtained with recycled plastic filament or the possibility of using different polymers should also be analyzed so that consistent properties and quality can be ensured. On the other hand, developing further a business case similar to the one proposed in this research could give interesting insights in defining a minimum investment and payback time. This would lead not only to further understand the feasibility of the project, but also to set new design goals and constraints especially in terms of material use and durability.



5.7 REFLECTION

Introduction

The graduation topic is developed within the framework of the “Living in a bottle” project, which aims to explore and develop 3d printed solutions for building components using recycled plastic as raw material. This subject has been combined with a personal interest in humanitarian and emergency architecture into the design of an envelope component for atmospheric water harvesting in developing countries.

The first choice of a subject has been performed in the early stages of the process. This decision was a combination of personal latest fascinations within the field of architecture and approaches I wanted to explore and learn throughout the year. For this reason, the passion for humanitarian architecture led to the definition of a societal problem, while the interest in digital fabrication provided a set of tools whose contribution towards the resolution of the problem could be investigated. To limit the scope and guide the study, the main research question was formulated as:

“How can AM (Additive Manufacturing) with rPET be used to design a building envelope component optimized for maximum passive atmospheric water harvesting and mitigate water stress in semi-arid regions?”

The goal was therefore not to design the best performing atmospheric water harvester possible, but rather to explore ways with which 3d printing can contribute to its development. However, the design had to be optimized for a given performance, introducing in this way new constraints and evaluative criteria to guide the creative process. Finally, the societal goal was expressed as “mitigating water stress”. This choice of words aimed to clarify that the research has not the presumption of solving world problems of this magnitude, but rather the hope of contributing towards their resolution.

The design phase is performed according to the methodology of design through prototyping. To do that, a 3d printer is used. The device is made available to me by the LAMA Lab so that I was able to use it from the second semester and in this way progress with the research. I am particularly grateful for the possibility I got, especially in the historical period we are living in now.

However, critically looking back at the process, the restrictions relating to the pandemic have partially affected my studies and would probably have done the same to any prototype-based research. Not being able to access any facility on campus for a long period, I had to get creative in finding ways to test the different steps of the design flow. At the same time, keeping a scientific approach that could be considered valid resulted to be hard in such a domestic setup.

Relationship Research & Design

At the beginning of the thesis, the two elements seemed segregated accordingly to the academic calendar in a more research-oriented first semester and a second one based on design and application. It was soon understood that such schematic division is not possible. Most of the preliminary literature review is performed in the initial period, but during the second semester only the approach is changed and research is performed in parallel with prototyping and experimental testing.

The methodology of design by prototyping is used. In this way, a final solution is developed progressively by validating different intermediate steps. The constant validation helps in approaching design more systematically and scientifically so that results are not just subjective decisions but supported by data. The process can be schematized as a linear sequence of iterative loops. The starting and ending points are clearly defined by the problem statement and research objective. However, the steps between them are not performed linearly, but rather in a circular way that is concluded when a valid result is achieved.

Over time, the benefits of this approach are visible. Multiple design directions are discarded and each design decision can be traced back and justified. On the other hand, it was the first time working in this way and it resulted confusing in certain moments. It is easy to get lost in these design loops and sometimes it is hard to get a realistic feeling of the progress of the overall research.

To achieve the research objective, the problem is broken down into a series of smaller design tasks. Functionality and 3d-printability are constantly used to evaluate the results and to progress the research. The two topics represent also the two specializations I decided to pursue during graduation.

Relationship Graduation topic & Master track

The thesis is developed within the Building Technology specializations of Design Informatics and Climate Design. In particular, the role of these subjects in the research can be summarized as:

- *Design Informatics*: an algorithmic approach is used to structure the research even when no computational tools are used. Problems are analyzed systematically and single parameters are usually evaluated so that generic workflows can be derived. Parametric tools are used in the process of geometrical modeling and configuration of the design iterations and results, while computational tools such as CFD engines are part of their evaluation. The exploration of digital fabrication’s potentials represents the main topic of the research and its main contribution to the field.

- *Climate design*: the thesis relates to it mainly in the definition and assessment of the design’s functionality. Environmental phenomena and their relationship with the built environment are investigated and simulated through models. Such models are then used to evaluate design options according to their required performance. An experimental approach is used throughout the whole process to validate the developed solutions.

Looking at the overall master track, the combination of new design and manufacturing tools and sustainable goals represents one of the main goals of the Building Technology track at TU Delft. The study and the development of new solutions that address the major challenges that we are facing represent some of the final objectives of the program and this research is trying to gradually approach these tasks. New potential applications for a rising technology such as 3d printing are explored, while taking into account the built environment and the impact that such solutions could have on it.

Research method

The academic calendar divides graduation into two semesters and sets a series of deadlines where the progress is evaluated. For this reason, personal planning and subdivision of the research tasks were done from the beginning. These steps have been used to guide the work and to build a linear storyline that can be divided in:

- Research context: the problem statement is presented and the research question is developed accordingly
- Foundation knowledge: the main part of the literature review is performed
- Pre-Design: literature review start to be more oriented towards the definition of a set of parameters and constraints that can be implemented into the design process
- Design: design by prototyping is performed. The design is developed systematically and prototyped. Design through prototyping method is used.
- Final Evaluation: the results of the design phase are evaluated from different points of view.

This general subdivision was followed throughout the whole process. However, many things changed from the more specific week planning presented in the initial graduation plan. It was initially planned to alternate weeks dedicated to prototyping and designing. As soon as fabrication and testing started, it was clear that such a strict subdivision was not possible as one part constantly informs the other in a more fluid back and forth process.

Moreover, the final evaluation was at the beginning planned to happen mainly experimentally. However, both new developments of the study and limitations related to the domestic setup in which the research took place, made me reconsider its relevance in the overall process. Different theoretical validation methods have been developed and the outdoor experiment has become one additional proof of concept. A more complete experiment would be needed for the research to take the next step, but the necessary conditions and their availability in a pandemic situation were probably underestimated in the early stages of the research.

It can be said that the methodology set at the beginning worked for the research. However, being the first time using the approach of research through prototyping, a lot was learned about how this process works and will be used again in a more aware definition of future research scopes or goals.

Research topic and societal relevance

The research contributions can be divided into different fields.

Technological relevance

The main goal of the thesis is to explore potential applications of Additive Manufacturing. The most relevant technological aspects, therefore, relate to it. The approach used for the design is that of developing a replicable solution, that can be adapted to different needs. This builds on the idea of an open-source community of makers that contributes to creating a network of production locations worldwide. The goal is then not only to develop a solution but to propose also a more general overview of a workflow that can be re-applied or improved.

3d-printing leads also to a practical understanding of material use and shape complexity. Being a slow production system, it becomes really important to minimize parameters such as printing time or printed mass. The result is a gradual optimization process that ends with a convenient solution. Moreover, the prototyping phase allows to test and understand more the properties of the material and can represent a starting point for new research.

Sustainability relevance

The main aspect in this field is again related to the fabrication technique. The design is thought for 3d-printing and to be realized locally with waste-plastic filament. The optimization of material is an intrinsic requirement of Additive Manufacturing if an efficient element wants to be realized. This means investing not only in a technology but also in a set of principles that care about reducing the use of resources. The only needed material is then plastic. However, plastic waste is usually available locally. In this way, the reuse of waste flows as local resources is promoted. The water-catcher design represents in this sense the starting point of a process that can look at AM as a way of pursuing sustainable development in developing communities.

Social relevance

The social aspect was one of the main driving forces of the research. In this sense, the goals were multiple and it can be said that at the end of this research they appear still promising and more feasible.

The first aim was to address a major societal issue that affects certain regions of the world, where mostly poor countries are located. Water scarcity slows down the development of these communities, which will have in the future less and less water. This means having access to it either by walking long distances daily or investing a lot of private earnings into private water supplies. The benefits of having a local and cheap water supply are undeniable. The water-catcher design aims to be this solution or at least part of it. The integration into the built environment and its optimization process are thought to maximize its collection abilities and consequently minimize the dependency on other supplies.

The second aspect is related to 3d-printing. Research is done to estimate a local production scenario and its economic feasibility. Introduce a production facility in developing communities could boost their growth. From this point of view, the water-catcher represents the way of teaching a set of different skills to people and bring new work and learning opportunities to the community. Moreover, thanks to the flexibility of a production system such as 3d-printing, these skills could be eventually used to move beyond the realization of the water-catchers and start realizing also other objects that can fulfill other needs. As it was for me performing this research, you can start from knowing almost zero about this technology and gradually gain knowledge and experience that can be applied to many different applications. In this way, technology not only helps relieve a basic need of people but contributes to the development of a more equal and resourceful society.

Future Research

Even if the results obtained so far are encouraging, more work needs to be done before a real-life application of the water-catcher can be thought. Different research directions can be identified and while some of them will be partially explored in the rest of the graduation period, others will remain as possible starting points for future studies.

The two main development are the realization of a 1:1 complete prototype and the setup of a more controlled experimental environment. In this way the validation of both printability and water-catching performance can be finalized. Moreover, the economic feasibility of the design can be explored in a more accurate way, so that a realistic business plan is developed. Lastly, the specific performance of recycled plastic filament needs to be assessed in practice, since it was used as a constraint in this research.

REFERENCES

1. United Nations, Sustainable Development Goal 6 Synthesis Report 2018 on Water and Sanitation, Geneva, United Nations Publications, 2018
2. M.M. Mekonnen, A.Y. Hoekstra, Four billion people facing severe water scarcity, *Science Advances* vol.2, 2016
3. Global Water Institute (E.Hameeteman), *Future Water (In)security: facts, figures and predictions*, 2013
4. J. Schyns, A. Hoekstra, A. Hamaideh, M.M. Mekonnen, *Mitigating the Risk of Extreme Water Scarcity and Dependency: the Case of Jordan*, 2015
5. United Nations, Department of Economic and Social Affairs, Population Division. *World Population Prospects 2019: Ten Key Findings*, 2019
6. United Nations, Department of Economic and Social Affairs, Population Division. *World Population Prospects 2019*, 2019
7. UNESCO, UN-Water, 2020: *United Nations World Water Development Report 2020: Water and Climate Change*, Paris, 2020
8. United Nations, Department of Economic and Social Affairs, Statistic Division, *SDG Report 2020*, 2020
9. L. Parker, The world's plastic pollution crisis explained, *National Geographic*, 2019
10. H. Ritchie, M. Roser, "Plastic Pollution". Published online at OurWorldInData.org. Retrieved from: 'https://ourworldindata.org/plastic-pollution' [Online Resource consulted last time 05/01/2021], 2018
11. Bluecycle presentation page. Available at: <https://bluecycle.com/en/about/> (Accessed: 08 May 2021)
12. M. Roser, "Future Population Growth". Published online at OurWorldInData.org. Retrieved from: 'https://ourworldindata.org/future-population-growth' [Online Resource consulted last time 05/01/2021], 2014
13. P. Comanns, *Passive water collection with the integument: mechanism and their biomimetic potential*, 2018
14. T. Nørregaard, M. Dacke, *Fog-basking behavior and water collection efficiency in Namib Desert Darkling beetles*, 2010
15. J. Guadarrama-Cetina, A.Mongruel, M.G. Medici, E. Baquero, A.R. Parker, I. Milimouk-Melnychuk, W.Gonzalez-Vinas and D.Beysens, *Dew condensation on desert beetle skin*, 2014
16. J.Ju, H. Bai, Y. Zheng, T. Zhao, R. Fang, L. Jiang, *A multi-structural and multi-functional integrated fog collection system in cactus*, 2012
17. P.S. Brown, B. Bhushan, *Bioinspired materials for water supply and management: water collection, water purification and separation of water from oil*, 2016
18. M. Ebner, T. Miranda, A. Roth-Nebelsick, *Efficient fog harvesting by stipagrostis sabulicola (Namib dune bushman grass)*, 2011
19. S. Vogel, *Desert geophytes under dew and fog: the curly whirlies of Namaqualand (south Africa)*, 2011
20. B. Khalil, J. Adamowski, A. Shabbir, C. Jang, M. Rojas, K. Reilly, B. Ozga-Zielinski, *A review: dew water collection from radiative passive collectors to recent developments of active collectors*, 2015
21. H. Jarimi, R. Powell, S. Riffat, *Review of sustainable methods for atmospheric water harvesting*. 2020
22. A.F.G. Jacobs, B.G. Heusinkveld, S.M. Berkowicz, *Passive dew collection in a grassland area, the Netherlands*, 2008
23. C.M. Regalado, A. Ritter, *The design of an optimal fog water collector, a theoretical analysis*, 2016
24. M. Rajaram, X. Heng, M. Oza, C. Luo, *Enhancement of fog-collection efficiency of a Raschel mesh using surface coatings and local geometric changes*, 2016
25. O. Klemm, R.S. Schemenauer, A. Lummerich, P. Cereceda, V. Marzol, D. Corell, J. van Heerden, D. Reinhard, T. Ghrezghither, J. Olivier, P. Osses, J. Sarsour, E. Frost, M.J. Estrela, J.A. Valiente, G.M. Fessehaye, *Fog as Fresh-water Resource: Overview and perspectives*, 2012
26. A. Lummerich, K.J. Tiedemann, *Fog water harvesting on the verge of economic competitiveness*, 2011
27. M. Azeem, L. Caminos, T. Dumais, M. Torres, *Optimal Design of multi-layer Fog Collectors*, 2020
28. R.M. Aynsley, *Shape and flow: the essence of Architectural Aerodynamics*, 2011
29. L. Chochran, R. Derickson, *Low-rise buildings and Architectural Aerodynamics*, 2005
30. E. Simiu, D. Yeo, *Wind effects on structures: modern structural design for wind*, John Wiley & Sons, pp. 73-104, 2019
31. T.Stathopoulos, *Introduction to Environmental Aerodynamics*, 2011
32. J. Rivera, *Aerodynamic collection efficiency of fog water collectors*, 2011
33. S. Hoerner, *Aerodynamic drag*, 1906
34. S. Daminabo, S. Grammatikos, S. Goel, H.Y. Nehzad, *FDM-based Additive Manufacturing (3d Printing): techniques for polymer material systems*, 2020
35. V. Piccioni, *The AM envelope: A mono-material façade element with complex geometries for structural and thermal performance produced by additive manufacturing (master's thesis)*, Delft; TU Delft; 2019
36. H.A. Little, N.G. Tanikella, M.J. Reich, M.J. Fiedler, S.L. Snabes, J.M. Pearce, *Towards distributed recycling with Additive Manufacturing of PET flake feedstocks*, 2020
37. J. Newman, *3D Printed Roofing Could Help Transform Low Income Housing* [Online Resource consulted last time 05/01/2021], 2014

³⁸ Benedict. Fluid Morphology: translucent 3D printed building facades with tunable ventilation, insulation, shading [Online Resource consulted last time 05/01/2021], 2017

³⁹ Sarakinioti, M.V., Turrin, M., Teeling, M., de Ruiter, P., van Erk, M., Tenpierik, M., Konstantinou, T., Knaack, U., Pronk, A., Teuffel, P., van Lier, A., Vorstermans, R., Dolkemade, E., de Klijn, M., Loonen, R., Hensen, J., Vlasblom, D. SPONG3D [Online Resource consulted last time 05/01/2021]

⁴⁰ Dermentzi, M. [video] This 3D printed green wall comes with an embedded irrigation system [Online Resource consulted last time 05/01/2021]

⁴¹ Emerging Objects, Cool brick [Online Resource consulted last time 05/01/2021], 2015

⁴² T.Nilsson, Initial experiments on dew collection in Sweden and Tanzania, 1996

⁴³ P. Gandhidasan, H.I. Abualhamayel, Modeling and testing of a dew collection system, 2005

⁴⁴ J. Wang, Y. Wu, Y. Cao, G. Li, Y. Liao, Influence of surface roughness on contact angle hysteresis and spreading work, 2020

⁴⁵ Italian Air Force weather data, (<http://www.meteoam.it/>)

⁴⁶ K. Steiros, M. Hultmark, Drag on Flat Plates of Arbitrary Porosity. J. Fluid Mech, 2018

⁴⁷ I. Lekouch, K. Lekouch, M. Muselli, A. Mongruel, B. Kabbachi, D. Beysens, Rooftop dew, fog and raing collection in southwest Morocco and predictive dew modeling using neural networks, 2012

⁴⁸ M.V. Marzol, J.L.S. Megia, Fog water Harvesting in Ifni, Morocco. An assessment of potential and demand, 2008

⁴⁹ S.D. Tripp, B. Bichelmeyer, Rapid prototyping: an alternative instructional design strategy, 1990

⁵⁰ B. Vayre, F. Vignat, F. Villeneuve, Designing for Additive Manufacturing, 2012

⁵¹ N. Boyard, M. Rivette, O. Christmann, S. Richir, A design methodology for parts using additive manufacturing, 2015

⁵² C. Alexander, Notes on the synthesis of form, Cambridge, MA: Harvard University, 1964

⁵³ W.Zuo, Introduction of Computational Fluid Dynamics, FAU Erlangen-Numberg, 2005

⁵⁴ H.A. Terré, Treball de fi de grau: structural optimization for dew-condensers using computational fluid dynamics, 2014

⁵⁵ S. Varagnolo, Study and control of drop motion on inclined surface

⁵⁶ World Bank Group, Feasibility study: production of recycled 3d print filament, 2016

⁵⁷ M.Gall, M. Wiener, C.C. de Oliveira, R.W. Lang, E.G. Hansen, Building a circular plastics economy with informal waste pickers: recyclate quality, business model and societal impacts, 2020

⁵⁸ A.L. Woern, J.R. McCaslin, A.M. Pringle, J.M. Pearce, RepRapable Recyclebot: Open source 3-D printable extruder for converting plastic to 3-D printing filament, 2018

⁵⁹ D.S. Lantagne, R. Quick, E.D. Mintz, Household Water Treatment and Safe Storage in Developing Countries, 2006

⁶⁰ A.G. Blum, C. Null, V. Hoffmann, Marketing household water treatment: willingness to pay. Results from an experiment in rural Kenya, 2014

⁶¹ R. Geyer, J.R. Jambeck, K. Lavender Law, Production, use and fate of all plastics ever made, 2017

⁶² K.R. Hart, J.B.Frketi, J.R. Brown, Recycling meal-ready-to-eat (MRE) pouches into polymer filament for material extrusion additive manufacturing, 2018

⁶³ Filament properties table, <https://www.simplify3d.com/support/materials-guide/properties-table/>, consulted on 19/06/2021

Radiative Condenser Calculations

The work and the formulas provided by Nilsson (1996) and Gandhidasan (2005) are taken into account for the following calculations. The formulas discussed in the following pages have been implemented into a mathematical simulation on Excel.

Heat Balance

$$P = LE + Q_{cond} + Q_{conv}$$

Calculating Qcond (Conduction heat exchange)

$$Q_{cond} = \frac{k}{x}(T_e - T_f)$$

Where k is the thermal conductivity of the material [W/mK] and x its thickness [m]

Calculating Qconv (Convection heat exchange)

$$Q_{conv} = h_c(T_e - T_f)$$

To Calculate Convection heat transfer coefficient

convection type	α_{conv}	v	Reference
forced	$\alpha_{conv} = 6 + 4v$	$v \geq 5 \text{ m/s}$	1
forced	$\alpha_{conv} = 7.41 \cdot v^{0.78}$	$v \leq 5 \text{ m/s}$	1
external wind Windward side	$\alpha_{conv} = 5 + 4.5 \cdot v - 0.14 \cdot v^2$	$v \leq 10 \text{ m/s}$	1
external wind Leeward side	$\alpha_{conv} = 5 + 1.5 \cdot v$	$v \leq 8 \text{ m/s}$	1
forced convection	$\alpha_{conv} = 10.45 - v + 10\sqrt{v}$	$2 \text{ m/s} \leq v \leq 20 \text{ m/s}$	2
natural convection interior surfaces	$\alpha_{conv} = 2 \cdot T_a - T_s ^{1/4}$	natural convection at interior surfaces	1

Table 1: α_{conv} for different situations by different authors. References: 1: Introduction to Building Physics, Carl-Eric Hagentoft, 2003; 2: Engineering toolbox.

Calculating P (Radiation heat exchange)

$$P = \epsilon_f \sigma (T_f^4 - T_{sky}^4)$$

Can be transformed into a formula similar to the convection and conduction heat exchange with

$$\alpha_{rad} = 4\epsilon_f \sigma \left(\frac{T_f + T_{sky}}{2} \right)^3$$

Where ϵ_f is the foil emissivity and σ the Stefan-Boltzmann constant [5,67E-08 W/(m²K⁴)]

Therefore,

$$P = \alpha_{rad}(T_f - T_{sky})$$

SVF (0 < SVF < 1) can be considered as reduction factor of the radiative cooling potential

$$P = SVF\alpha_{rad}(T_f - T_{sky})$$

To calculate Tsky

$$T_{sky}^4 = \varepsilon_a T_e^4$$

Where ε_a is the effective emissivity of the sky. For Unsworth (1975), with (D=0,84 and c= cloud coverage)

$$\varepsilon_a = \varepsilon_0(1 - Dc) + Dc$$

Where ε_0 represents the clear sky emissivity and is equal to (A=0,745 and B=0,0056 for an average situation)

$$\varepsilon_0 = A + BT_{dew}$$

With dew temperature equal to

$$T_{dew} = T_e - \frac{100 - RH\%}{5}$$

Combining the formulas to find Tf

$$P = \varepsilon_f \sigma (T_f^4 - T_{sky}^4)$$

Becomes

$$SVF\alpha_{rad}(T_f - T_{sky}) = LE + \alpha_{conv}(T_e - T_f) + \frac{k}{x}(T_e - T_f)$$

And therefore Tf

$$T_f = \frac{LE + \alpha_{conv}T_e + \frac{k}{x}T_e + SVF\alpha_{rad}T_{sky}}{SVF\alpha_{rad} + \alpha_{conv} + \frac{k}{x}}$$

As also E is an unknown in this calculation, iterative calculations are required.

For Nilsson (1996)

$$LE = \frac{h_c(e_{amb} - e_f)}{\xi}$$

Where L is the water latent heat of vaporization [628 Wh/kg], ξ the Psychrometric constant [66 Pa/K] and $e_{amb} - e_f$ the difference between the vapor pressure of the ambient and the one closer to the foil [Pa]

$$E = \frac{h(RHe'_{amb} - e'_f)}{L\xi}$$

The formulas are iteratively solved (100 iterations) and values for Tf, E and α_{rad} are obtained.

Fog Collection Calculations

The calculations provided by Azeem (2020) are used as reference for the simulation on the fog harvesting process in Excel. The main formulas are presented below. The case of a multilayer harp collector is assumed.

Total efficiency of a fog collector

$$\eta_{tot} = \frac{J}{LWCv_w}$$

Where J represent the total mass rate [g/sm²], LWC the total fog liquid water content [g/m³] and v_w the airstream velocity [m/s].

The total efficiency can be seen also as

$$\eta_{tot} = \eta_{ACE}\eta_{capt}\eta_{drain}$$

When assuming a minimization of the thread diameter, the capturing and draining efficiencies can be assumed to be 1. Therefore

$$\eta_{tot} = \eta_{ACE}$$

It results that

$$\lim_{d \rightarrow \infty} \eta_{tot} = \eta_{ACE} = \frac{A_\infty}{A} [(1 - (1 - s)^N)]$$

Where s represent the solid fraction (or shade coefficient) and N the number of collecting layers. This can be seen as

$$\eta_{ACE} = \varphi\chi$$

Where are the two factors are the filtered fog fraction and the incident fog fraction. The filtered fog fraction results equal to

$$\varphi = \sqrt{\frac{C_D}{k}}$$

Where Cd is the pressure drag coefficient and k the pressure loss coefficient.

Steiros (2018) provides implicit formulas to calculate both of them

$$C_D = \frac{4(1 - \varphi)(2 + \varphi)}{3(2 - \varphi)}$$

$$k = N \left(\left(\frac{1}{(1 - s)^2} - 1 \right) - \frac{4}{3} \frac{(1 - \varphi)^3}{\varphi^2(2 - \varphi)^2} \right)$$

This formulas are calculated through the function GoalSeek in Excel.

Incident fog fraction is calculated as

$$\chi = (1 - (1 - s)^N)$$



PET-G (Polyethylene terephthalate) is a very strong, water-repellent material that gives your 3D-prints a beautiful shine. Most people are already familiar with PET as soda bottles. PET-G filament is rapidly increasing in popularity within the 3D-print community because it has the easy characteristics of PLA and the strong durability of ABS.

Diameter

Diameter	Tolerance	Roundness
1,75 mm	0,05 mm	95%
2,85 mm	0,1 mm	95%

Characteristics

Physical characteristics	Test method	Typical value
Specific gravity	ASTM D1505	1,27g/cc
MFI	-	-
Tensile strength	ASTM D638	50 MPa 7300 psi
Elongation at break	ASTM D638	28 MPa 4100 psi
Tensile modulus	ASTM D790	2100 MPa 305000 psi
Impact strength	-	33 joules

Thermal characteristics

Description	Test method	Typical value
Print temperature	-	230 - 250 C
Melt temperature	-	250 C +/- 10 C
Melting point	-	-
Vicat softening temperature	ISO 305	+/- 85 C

Technical Data Sheet

Ultrafuse PET

Date / Revised: 14.11.2019

Version No.: 3.2

General information

Components

Amorphous Polyethylene Terephthalate based filament for Fused Filament Fabrication.

Product Description

Ultrafuse PET is made from a premium PET and prints as easy as PLA, but is much stronger. The filament has a large operating window for printing (temperature vs. speed), so it can be used on every 3D-printer. PET will give you outstanding printing results: a good layer adhesion, a high resolution and it is easy to handle. Ultrafuse PET can be 100% recycled, is watertight and has great colors and finish.

Delivery form and warehousing

Ultrafuse PET filament should be stored at 15 - 25°C in its originally sealed package in a clean and dry environment. If the recommended storage conditions are observed the products will have a minimum shelf life of 12 months.

Product safety

Recommended: Process materials in a well ventilated room, or use professional extraction systems. For further and more detailed information please consult the corresponding material safety data sheets.

Notice

The data contained in this publication are based on our current knowledge and experience. In view of the many factors that may affect processing and application of our product, these data do not relieve processors from carrying out their own investigations and tests; neither do these data imply any guarantee of certain properties, nor the suitability of the product for a specific purpose. Any descriptions, drawings, photographs, data, proportions, weights etc. given herein may change without prior information and do not constitute the agreed contractual quality of the product. It is the responsibility of the recipient of our products to ensure that any proprietary rights and existing laws and legislation are observed.

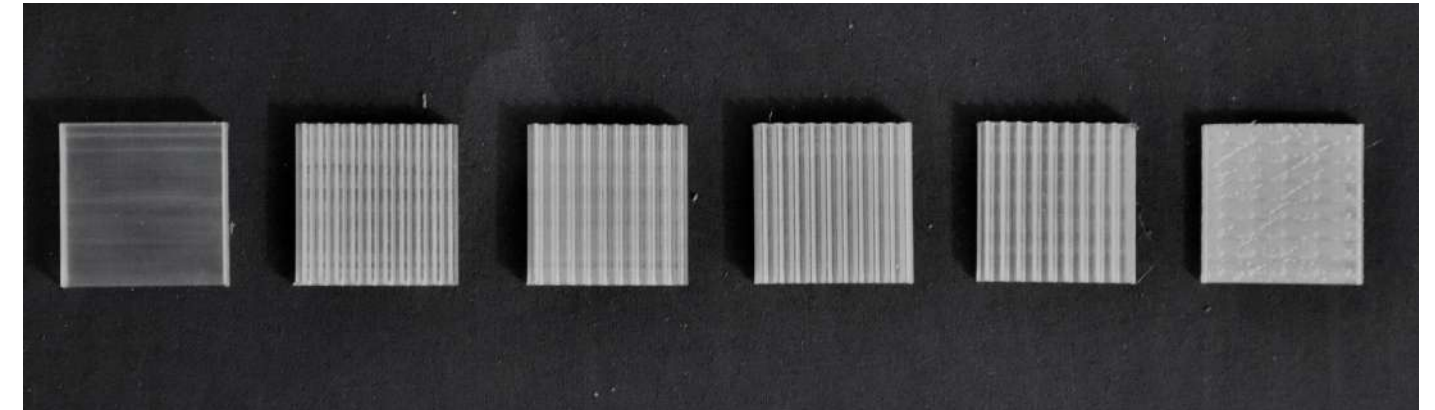
Recommended 3D-Print processing parameters	
Nozzle Temperature	210 – 230 °C / 410 – 446 °F
Build Chamber Temperature	-
Bed Temperature	60 – 80 °C / 140 – 176 °F
Bed Material	Glass
Nozzle Diameter	≥ 0.4 mm
Print Speed	40 - 80 mm/s

Drying Recommendations	
Drying recommendations to ensure printability	60 °C in a hot air dryer or vacuum oven for 4 to 16 hours
Please note: To ensure constant material properties the material should always be kept dry.	

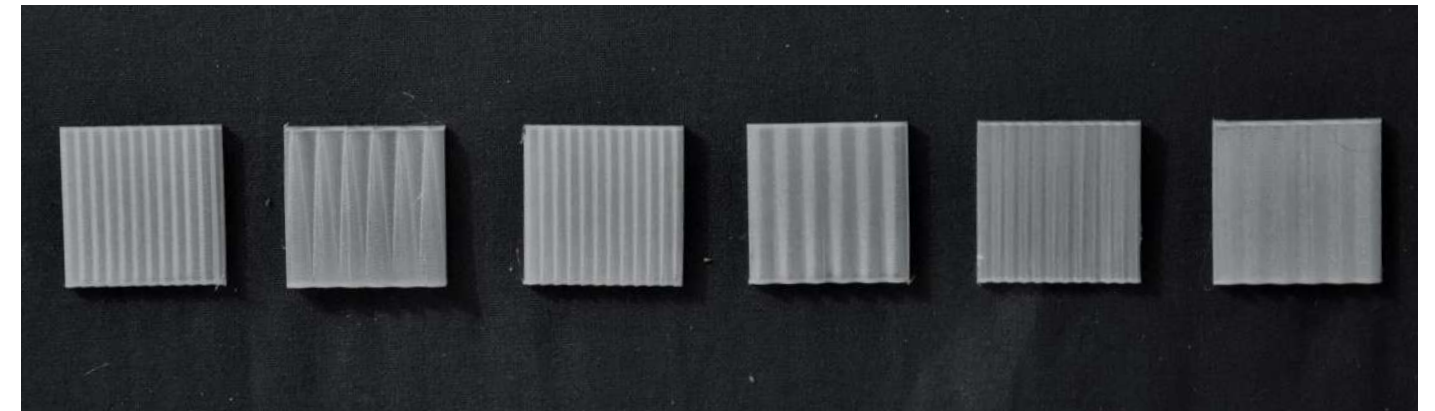
General Properties		Standard
Printed Part Density	1329 kg/m ³ / 83.0 lb/ft ³	ISO 1183-1

Thermal Properties		Standard
HDT at 1.8 MPa	61 °C / 142 °F	ISO 75-2
HDT at 0.45 MPa	63 °C / 145 °F	ISO 75-2
Glass Transition Temperature	71 °C / 160 °F	ISO 11357-2
Melt Volume Rate	16.3 cm ³ /10 min / 0.99 in ³ /10 min (220 °C, 2.16 kg)	ISO 1133

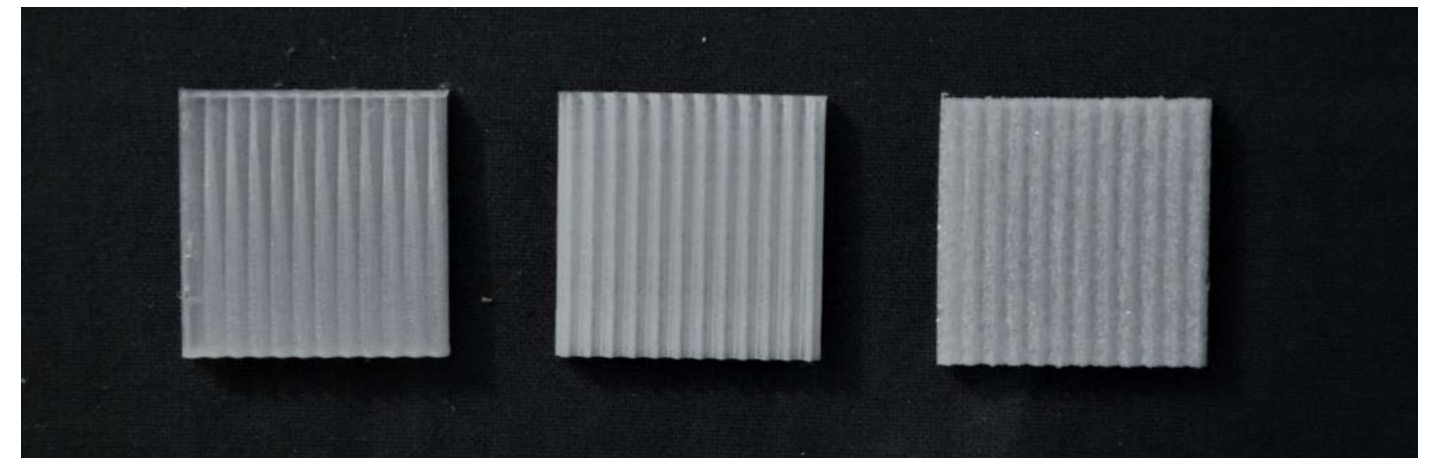
APPENDIX IV



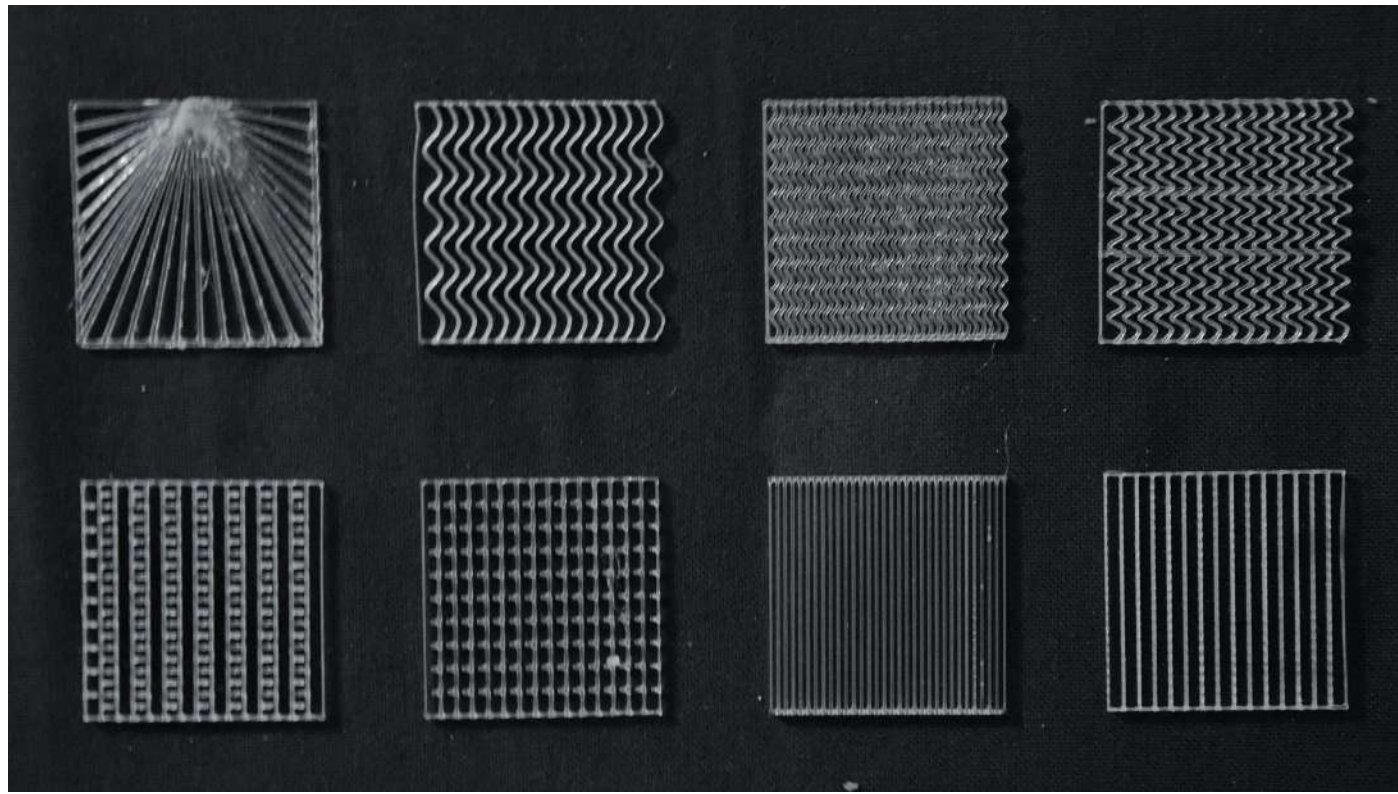
Condensing surface experiment. Nucleation's rate on different surfaces.



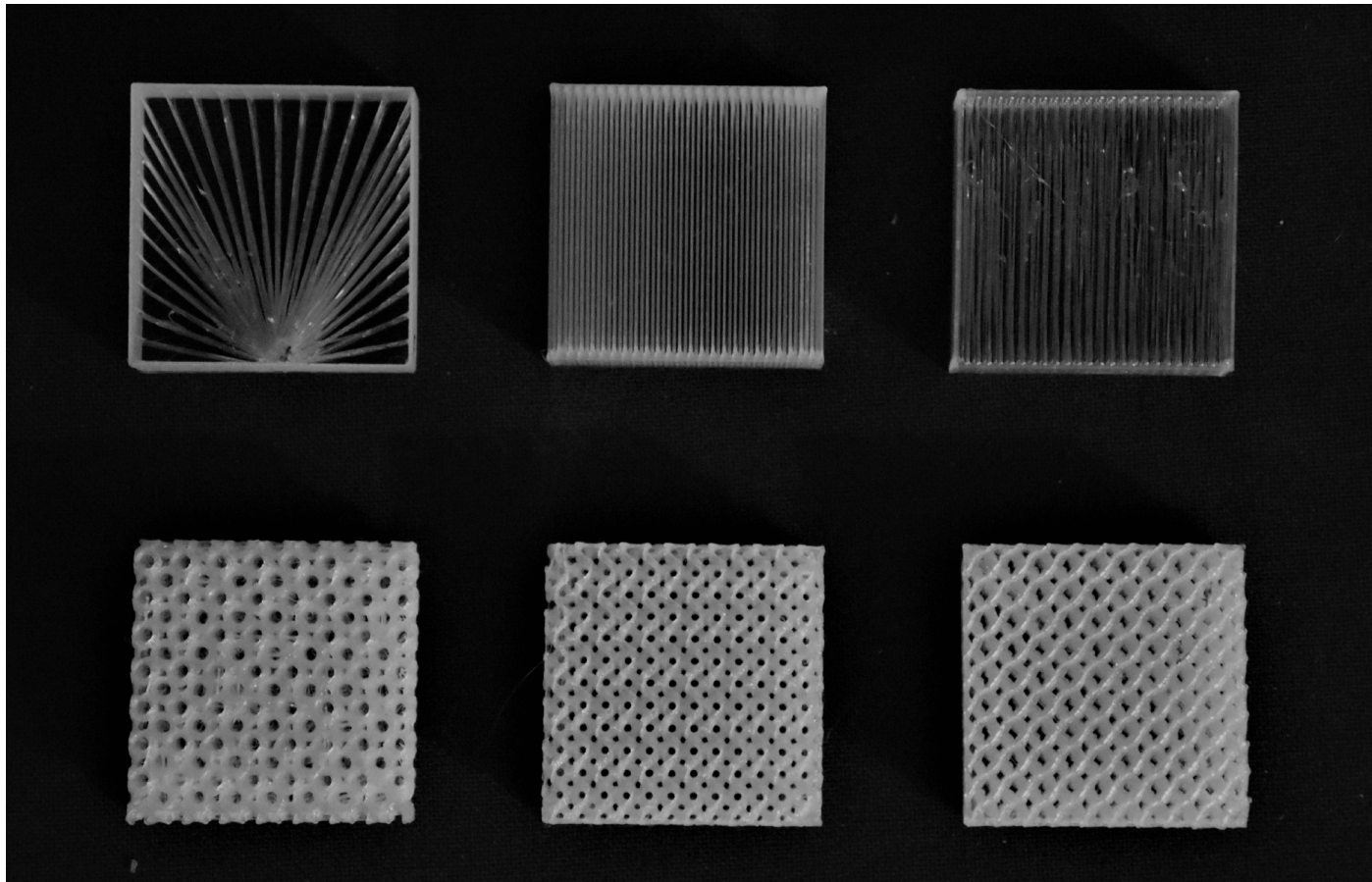
Condensing surface experiment. Nucleation's rate on different undulated surfaces.



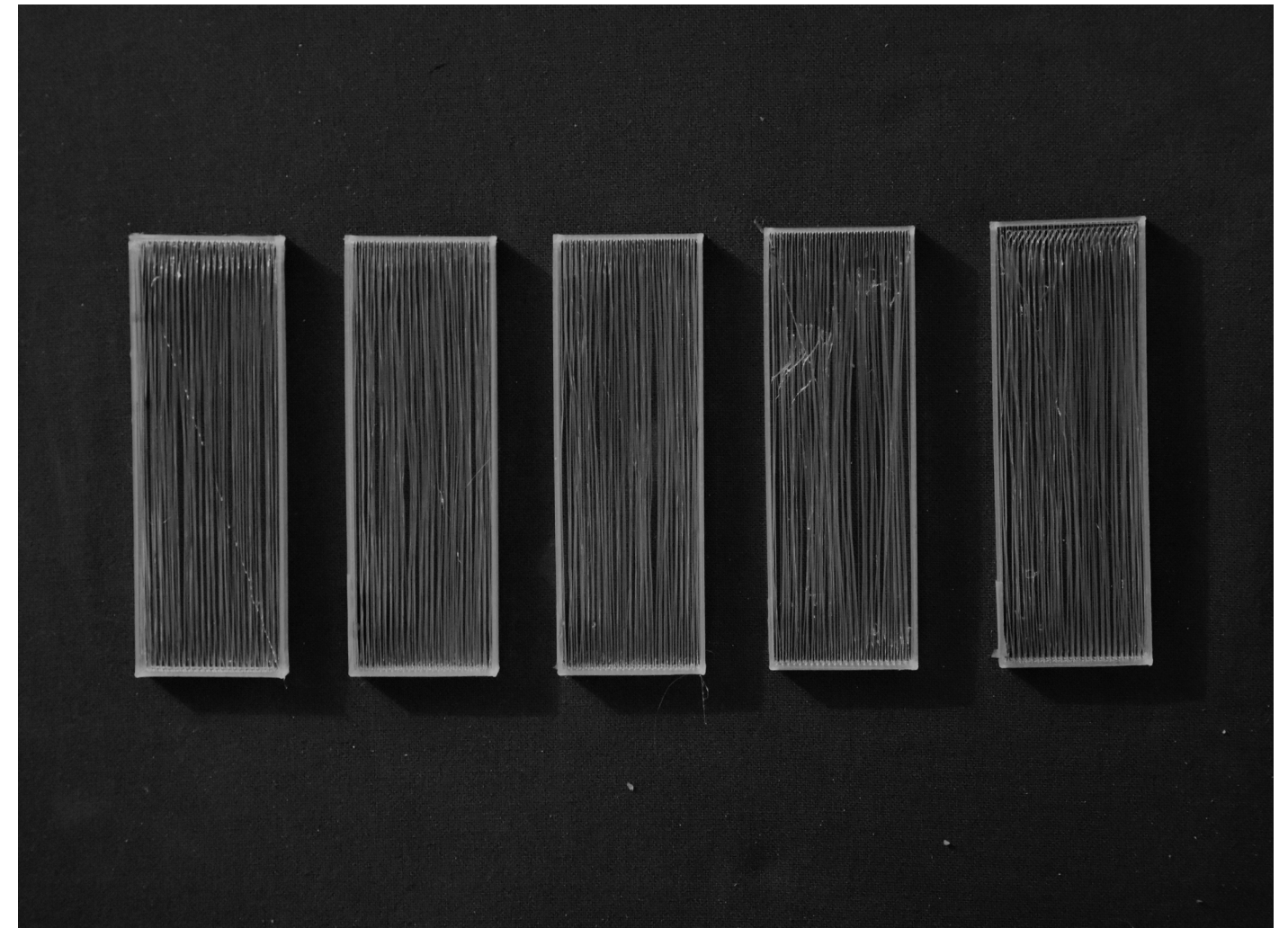
Condensing surface experiment. Impact of roughness and print layer orientation on nucleation's rate.



Fog collecting surface. Single-layer collection efficiency



Fog collecting surface. Multi-layer collection efficiency



Fog collecting surface. Maximum bridging distance

APPENDIX V

This appendix gives further details in the calculation process of the weighting coefficient used in the evaluation process of the best possible orientation for the water catcher. The calculations refer to the experimental data recorded in Morocco and reported by Lekouch (2012). The cumulative water mass collected through fog and dew are compared. The comparison is considered valid for the chosen case study of Rabat, as the city of Mirleft is another coastal city of Morocco.

Experimental period (mm/dd/yyyy)	05/01/2007–04/30/2008					07/01/2007–09/30/2007			
	Mirleft					Id Ouasskssou			
Yields (L m ⁻²)	Rain days	Dew days 178 (48.6%)				Fog days	Rain days	Dew days	Fog days
	31 (8.5%)	East side	West side	North side	South side	20 (5.5%)	6 (6.5%)	50 (54.3%)	16 (17.4%)
Minimum	0.05	0.005	0.005	0.005	0.005	0.000	0.23	0.05	0.10
Maximum	12.32	0.45	0.43	0.50	0.44	0.425	11.56	0.50	1.40
Mean	1.57	0.10	0.10	0.11	0.10	0.071	13.83	0.14	0.41
Cumulative	48.7	18.3	17.7	18.9	18.3	1.4	15.6	7.1	6.5
Uncertainty	7	2	2	2	2	-0.2/+0.4	2	0.3	-0.1/+1.8

The ratio between the amount of dew and fog collected is equal to 52,3. Dew collection is considered over a period of approximately one year 52 times more efficient than fog catching. For this reason the estimated amount of fog is divided by the same value.

	Fog	0,00194	Total	Weighting formula	Weighted total
Vertical	2,2	1,9E-03	2,2	= Fog/52+Dew	0,04
Horizontal	1,8	1,5E-02	1,8	= Fog/52+Dew	0,05

For this reason, a roof component is considered potentially more efficient than a facade element,

APPENDIX VI



STANDALONE COMPONENT



MODULAR WALL COMPONENT

